

**NATIONAL METALLURGICAL LABORATORY  
MADRAS CENTRE, CSIR COMPLEX  
TARAMANI, CHENNAI**

**Dr T.S.N. SANKARA NARAYANAN**  
Scientist E1  
Research Supervisor

*Fax:* 91-44-2254 1027  
*E-mail:* [tsnsn@rediffmail.com](mailto:tsnsn@rediffmail.com)

**CERTIFICATE**

I hereby certify that the thesis, entitled **“STUDIES ON Ni-B AND Ni-B-Si<sub>3</sub>N<sub>4</sub> COMPOSITE COATINGS OBTAINED BY ELECTRO- AND ELECTROLESS DEPOSITION PROCESSES”** submitted to the University of Madras, is a record of research work done by **Ms. K. KRISHNAVENI** during the period from April 2002 to October 2006 under my supervision and the thesis has not formed previously the basis for the award of any Degree, Diploma, Associateship, Fellowship or other similar titles.

**(Dr. T.S.N. SANKARA NARAYANAN)**

Chennai-600 113  
October 18, 2006.

**NATIONAL METALLURGICAL LABORATORY  
MADRAS CENTRE, CSIR COMPLEX  
TARAMANI, CHENNAI**

**Dr T.S.N. SANKARA NARAYANAN**  
Scientist E1  
Research Supervisor

*Fax:* 91-44-2254 1027  
*E-mail:* [tsnsn@rediffmail.com](mailto:tsnsn@rediffmail.com)

**STATEMENT**

The thesis, entitled **“STUDIES ON Ni-B AND Ni-B-Si<sub>3</sub>N<sub>4</sub> COMPOSITE COATINGS OBTAINED BY ELECTRO- AND ELECTROLESS DEPOSITION PROCESSES”** submitted by **Ms. K. KRISHNAVENI** to the University of Madras, for the Degree of Doctor of Philosophy is the original and independent work carried out by her at the National Metallurgical Laboratory, Madras Centre, CSIR Complex, Taramani, Chennai, under my supervision during the period from April 2002 to October 2006.

**(Dr. T.S.N. SANKARA NARAYANAN)**

Chennai-600 113  
October 18, 2006.

## DECLARATION

I hereby declare that the Ph.D. thesis entitled “**STUDIES ON Ni-B AND Ni-B-Si<sub>3</sub>N<sub>4</sub> COMPOSITE COATINGS OBTAINED BY ELECTRO- AND ELECTROLESS DEPOSITION PROCESSES**” submitted for the award of degree of Doctor of Philosophy is the bonafide record of independent research work done by me in National Metallurgical Laboratory, Madras Centre, during the period from April 2002 to October 2006 under the supervision of **Dr. T.S.N. SANKARA NARAYANAN**, Scientist, National Metallurgical Laboratory, Madras Centre, CSIR Complex, Taramani, Chennai-600 113 and has not formed the basis for the award of any degree, diploma, associateship, fellowship or similar titles in this University or any other University.

National Metallurgical Laboratory  
Madras Centre, CSIR Complex  
Taramani, Chennai-600 113

**K. KRISHNAVENI**

October 2006.

# TABLE OF CONTENTS

Abstract	(i)
<b>Chapter</b>	<b>Page</b>
<b>I INTRODUCTION</b>	
1.1 Surface Engineering	1
1.2 Electrodeposition	2
1.3 Electroless deposition	4
1.4 Ni-B coatings	6
1.4.1 Structure of Ni-B coatings	11
1.4.2 Hardness of Ni-B coatings	15
1.4.3 Wear resistance of Ni-B coatings	17
1.4.4 Corrosion resistance of Ni-B coatings	18
1.4.5 Applications of Ni-B coatings	19
1.5 Composite coatings	20
1.5.1 Factors influencing particle incorporation	21
1.5.2 Mechanism of electro- and electroless codeposition	30
1.5.3 Structure of composite coatings	35
1.5.4 Hardness of composite coatings	35
1.5.5 Friction, wear and abrasion resistance of composite coatings	37
1.5.6 Corrosion resistance of composite coatings	44
1.5.7 Applications of composite coatings	48
<b>II STATE-OF-THE-ART AND THE SCOPE OF PRESENT INVESTIGATION</b>	49
<b>III MATERIALS AND METHODS</b>	
3.1 Materials used	54
3.2 Methodology of synthesis of Ni-B and Ni-B-Si <sub>3</sub> N <sub>4</sub> composite coatings	54



<b>Chapter</b>		<b>Page</b>
3.3	Characterization of the Ni-B and Ni-B-Si <sub>3</sub> N <sub>4</sub> composite coatings	58
3.3.1	Evaluation of chemical composition of the coatings	58
3.3.2	Evaluation of coatings using optical and scanning electron microscopes	59
3.3.3	Evaluation of structural characteristics	60
3.3.4	Evaluation of microhardness	61
3.3.5	Evaluation of wear resistance	61
3.3.6	Evaluation of corrosion resistance	63

## **IV RESULTS AND DISCUSSION**

### **Part A – Electro- and Electroless deposited Ni-B coatings**

4.1	Electrodeposited Ni-B coatings	
4.1.1	Coating synthesis	64
4.1.2	Surface morphology	66
4.1.3	Structural characteristics	67
4.1.4	Thermal characteristics	74
4.1.5	Microhardness	77
4.1.6	Wear resistance	78
4.1.7	Corrosion resistance	81
4.2	Electroless Ni-B coatings	
4.2.1	Coating synthesis	85
4.2.2	Surface morphology	86
4.2.3	Structural characteristics	87
4.2.4	Thermal characteristics	89

<b>Chapter</b>	<b>Page</b>
4.2.5 Microhardness	90
4.2.6 Wear resistance	91
4.2.7 Corrosion resistance	93
<b>Part B – Electro- and Electroless deposited Ni-B-Si<sub>3</sub>N<sub>4</sub> composite coatings</b>	
4.3 Electrodeposited Ni-B-Si <sub>3</sub> N <sub>4</sub> composite coatings	
4.3.1 Coating synthesis	98
4.3.2 Plating rate and chemical composition	103
4.3.3 Surface topography and morphology	104
4.3.4 Structural characteristics	105
4.3.5 Microhardness	107
4.3.6 Wear resistance	108
4.3.7 Corrosion resistance	112
4.4 Electroless Ni-B-Si <sub>3</sub> N <sub>4</sub> composite coatings	
4.4.1 Coating synthesis	118
4.4.2 Plating rate and chemical composition	120
4.4.3 Surface finish and morphology	121
4.4.4 Structural characteristics	121
4.4.5 Microhardness	122
4.4.6 Wear resistance	123
4.4.7 Corrosion resistance	127
<b>Part C – Duplex, multilayer and graded coatings</b>	
4.5 Electroless Ni-P/Ni-B duplex coatings	133
4.5.1 Coating synthesis	133
4.5.2 Plating rate and chemical composition	133
4.5.3 Structural characteristics	134
4.5.4 Microhardness	136

<b>Chapter</b>	<b>Page</b>
4.5.5 Wear resistance	137
4.5.6 Corrosion resistance	138
4.6 Multilayered coatings	141
4.7 Graded coatings	143
4.8 Comparison of important characteristics of Ni-B and Ni-B-Si <sub>3</sub> N <sub>4</sub> composite coating	146
<b>V SUMMARY AND CONCLUSIONS</b>	147
<b>REFERENCES</b>	156

## ACKNOWLEDGEMENT

I express my gratitude to my guide, **Dr. T.S.N. Sankara Narayanan**, Scientist, NML Madras Centre, for his constant encouragement, motivation and guidance. His enthusiasm, helping tendency and spirited nature inspired me. Apart from research, he introduced me the joy of helping others without expectations.

I thank **Prof. S.P. Meharotra**, Director, NML, Jamshedpur and **Dr. S. Srikanth**, Scientist-in-charge, NML Madras Centre, for providing permission and the necessary facilities to carry out my research work.

I thank the **Council of Scientific and Industrial Research (CSIR)** for providing me the Research Fellowship to carry out the research work.

I am grateful to **Prof. S.K. Seshadri**, Department of Metallurgical Engineering, Indian Institute of Technology-Madras, Chennai, for his valuable suggestions and guidance.

I thank **Dr. B.R.V. Narasimhan**, Technical Officer NML Madras Centre and **Mr. Satender Kumar** for their encouragement and support. I also thank all the scientists and technical officers of NML Madras Centre for their help during the course my work.

I express my sincere thanks to **Dr. R. Parimala** for being an inspiration for my research work. My heartfelt thanks are due to **Mr. I. Baskaran**, Research Scholar, University of Madras, for his timely help.

I express my sincere thanks to **Mr. Sasikumar**, research scholar and **Mr. Kumaran**, Graduate trainee, for their help in preparing the metallographic samples. I also thank **Mr. V. Vaidhyanathan** for assisting me in sample preparation.

I thank **Dr. R. Narayanan** and **Dr. M. Palaniappa**, IIT, Chennai, for their support and help in doing the wear resistance studies.

I thank all the research scholars and my friends at NML Madras Centre for their timely help and in boosting me up during my tough times.

I thank my parents, my sisters, Ms. Vidhya, Ms. Krithika and, my in-laws for their prayers, wishes, encouragement and support. Special thanks are due to my husband for encouraging me in all possible ways.

(K. KRISHNAVENI)

## LIST OF SYMBOLS AND ABBREVIATIONS

### *List of symbols*

K	-	Kelvin
$E_{\text{corr}}$	-	Corrosion potential
$I_{\text{corr}}$	-	Corrosion current density
$R_{\text{ct}}$	-	Charge transfer resistance
$C_{\text{dl}}$	-	Double layer capacitance
mV	-	Millivolt
mA	-	Milliampere
$\mu\text{A}$	-	Microampere
$R_a$	-	Surface roughness
$\mu_{\text{av}}$	-	Average friction coefficient

### *List of abbreviations*

DMAB	-	Dimethylamine borne
SCE	-	Saturated calomel electrode
OCP	-	Open circuit potential
XRD	-	X-ray diffraction
DSC	-	Differential Scanning Calorimetry
LSM	-	Laser scanning microscope
SEM	-	Scanning electron microscope
TEM	-	Transmission electron microscope
EDX	-	Energy dispersive X-ray spectrometry
EIS	-	Electrochemical impedance spectroscopy
ASTM	-	American Society for Testing and Materials
ED	-	Electrodeposited
EL	-	Electroless

# CHAPTER I

## INTRODUCTION

### 1.1 SURFACE ENGINEERING

A vast majority of engineering components can degrade or fail catastrophically in service through surface related phenomena such as wear, corrosion and fatigue. This has led to the development of an interdisciplinary subject called as surface engineering in the early 1980's (Bell, 1991). According to Bell, surface engineering can be defined as *“the design of a substrate and surface together as a system to produce a cost-effective performance enhancement of which neither is capable on its own”* (Bell, 1991). Surface engineering has been practiced in crude forms in Europe and Asia for several thousand years. In medieval times there were many references to a wide variety of nitrogenous compounds used to engineer the surface of weapons and agricultural implements. Increasing number of surface technologies including chemical vapour deposition (CVD), physical vapour deposition (PVD), ion implantation, laser surface modification, plasma thermochemical treatments and various other plasma spray technologies have attained commercial maturity in 1980's. In addition to the manufacturing industry including the aerospace, automotive, nuclear, mining and general engineering sectors, the new surface engineering technologies are being adopted by the electronics, medical and decorative sectors as well (Bell, 1991). Among the various surface modification processes, electro- and electroless deposition processes are widely accepted owing to their cost-effectiveness, higher production rate and ease of operation.

## 1.2 ELECTRODEPOSITION

Electrodeposition can be defined as the deposition of an adherent metallic coating for the purpose of securing a surface with properties or dimensions different from those of the base material. Electrodeposits are applied to metal substrates for decoration, corrosion resistance, wear resistance, electrical and magnetic properties, solderability, etc. In electrodeposition of metals, a direct current is made to flow between two electrodes immersed in a conductive aqueous solution containing the metal salts to be deposited. The flow of current causes one of the electrodes (the anode) to dissolve and the other electrode (the cathode) to become covered with the deposited metal. The metal to be deposited is available as positively charged ions. When the current flows, the positively charged ions react with the electrons and are converted to metallic atoms at the cathode surface. The reverse occurs at the anode where the metal is dissolved to form positively charged metal ions which enter the solution (Lowenheim, 1974; Schlesinger and Paunovic, 2000). The various constituents of the electrolyte solutions used for electrodeposition of metals and their functions are listed in **Table 1.1**.

Alloy deposition is subjected to the same principles as single metal plating. The deposition potential of a given metal is determined by the standard electrode potential ( $E^0$ ) and ionic activity. The ionic activity is proportional to the ionic concentration. The electrodeposition of an alloy requires codeposition of two or more metals. For achieving the deposition of an alloy, the metal ions must be present in the electrolyte solution that provides a cathode film where their individual deposition potential can be made to be close or even the same.

If the deposition potential differs a lot then the only way to achieve the deposition of the alloy is by controlling the activity of the ions by changing their concentration (Brenner, 1963). Alloy deposition often provides deposits with properties not obtained by employing electrodeposition of single metals. The three main stages of alloy deposition are:

*Ionic migration:* The hydrated ions in the electrolyte migrate towards the cathode under the influence of the applied potential as well as through diffusion and/or convection.

*Electron transfer:* At the cathode surface, the hydrated metal ions enter the diffusion double layer where the water molecules of the hydrated ion are aligned by the field present in this layer. Subsequently the metal ions enter the fixed double layer where because of the higher field present, the hydrated shell is lost. Then on the cathode surface, the individual ion may be neutralized and gets adsorbed.

*Incorporation:* The adsorbed atom wanders to a growth point on the cathode and is subsequently incorporated in the growing lattice.

Some key issues in alloy deposition are as follows:

- (i) If an alloy plating bath, which is in continuous operation, is replenished with two metals in a constant ratio, the ratio of metals in the deposit will approach and ultimately take on that value.
- (ii) In alloy deposition, the ratio of the concentration of the more readily depositable metal to the other is smaller at the cathode-solution interface than in the bulk of the bath.



- (iii) An increase in the metal percentage of a parent metal in an alloy plating bath results in an increase in its percentage in the deposit.
- (iv) In the deposition of alloys from the normal alloy plating systems, the most fundamental mechanism is the tendency of the concentration of the metal ions at the cathode-solution interface to approach mutual equilibrium with respect to the two parent metals.
- (v) A variation in a plating condition that brings closer together the potentials for the deposition of the parent metals increases the percentage of the less noble metal in the electrodeposited alloy.

### **1.3 ELECTROLESS DEPOSITION**

Electroless plating was an accidental discovery by Brenner and Riddell in the year 1946, when they tried to electroplate Ni-W alloy on the inner side of a steel tube using a citrate bath. As the Ni-W alloy deposit exhibits a high level of internal stress and cracking due to oxidation of the organic components in the bath, they attempted modification of the plating bath using several reducing agents including sodium hypophosphite. To their surprise, they found that the exterior surface of the steel tube was also coated and this had accounted for the increased current efficiency, totaling up to 120% of the theoretical value. After careful analysis they concluded that the coating formed on the exterior of the steel tube might have formed by chemical reduction induced by hypophosphite, which happened to be a good reducing agent (the reduction potential of hypophosphite is -0.499 V at pH 4-6 and -1.57 at pH 7-10). In this process the chemical reducing agent provides electrons necessary to produce a metallic

deposit rather than external electric current (as in electroplating). Hence, the process was named as chemical nickel plating. Based on its analogy with electroplating process, William Blum coined the term “Electroless Plating” for this process. Electroless plating process as we know today is an improved version of the process developed by Brenner and Riddell.

Among the variety of metals that can be plated using this method, electroless nickel has proved its supremacy for producing coatings with excellent corrosion and wear resistance (Gawrilov, 1979; Mallory and Hajdu, 1991; Riedel, 1991). Compared to electrodeposition, coatings obtained using the electroless plating technique is uniform and they possess a very homogeneous distribution regardless of the substrate geometry (Okinaka et al. 1994). Since no current flow is involved in the electroless deposition process, the rate of deposition on all areas should be equal as long as the solution conditions are maintained properly. This attribute of electroless plated coatings is beneficial when coating complex parts with critical dimensions, such as ball valves or threaded components.

The essential components of the electroless plating bath (**Table 1.2**) are metal salt, reducing agent, complexing agent, accelerators, buffers, pH regulators, stabilizers and wetting agents. Most of the applications of electroless nickel coating are based on their wear and corrosion resistance. **Table 1.3** enumerates the various applications of electroless nickel based coatings (Agarwala and Agarwala, 2003). Electroless nickel processes are grouped as Ni-P, Ni-B and pure Ni, respectively, based on the reducing agents used i.e., hypophosphite, borohydride or dialkyl amino borane and hydrazine,

in the plating bath. Hypophosphite-reduced electroless nickel plating process has received commercial success because of its low cost, ease of control, and ability to offer good corrosion resistance (Gawrilov, 1979; Mallory and Hajdu, 1991; Riedel, 1991). Recently, much attention is being paid towards amino-borane and borohydride-reduced electroless nickel plating.

#### **1.4 Ni-B COATINGS**

The following sections address the various aspects of deposition of Ni-B alloy coatings by electro- and electroless deposition processes, the mechanism of deposition, the characteristics properties and applications of Ni-B coatings.

ED Ni-B coatings are prepared using dialkylamine borane modified nickel plating baths, in which the dialkylamine borane forms the source of boron in these coatings. The mechanism of alloying of boron with nickel is not fully understood. It is believed that the adsorption of DMAB on the already formed nickel surface and its subsequent decomposition to elementary boron leads to the alloying of boron with nickel (Onada et al., 1998, 1999). Hence, the amount of boron alloying with nickel is determined mainly by the distribution of DMAB, and the thickness of the diffusion layer at the cathode surface, regardless of the electrode potential.

For electroless plating of Ni-B alloy coatings, boron-containing reducing agents such as sodium borohydride or dimethylamine borane (DMAB) are commonly used. The former requires high temperature and strong alkaline conditions, while the latter can be used under relatively lower temperature and neutral or weakly acidic conditions (Masui, 1986). Sodium

borohydride is one of the most powerful reducing agents for producing electroless Ni-B coatings. The reduction efficiency of sodium borohydride is much higher than that of DMAB and sodium hypophosphite. It can provide up to eight electrons for reduction of some metals as opposed to two electrons that can be provided by sodium hypophosphite, for the same reaction (Duncan and Arney, 1984). Besides the high reduction efficiency, borohydride-reduced baths are preferred to DMAB based baths in terms of cost-effectiveness of operation (Lo and Hwang, 1994). However, borohydride ions hydrolyze readily in acid or neutral solutions and will spontaneously yield nickel boride in presence of nickel ions in the plating bath (Duncan and Arney, 1984; Lo and Hwang, 1994). Hence, control of pH is important to avoid the spontaneous decomposition of the bath solution and to decrease the cost of operation. Because of the high operating pH, borohydride baths cannot be used for producing Ni-B coatings on aluminium substrates (Dadvand et al., 2003). Using sodium borohydride as the reducing agent, electroless Ni-B coatings with 3-8 wt.% B content can be obtained. This kind of EL Ni-B coating is known for its high hardness and wear resistance, as well as corrosion resistance and specific electrical and magnetic properties (Rao et al., 2001; Valsiunene, 1988). In general, borohydride-reduced electroless nickel coatings provide superior hardness, wear resistance, lubricity and have more consistent properties than coatings reduced with other boron compounds (Duncan and Arney, 1984; Rao et al., 2001).

DMAB-reduced electroless nickel plating baths can be operated over a wide pH range from weak acidic to strong alkaline conditions (Kosov et al., 1989). They offer a wide window of opportunity to produce electroless Ni-B

coatings and these baths are even suitable for the metallization of plastics. These baths have an exceptionally long bath life due to high solubility of the products of the deposition reaction and moderate operating temperature. The electroless Ni-B coatings obtained from such baths have low electrical resistivity and high as-plated hardness (Mallory, 1971). The main limitation of DMAB-reduced electroless plating baths is that they are unsuitable for producing Ni-B coatings having relatively higher boron content of the order of 5-6 wt.% and above.

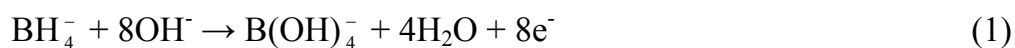
Electroless plating is defined as the autocatalytic deposition (reduction) of metal ions in the presence of a reducing agent (hypophosphite, aminoborane or borohydride). Initiation of electroless nickel deposition occurs readily with metals such as iron, nickel, and cobalt. Once the initial nickel layer has deposited on the catalytic substrate, it acts as a catalyst for the process and the deposition continues unaided. This is referred to as autocatalysis of the deposition reaction. This unique property of electroless plating makes it possible to coat internal surfaces of pipes, valves, nuts and bolts, and other complex geometries that are very difficult or impossible to be coated by conventional electroplating techniques.

Paunovic (1968) was the first to identify electroless metal deposition in terms of mixed potential theory. He suggested that electroless metal deposition mechanisms could be predicted from the polarization curves of the partial anodic and cathodic processes. In simple terms, mixed potential theory leads to the assumption that electroless nickel plating can be considered as the superposition of anodic and cathodic reaction at the mixed (deposition)

potential,  $E_m$ . Accordingly, the rates of the anodic reactions are independent of the cathodic reactions occurring simultaneously at the catalytic surface, and the rates of separate partial reactions depend only on the electrode potential, the mixed potential.

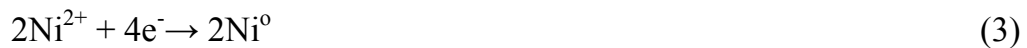
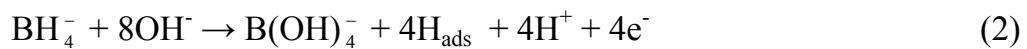
Homma et al. (2003) studied the reaction mechanism of electroless deposition using dimethylamine borane (DMAB) using *ab initio* molecular orbital approaches such as Hartree-Fock (HF) and second order Møller-Plesset (MP2) calculations. They have suggested that the oxidation reaction of DMAB proceeds via five-coordinate intermediates in which  $\text{OH}^-$  coordinates to B before the elimination of H radical and that the total oxidation reaction is stabilized by the generation of  $\text{H}_2$  (**Fig. 1.1**). They also suggest that the reaction preferably proceeds in the electric double layer that is formed at the surface region of the deposited metals, rather than in the bulk solution. Furthermore, it is expected that the metal surface stabilizes this reaction due to its electron receptivity, which enhances the electron emitting reaction of the reductant.

Sodium borohydride and DMAB are the most widely used reducing agents for preparing electroless Ni-B coatings. Borohydride is a powerful reducing agent. The redox potential of  $\text{NaBH}_4$  is calculated to be  $E = -1.24 \text{ V}$ . In basic solutions, the decomposition of the  $\text{BH}_4^-$  unit yields 8 electrons for the reduction reaction.

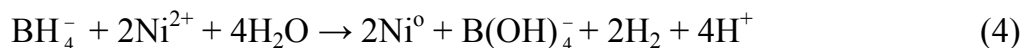


However, it has been found experimentally that one mole of borohydride reduces approximately one mole of nickel. Based on this observation many

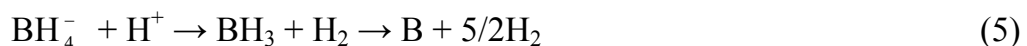
mechanisms were proposed. The most widely accepted mechanism was proposed by Gorbunova et al. (1973).



Equations (2) and (3) can be combined to give



Reduction of boron

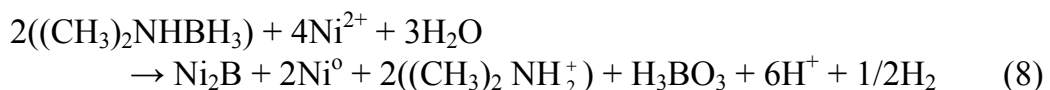


hydrolysis of borohydride

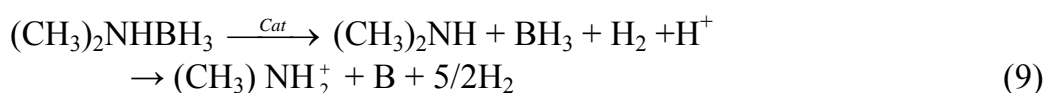


This mechanism indicates that the mole ratio of nickel reduced to borohydride consumed is 1:1, which was supported by experimental evidence (Gorbunova et al., 1973).

DMAB has three active hydrogens bonded to the boron atom and, therefore, should theoretically reduce three nickel ions for each DMAB molecule consumed (each borohydride will theoretically reduce four nickel ions). The reduction of nickel ions with DMAB is described by the following equations:

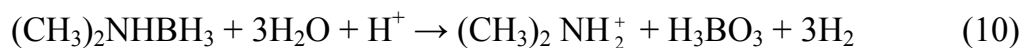


Boron reduction:

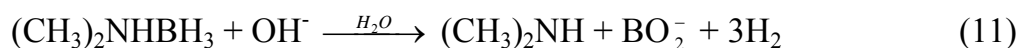


In addition to the above useful reactions, DMAB can be consumed by wasteful hydrolysis:

Acid:



Alkaline:



In acidic solutions, the first stage of the process is the dissociation of water ( $\text{H}_2\text{O} \rightarrow \text{H}^+ + \text{OH}^-$ ) at the catalytic surface. The hydroxyl ions ( $\text{OH}^-$ ) replace the hydrogen in the B-H bond of DMAB and as a result, an electron and a hydrogen atom are produced. The consumption of  $\text{OH}^-$  ions results in the accumulation of hydrogen ions ( $\text{H}^+$ ) in the solution with a concurrent decrease in pH of the solution. In alkaline solutions, the sources of hydroxyl ions are the basic compounds ( $\text{NaOH}$ ,  $\text{NH}_4\text{OH}$ , etc.) that are added to the plating solution to adjust the pH into the alkaline range of 7.0 to 14.0. As a result of the reaction of  $\text{OH}^-$  with the B-H bond, the pH also decreases in the alkaline solution. In this case, however, the pH decrease is due to the consumption of  $\text{OH}^-$  ions rather than the formation and accumulation of  $\text{H}^+$  ions. As can be deduced from reactions (1) to (5) and (7) to (9), the electroless nickel coating is not pure nickel, unlike for electroplating, but a nickel-boron alloy coating.

#### 1.4.1 Structure of Ni-B coatings

In as-deposited condition, ED and EL Ni-B coatings are metastable, supersaturated metal-metalloid alloy coating. The equilibrium phase diagrams of Ni-B alloy showed in **Fig. 1.2** exhibits no solubility of boron in nickel at ambient temperatures. Hence, under equilibrium conditions, the Ni-B alloys



should essentially consist of pure nickel and the intermetallic compound,  $\text{Ni}_3\text{B}$ . However, the conditions that exist during deposition do not permit the formation of the  $\text{Ni}_3\text{B}$ , the stable intermetallic in the Ni-B system. Growth of even tiny crystals of  $\text{Ni}_3\text{B}$  would involve the movement of large numbers of atoms by surface diffusion in order to achieve correct stoichiometry of three nickel atoms to one boron atom. This movement cannot occur before the next layer of atoms has been laid down. Thus, the boron atoms are trapped between nickel atoms, resulting in supersaturation. It is also likely that boron atoms so trapped are not uniformly distributed. The enrichment of boron makes it impossible for nickel to maintain the f.c.c. structure over a long range and the structure becomes amorphous (Sampath Kumar and Kesavan Nair, 1995).

The structural characteristics of ED and EL Ni-B coatings are directly related to their boron content. The crystal structure of nickel is face-centred cubic (f.c.c.), in which each atom has 12 neighbours. The entrapment of boron makes it impossible for this atom arrangement to extend over large surfaces. The volume of material within which the f.c.c. atom arrangement can be maintained is called a grain. Grain sizes are thus very small in ED and EL Ni-B coatings. If the f.c.c. structure cannot be maintained at all, the structure is equivalent to that of a liquid and is considered to be amorphous.

The detailed structure of ED and EL Ni-B coating is not fully understood but in as-plated conditions they are reported to be either crystalline, amorphous, or a combination of the two depending on the boron content of the alloy. The amorphous state of the Ni-B coatings could have resulted from the increase in the level of boron inclusion in the coatings following the higher

concentration of reducing agents used in the plating bath (Watanabe and Tanabe, 1976). Some studies based on XRD measurements suggest that the Ni-B alloy is in a state of transition between amorphous and very finely crystalline structures (Duncan and Arney, 1984). The structural information obtained from the morphological studies and XRD measurements indicate that the Ni-B coatings are developed through a nucleation and growth type process involving island formation of microcrystalline nickel and lateral growth. The coating structure generated was a supersaturated solid solution of boron in nickel with a level of free energy higher than the equilibrium configuration (Bedingfield et al., 1991). It has been suggested that the structure of the Ni-B coating is in the process of transition from a crystalline to non-crystalline state, i.e., the as-plated Ni-B coating possess a nucleated structure of short-range order (Zhang et al., 1993). According to Rao et al. (2001) the XRD pattern of an as-plated Ni-B coating consists of a broad peak and a superimposing sharp one. Accordingly, the microstructure of the coating is a mixture of microcrystalline and non-crystalline containing (i) a solid solution of boron and hydrogen in f.c.c. cubic nickel; and (ii) an amorphous phase. The main constitution of the microcrystalline was probably a supersaturated solid solution of boron in nickel.

EL Ni-B alloy coating deposited using DMAB-reduced electroless nickel plating bath with a pH of 6 is nearly amorphous whereas the one deposited at a pH of 9 exhibits a diffraction pattern characteristic of f.c.c. nickel. As the metallizing solution pH increases, the size of the grains increases and there is a distinct increase in the initial degree of crystallinity, which is confirmed by the changes in the width, and clearer definition of the individual

diffraction rings. Evans and Schlesinger (1994) and Masui (1986) have suggested that the EL Ni-B coating having  $< 4\%$  B exists in a mixed state of supersaturated and amorphous phase, which are different thermodynamically, from one another.

Annealing of Ni-B coatings enables them to release the compressive stress and enlarge the structure cell and the interplanar distance. Annealing results in the formation of f.c.c. nickel crystallites of varying dimensions and causes the migration of boron to the surface. Like phosphorus, boron could also act like a crystallization inhibitor. Heat-treatment brings the bulk of boron of the Ni-B coating to the coating surface and causes a higher degree of crystallization. Annealing of the Ni-B coatings at  $300^{\circ}\text{C}$  results in a large amount of diffusion of boron to the surface and causes precipitation of nickel boride phases. Heat-treatment at temperatures higher than  $400^{\circ}\text{C}$  leads to precipitation of  $\text{Ni}_2\text{B}$  and  $\text{Ni}_7\text{B}_3$  phases (Duncan and Arney, 1989). Annealing at  $500^{\circ}\text{C}$  essentially removes all the boron from the bulk of the coating by diffusing it to the film's surface (Evans and Schlesinger, 1994). The type of boride formed depends upon heat treatment temperature and the boron content of the coating. Increase in the annealing temperature to  $600^{\circ}\text{C}$  results in coarsening of the crystals and indicate the absence of  $\text{Ni}_2\text{B}$  phase and predominance of nickel and  $\text{Ni}_3\text{B}$  phases in the coating. Further annealing at  $600^{\circ}\text{C}$  results in growth of crystalline nickel and dissolution of  $\text{Ni}_2\text{B}$  precipitates giving way to  $\text{Ni}_3\text{B}$  precipitation, a more stable phase.

The process of crystallization of Ni-B alloys can be classified into two types depending on their boron content. In alloys with lower boron content

(approximately 7-18 at.% B) fine f.c.c. nickel particle precipitated from an amorphous (or supersaturated solid solution) matrix at approximately 200°C and upon further heating, the remaining matrix was transformed into a stable phase of (Ni+ Ni<sub>3</sub>B) by eutectic crystallization at 300-400°C. In alloys with higher boron content (approximately 20-25 at.% B) the amorphous solid is directly converted into stable crystal phases of Ni<sub>3</sub>B and Ni at 300-350°C (Masui et al., 1985; Gaevskaya et al., 1996).

#### **1.4.2 Hardness of Ni-B coatings**

One of the outstanding characteristics of ED and EL Ni-B coatings is their high hardness even in as-plated condition, which increases further after heat-treatment at appropriate temperatures. The hardness of ED and EL Ni-B coatings is especially important when superior wear and abrasion resistance of these coatings are warranted. The three major parameters, which influence the hardness of ED and EL Ni-B coatings, are the boron content of the coating, the heat-treatment temperature and time (Rao et al., 2001). The microhardness of ED Ni-B coatings is of the order of 600 HV<sub>0.1</sub> for as-plated coatings and 750 HV<sub>0.1</sub> for coatings heat-treated at 400°C for 1 hour. The hardness of EL Ni-B coatings is of the order of 550-750 HV<sub>0.1</sub> in as-plated condition and 950-1230 HV<sub>0.1</sub> after heat-treatment at 400°C for 1 hour (Duncan and Arney, 1984; Zhang et al., 1993; Sankara Narayanan et al., 2003, 2006).

The variation in hardness of ED and EL Ni-B coatings as a function of heat-treatment temperature is related to their microstructure and the nature of phases formed during the heat-treatment process. The slight increase in microhardness observed around 250°C, which is slightly earlier than the

crystallization temperature, confirms the effect of precipitation hardening. The formation of crystallized nickel leads to a large lattice distortion and a rapid increase in hardness of the coating. The peak hardness is attained around 350°C, well after the completion of the reaction. The increase in plating hardness after isothermal annealing appears to be due to both the dispersion hardening because of  $\text{Ni}_3\text{B}$  and  $\text{Ni}_2\text{B}$  phase formation and their high hardness values. Because crystallization is gradual and  $\text{Ni}_3\text{B}$  is formed with increasing temperature, a maximum value of hardness is obtained, which then falls with coalescence and coarsening of the  $\text{Ni}_3\text{B}$  phase. The hardening mechanism is dispersion strengthening. The decrease in hardness after reaching its maximum value can be considered to be the result of relaxation of the internal stresses and coarsening of boride particles (Gorbunova et al., 1973). Particle coarsening and loss of coherency are considered responsible for the observed decrease in hardness at 450°C. Additional matrix softening occurs at 600°C (Bedingfield et al., 1991).

The microhardness values of heat-treated ED and EL Ni-B coatings are also related to the specific borides formed during heat-treatment. When the coating contains only the  $\text{Ni}_3\text{B}$  phase, the microhardness values reach around 1100-1200  $\text{HV}_{0.1}$  whereas when the  $\text{Ni}_2\text{B}$  phase exist in the coatings, the hardness values reach around 1200-1300  $\text{HV}_{0.1}$  and with  $\text{Ni}_4\text{B}_3$  phase the hardness attains around 1400  $\text{HV}_{0.1}$  (Rao et al., 2001). Very long term (30-40 weeks) treatments at 200-300°C can produce hardness values ranging from 1700-2000  $\text{HV}_{0.1}$ . Heat-treatment at these temperatures cause a finer dispersion of nickel boride compared to treatment at higher temperatures (400°C and above) and also allows the formation of iron borides such as  $\text{Fe}_2\text{B}$  and

$\text{Fe}_3\text{C}_{0.2}\text{B}_{0.8}$  from substrate diffusion into the coating (Duncan and Arney, 1984). Though appropriate heat treatment of Ni-B coatings lead to very high hardness values, the heat-treated coating become too brittle and fragile. Hence, the choice of heat-treatment temperature should be made in such a way to obtain the best compromise between hardness and wear resistance without brittleness of the coating (Delaunois et al., 2000).

### **1.4.3 Wear resistance of Ni-B coatings**

The principal advantages of borohydride-reduced electroless nickel coatings are its hardness and superior wear and abrasion resistance in the as-deposited condition (Duncan 1986; Gorbunova et al., 1973; Delaunois and Lienard, 2002). EL Ni-B-Tl coatings with higher boron content are very hard and provide excellent resistance to wear and fretting (Laitinen, 1992). The wear resistance of borohydride reduced electroless nickel is outstanding and after heat-treatment equals or exceeds that of tool steel and hard chromium coatings (Duncan and Arney, 1984; Bielinski et al., 1990; Zhang et al., 1993; Delaunois et al., 2000). The columnar structure of Ni-B coatings composed of uniformly deposited nodules is expected to provide a low friction surface by reducing the surface area of contact. Besides, this type of structural feature also contributes to an enhanced coating toughness and they are also useful in retaining lubricants under conditions of adhesive wear (Gawrilov, 1979; Dadvand et al., 2003). Heat-treatment of ED and EL Ni-B coating allows extremely hard and uniform deposition of nickel boride phases, providing them with incredible wear and abrasion resistance.

#### **1.4.4 Corrosion resistance of Ni-B coatings**

Several factors could influence the corrosion resistance of ED and EL Ni-B coatings. These include boron content, coating thickness, porosity, type of heat treatment, and induced tensile stress of substrates caused by machining or surface finishing operations. The most important factors that determine the corrosion resistance of ED and EL Ni-B coatings are: (Mallory and Hajdu, 1991):

- ❖ Substrate composition, structure and surface finish
- ❖ Pretreatment of the substrate to achieve a clean, uniform surface
- ❖ Adequate deposit thickness to meet the severity and time of exposure to corrosive conditions
- ❖ The properties of the deposit (composition, porosity, internal stress etc.) which depends on pH, formulation and prolonged use (turnover) of the plating solution
- ❖ Post plating treatments of the coating such as passivation and annealing
- ❖ The aggressiveness of the corrosive environment condition

Electroless Ni-B coatings are considered to have lesser resistance to corrosion when compared to electroless Ni-P coatings. In environments that cause little corrosion of high-phosphorus coatings (e.g., alkalis and solvents), electroless Ni-B is also very resistant. However, in environments that cause moderate attack of nickel-phosphorus (e.g., acids and ammonia solutions), nickel-boron coatings can be severely corroded. In strongly oxidizing media neither coating is satisfactory (Duncan and Arney, 1989). The difference in corrosion resistance of Ni-P and Ni-B coatings is due to the difference in their

structures. Ni-B coatings are not fully amorphous and the passive layers that form are not as glassy and protective as that of Ni-P coatings (Duncan and Arney, 1984).

Porosity is an important factor that promotes the corrosion of ED and EL Ni-B coatings. In general, thicker coatings have fewer pores and hence provide an increase in corrosion resistance. Apart from porosity and coating thickness, the corrosion performance of these coatings also depends on the surface roughness. Upon heat treatment, both ED and EL Ni-B coatings undergo shrinkage in volume which might cause cracks through the coating. This, in turn, would impair the corrosion resistance of the heat-treated coatings.

#### **1.4.5 Applications of Ni-B coatings**

ED and EL Ni-B coatings find applications in aerospace, automotive, chemical, electrical, mechanical, mining, molding and casting, optical, pulp and paper, textiles and weapon industries. ED and EL Ni-B coatings have become an integral part of the manufacturing process in electronic industries. These coatings are useful in improving reliability, extending equipment life and reducing cost. The maskless selective area nature and the electroless feature have made EL Ni-B coating a popular choice with widespread application in the electronic packaging industry. Typical e.g., of applications include metal finishing of PCB, filling of via-holes in multilevel interconnection, fabrication of multi-chip modules and the formation of solder bumps in tape-automated bonding technology. EL Ni-B coatings are logical choices by virtue of their solderability, diffusion-barrier effectiveness and bondability. Dual-inline sockets, transformer copper contacts, TO-5 header and pins and metallized



ceramic resistors are currently plated with Ni-B in the place of gold. These coatings are also recommended for the replacement of gold and silver coatings in different devices and microelectronic devices. Silicon wafers once finished with gold are now plated with Ni-0.2% B alloy coating from an alkaline electroless nickel plating bath. For many applications, the characteristics of electroless Ni-B coatings enables them to function as well or better than gold, or as an excellent barrier underplate for thin gold deposits. Wire bonding to electroless Ni-B coatings is superior compared to wire bonding to gold. Eutectic diode bonding to electroless nickel is equal or superior to eutectic diode bonding to gold. Ni-B coatings exhibit satisfactory solderability with nonactive fluxes and ultrasonic weldability with aluminium. Over the recent years, there has been a large increase in the use of electroless Ni-B coatings for wear-resistant and corrosion resistant applications (Laitinen, 1991).

## **1.5 COMPOSITE COATINGS**

The idea of codepositing various second phase particles in electro- or electroless deposited metals or alloy matrix and thereby taking advantage of their desirable qualities, such as hardness, wear and abrasion resistance, corrosion resistance, etc. has led to the development of composite coatings with a wide range of possible combination and properties (Pushpavanam and Sheno, 1977; Gawrilov, 1979; Joshi and Totlani, 1981; Zahavi and Hazan, 1983; Ramesh et al., 1991; Mallory and Hajdu, 1991; Riedel, 1991; Okinaka et al., 1994; Yeh et al. 1994, 1995, 1997; Garcia et al., 2001, 2003; Agarwala and Agarwala, 2003; Ramesh and Seshadri, 2003, Balaraju et al., 2003; Aruna et al. 2006). Almost any particle which can be held in suspension without

reacting with the plating bath can be codeposited by electro- and electroless deposition. The potential of electrodeposition as a method to produce composite coatings was reported way back in 1928 whereas the work dealing with the incorporation of second phase particles in the electroless deposited metal matrix began in the 1960's (Metzger and Florian, 1976). Both methods basically involve incorporation of small insoluble solid particles in the metal matrix during plating. The solid particles should be kept in suspension in the plating bath by agitation. The particles used for codeposition with the metal matrix ranged from hard particles like oxides of Al, Ce, Si, Ti, Th, Zr, carbides of Si, B, Ti, W, Cr, nitrides of Si, B and borides of Ti and Zr, synthetic and natural diamond to soft particles like, graphite, barium sulphate, calcium fluoride, molybdenum disulphide, PTFE and advanced materials like carbon nanotubes and inorganic fullerenes.

### **1.5.1 Factors influencing particle incorporation**

Several factors influence the incorporation of hard and soft particles in an electro- and electroless deposited metal matrix, which include, size, shape, conductivity and pretreatment of the particles, the concentration of particles in the plating bath, current density, additives, the method and degree of agitation, compatibility of the particle with the matrix, orientation of the substrate, etc. (Sharp, 1975; Agarwala and Agarwala, 2003).

#### ***Size and shape of the particles***

In electro-codeposition, fine particles (up to 10  $\mu\text{m}$ ) have been found to codeposit readily with high incorporation compared to coarse particles

(Kedward, 1972; Berkh et al., 1995). The mass/charge ratio of the particles in an electrolytic bath is shown to be the key factor. With increase in size of the particles, the mass/charge ratio of the particles increases considerably. This reduces both adsorption and electrophoretic movement of the particles in the electrical double layer at the cathode (Brandes and Goldthorpe, 1967), thus reducing the codeposition. Larger particles, however, have been codeposited easily at higher current densities (Ruimi and Martinou, 1989; Berkh et al., 1995).

The size of the particles also has a definite impact on their incorporation in the electroless deposited metal matrix (Grosjean et al., 2000; Brown, 1985; Apachitei et al., 1998a, 1998b). In general, it is recommended that the particles must be large and heavy enough to settle in the solution yet not so large as to make the deposit rough or make it difficult for them to be held in suspension (Brown, 1985). Also, the size of the particles should be selected with reference to the thickness of the electroless deposit, as attempts made to incorporate 10  $\mu\text{m}$  size particles in a 7  $\mu\text{m}$  thick electroless deposit has resulted in unsatisfactory finish and incorporation of 10  $\mu\text{m}$  size particles even in a 25  $\mu\text{m}$  thick deposit physically weakened it (Brown, 1985). It is suggested that particles in the size range of 2-7  $\mu\text{m}$  might be suitable for codeposition in an electroless nickel matrix, with particles in the size range 4-7  $\mu\text{m}$  being easiest to work with (Brown, 1985). Grosjean et al. (2000) have suggested that whatever the concentration of silicon carbide particles in the bath, the majority of the particles incorporated in the electroless Ni-P matrix are in the range 0.3-1.8  $\mu\text{m}$  diameter. Apachitei et al. (1998a) have found that, under similar

operating conditions, smaller particles in a narrow size distribution yields maximum incorporation. Reddy et al. (2000) recommended that for achieving a better integrity between the particles and the electroless Ni-P matrix, the size of the particles should be small so that they can be firmly held by the matrix.

In both electro- and electroless codeposition processes, particle shape plays a vital role in determining their level of incorporation in the metal matrix. It is generally believed that angular shaped particles will have a greater tendency to hold on to the surface upon impingement than the round ones. Apachitei et al. (1998a, 1998b) have, however, shown that spherical shaped alumina particles resulted in better incorporation than irregular ones. The difference in particle shape also has a bearing on the type of finish of the deposit. Very smooth and very rough surfaces were obtained, respectively, from small rounded particles and large angular particles.

### ***Conductivity of the particle***

In electro-codeposition, conducting particles show higher codeposition than the non-conducting ones. However, the composite coatings are uniform, contain a homogeneous distribution of particles and have a smooth finish only with the incorporation of non-conducting particles. This is due to the fact that conducting particles are rapidly and completely enveloped with the growing metal, codepositing upon each other, resulting in the formation of agglomerates whereas non-conducting particles are engulfed only at cathode areas adjacent to them, resulting in a uniform distribution (Tomaszewski et al., 1969). Conductivity of the particles has no influence on particle incorporation in electroless deposition.

### ***Pretreatment of particles***

Pretreatment of particles prior to addition to the electrolyte has been reported to improve the incorporation considerably (Sautter, 1963; Greco and Baldauf, 1968; Gupta et al., 1982; Zahavi and Hazan, 1983). The surface of the particles used for codeposition may be contaminated due to adsorption of various organic and inorganic impurities, which need to be removed, for better codeposition. Prevention of agglomeration and uniform distribution of the particles in the plating bath could be achieved by blending the particles with a small quantity of the plating bath in a mortar (Pushpavanam and Shenoi, 1977; Pushpavanam et al., 1974, Balaraju, 2000). Surface treatments like ball milling could induce electrostatic surface charge on individual particles.

### ***Composition of the plating bath***

The efficiency of the plating bath to codeposit particles in the metal matrix is found to be different for different electrolytes of the same metal. For example, codeposition of  $\text{Al}_2\text{O}_3$ , SiC, etc. is found to be less from an acid copper sulphate bath than from alkaline copper cyanide and fluoborate baths, in spite of these baths being operated at close to 100% efficiency (Tomaszewski et al., 1969). The difference is mainly due to the adsorption of cations on the particle surface. Since cation adsorption on particles in acid copper sulphate bath is small, the attractive force for the cathode surface is not strong enough to cause a higher level of incorporation. Similarly, for codeposition of insoluble inorganic particles, Watt's nickel bath (high sulphate bath) is found to be more effective than the chloride and fluoborate baths at the same temperature and pH (Tomaszewski et al., 1969). Microthrowing power is an important parameter

for codeposition of particles; plating baths having a poor microthrowing power enable easier entrapment of particle in the metal matrix.

### ***Concentration of particles in the bath***

Concentration of particles in the plating bath also plays a major role in influencing the particle incorporation level. Bath loadings of 5-200 g/l are quite common in electrodeposition whereas relatively lower concentrations are used in electroless deposition. In electro-codeposition, incorporation of particles in the metal matrix varies either linearly or logarithmically. Under steady state condition, the number of codeposited particles equals that approaching the cathode surface, thus exhibiting a linear relationship. However, beyond a critical concentration, collision among the moving particles inhibits the entrapment, which results in a plateau in the level of incorporation. In electroless codeposition, particle incorporation in the metal matrix exhibits a logarithmic relationship. In some instances, a slight decrease in the level of incorporation is also observed (Balaraju, 2000, Balaraju et al., 2003).

The critical concentration at which particles exhibit saturation in incorporation is not very different for various hard and soft particles in electroless codeposition whereas in electro-codeposition, the critical concentration for saturation in incorporation level varies with type of particles (Gawrilov, 1979; Balaraju, 2000; Dennis et al., 1981; Pushpavanam and Sheno, 1977; Pushpavanam, 1992; Izzard and Dennis, 1987; Balaraju and Seshadri, 1999; Abdel Hamid and Elkhair, 2002). Compared to electrodeposited composite coatings, incorporation of particles for a given concentration is considerably higher for electroless composite coatings.

Moreover, it is observed that to obtain a particular level of incorporation, a greater amount of particles in the bath is required in the case of electro-codeposition than electroless codeposition (Gawrilov, 1979; Indira Rajagopal, 1989; Dennis et al., 1981; Pushpavanam and Shenoi, 1977; Pushpavanam, 1992, Balaraju, 2000).

### ***Current Density***

Current density is one of the most important factors influencing the codeposition of particles in the metal matrix in electro-codeposition process. The range of current density suitable for codeposition, however, is not the same for all the baths and changes from metal to metal. For example, while most of the composites of metals such as Cu, Ni, Fe and Co can be codeposited in the range of 0.1-1 A/dm<sup>2</sup>, a very high current density of 10-60 A/dm<sup>2</sup>, is required for chromium based composite coatings. The variation in the level of incorporation of particles as a function of current density can be classified in to three types:

- ❖ A linear increase in incorporation with current density; e.g., Ni-Al<sub>2</sub>O<sub>3</sub> (Joshi and Totlani, 1981), Ni-TiO<sub>2</sub> (Ramesh Babu et al., 1991) and Ni-SiC (Viswanathan, 1973; Joshi and Totlani, 1981).
- ❖ A linear decrease in incorporation with current density; e.g., Ni-Cr<sub>3</sub>C<sub>2</sub> (Zahavi and Kerbel, 1982), Ni-Flyash (Ramesh et al., 1991), Ni-CeO<sub>2</sub> (Balathandan and Seshadri, 1992), Ni-graphite (Viswanathan and Ghouse, 1979) and Ni-Al<sub>2</sub>O<sub>3</sub>, (Greco and Baldauf, 1968; Sinha et al., 1973; Zahavi and Kerbel, 1982) etc.

- ❖ An increase followed by decrease with current density, the maximum being at a critical current density; e.g., Ni- $\gamma$ Al<sub>2</sub>O<sub>3</sub> (Webb and Robertson, 1994).

Among the three categories, the later one is followed by most of the systems. At low current densities (below 0.4 A/dm<sup>2</sup>), incorporation of the particles generally increase with increase in current density for most of the systems. However, after a critical current density, which is specific for individual bath, the incorporation decreases with further increase in current density. This is irrespective of the temperature and pH of the bath (White and Foster, 1981).

### ***Agitation***

To obtain a uniform distribution of the particles in the metal matrix without agglomeration, a homogeneous dispersion of the particles in the plating bath is very important, which can be accomplished by an efficient agitation of the plating bath. Various methods of agitation employed include mechanical agitation, circulation by pumping, purging of air, oxygen, nitrogen, ultrasonic agitation, and the plate-pumping technique. In practice, circulation by pumping or controlled air sparging is the best way to agitate the plating bath for obtaining maximum incorporation of particles in the metal matrix. In general if the agitation is too slow (laminar flow), the particles in the bath may not disperse completely, except when their density is low. On the other hand, if the agitation is too high (turbulent), particles will not have sufficient time to get attached to the surface, and this results in poor particle incorporation. The stirring speed should be optimized based on the size of the second phase particles to be incorporated. Kalantary et al. (1993) have suggested that the



laminar-turbulent transition region is the most effective agitation condition for maximizing incorporation of particles in electroless composite plating. Xiang et al. (2001) studied the effect of various modes of agitation on the level of incorporation of nano-sized diamond particles in the electroless Ni-P matrix. Mechanical agitation resulted in lesser incorporation due to the directional flow in the bath. Although agitation by nitrogen avoids the directional flow, it does not help to decrease the extent of aggregation of nano-sized diamond particles in the bath. Injection agitation mode helps to shatter the aggregation of nano-sized diamond particles and results in higher levels of incorporation of particles in the electroless Ni-P matrix.

### *Additives*

Organic substances such as thiourea, ethylenediamine, tetraethylene pentamine, ethylenediamine tetra acetic acid, glycine, alanine, taurin, asparagine, etc. helps to promote the co-deposition of particles in metal matrix obtained by electrodeposition. Monovalent cations such as, thallium, caesium, rubidium also helps to promote the electro-codeposition of particles and among them thallium is the most effective one. Besides, some special additives, mostly surfactants, play a major role in the incorporation of particles. Small amount of sodium lauryl sulphate (SLS), which is usually added in plating baths as an anti-pitting agent, helps to effectively disperse the particles in the plating bath and promote codeposition of particles. Wu et al. (2000a) reported that addition of SLS in the plating bath increases the dispersion and wettability of the silicon carbide particles. Grosjean et al. (1997) have shown that with the addition of 'Forafac-500', the incorporation of silicon carbide particles could be raised

from 19 to 53 vol.%. Surfactant additives are especially important in the incorporation of soft particles like polytetra fluoroethylene (PTFE), graphite and molybdenum disulphide (Izzard and Dennis, 1987; Nishira and Takano, 1994; Nishira et al., 1996; Matsuda et al., 1995; Hu et al., 1997; Moonir-Vaghefi et al., 1997a, 1997b, 1997c; Ger and Hwang, 2002). Ger et al. (2003) have suggested that, though surfactant additives enable a higher level of incorporation of PTFE particles, their concentration in the bath is critical. Beyond a certain concentration, surfactants tend to promote agglomeration of the particle in the plating bath. Moreover, adsorption of the surfactants on the substrate could act as a barrier for the codeposition of particles. Hence, it is recommended that while modifying the plating bath using special additives, such as, surfactants, a better understanding of the role of surfactants to achieve higher levels of particle incorporation is required.

### ***Orientation of the substrate***

The other important factor that determines particle incorporation is the orientation of the work piece. During plating the substrates can be held either vertically or horizontally. Substrates held vertically under uniform agitation, showed good incorporation. However, surfaces held horizontally and facing upwards were found to contain twice as many particles in comparison with those obtained using the vertical orientation (Sheela and Pushpavanam, 2002). Nevertheless, in such an orientation, very few particles were incorporated on the surface facing downwards. Hence, it is recommended that the objects be rotated and/or tumbled in such a way that all parts of the surface are regularly presented upwards (Hussain and Such, 1981).

It is clear from the above that several factors influence the incorporation of second phase particles in electro- and electroless deposited metal matrix and under actual process conditions more than one factor plays a predominant role. A thorough knowledge of the influence of process parameters and conditions on deposition of the metal matrix and the characteristic properties of the second phase particles used for incorporation are an essential prerequisite to achieve maximum particle incorporation. An essential advantage of preparing composite coatings by electroless codeposition compared to electro-codeposition is that the former allows accurate reproduction of the base geometry and eliminates the need for subsequent mechanical finishing.

### **1.5.2 Mechanism of electro- and electroless codeposition**

Various models were proposed to explain the mechanism of electro-codeposition:

#### ***(i) Model of Saifullin and Kahlilova (1970)***

This is an empirical model, based on the assumption that the particle concentration in the coating is the same as that in the bulk of the solution.

#### ***(ii) Model of Bazzard and Boden (1971)***

This model is based on the assumption that the particle size has an influence on codeposition, which depends on the frequency of collision of the particles with the cathode. Based on this approach, an empirical correlation was found between particle size, plating time and current density used for codeposition with weight percent incorporation of the particles in the matrix.

**(iii) Model of Guglielmi (1972)**

This was the first model which accounts for the electro-codeposition mechanism. The proposed mechanism is based on two consecutive adsorption steps (**Fig. 1.3**).

- (i) *The first step is postulated to be substantially physical in character and to produce a layer of loosely adsorbed particles with a rather high coverage.*
- (ii) *The second adsorption step is thought to be field-assisted and hence substantially electrochemical in character and results in strong adsorption of the particles on to the electrode. The strongly adsorbed particles are then progressively submerged by the growing metal.*

Several investigators have demonstrated the validity of Guglielmi's model for various systems, such as Ni-WC (Gupta et al., 1982), Cu- $\alpha$ -Al<sub>2</sub>O<sub>3</sub> and Cu- $\gamma$ -Al<sub>2</sub>O<sub>3</sub> (Celis and Roos, 1977), Cr-graphite (Narayan and Narayan, 1981) Ni-SiC (Guglielmi, 1972), Ni-TiO<sub>2</sub> (Guglielmi, 1972). However, the model did not take into account, the hydrodynamic situation prevalent in an electrolytic bath.

**(iv) Model of Kariapper and Foster (1974)**

This model is a modification of Guglielmi's model, where an attempt has been made to take into consideration the hydrodynamic factors of the bath. This model retains the assumptions of the Guglielmi's model. In addition, it assumes that both the volume fraction of the codeposited particles and current density are proportional to the stirring velocity, which shows maxima, and that

only those particles with an impact velocity below a certain critical value will be codeposited. However, the above relationship is dependent on the rate of metal deposition and rate of particle adsorption on to the cathode. When the rate of metal deposition exceeds the rate of particle adsorption, the volume fraction of particles in the deposit will further increase with current density.

(v) ***Model of Celis, Roos and Buelens (1987)***

Here, the proposed mechanism of electrolytic codeposition of inert particles with metals is based on two fundamental postulates:

- (i) *An adsorbed layer of ionic species is created around the inert particles at the time the particles are added to the plating solution or during the pretreatment of these particles in ionic solutions.*
- (ii) *The reduction of some of these adsorbed ionic species is required for the incorporation of particles in the metallic matrix.*

On its way from the bulk of the solution to the site of incorporation at the active cathode surface the inert particle has to proceed through five stages (**Fig. 1.4**):

- (i) *Adsorption of ionic species upon the particle surface;*
- (ii) *Movement of the particle by forced convection towards the hydrodynamic boundary layer at the cathode;*
- (iii) *Diffusion of the particle through the diffusion double layer;*
- (iv) *Adsorption of the particle, still with its adsorbed ionic cloud, at the cathode surface; and*
- (v) *Reduction of some adsorbed ionic species by which the particle becomes irreversibly incorporated in the metal matrix.*

This model was found to be valid for the electrolytic codeposition of Cu-Al<sub>2</sub>O<sub>3</sub> from acid sulphate bath and Au-Al<sub>2</sub>O<sub>3</sub> from cyanide bath (Celis et al., 1987).

**(vi) *EIPET Model (1987)***

The electrode-ion-particle-electron transfer (EIPET) was proposed by Valdes (1987), by taking into account the electrochemical nature of the particle metal codeposition. It is assumed that, the electrochemical reduction of the metal ions adsorbed on the particle surface, at the cathode, provides the essential surface binding interaction, which is responsible for codeposition. This model was found to be in agreement with codeposition of Al<sub>2</sub>O<sub>3</sub> from an acid copper sulphate bath (White and Foster, 1981).

**(vii) *The Trajectory Model (1992)***

This model is for electrolytic codeposition of spherical particles with metals on a rotating disc electrode based on a trajectory analysis of the particle codeposition, including convective mass transport, geometrical interception and migration under specific forces, coupled to a surface immobilization reaction. Theoretical predictions of this model were comparable with experimental results for the codeposition of spherical polystyrene particles with copper during electrolysis from an acid copper sulphate solution (Fransaer et al., 1992).

**(viii) *Hwang and Hwang model of Codeposition (1993)***

This model is developed on the similar basis as in the original Guglielmi's model. However, it was assumed that unlike in Guglielmi's model

where only metal ions are adsorbed on the particles, here both hydrogen ions ( $H^+$ ) and metal ions ( $M^{2+}$ ) are adsorbed on the particle surface. Therefore, the particle deposition rate is determined by the reduction of these adsorbed ions on the particles. At low applied current densities, the reduction of the adsorbed hydrogen ions are favoured and therefore the particle deposition rates are determined mainly by the reduction of  $H^+$  ions on the particle. At high current density, however, the reduction of both  $H^+$  as well as metal ions is important to the deposition rate of the particle.

**(ix) *Modified Guglielmi's model (1993)***

Guglielmi's model was derived based on the assumption that metal deposition is an activation controlled process, which is not always true. Hence, in the case of diffusion controlled metal deposition process, such as that taking place in cobalt metal deposition, a modified model has been suggested by Rajiv and Seshadri (1993). This modified model was found to be satisfactory for Co-TiO<sub>2</sub>, Co-PSZ and Co-Si<sub>3</sub>N<sub>4</sub> systems (Rajiv and Seshadri, 1993).

The electroless composite coating is formed by the impingement and settling of particles on the surface of the substrate, and subsequent envelopment of these particles by the matrix metal as it is deposited. There is no molecular bonding between particles and metal matrix (Hubbel, 1978a, 1978b). The mechanism of particle incorporation in electroless Ni-P matrix has received very little attention. Grosjean et al. (1998) have studied the incorporation of SiC in an electroless Ni-P matrix using Guglielmi's mathematical model (Guglielmi, 1972). They suggest that the experimental results are in agreement with the mechanism proposed by Guglielmi (1972).

### **1.5.3 Structure of composite coatings**

Hansen and Moller (1990), Balaraju (2000), Balaraju and Seshadri (1999) and Balaraju et al. (2006b) have studied the effect of incorporation of TiC, Si<sub>3</sub>N<sub>4</sub>, CeO<sub>2</sub> and TiO<sub>2</sub> particles and suggest that incorporation of these particles does not alter the structure of the electroless Ni-P matrix. However, incorporation of B<sub>4</sub>C particles is found to affect the orientation of nickel crystallites without influencing the crystallite dimensions; nickel tends to be less oriented in layers with B<sub>4</sub>C particles (Bozzini et al., 1999). Incorporation of SiC particles helps to increase nucleation centres, degree of crystallization, microstructural stability and prevents grain growth and aggregation of the matrix (Wu et al., 2000b). McCormack et al. (2003) have shown that addition of yttria particles to a Watt's nickel plating bath significantly changes the surface morphology and the preferred crystallographic orientation of the Ni-yttria composite coatings.

### **1.5.4 Hardness of composite coatings**

The hardness of electro- and electroless deposited composite coatings increases with the incorporation of hard particles whereas with soft particles, the hardness tends to decrease (Kedward and Kiernan, 1967; Greco and Baldauf, 1968; Gladman et al., 1971; Sinha et al., 1973; Pushpavanam et al., 1974; Pushpavanam and Sheno, 1977; Viswanathan and Ghouse, 1979; Ghouse et al., 1980; Joshi and Totlani, 1981; Lausmann, 1984; Ramesh et al., 1990, 1991; Balathandan and Seshadri, 1992a; Metzger and Florian, 1974; Hubbell, 1978a, 1978b; Brown, 1985; Apachitei et al. 1998a, 1998b; Hussain and Such, 1981; Balaraju, 2000; Xiang et al., 2001; Dennis et al., 1981;



Pushpavanam, 1992; Izzard and Dennis, 1987; Duncan, 1989; Balaraju and Seshadri 1998, 1999; Balaraju, 2000; Leon et al., 1999; Abdel Hamid and Abou Elkhair, 2002; Nishira and Takano, 1994; Moonir-Vaghefi et al., 1997a, 1997b; Wu et al., 2000a, 2000b; Chen et al., 2003a). The hardness of several ED Ni based composite coatings and EL Ni-P composite coatings are presented in **Tables 1.4 and 1.5**, respectively. The level of incorporation of particles, the alloying elements of the metal matrix and heat-treatment determines the hardness of these coatings. Annealing of ED nickel composite coatings in inert atmosphere or vacuum generally reduces the microhardness. However, the extent of reduction in hardness with annealing temperature for composites is much less when compared to pure nickel under similar circumstances.

When hard particles, like SiC, are incorporated in EL Ni-P matrix, an increase in hardness is noticed in all the deposits irrespective of their phosphorus content (2-13 wt % P) (Xinmin and Zonggang, 1992). However, the influence of phosphorous can be seen on annealing these coatings arising from the formation of large amounts of hard Ni<sub>3</sub>P phase when the phosphorus content of the coating is higher than 7 wt %.

The influence of heat treatment on the hardness of EL Ni-P-SiC and Ni-P-PTFE coatings in comparison with EL Ni-P coating is shown in **Fig. 1.5**. The change in hardness with heat treatment temperature exhibits a similar trend for these coatings, which suggests that the hardening mechanism upon annealing is the same for both EL Ni-P and Ni-P composite coatings. Increase in hardness up to 400°C is due to precipitation hardening because of the formation of the intermetallic Ni<sub>3</sub>P phase. The decrease in lattice defects and

coarsening of the  $\text{Ni}_3\text{P}$  particles cause a reduction in hardness when these coatings were annealed beyond  $400^\circ\text{C}$ .

### **1.5.5 Friction, wear and abrasion resistance of composite coatings**

Friction is the resistance to motion when bodies slide over one another (Bowden and Tabor, 1964; Halling, 1975, 1983). Modification of the surface to impart dry lubrication is best achieved with the use of coatings. The natural lubricity of phosphorus and boron enables electro- and electroless deposited Ni-P and Ni-B coatings to exhibit a good lubrication property. However, under unlubricated conditions prolonged testing results in galling or seizure failure of ED and EL Ni-P and Ni-B coatings (Gawrilov, 1979; Riedel, 1991). One of the options available to reduce such failures is the use of ED and EL Ni-P/Ni-B composite coatings.

ED and EL Ni-based composite coatings containing hard particles such as SiC generally exhibit poor lubrication property when compared with their plain matrix counterpart, regardless of the extent of particle incorporation, due to their high surface roughness and high mechanical interlocking force (Grosjean et al., 2001). In contrast, ED and EL composite coatings incorporated with soft particles like PTFE and graphite provide good lubrication when tested under unlubricated conditions due to their ability to prevent adhesion between the mating surfaces (Izzard and Dennis, 1987; Nishira et al., 1996; Yu and Zhang, 1994; Broszeit, 1982; Tulsi, 1983a, 1983b; Tulsi, 1985; Ebdon, 1987, 1988; Assoul et al., 1998; Ger et al., 2003). ED Ni-MoS<sub>2</sub> coatings containing 60 vol.% of MoS<sub>2</sub> particles exhibit a low friction coefficient of the order of 0.05 to 0.18. ED Ni-h-BN composite

coatings are found to be superior to Ni-MoS<sub>2</sub> and nickel-graphite composite coatings in offering a better lubrication property. However, at low temperatures, ED Ni-h-BN composite coating was found marginally inferior to ED Ni-PTFE composite coatings (Pushpavanam and Natarajan, 1995).

Tulsi (1983a, 1983b, 1985), Hadley and Harland (1987) and Ebdon (1987, 1988) have suggested that the low coefficient of friction of EL Ni-P-PTFE composite coatings is due to the transfer of PTFE to the counterface material (**Table 1.6**). Nishira and Takano (1994) suggest that these coatings have lower coefficient of friction compared to EL Ni-P coatings, in both as-plated and heat-treated (400°C, 1 hour) conditions and the coefficient of friction is an inverse function of PTFE content. These coatings possess excellent lubrication properties in the temperature range from cryogenic to 290°C. Izzard and Dennis (1987) observed that EL Ni-P-graphite (6 vol %) coatings fail to provide efficient lubrication when run against a steel counterface and the coefficient of friction is low when EL Ni-P-graphite composite coating is run against itself. Hexagonal boron nitride, molybdenum disulphide, inorganic fullerene-WS<sub>2</sub> and carbon nanotubes are the other particles capable of providing a low coefficient of friction when incorporated in the EL Ni-P matrix (Moonir-Vaghefi, 1997c; Leon et al., 1999; Chen et al., 2002b, 2003a, 2003b).

Wear is defined as 'damage to a solid surface, generally, involving the progressive loss of material, due to relative motion between that surface and a contacting substance or substances' (ASTM, 1993). Incorporation of second phase particles in a metal matrix could offer excellent wear resistance. The

developments made in automobile and aerospace industries in recent years, such as in advanced engines, require materials that can withstand increasingly high working temperatures and running speeds. The conditions in such applications warrant that the coating must be able to support the load without distortion, deformation or fracture during performance and must be able to maintain controlled friction and wear over long periods without seizure under the working conditions (Lancaster, 1983). ED and EL composite coatings will be a useful choice for such applications.

The wear resistance of ED and EL composite coatings is influenced by the type of particle incorporated in the deposit, the level of incorporation, the size and hardness of the particles as well as the hardness of the matrix. ED and EL Ni-based composite coatings incorporated with hard particles such as diamond (Zahavi and Hazan, 1983),  $\text{Cr}_3\text{C}_2$  (Zahavi and Kerbel, 1982), SiC (Sasame, 1974), TiC (Ramesh Bapu, 1994), etc. were reported to offer better wear resistance than their plain matrix counterpart. This is due to the fact that the hard particles present in the matrix take up the wear load exerted by the sliding counterface material after being exposed by the removal of the upper metal layer. However, to achieve the improvement in wear resistance, the wear load should not exceed the compression yield strength of the matrix material. Kedward (1972) have observed that metal-to-metal contact was inevitable due to the non-uniformity of the applied load over the wearing surface. Therefore, the wear resistance of composite coatings depends on both the nature of the second phase particles and the metal matrix. According to him, maximum wear resistance would be obtained only when hard particles are dispersed in a hard and wear resistant matrix. Increase in the level of incorporation of hard

particles in the metal matrix is reported to increase the wear resistance of ED and EL Ni-based composite coatings. There seems to be an optimum particle size for best wear resistance. A study showed that wear resistance was highest with 3 to 6 micron size natural or synthetic diamond particles (Zahavi and Hazan, 1983). Wear resistance decreases with the use of smaller or larger particles.

Heat treatment causes a significant change in the wear behaviour of the composite coatings. When ED Ni-Cr<sub>3</sub>C<sub>2</sub> composite coating was annealed at 400, 600, 800 and 1000°C for 30 minutes, it was found that the coating heat-treated at 400°C showed a reduced wear resistance whereas the wear resistance of those annealed at 600, 800 and 1000°C was similar to that of un-annealed deposits (Zahavi and Kerbel, 1982). Heat treatment of ED Ni-SiC composite coating causes a further improvement in the wear resistance of the coatings in spite of the decrease in hardness due to the formation of Ni<sub>5</sub>Si<sub>2</sub> phase (Ghouse et al., 1980). The wear resistance of heat treated ED-Ni, ED Ni-SiC and ED Ni-P-SiC coatings exhibit a peak at 400°C (Chaggeng et al., 1988). The precipitation hardening effect of heat treatment at 400°C resulted in minimum wear for the ED Ni-P-SiC coatings. The precipitated Ni<sub>3</sub>P phase increased resistance to plastic deformation during wear testing (Chaggeng et al., 1988).

Metzger and Florian (1976), Brown (1985), Parker (1974) and Feldstein et al. (1983) have reviewed the wear resistance of electroless nickel composite coatings with various ceramic (hard) particles (**Table 1.7**). Gould (1988) has reviewed the suitability of these coatings to combat adhesive and abrasive wear. Adhesive and abrasive wear are the most frequently encountered wear

mechanisms in EL Ni-P coatings. Straffelini et al. (1999) suggest that wear of EL Ni-P composite coatings occurs in two stages. During stage I, the deposits undergo a mild abrasive wear whereas during stage II the wear is severe and characterized by the brittle detachment of debris. Stage I represent the initial wear damage and reflect the surface durability.

Wear resistance of EL Ni-P-SiC composite coatings has been studied by several authors (Brozeit, 1982; Xinmin and Zonggang, 1992,1993; Subramanian and Pallotta, 1996; Li, 1997; Wu et al., 2000a, 2000b; Sale, 1979; Apachitei et al., 2001, 2002; Chen et al., 2002a; Zonggang and Xinmin, 1987). Increase in wear resistance with increase in SiC incorporation level is reported by Sale (1979). Wu et al. (2000b) suggest that the dispersion strengthening effect of SiC particles and the strengthening effect of the Ni-P alloy matrix enables such coatings to provide better wear resistance. Zonggang and Xinmin (1987, Xinmin and Zonggang, 1992,1993) argue that the Ni-P matrix should posses high phosphorus content ( $>7$  wt %) in order to be capable of supporting the SiC particle to offer superior wear resistance, both in as plated and heat-treated conditions. The effect of heat treatment on the wear resistance of EL Ni-P-SiC composite coatings reveals that wear resistance increases with increase in heat-treatment temperature up to  $350^{\circ}\text{C}$ . Further increase in temperature (up to  $600^{\circ}\text{C}$ ) results in increase in the wear rate with further deterioration at higher temperatures ( $\sim 800^{\circ}\text{C}$ ). The possibility of reaction between nickel and SiC around  $580^{\circ}\text{C}$  and a partial melting of Ni-P eutectic at  $880^{\circ}\text{C}$  are responsible for the poor wear characteristics at high temperatures (Broszeit, 1982). The formation of nickel silicide ( $\text{Ni}_3\text{Si}$ ) is governed by the diffusion of nickel atoms into the SiC lattice and it occurs at the SiC/Ni-P

matrix interface upon heat-treatment at 500°C for 1 hour. The  $\text{Ni}_3\text{Si}$  formation increases the adhesion between the reinforcement and the matrix and decreases the abrasive wear behaviour (Apachitei et al., 2001, 2002). Chen et al. (2002a) have identified the formation of  $\gamma\text{-Ni}_5\text{Si}_2$  and  $\beta_1\text{-Ni}_3\text{Si}$  phases up on annealing above 450°C. However, further annealing at 500°C leads to the incorporation of phosphorous into the  $\text{Ni}_5\text{Si}_2$  lattice and results in the formation of  $\text{Ni}_5(\text{Si}_{1-x}\text{P}_x)_2$  solid solution.

The incorporation of  $\text{Cr}_3\text{C}_2$  particles (27 vol. %) in the Ni-P matrix is found to increase the wear resistance when evaluated by pin-on-disc and simulated hot forging tests (Dennis et al., 1981). Heat-treatment at 400°C for 1 hour further enhances the wear resistance of these coatings. Leon et al. (1999) suggest that even in as-plated condition, electroless Ni-P-h-BN composite coating is capable of providing higher wear resistance than plain electroless Ni-P coating heat-treated at 400°C for 1 hour. Wear decreased by nearly two orders of magnitude when the Ni-P matrix is incorporated with 33 vol.% hexagonal BN particles (Leon et al., 1998, 1999). Increase in wear temperature decreases the wear resistance. At high temperatures of the order of 400°C, a mixed adhesive and fatigue wear mechanism, accompanied by a large plastic deformation of coatings and high coating transfer to the counterface material was observed (Leon et al., 2003). This indicates that the tribological response of composite coatings at high temperatures is related to the mechanical properties of the Ni-P matrix, that is, to its behaviour to withstand the applied stresses as the temperature increases, irrespective of the nature and properties of the codeposited particles. Incorporation of inorganic fullurene- $\text{WS}_2$  nanoparticles in the EL Ni-P matrix increases the wear resistance under

oil lubricated conditions and in this respect these coatings are better than Ni-P, Ni-P-2H-WS<sub>2</sub> and Ni-P-graphite coatings. The improvement in wear resistance following the incorporation of inorganic fullurene-WS<sub>2</sub> nanoparticles is due to its ability to serve as spacers between the asperities of two mating metal surfaces (Chen et al., 2002b). Carbon nanotubes, when incorporated in an electroless Ni-P matrix (12 vol %), increases the wear resistance both in as-plated and heat-treated conditions (Chen et al., 2002c, 2003a, 2003b). The wear resistance offered by these coatings is better than that of EL Ni-P-SiC and Ni-P-graphite coatings.

Graham and Gibbs (1975) investigated the difference in wear behaviour of EL Ni-P composite coatings having natural and shock synthesized diamond particles by examining the yarnline wear groove with the help of SEM. Synthetic diamond particles appear to give a superior wear resistance. This has been ascribed to the much stronger bonding between the EL Ni-P matrix and the rough and irregularly shaped synthetic diamond particles. In contrast, natural diamond particles, which are relatively smooth, are incorporated only to a lesser extent and such coatings wear to a greater extent, under identical testing conditions. Reddy et al. (2000) studied the wear resistance of EL Ni-P composite coatings incorporated with diamond particles of different size ranges (3-40 microns). Coatings incorporating finer diamond particles (3-6 microns and 6-12 microns) are more wear resistant compared to those with coarse diamond particles (20-40 microns). This effect is largely a function of the degree of incorporation of diamond particles for a given coating thickness, which is higher for finer diamond particles. For achieving higher wear resistance, the integrity between particle and the EL Ni-P matrix should be



better, which is decided by the ratio of the coating thickness to the size of the particles.

Incorporation of ceramic (hard) particles might also have a deleterious effect. Hard particles, such as, tungsten carbide and diamond cause pronounced abrasion of the counterface materials (Parker 1974). Similarly, higher levels of  $B_4C$  particles incorporated in the Ni-P matrix is reported to increase the wear rate, due to the protrusion of the  $B_4C$  particles, which increases the supporting points and causes increased wearability (Ge et al., 1998). The results of the Falex test performed on electroless Ni-P and Ni-P- $Si_3N_4$  composite coatings suggest that these coatings are safer to use only under lubricated condition (Balaraju, 2000).

### **1.5.6 Corrosion resistance of composite coatings**

Literature reports on ED and EL composite coatings unanimously agree that the incorporation of hard particles increases the hardness and wear resistance whereas soft particles reduce the hardness and offer better frictional properties. However, the corrosion resistance of ED and EL composite coatings has been a debatable issue. A survey of the corrosion resistance of electro- and electroless deposited Ni-based composite coatings is compiled in **Table 1.8**. Incorporation of  $Al_2O_3$ , SiC,  $Si_3N_4$ , BN,  $TiO_2$ , polyethylene, carbon nanotubes (CNT), etc. and metal particles such as Nb, etc. in ED Ni matrix (Ahmed et al., 1967; Ramesh et al., 1991; Ramesh Bapu, 1995; Medeliene, 2002; Abdel Hamid and Ghayad, 2002; Fratari and Robin, 2006; Li et al., 2005; Chen et al., 2005), ultrafine diamond in ED Ni-P matrix (Shi et al., 2004), WC and TiCN in ED Cr matrix (Abdel Hamid et al., 2005; Surviliene et al., 2004), nano-SiC

particles in ED Ni-Co matrix (Shi et al. 2006),  $\text{ZrO}_2$  particles in ED Cu matrix (Benea et al., 2000),  $\alpha\text{-Al}_2\text{O}_3$  particles in ED Fe matrix (Revenko et al., 2003), SiC,  $\text{Si}_3\text{N}_4$ ,  $\text{CeO}_2$ ,  $\text{TiO}_2$ ,  $\text{Al}_2\text{O}_3$ , CNT, nano-diamond, PTFE, polyacrylamide (PAM) particles in EL Ni-P matrix (Balaraju and Seshadri, 1998; Shoeib et al., 1998; Zhang et al., 1998; Mitoseriu and Mitoseriu, 2002; Balaraju et al., 2001, 2003, 2006a; Yang et al., 2004a, 2004b, 2005; John et al., 2005; Xu et al., 2005; Srinivasan and John 2005) was reported to increase the corrosion resistance of the corresponding metal matrix. Several reasons were suggested for the observed increase in corrosion resistance, which include decrease in porosity, change in coating microstructure from columnar to non-columnar structure, microstructural features causing smaller pores, favourable chemical stability due to reduction in defect size that also prevents the growth of corrosion pits and accelerates the passivation process, retardation of oxygen reduction reaction by the particles embedded in the matrix, screening of the matrix by the dispersed particles, prevention of preferential corrosion of grain boundaries and triple junctions by the dispersion of nano-sized particles in the matrix.

In contrast, Medeliene (2002) have reported that conducting nature of the  $\text{B}_4\text{C}$  particles increases the surface activity of the ED Ni- $\text{B}_4\text{C}$  composite coating and decreases the stability of the matrix. Erler et al. (2003) have reported that  $\text{Al}_2\text{O}_3$  and  $\text{TiO}_2$  particles incorporated in ED Ni matrix enables an accelerated diffusion of chloride ions along the interface between the Ni and the incorporated particles, thus causing a deterioration in corrosion resistance. Surender et al. (2004a) have reported that incorporation of WC in ED Ni matrix decreased the stability of the passive film, which is evident from the positive

shift in the passivation potential, reduction in the passivation range and higher passive current density. Starosta and Zielinski (2004) have reported that incorporation of  $\text{Al}_2\text{O}_3$  particles in ED Ni and Ni-19%Fe matrix decreases the corrosion resistance. The reasons suggested for the observed decrease in corrosion resistance are increase in surface roughness, increase in porosity, inhomogeneity of the coatings and formation of electrochemical cells. They have also observed that increase in level of incorporation of  $\text{Al}_2\text{O}_3$  particles decreases the corrosion resistance further (Starosta and Zielinski, 2004). The corrosion resistance of ED Ni-colloidal silica composite coating was also found to decrease with increasing percentage of colloidal silica in the ED Ni matrix, in both 3.5 % NaCl and 1 N sulphuric acid (Ramkrishna, 1990). Similarly, incorporation of SiC,  $\text{Al}_2\text{O}_3$ , PTFE (at higher levels of incorporation/high bath loading), polyvinyl chloride (PVC), europium doped yttrium vanadate in EL Ni-P matrix was found to decrease the corrosion resistance (Shoeib et al., 1998; Das et al., 2002; Huang et al., 2004; Huang et al., 2004; Zhao and Liu, 2005a; Wu et al., 2005a, 2005b; Balaraju et al. 2006a).

In some cases, incorporation of particles such as PTFE did not significantly improve the corrosion resistance of a metal matrix like nickel (Ebdon, 1988). Similarly, incorporation of SiC, PTFE, polyvinyl alcohol (PVA) does not exhibit much change in corrosion resistance or a slight decrease in corrosion resistance (Huang et al., 2004; Shoeib et al., 1998).

It is interesting to note that incorporation of WC in ED Cr matrix causes a marked increase in corrosion resistance whereas incorporation of the same particle in ED Ni matrix decreases the stability of passive film (Abdel Hamid

et al., 2005; Surender et al., 2004a). Similarly, incorporation of CNT in ED Ni matrix was reported to increase the corrosion resistance (Chen et al., 2005) whereas incorporation of CNT in ED Ni-P matrix was reported to decrease the corrosion resistance (Shi et al. 2005). Also, it is interesting to note that in case of ED Ni-Si<sub>3</sub>N<sub>4</sub> composite coatings increase in level of incorporation increases the corrosion resistance (Ramesh et al., 1991) whereas a decrease in corrosion resistance was observed by Starosta and Zielinski (2004) with an increase in the level of incorporation of Al<sub>2</sub>O<sub>3</sub> particles in ED Ni and Ni-19% Fe matrix. Similarly, increase in the level of incorporation of CNT from 1 to 5 wt.% decreases the corrosion resistance of EL Ni-P-CNT composite coatings (Yang et al., 2005). Starosta and Zielinski (2004) have reported that in case of ED Ni-41% Fe matrix increase in the level of incorporation of Al<sub>2</sub>O<sub>3</sub> particles decreases the corrosion resistance. Similarly, ED Ni-Si composite coating is reported to have a higher passive current density compared to ED Ni, in spite of the fact the Si particles are electrically neutral and more uniformly distributed in the ED Ni matrix.

The corrosion resistance of electro- and electroless composite coatings is influenced by a variety of factors such as method of deposition, nature of metal matrix, level of incorporation of particles, distribution of particles in the metal matrix, the particle characteristics, such as size and conductivity, ability of the particles to get impregnated in the pores, roughness and heterogeneity of the coating, porosity of the coating, nature of corrosive medium, method of testing, etc. There are some agreeable and a few conflicting issues existing among the researchers regarding the corrosion resistance of electro- and electroless composite coatings. The improvement or impairment of corrosion

resistance of ED and EL composite coatings depends on the chemical stability of the particle, structural state or microstructural feature of the coating, porosity or defect size of the coating, ability to prevent diffusion of chloride ions along the interface between the metal and the particle, the ability of the particle to prevent the corrosive pits from growing up, etc. Ebdon (1988) and Henry (1990) have recommended a duplex coating, consisting of an initial electroless Ni-P coating followed by an electroless Ni-P composite coating for applications requiring good corrosion resistance. Rossi et al. (2003) have also ascertained the importance of such a duplex layer. They have suggested that the inner EL Ni-P layer (without PTFE particles) could provide a better corrosion protection by barrier-effect and improve the coating-substrate adhesion.

### **1.5.7 Applications of composite coatings**

The applications of ED and EL Ni-based composite coatings can be broadly classified into three categories, providing (a) wear resistance; (b) a surface with a desired friction coefficient; and (c) a hard surface for machining and finishing tools (Metzger and Florian, 1976; Hubbel, 1978; Tulsi, 1983; Lukschandel, 1978; Teranishi, 2000). **Table 1.9** gives the applications of ED and EL Ni-based composite coatings in various industries.

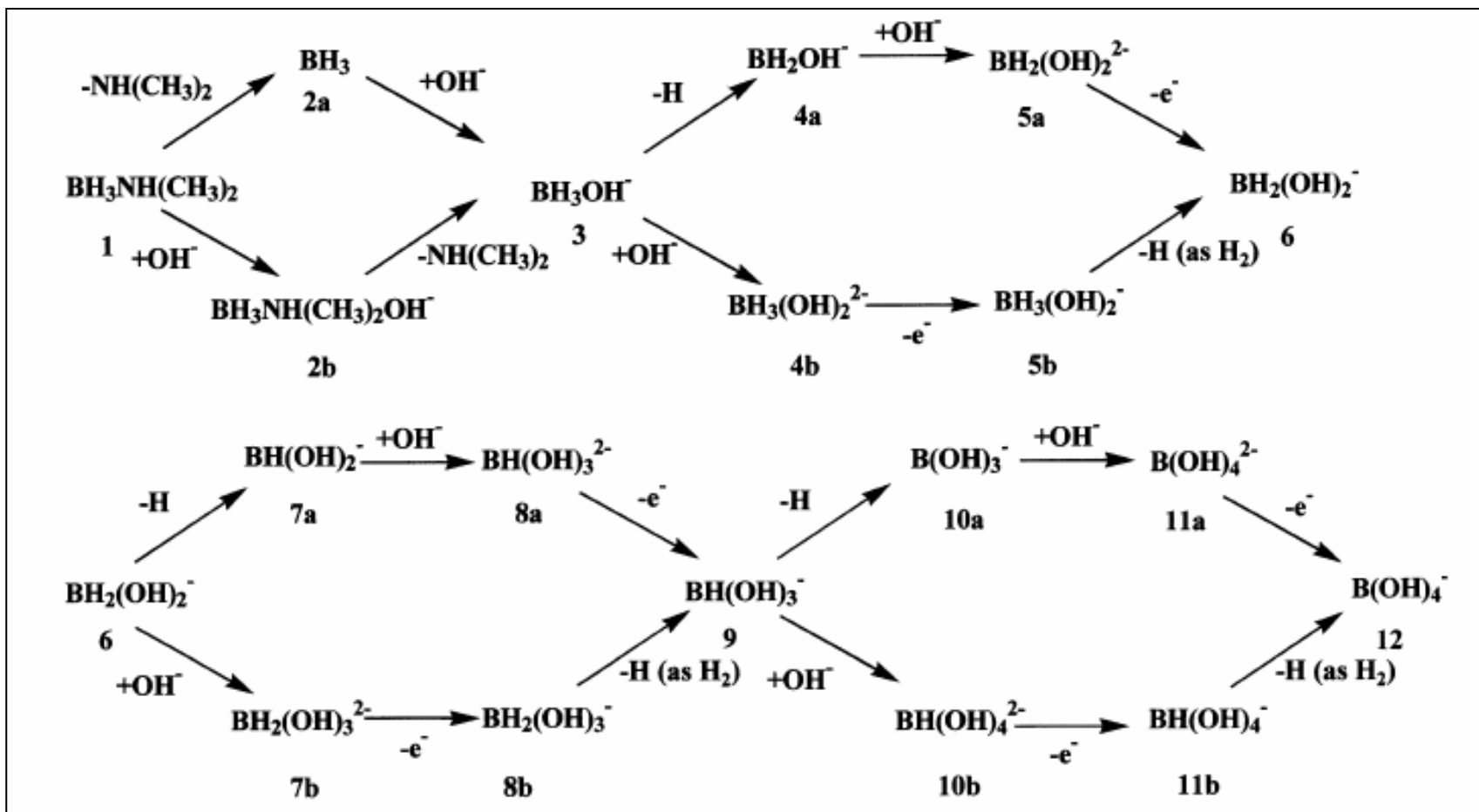


Fig. 1.1 Reaction pathways for the oxidation process of dimethylamine borane (DMAB) via three-coordinate intermediates (2a, 4a, 5a, 7a, 8a, 10a and 11a) and five-coordinate intermediates (2b, 4b, 5b, 7b, 8b, 10b and 11b) (adapted from Homma et al. 2003)

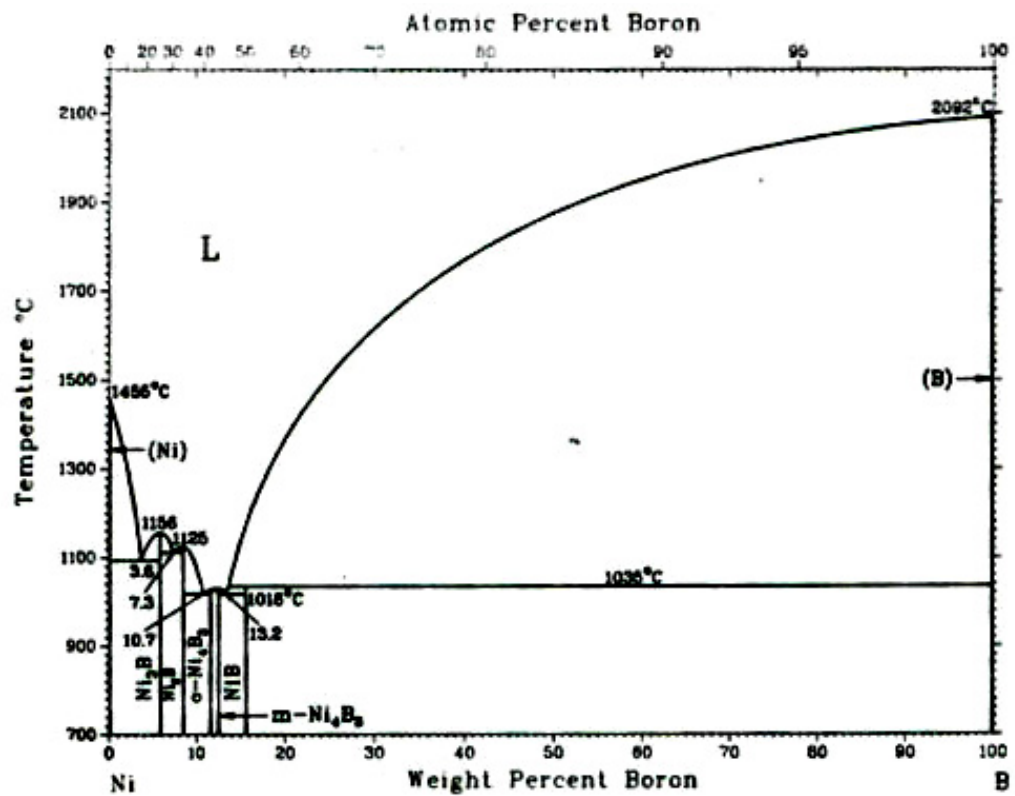
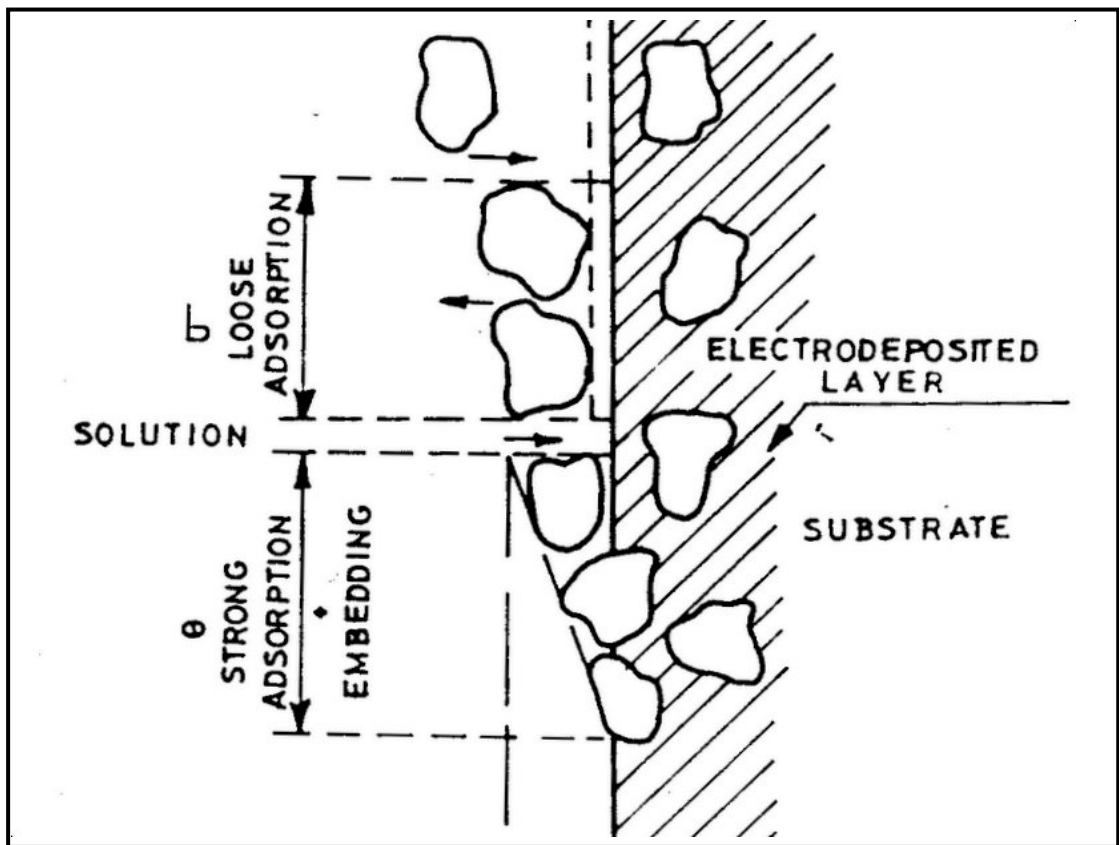


Fig. 1.2 Binary alloy phase diagram of Ni-B system  
(Adapted from ASM Metals Handbook Vol. 3, 1991)



**Fig. 1.3 Pictorial representation of the two stage model proposed to explain the incorporation of second phase particles in electrodeposited metal matrix**



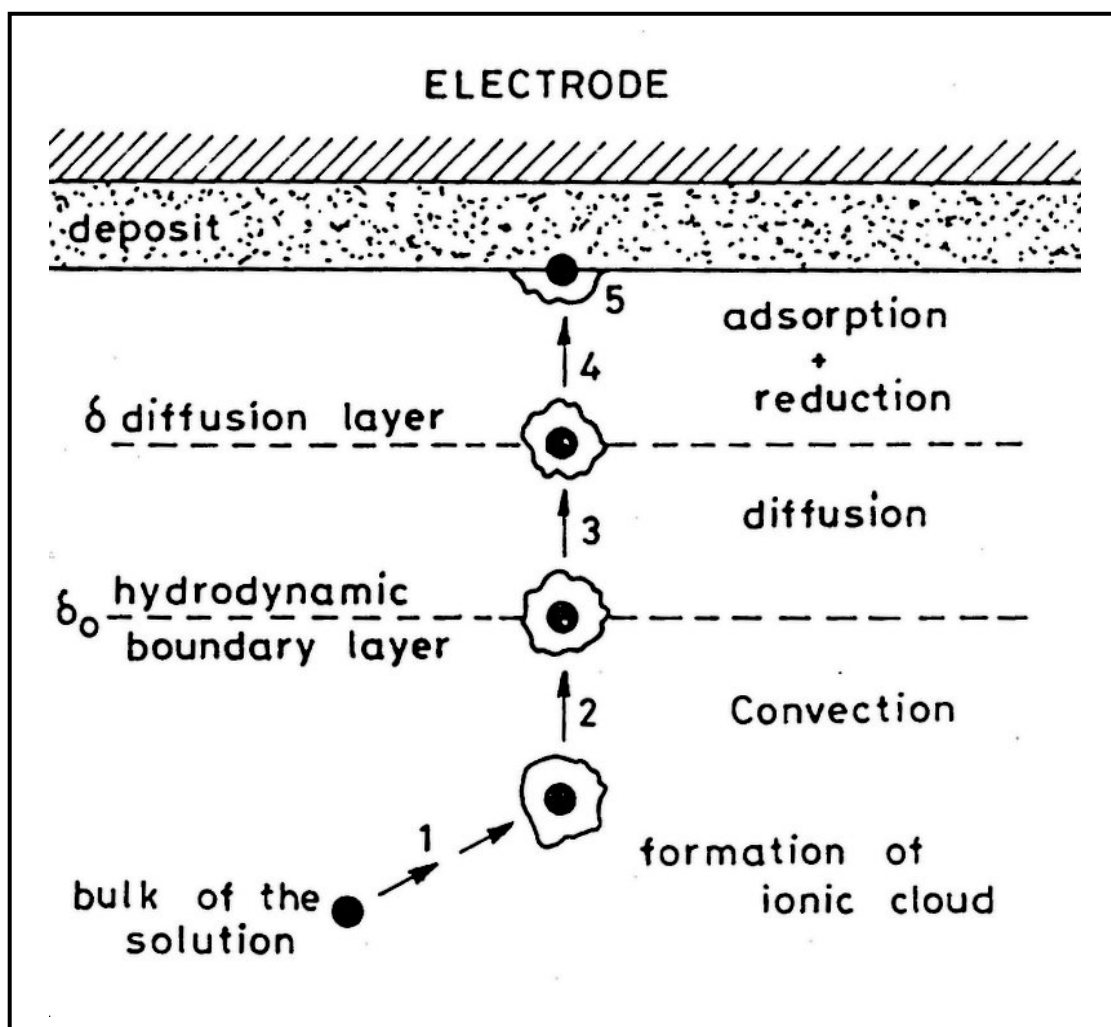
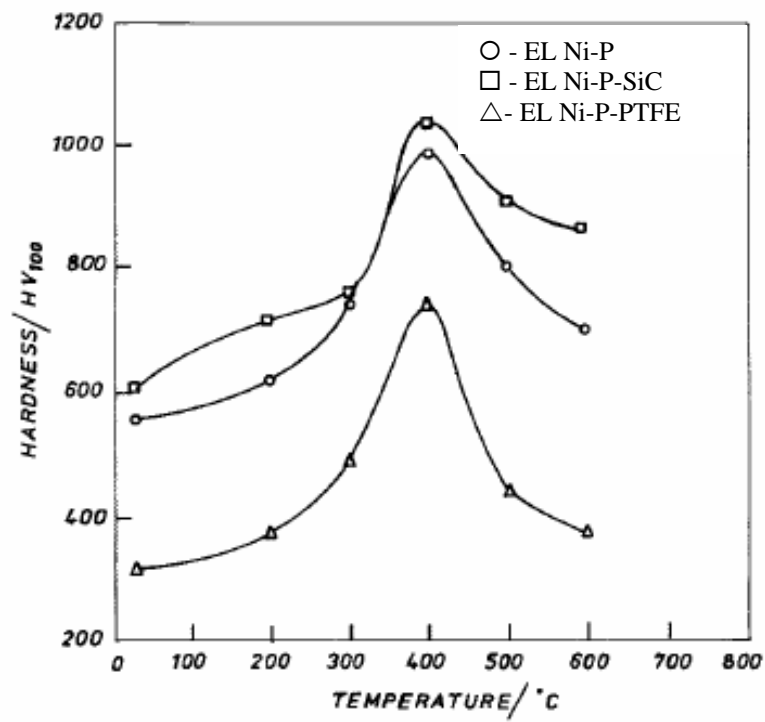


Fig. 1.4 Pictorial representation of the five stage model proposed to explain the incorporation of second phase particles in electrodeposited metal matrix



**Fig. 1.5 Comparison of change in hardness with heat treatment temperature for electroless Ni-P, Ni-P-SiC and Ni-P-PTFE (Data adapted from Nishira and Takano (1994) and Li (1997))**

**Table 1.1: Various constituents of the electrolyte solutions used for electrodeposition of metals**

<b>Constituent</b>	<b>Functions</b>
Metal salt	To supply metal ions
Complexant	Stabilize metal in soluble form; Influence the mode of ion discharge
Complexant stabilizer	Excess complexant, acid or alkaline reagent
Buffer salt	Stabilize pH at optimum value
Anode depassivator	Smooth anode dissolution and oxide film disruption
Addition agents	Surfactant for hydrogen bubble dispersal Brightener for bright deposits Levelling agent for grain refinement Stress reliever

**Table 1.2: The various components of electroless plating bath and their functions (Riedel, 1991)**

<b>Component</b>	<b>Function</b>
Nickel Ion	Source of Metal
Hypophosphite/Borohydride/DMAB	Reducing agent
Complexants	Stabilizes the solution
Accelerators	Activate reducing agent
Buffers	Controlling pH (longer term)
pH regulators	Regulates the pH of the solution
Stabilizer	Prevents solution breakdown
Wetting agents	Increases wettability of surfaces

**Table 1.3: Application of electroless Ni-P coatings (adapted from Agarwala and Agarwala, 2003)**

Application avenue	Components	Coating thickness ( $\mu\text{m}$ )
Automotive	Heat sinks, carburettor components, fuel injection, ball studs, differential pinion ball shafts, disk brake pistons and pad holders, transmission thrust washers, synchromesh gears, knuckle pins, exhaust manifolds and pipes, mufflers, shock absorbers, lock components, hose couplings, gear and gear assemblies. Fuel pump motors, aluminium wheels, water pump components, steering column wheel components, air bag hardware, air conditioning compressor components, decorative plastics and slip yokes	2–38
Air craft/ aerospace	Bearing journals, servo valves, compressor blades, hot zone hardware, pistons heads, engine main shafts and propellers, hydraulic actuator splines, seal snaps and spacers, landing gear components, pilot tables, gyro parts, engine mounts, oil nozzle components, turbine front bearing cases, engine mount insulator housing, flanges, sun gears, breech caps, shear bolts, engine oil feed tubes, flexible bearing supports, break attach bolts, antirotational plates, wing flap universal joints and titanium thruster tracks	10–50
Chemical & petroleum	Pressure vessels, reactors, mixer shafts, pumps and impellers, heat exchangers, filters and components, turbine blades and rotor assemblies, compressor blades and impellers, spray nozzles, valves: ball, gate, plug, check and butterfly, stainless steel valves, chokes and control valves, oil field tools, oil well packers and equipment, oil well turbine and pumps, drilling mud pumps, hydraulic systems actuators and blowout preventors	25–125
Electrical	Motor shafts, rotor blades of stator rings	12–25
Electronics	Head sinks, computer drive mechanisms, chassis memory drums and discs, terminals of lead wires, connectors, diode and transistor cans, interlocks, junction fittings and PCB	2–25
Food	Pneumatic canning machinery, baking pans, moulds, grills and freezers, mixing louts, bun warmers and feed screw and extruders	12–25
Marine	Marine hardware, pumps and equipment	25–50
Material handling	Hydraulic cylinders and shafts, extruders, link drive belts, gears and clutches	12–75
Medical & pharmaceutical	Disposable surgical instruments and equipment, sizing screens, pill sorters and feed screws and extruders	12–25
Military	Fuse assemblies, tank tarred bearings, radar wave guides, mirrors, motors, detonators and firearms	8–75
Mining	Hydraulic systems, jetting pump heads, mine engine components, piping connections, framing hardware	30–60
Moulds & dies	Zinc dies, cast dies, glass moulds and plastic injection moulds of plastic extrusion dies	15–50
Printing	Printing rolls and press beds	~ 38
Rail road	Tank cars, diesel engine shafts and car hardware	20–90
Textiles	Feeds and guides, fabric knives, spinnerets, loom ratchets and knitting needles	12–50
Wood & paper	Knife holder corer plates, abrading plates and machine parts.	~ 30
Miscellaneous	Chain saw engine	~ 25
	Drills and taps	~ 12
	Precision tools	~ 12
	Shower blades and heads	~ 8
	Pen tips	~ 5

**Table 1.4 Hardness of electrodeposited Ni-based composite coatings**

Type of particle	Particle Size (microns)	Level of incorporation (wt.%)	Hardness (kg/mm <sup>2</sup> )	Reference
Al <sub>2</sub> O <sub>3</sub>	0.01-0.05	24.0	230-270	Greco and Baldauf (1968)
Al <sub>2</sub> O <sub>3</sub>	1-2	50	562	Kedward and Kiernan (1967)
Cr <sub>3</sub> C <sub>2</sub>	2-3	40.0	420	Kedward and Kiernan (1967)
Cr <sub>2</sub> O <sub>3</sub>	1.0	30.0	533	Kedward and Kiernan (1967)
SiC	3-5	40	515	Kedward and Kiernan (1967)
Si <sub>3</sub> N <sub>4</sub>	1.0	8.2	489-496	Ramesh et al (1990)
CeO <sub>2</sub>	1-5	10.3	425-445	Balathandan and Seshadri (1992a)
TaC	3.5	40.0	518	Kedward and Kiernan (1967)
TiC	3.4	40.0	504	Kedward and Kiernan (1967)
TiO <sub>2</sub>	0.2	10.0	300-420	Greco and Baldauf (1968)
WC	2-3	40.0	515	Kedward and Kiernan (1967)
ZrC	3-5	40.0	533	Kedward and Kiernan (1967)

**Table 1.5 Hardness of electroless Ni-P composite coatings**

Type of electroless Ni-P coating	Phosphorus content of the coating (wt.%)	Particle content in the Ni-P matrix	Hardness (HV <sub>0.1</sub> )		Reference
			As plated	Heat-treated*	
Ni-P	8.00-9.10	-	410-600	979-1136	Apachitei et al. (1998a, 1998b); Xiang et al. (2001); Dennis et al. (1981)
Ni-P-nano diamond	7.60	0.52 wt.%	470	939	Xiang et al. (2001)
Ni-P-nano diamond	6.27	2.21 wt.%	755	966	Xiang et al. (2001)
Ni-P-SiC (irregular)	8.22	19.60 vol.%	705	1143	Apachitei et al. (1998a, 1998b)
Ni-P-Al <sub>2</sub> O <sub>3</sub> (irregular)	8.22	9.70 vol.%	643	1139	Apachitei et al. (1998a, 1998b)
Ni-P-Al <sub>2</sub> O <sub>3</sub> (spherical)	8.22	28.60 vol.%	743	1248	Apachitei et al. (1998a, 1998b)
Ni-P-Al <sub>2</sub> O <sub>3</sub> (fibres)	8.22	10.70 vol.%	640	1147	Apachitei et al. (1998a, 1998b)
Ni-P-Cr <sub>2</sub> C <sub>3</sub>	7.20	27.00 vol.%	645	1195 <sup>a</sup>	Dennis et al. (1981)
Ni-P-PTFE	9.5-10.0	25.00 vol.%	275 <sup>b</sup>	450 <sup>b, c</sup>	Duncan (1989)
Ni-P-hexagonal BN	5.5	33.00 vol.%	486 <sup>d</sup>	753	Leon et al. (1999)
Ni-P-Si <sub>3</sub> N <sub>4</sub>	10.10	8.01 wt.%	720	1171	Balaraju (2000); Balaraju and Seshadri (1998)
Ni-P-CeO <sub>2</sub>	10.18	7.44 wt.%	676	1136	Balaraju (2000)
Ni-P-TiO <sub>2</sub>	10.40	5.42 wt.%	642	1104	Balaraju (2000)
Ni-P-CNT	> 7.00	12.0 vol.%	520	1035	Chen et al. (2003)

\*Heat-treated at 400°C/1 hour unless otherwise indicated; (a) 500°C/12 hours; (b) load 50 g; (c) 350°C/2 hour; (d) Knoop hardness.

**Table 1.6 Friction coefficient of electroless Ni-P-PTFE composite coating measured by pin and ring machine  
(Data adapted from Tulsi, 1983a, 1983b)**

Coating on pin	Coating on ring	Coefficient of friction
Electroless Ni-P	Cr steel	0.6 - 0.7
Electroless Ni-P-PTFE	Cr steel	0.2 - 0.3
Electroless Ni-P-PTFE	Electroless Ni-P-PTFE	0.1 - 0.2
Electroless Ni-P-PTFE*	Cr steel	0.2 - 0.5
Electroless Ni-P-PTFE <sup>*</sup>	Electroless Ni-P-PTFE	0.1 - 0.7

\* - Heated at 400°C for 4 hours.



**Table 1.7 Abrasive wear of electroless Ni-P composite coatings**  
**(Data adapted from Parker, 1974)**

Type of coating	Taber wear index <sup>a</sup>	
	As plated	Heat Treated <sup>b</sup>
EL Ni-P	18	8
EL Ni-P-Cr <sub>3</sub> C <sub>2</sub>	8	2
EL Ni-P-Al <sub>2</sub> O <sub>3</sub>	10	5
EL Ni-P-TiC	3	5
EL Ni-P-SiC	3	2
EL Ni-P-B <sub>4</sub> C	2	1
EL Ni-P-Diamond	2	2
Hard chromium	3	-
Aluminium hard coat	2	-

a - Weight loss in mg/1000 cycles (average of 5000 cycles) with CS 10 wheels and a 1000 g load.

b - Heated 10 to 16 hr at 290°C.

**Table 1.8 Survey of the corrosion resistance of electro- and electroless deposited Ni-based composite coatings**

<b>Corrosion resistance of ED and EL composite coatings compared to their plain counterparts</b>	<b>Types of coating</b>	<b>Reference</b>
Increase in corrosion resistance	EL Ni-P-SiC	Mitoseriu and Mitoseriu (2002)
	EL Ni-P-Si <sub>3</sub> N <sub>4</sub>	Balaraju and Seshadri (1998); Balaraju et al. (2001, 2003)
	EL Ni-P-TiO <sub>2</sub>	Balaraju et al. (2001, 2003) John et al. (2005)
	EL Ni-P-CeO <sub>2</sub>	Balaraju et al (2001, 2003)
	EL Ni-P-Al <sub>2</sub> O <sub>3</sub>	Balaraju et al. (2006a)
	EL Ni-P-CNT	Yang et al. (2004, 2005)
	EL Ni-P-nano diamond	Xu et al. (2005)
	EL Ni-P-PTFE	Zhang et al. (1998) Srinivasan and John (2005)
	EL Ni-P-Polyacrylamide	Shoeib et al. (1998)
	EL Ni-P/Ni-P-PTFE (Duplex)	Rossi et al. (2003)
	EL Ni-Cu-P-PTFE (graded)	Zhao and Liu (2004, 2005)
	EL Ni-P-PTFE-SiC	Huang et al. (2005)
	ED Ni-Nb	Fratari and Robin (2006)
	ED Ni-Cr and ED Ni-Si	Desyatkova et al. (2002)
	ED Ni-B	Szeptycka (2002)
	ED Ni-Diamond	Yagodkina et al. (1997) Szeptycka (2002)

**Table 1.8 (Contd...)**

ED Ni-Si <sub>3</sub> N <sub>4</sub>	Szeptycka (2002)
ED Ni-CeO <sub>2</sub>	Aruna et al. (2006)
ED Ni-TiO <sub>2</sub>	Li et al. (2005)
ED Ni-Al <sub>2</sub> O <sub>3</sub>	Medeliene et al. (2001) Szczygiel and Kołodziej (2005a, 2005b)
ED-Ni-SiC	Medeliene (2002); Szeptycka (2002) Garcia et al. (2003); Lekka et al. (2005)
ED Ni-CNT	Chen et al. (2005)
ED Ni-PTFE	Shoeib (2002); Szeptycka (2002)
ED Ni-B <sub>4</sub> C	Szeptycka (2002)
ED Ni-SiO <sub>2</sub>	Yar-Mukhamedova, (2000) Szeptycka (2002)
ED Ni-Polyethylene	Abdel Hamid and Ghayad (2002)
ED Ni-SiC-fluoropolymer	Szeptycka and Gajewska (2005)
ED Ni-liquid microcapsule with lubricant oil	Szeptycka (2002) Zhu et al. (2004)
ED Ni-P-Ultrafine Dimond	Shi et al. (2004)
ED Ni-W-P-SiC	Guo et al. (2001)
ED Ni-P-B <sub>4</sub> C	Bozzini et al. (2001b)
ED Ni-P-SiC	Malfatti et al. (2005)
ED Ni-W-B-ZrO <sub>2</sub>	Yang et al. (2004)
ED Ni-41%Fe-Al <sub>2</sub> O <sub>3</sub>	Starosta and Zielinski (2004)
ED Ni-Co-SiC	Shi et al. (2006)
ED Ni-RE-W-P-SiC	Guo et al. (2001)
ED Ni-RE-W-B-SiC	Guo et al. (2003)

**Table 1.8 (Contd...)**

Not much change in corrosion resistance/slight decrease in corrosion resistance	EL Ni-P-SiC	Huang et al. (2004)
	EL Ni-P-PTFE	Huang et al. (2004)
	EL Ni-P-Polyvinyl alcohol	Shoeib et al. (1998)
	ED Ni-SiC and ED Ni-B <sub>4</sub> C	Medeline et al. (2002)
Decrease in corrosion resistance	EL Ni-P-SiC	Huang et al. (2004)
	EL Ni-P-Al <sub>2</sub> O <sub>3</sub>	Balaraju et al. (2006)
	EL Ni-P-PTFE (at higher levels of incorporation/high bath loading)	Huang et al. (2004) Zhao and Liu (2005) Wu et al. (2005a, 2005b)
	EL Ni-Cu-P-PTFE	Zhao and Liu (2005a)
	EL Ni-P-SiC-PTFE	Huang et al. (2004)
	EL Ni-P-Polyvinyl chloride	Shoeib et al. (1998)
	EL Ni-P-Europium doped yttrium vanadate)	Das et al. (2002)
	ED Ni-WC	Surender et al. (2004)
	ED Ni-Al <sub>2</sub> O <sub>3</sub> and ED Ni-TiO <sub>2</sub>	Erler et al. (2003)
	ED Ni-B <sub>4</sub> C	Medeliene (2002)
	ED Ni-19%Fe-Al <sub>2</sub> O <sub>3</sub> and ED Ni-29%Fe-Al <sub>2</sub> O <sub>3</sub>	Starosta and Zielinski (2004)
	ED Ni-Si	Desyatkova et al. (2002)
	ED Ni-P-SiC	Berkh et al. (1996)
	ED Ni-P-CNT	Shi et al. (2004)
	ED Ni-Y <sub>2</sub> O <sub>3</sub> (more electrochemically active)	Veleva et al. (2003)

**Table 1.9 Applications of electro- and electroless deposited composite coatings in various industries**

<b>Type of industry/ Application</b>	<b>Component/ Assembly</b>	<b>Problem, conventionally used coatings and normal service life</b>	<b>Improvement in performance by adopting ED and EL Ni-based composite coatings</b>	<b>Reference</b>
Rubber and plastic industry	Moulds	The life of moulds for plastics, rubber etc. usually last for 10,000 mouldings	A 50 $\mu\text{m}$ thick ED and EL Ni–P–SiC coating increases the service life by 15 times	Metzger and Florian (1976); Chaggeng et al. (1988)
	Moulds	Accelerated corrosion of moulds – chrome plating	EL Ni–P–SiC and EL Ni-P-PTFE coatings prevent accelerated corrosion of abrasion moulds and its performance is superior to the conventionally used chrome plating	Metzger and Florian (1976); Tulsi (1983)
Foundries	Core boxes	Wear and release of sand cores without breakage	EL Ni–P–SiC coating has been found to reduce wear and helps to release sand cores, without breakage, from core boxes	Hubbell (1978)
Oil and gas industry	butterfly valves	Pick up and galling; Increase in the leak rate – unsafe operation of the valves	A Ni–P–PTFE composite coating applied to a butterfly valve prevents pick up and galling and decreases the leak rate and enables safe operation of the valve for cryogenic applications	Tulsi (1983)
Textile industry	Thread guides yarn brakes, gears, friction clutches	Wear and friction	EL Ni–P–diamond coatings enable slipless transmission of very high rotational speed, an essential requirement of yarn brakes, infinitely variable gears, and friction clutches	Lukschandel (1978)

**Table 1.9 (contd...)**

Automobile industry	Carburetor parts Choke shafts Piston Cylinder liners Gears, etc.	Pickup and galling arise during forming and drawing operations  Friction and dry lubrication  Build-up of gummy deposits  Wear	Electroless Ni-P-SiC coating has been used to overcome problems due to pickup and galling, arise during forming and drawing operations ED and EL Ni-P-PTFE on carburetor parts makes it nonstick, provides dry lubrication and low coefficient of friction properties EL Ni-P-PTFE coating minimizes build-up of gummy deposits on the choke shafts ED Ni-SiC composite coating offers enhanced wear resistance	Hubbell (1978a, 1978b) Tulsi (1983) Wasserman (1989)
Aerospace industry	Aircraft turbine blades and turbine engine components	Wear resistance	ED Ni-Cubic BN composite coating offers enhanced wear resistance ED Ni-SiC, Ni-Al <sub>2</sub> O <sub>3</sub> and Ni-Cr <sub>2</sub> O <sub>3</sub> composite coating also offers an improved performance	Furukawa and Hayashi (1984)
Cutting tools and grinding wheels	Profiled diamond tools or micro-inishing, screw threads,  Razor blades	High accuracy micro-finishing – very difficult with conventional electroplating  Wear resistance	EL Ni-P-diamond, ED Ni-SiC, Ni-diamond and Ni-garnet composite offer improved performance  ED Ni-MoS <sub>2</sub> and Ni-h BN composite coatings offers enhanced wear resistance	Futterer (1967)

## **CHAPTER II**

### **STATE-OF-THE-ART AND SCOPE OF PRESENT INVESTIGATION**

Surface degradation processes such as wear, oxidation, corrosion and fatigue cause failure of many engineering components under varied circumstances. Although a variety of techniques, such as physical vapour deposition (PVD), chemical vapour deposition (CVD), etc., are available for engineering the surfaces to impart the desirable characteristics, electro- and electroless plating processes have received widespread acceptance following their less complex processing sequence and cost-effectiveness. Electro- and electroless plated nickel coatings are widely used in engineering applications. Alloying of phosphorous or boron along with nickel improved the hardness, corrosion resistance and wear resistance. Numerous reports are available on the formation and characterization of electro- and electroless plated Ni-P coatings (Ratzker et al., 1986; Carbajal and White, 1988; Lewis and Marshall, 1996; Morikawa et al., 1997; Daly and Barry, 2003; Lin et al. 2005; Gawrilov, 1979; Mallory and Hajdu, 1991; Riedel, 1991; Duncan, 1986; Keong et al., 2002a, 2002b; Guo et al. 2003, Balaraju, 2000). However, studies on Ni-B coatings are rather limited. A few reports are available on the formation and characterization of electroless Ni-B coatings (Mallory, 1971; Gorbunova et al., 1973; Duncan and Arney, 1984; Mausi et al., 1985; Mausi, 1986; Srivastava et al., 1992; Evans and Schlesinger, 1994; Delaunois et al., 2000, Delaunois and Lienard, 2002; Sankara Narayanan and Seshadri, 2004) whereas Ni-B coatings obtained by electrodeposition route are not studied in detail.

Several type of plating baths are available for preparing electrodeposited (ED) nickel coating, which include Watts' nickel bath, sulphamate bath, fluoborate bath etc. Tomaszewski et al. (1969) have reported that the Watt's nickel bath is more effective than the chloride and fluoborate baths at the same temperature and pH for codeposition of insoluble inorganic particles. Watts' nickel plating bath was chosen for the present investigation for the preparation of ED Ni-B coating. Several boron containing compounds can be used as a source of boron in the plating baths for preparing ED Ni-B coatings. Onada et al. (1998, 1999), Lee et al. (2005) and Gaevskaya et al. (1996) have used dimethylamine borane (DMAB), trimethylamine borane (TMAB) and sodium decahydridodecaborate ( $\text{Na}_2\text{B}_{10}\text{H}_{10}$ ) as a source of boron to prepare ED Ni-B coatings. In the present investigation DMAB was chosen as the source of boron in the Watt's nickel plating bath to prepare the ED Ni-B coating. Wehner et al. (2003) have reported that the throwing power of DMAB is higher than that of sodium hypophosphite. The structural characteristics, textural aspects and evaluation of characteristic properties such as microhardness, wear resistance and corrosion resistance of ED Ni-B coatings are yet to be explored.

For preparing electroless (EL) Ni-B coatings, boron containing reducing agents such as, sodium borohydride or dimethylamine borane are commonly used. The reduction efficiency of sodium borohydride is much higher than that of dimethylamine borane and sodium hypophosphite. It can provide up to eight electrons for reduction of some metals as opposed to two electrons that can be provided by sodium hypophosphite for the same reaction (Duncan and Arney, 1984). Besides the high reduction efficiency, borohydride baths are preferred to dimethylamine borane baths in terms of cost-effectiveness of operation (Lo and



Huang, 1994). However, borohydride ions hydrolyze readily in acid or neutral solutions and will spontaneously yield nickel boride in presence of nickel ions in the plating bath (Duncan and Arney, 1984; Lo and Huang, 1994; Gorbunova et al., 1973). Hence, control of pH is important to avoid the spontaneous decomposition of the bath solution and to decrease the cost of operation. The properties of sodium borohydride reduced electroless nickel coatings are often superior to those of deposits reduced with other boron compounds or with sodium hypophosphite (Baudrand, 1994; Delaunois and Lienard, 2002). The principal advantages of borohydride-reduced electroless nickel coatings are its hardness and superior wear resistance in the as-deposited condition (Duncan and Arney, 1984; Gorbunova et al., 1973; Baudrand, 1994; Delaunois and Lienard, 2002). EL Ni-B coatings are more wear resistant than tool steel and hard chromium coatings and it can replace gold in electronic industries (Duncan and Arney, 1984). The columnar structure of EL Ni-B coatings is useful in retaining lubricants under conditions of adhesive wear (Gawrilov, 1979; Baudrand, 1994). The rapid changing needs of engineering industries warrant the development of coatings that possess high hardness, good wear and abrasion resistance and in this respect one such coating which seems promising is the borohydride-reduced electroless nickel coating. Much remain to be explored about borohydride-reduced electroless nickel coatings so that they can be effectively manipulated to suit the needs. Though some studies on EL Ni-B coatings are available in the literature, the structural characteristics, phase transformation behaviour and evaluation of characteristic properties such as microhardness, wear resistance and corrosion resistance of EL Ni-B coatings are not yet studied in detail.

The idea of codepositing various second phase particles in electro- or electroless deposited metals or alloy matrix and thereby taking advantage of its desirable qualities, such as hardness, wear and abrasion resistance, corrosion resistance, etc. has led to the development of composite coatings with a wide range of possible combination and properties (Musiani, 2000; Low et al., 2006; Agarwala and Agarwala, 2003; Balaraju et al., 2003). ED and EL composite coatings provide specific engineering properties otherwise unobtainable with the single plated coatings. Much research has been directed towards the optimization of the deposition process in relation to the main coatings properties such as uniform deposition of particles, microhardness, corrosion and wear resistance (Staia et al., 1996, 2002). A number of oxides, carbides and nitrides are used as second phase particles to produce composite coatings. A compilation of ED and EL Ni-based composite coatings obtained by the incorporation of various hard and soft particles is given in **Table 2.1**. It is obvious that only a few studies are made on ED and EL Ni-based composite coatings containing silicon nitride particles. Silicon nitride ( $\text{Si}_3\text{N}_4$ ) is a very hard ceramic material, which retains its room temperature strength up to  $1200^\circ\text{C}$  and has excellent dimensional stability and oxidation resistance (Joshi and Totlani, 1981). Ramesh and Seshadri (2003) have reported that incorporation of  $\text{Si}_3\text{N}_4$  particles in ED Ni matrix results in a significant improvement in hardness and wear resistance. Balaraju (2000) have studied EL Ni-P composite coatings with three different particles, namely,  $\text{CeO}_2$ ,  $\text{TiO}_2$  and  $\text{Si}_3\text{N}_4$ . Among them, EL Ni-P- $\text{Si}_3\text{N}_4$  composite coating was found to possess superior properties (Balaraju, 2000). Literature reports on ED and EL composite coatings prepared by incorporating various second phase particle in

the Ni-B matrix are scarce. In this context, the present investigation aims to study the formation of Ni-B and Ni-B-Si<sub>3</sub>N<sub>4</sub> composite coatings by electro- and electroless deposition processes and evaluation of their characteristic properties. Besides, the present study also aims to study the formation and characteristics of EL Ni-P/Ni-B duplex coatings and explores the possibility of preparing ED Ni-B multilayered and graded coatings. The flow chart depicting the work plan of the present investigation is given in **Fig. 2.1**.

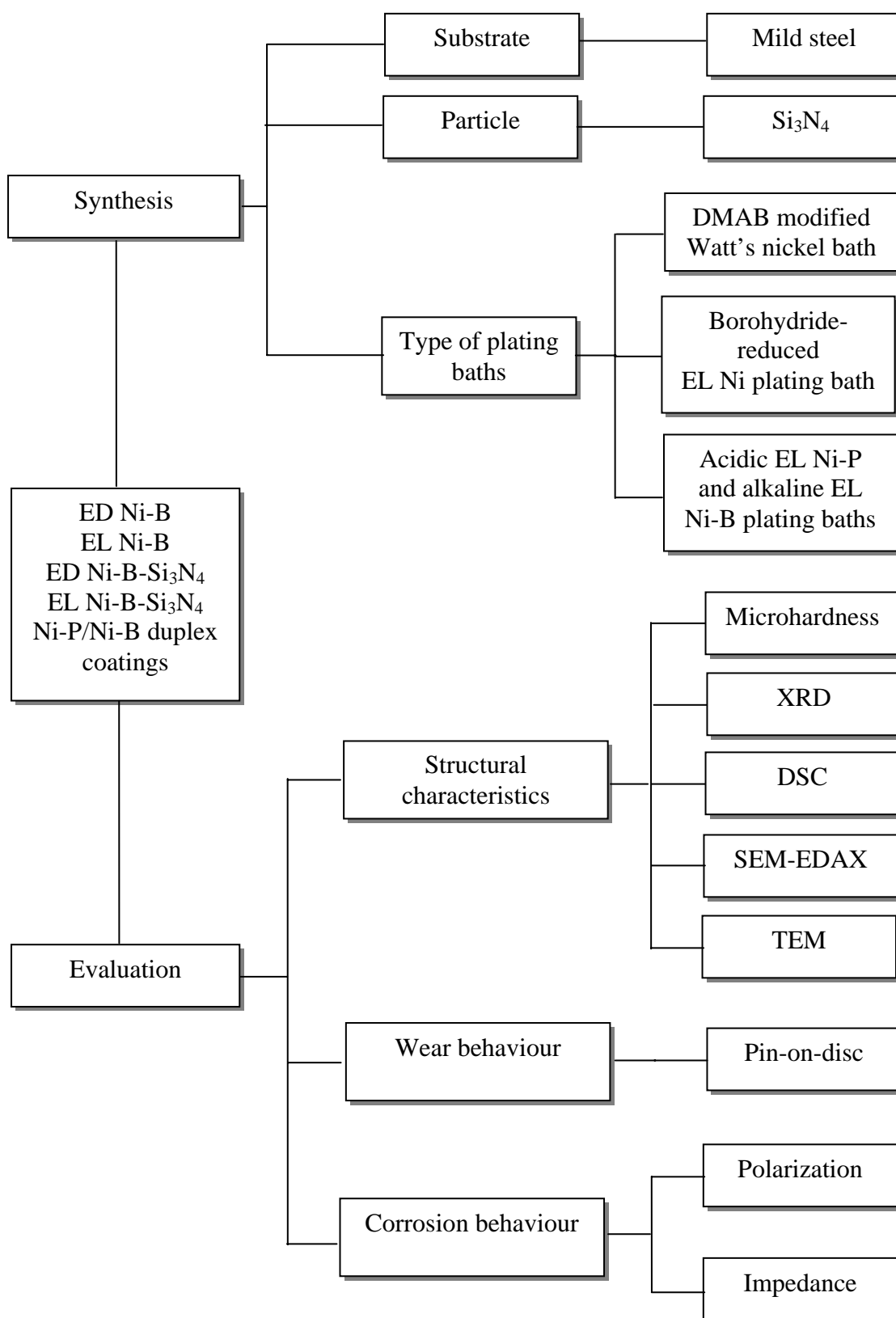


**Fig. 2.1 Flow chart depicting the work plan of the present investigation**

**Table 2.1 Survey of the literature reports on electrodeposited (ED) and electroless deposited (EL) Ni-based composite coatings incorporated with various hard and soft particles**

<b>Matrix</b>	<b>Reference</b>
ED Ni-SiC	Sasame (1974); Yeh et al. (1994, 1995, 1997) Kim et al. (1998); Nowak et al. (2000) Garcia et al. (2001, 2003); Medeliene (2002) Benea et al. (2002a); Socha et al., (2002); Hou et al., (2002) Zimmerman et al. (2002a, 2002b); Wang et al. (2003b); Shrestha et al. (2003)
ED Ni-Si <sub>3</sub> N <sub>4</sub>	Ramesh and Seshadri (2003); Joshi and Totlani (1981)
ED Ni-Al <sub>2</sub> O <sub>3</sub>	Pushpavanam and Shenoi (1977) Banovic et al. (1999) Shrestha et al. (2001); Vidrine et al. (2001) Wang et al. (2003b); Shao et al. (2002)
ED Ni-Diamond	Lee et al. (1999); Zahavi and Hazan (1983);
ED Ni-B <sub>4</sub> C	Medeliene (2002); Bozzini et al. (1999)
ED Ni-ZrO <sub>2</sub>	Moller and Hahn (1999); Wang et al. (2000)
ED Ni-CeO <sub>2</sub>	Balathandan and Seshadri (1992a) Aruna et al. (2006); Xue et al., (2006)
ED Ni-TiO <sub>2</sub>	Pushpavanam et al. (1989); Ramesh Babu et al. (1991); Li et al. (2005)
ED Ni-WC	Wang et al. (2002a) Surender et al. (2004a, 2004b);
ED Ni-Flyash	Ramesh et al. (1991, 2003)
ED Ni-CaF <sub>2</sub>	Ramesh et al. (2003)

Matrix	Reference
ED Ni-BN	Shrestha et al. (2001) Wang et al. (2001)
ED Ni-PSZ	Jun et al. (1997)
ED Ni-Co <sub>3</sub> O <sub>4</sub>	Bonino et al. (1998)
ED Ni-Yttrium oxide	Veleva et al. (2003); McCormack et al. (2003)
ED Ni-Fluorographite	Plumier et al. (2003)
ED Ni-Polyethylene	Abdel Hamid and Ghayad (2002)
ED Ni-Polystyrene	Filiatre et al. (1999)
ED Ni-SiO <sub>2</sub>	Nowak et al. (2000)
ED Ni-ZrB <sub>2</sub>	Pushpavanam and Natarajan (1992)
ED Ni-Al	Susan et al. (1997)
ED Ni-B	Fellner and Cong (1996)
ED Ni-Ti	Serek and Budniok (2003)
ED Ni-CeO <sub>2</sub> -ZrO <sub>2</sub>	Balathandan and Seshadri (1992b)
ED Ni-P-SiC	Berkh et al. (1995, 1996)
ED Ni-P-TiO <sub>2</sub>	Gierlotka et al. (1997)
ED Ni-Fe-Si <sub>3</sub> N <sub>4</sub>	Li and Li (2003)
ED Ni-Co-Si <sub>3</sub> N <sub>4</sub>	Shi et al. (2005)
ED Ni-Co-P-Si <sub>3</sub> N <sub>4</sub>	Hiratsuka et al. (2001)
ED Ni-W-B-ZrO <sub>2</sub>	Liqun et al. (2001)
EL Ni-P-SiC	Grosjean et al. (1997); Li (1997) Apachitei et al. (1998, 2001, 2002) Wu et al. (2000a, 2000b) Chen et al. (2002a) Jiaqiang et al. (200)
EL Ni-P-Al <sub>2</sub> O <sub>3</sub>	Apachitei et al. (1998a, 1998b) Abdel Hamid and Abou Elkhair (2002) Balaraju et al. (2006) Alirezaei et al. (2004) Oh et al. (2005)
EL Ni-P-Diamond	Reddy et al. (2000) Bozzini et al. (2001a) Sheela and Pushpavanam (2002) Xu et al. (2005) Chao et al. (2006)

Matrix	Reference
EL Ni-P-B <sub>4</sub> C	Moonir-Vaghefi et al (2003) Bozzini et al. (1999, 2001b) Ge et al. (1998)
EL Ni-P-BN(h)	Leon et al. (1998, 2003) Straffelini et al. (1999)
EL Ni-P-Si <sub>3</sub> N <sub>4</sub>	Balaraju et al. (2000); Das et al., (2006)
EL Ni-P-CeO <sub>2</sub>	Balaraju et al (2000)
EL Ni-P-TiO <sub>2</sub>	Balaraju et al (2000) Abdel Hamid and Abou ElKhair (2002) John et al. (2005) Novakovic et al. (2006)
EL Ni-P-ZrO <sub>2</sub>	Abdel Hamid and Abou ElKhair (2002)
EL Ni-P-MoS <sub>2</sub>	Moonir-Vaghefi et al., (1997a, 1997b, 1997c) Straffelini et al., (1999)
EL Ni-P-PTFE	Parker 1972 Zhang et al (1998) Pena-Munoz et al. (1998) Zhao and Liu (2005a) Straffelini et al. (1999) Ger and Hwang (2002) Ger et al. (2003) Zhao et al., (2002) Srinivasan and John (2005)
EL Ni-P- Carbon nanotubes (CNTs)	Chen et al (2002c, 2003a, 200b, 2005, 2006) Li et al. (2006) Yang et al (2004, 2005) Chao et al. (2006)
EL Ni-P-nano-IF-WS <sub>2</sub>	Chen et al., (2002b)
EL Ni-P-B	Apachitei et al. (1998b)
EL Ni-P-Polyvinyl alcohol EL Ni-P- Polyvinyl chloride EL Ni-P- Polyacrylamide	Shoeib et al. (1998)
EL Ni-P-ZnO	Shibli et al. (2006a, 2006b)
EL Ni-Cu-P-PTFE	Zhao and Liu (2004, 2005b)
EL Ni-P-PTFE-SiC	Straffelini et al.(1999) Huang et al., (2003, 2004, 2005) Wu et al. (2006)

## **CHAPTER III**

### **MATERIALS AND METHODS**

The present chapter gives a detailed account of the synthesis of Ni-B and Ni-B-Si<sub>3</sub>N<sub>4</sub> composite coatings by electro- and electroless deposition processes and evaluation of their characteristic properties, namely, structural characteristics, phase transformation behaviour, microhardness, wear resistance and corrosion resistance. The details regarding the formation and characteristics of EL Ni-P/Ni-B duplex coatings, ED Ni-B multilayer and ED Ni-B graded coatings are given in part C of Chapter IV in sections 4.5, 4.6 and 4.7, respectively.

### **3.1 MATERIALS USED**

#### **3.1.1 Choice of the substrate**

Mild steel discs (30 mm diameter and 5 mm thick, having a composition of C: 0.16%; Si: 0.18%; Mn: 0.62%; P: 0.012%; S: 0.016%; Cr: 0.01%; Ni: 0.1%; Fe: Balance), copper (electrolytic grade) and stainless steel (AISI 304 grade) were used as substrate materials for the deposition of Ni-B and Ni-B-Si<sub>3</sub>N<sub>4</sub> composite coatings by electro- and electroless deposition processes. Copper substrate was employed to assess the plating rate. Stainless steel substrate was used to prepare thin foils of Ni-B and Ni-B-Si<sub>3</sub>N<sub>4</sub> composite coatings, which were subsequently peeled off and used for chemical analysis, structural characterization by transmission electron microscopy (TEM) and to study the phase transformation behavior by differential scanning calorimetry (DSC). Ni-B and Ni-B-Si<sub>3</sub>N<sub>4</sub> composite coated mild steel discs were used for



evaluating microhardness, structural characterization by X-ray diffraction, surface topography and roughness by laser scanning microscope (LSM), surface morphology by scanning electron microscope (SEM), chemical analysis by energy dispersive X-ray spectroscopy (EDX), X-ray mapping and corrosion resistance while Ni-B and Ni-B-Si<sub>3</sub>N<sub>4</sub> composite coated mild steel pins were used for evaluating the wear resistance.

### **3.1.2 Choice of the metal matrix and second phase particle**

The metal matrix chosen for the present investigation is Ni-B. The Ni-B matrix is prepared by both electro- and electroless deposition processes. Silicon nitride (Si<sub>3</sub>N<sub>4</sub>) was chosen as the second phase particle for the present study. The characteristic properties of Si<sub>3</sub>N<sub>4</sub> particles are given in **Table 3.1**. The Si<sub>3</sub>N<sub>4</sub> particles used in the present has a d<sub>10</sub>, d<sub>50</sub> and d<sub>80</sub> of 0.08, 0.39 and 0.92 µm, respectively, with a mean diameter of 0.80 µm.

## **3.2 METHODOLOGY OF THE SYNTHESIS OF Ni-B AND Ni-B-Si<sub>3</sub>N<sub>4</sub> COMPOSITE COATINGS**

### **3.2.1 Surface preparation of the substrate material**

The mild steel discs were surface ground to a roughness of 0.45 µm, electrolytically cleaned using a mixture of sodium hydroxide-sodium carbonate-sodium lauryl sulphate and electrolytically etched in the plating bath before subjecting them for plating. In case of electrodeposition of Ni-B and Ni-B-Si<sub>3</sub>N<sub>4</sub> composite coatings, a nickel strike at low current density was given with the plating solution itself to get a brittle-free, adherent deposit. During plating, the pH of the bath is maintained at ± 0.2 and temperature at ±1°C.

Also, the plating bath was agitated using a magnetic stirrer (600 rpm) to ensure a uniform supply of the electrolyte solution and the  $\text{Si}_3\text{N}_4$  particles to the cathode-solution interface. In case of EL Ni-B and Ni-B- $\text{Si}_3\text{N}_4$  composite coatings, a nickel strike using Watt's nickel bath was given to substrates prior to their immersion in electroless plating bath.

### **3.2.2 Bath composition and operating conditions of the plating bath employed for the preparation of electrodeposited Ni-B coatings**

ED Ni-B coatings were prepared using Watt's nickel bath modified with the addition of dimethylamine borane (DMAB), which also serves as the source of boron. The details of the chemical composition of the bath and its operating conditions are given in **Table 3.2**. The plating was done at different current densities ranging from 0.4 to 4  $\text{A}/\text{dm}^2$ . During plating, the pH and the temperature of the bath were maintained at 3.5 and at  $45 \pm 2^\circ\text{C}$ , respectively. Also, the bath solution is agitated mechanically using a magnetic stirrer and Teflon coated iron paddle. Using the chemical composition and operating conditions given in Table 3.2, the plating bath was capable of depositing 10-12  $\mu\text{m}/\text{hour}$  at 1  $\text{A}/\text{dm}^2$ . Depending on the applied current density, the time of plating was varied to prepare coatings of equal thickness, which were subsequently used for characterization.

### **3.2.3 Bath composition and operating conditions of the plating bath employed for the preparation of electroless Ni-B coatings**

An alkaline bath having nickel chloride as the source of nickel and sodium borohydride as the reducing agent was used to prepare EL Ni-B coating. Besides nickel salt and borohydride, the plating bath also contained

suitable quantities of ethylenediamine as a complexing agent and sufficient quantities of sodium hydroxide. Thallium acetate was used as the stabilizer. While preparing the plating bath, the order of addition is very important. Nickel ions in nickel chloride solution were first complexed by the addition of the complexing agent, ethylenediamine. Then sufficient quantities of sodium hydroxide were added to maintain the pH at 14. Thallium acetate (stabilizer) and sodium borohydride (reducing agent) are added after the bath has attained a temperature of  $95\pm 1^\circ\text{C}$ . This methodology was adopted to achieve greater uniformity of EL Ni-B coatings. The details of the chemical composition of the plating bath and its operating conditions are given in **Table 3.3**. Using the chemical composition and operating conditions given in Table 3.3, the borohydride-reduced electroless nickel plating bath was capable of depositing 18-20  $\mu\text{m}/\text{hour}$ .

#### **3.2.4 Conditioning of the plating baths for preparing ED and EL Ni-B-Si<sub>3</sub>N<sub>4</sub> composite coating**

Required amount of Si<sub>3</sub>N<sub>4</sub> particles were taken in a mortar and they were blended thoroughly with a small quantity of the plating bath. This procedure ensures the prevention of agglomeration and enables uniform distribution of Si<sub>3</sub>N<sub>4</sub> particles in the plating bath. Blending of the particles with a small quantity of plating bath before adding the particles to the bath has been proved to be useful and recommended by many researchers (Ghouse et al., 1980; Joshi and Totlani, 1981; Ramesh et al., 1991; Balaraju, 2000). The resulting slurry was then transferred to the plating bath. The plating solution was then made up to the required volume. The plating bath containing Si<sub>3</sub>N<sub>4</sub> particles was mechanically agitated for 30 minutes before the commencement

of the deposition process (i.e., before the addition of DMAB and application of d.c. power supply in the case of electrodeposition and before the addition of sodium borohydride in the case of electroless deposition.)

### **3.2.5 Methodology of electro- and electroless deposition of Ni-B and Ni-B-Si<sub>3</sub>N<sub>4</sub> composite coatings**

The schematic of the experimental set up used for electrodeposition and electroless deposition of plain Ni-B coatings and Ni-B-Si<sub>3</sub>N<sub>4</sub> composite coatings is shown in **Figs. 3.1** and **3.2**, respectively. The plating cell used for electrodeposition consists of two graphite disc anodes (diameter: 6 cm) placed on both sides of the cathode to ensure uniform deposition on all sides of the mild steel cathode (diameter 3.2 cm). Anode bags made up of muslin cloth were used to prevent contamination of the plating bath by graphite particles. The graphite particles if entered in the plating bath would lead the formation of rough coatings. Mild steel discs prepared according to the procedures described in section 3.2.1 were subjected to electro- and electroless deposition of Ni-B and Ni-B-Si<sub>3</sub>N<sub>4</sub> composite coatings. Mechanical agitation of the plating bath during plating ensures uniform supply of the Si<sub>3</sub>N<sub>4</sub> particles towards the electrode surface and enables uniform distribution of Si<sub>3</sub>N<sub>4</sub> particles throughout the depth of the ED and EL Ni-B matrix.

## **3.3 CHARACTERIZATION OF THE Ni-B AND Ni-B-Si<sub>3</sub>N<sub>4</sub> COMPOSITE COATINGS**

### **3.3.1 Evaluation of chemical composition of the coatings**

The nickel content of the Ni-B coatings was determined by gravimetric technique after precipitating the nickel as Ni-DMG complex whereas the boron

and thallium content was analyzed by atomic absorption spectrophotometer (GBC Avanta). The level of incorporation of  $\text{Si}_3\text{N}_4$  particles in both ED and EL Ni-B matrix is determined by wet chemical method. A weighed quantity of the Ni-B- $\text{Si}_3\text{N}_4$  composite coating was dissolved in 1:1 nitric acid. After complete dissolution of the coating, the solution was diluted with deionized water and filtered through an ashless filter paper (Whatman, No.41, weight of the ash 0.01%). The filtered mass was then incinerated in a platinum crucible and the residual ceramic material was weighed. Based on the weight of the particles determined above and the amount of  $\text{Si}_3\text{N}_4$  particles present in the plating bath, the weight percentage of  $\text{Si}_3\text{N}_4$  particles incorporated in the Ni-B matrix was calculated.

### **3.3.2 Evaluation of coatings using optical and scanning electron microscopes**

The Ni-B and Ni-B- $\text{Si}_3\text{N}_4$  composite coated mild steel discs were ground successively on 1/0, 2/0, 3/0 and 4/0 emery papers followed by lapping on sylvet cloth mounted on rotating discs using alumina as the abrasive material. The surface of the coating thus prepared was examined by optical microscope (Leica Qwin) at 100 and 500X magnifications. A scanning electron microscope (SEM) was used to assess the surface morphology of Ni-B and Ni-B- $\text{Si}_3\text{N}_4$  composite coatings at suitable magnifications. In order to assess the cross section of the selected coatings, the coated mild steel discs were cut along its diameter. A thin layer of copper was electrodeposited to protect the edges from damage during cutting. The cut specimens were mounted in bakelite resin, thoroughly polished, etched with “Nital” and were examined by optical or scanning electron microscopy at suitable magnifications.

### 3.3.3 Evaluation of structural characteristics

The structure of Ni-B coatings largely depends on boron content of the coating which in turn is influenced by the type of plating bath used and its operating conditions. The structure of Ni-B and Ni-B-Si<sub>3</sub>N<sub>4</sub> composite coatings, both in as-plated and heat treated conditions, was determined by X-ray diffraction (XRD) measurements using Cu K $\alpha$  ( $\lambda = 1.5418 \text{ \AA}$ ) or Co K $\alpha$  ( $\lambda = 1.7902 \text{ \AA}$ ) radiation. The phase transformation behaviour of ED and EL Ni-B coatings was studied by differential scanning calorimetry (DSC). To enable DSC studies, Ni-B coatings were deposited on stainless steel substrates and were subsequently peeled off from the substrate to serve as thin foils. The DSC traces were obtained using a NETZSCH-Geratebau GmbH thermal analyzer. Thin foils of Ni-B coatings, similar to that used in DSC measurements were also employed for structural characterization by transmission electron microscopy (TEM). TEM studies were performed using a Philips transmission electron microscope (Model CM 12), operated at 120 KV. The thin foils of Ni-B coatings were suitably thinned by twin jet polishing using perchloric acid-methanol mixture at very low temperatures (about 5°C) and carefully placed inside a copper grid for analysis. The TEM micrographs were taken at different locations with suitable magnifications. Besides this, diffraction patterns were also made at selected regions (SAD patterns) to have a better insight about the structure of the Ni-B coatings.

A scanning electron microscope (SEM) was used to assess the surface morphology of the Ni-B and Ni-B-Si<sub>3</sub>N<sub>4</sub> composite coatings. Energy dispersive

X-ray spectrometer (EDAX) attached with the SEM facilitates chemical analysis of the constituents present in coating at selected areas. The EDAX analysis was performed on both the Ni-B matrix region as well as in the region rich in incorporated  $\text{Si}_3\text{N}_4$  particles. EDAX line scanning was also performed across selected regions of the Ni-B- $\text{Si}_3\text{N}_4$  composite coatings. X-ray elemental mapping of nickel, silicon and nitrogen was also recorded to assess the distribution of the  $\text{Si}_3\text{N}_4$  particles in the Ni-B matrix.

### **3.3.4 Evaluation of microhardness**

The microhardness of Ni-B and Ni-B- $\text{Si}_3\text{N}_4$  composite coatings was determined both in as-plated as well as heat treated (200, 300, 400, 500, 600°C for 1 hour) conditions. All coatings used for microhardness measurements have a thickness of around 20  $\mu\text{m}$ . A constant load of 100-g (0.98 N) was applied to cause the indentations in all the coatings. The coating hardness was measured on the surface using a Leica microhardness tester with a Vickers diamond indenter under a 100-g load (0.98 N). The lap time for each indentation was 15 seconds and the values reported represent the average and standard deviation of a minimum of five measurements.

### **3.3.5 Evaluation of wear resistance**

Sliding wear tests are primarily meant for assessing the adhesive wear resistance of metals. As electro- and electroless deposited coatings encounter adhesive wear failure, it is essential to evaluate the sliding wear behavior of ED and EL Ni-B and Ni-B- $\text{Si}_3\text{N}_4$  composite coatings. Among the various test methods that are available for assessing the sliding wear resistance, the pin-on-

disc method is used in the present investigation. The wear resistance of ED and EL Ni-B and Ni-B-Si<sub>3</sub>N<sub>4</sub> composite coatings, both in as-plated and heat-treated conditions was evaluated using a pin-on-disc apparatus (DUCOM, India). In this method the pin and disc are arranged in such a way that the rotating disc served as the counter face material while the stationary pin served as the test specimen. Steel discs (composition conforming to EN 31 specification) of 10 cm diameter and 5 mm thickness were chosen as counter face materials to slide against the test specimens. These discs were fully hardened ( $R_c$  63) and surface ground to a finish ( $R_a$ ) of 0.02  $\mu$ m. The applied normal loads were 8, 10 and 12 N for ED Ni-B and ED Ni-B-Si<sub>3</sub>N<sub>4</sub> composite coatings and 20, 30 and 40 N for EL Ni-B and EL Ni-B-Si<sub>3</sub>N<sub>4</sub> composite coatings. The sliding speed was kept constant at 0.5 m/s for all the tests by adjusting the diameter of the wear track and the rotational speed of the disc. All coatings used for wear resistance studies have a thickness of 20  $\mu$ m. Tests were done in air at 25°C with a relative humidity of about 35-45% RH. The frictional force was recorded continuously during the test using a transducer linked to a personal computer. In this way the coefficient of friction was continuously monitored during the test. After the wear tests, the pins were cleaned in acetone in an ultrasonic bath for about 10 minutes to remove the loose particles and wear debris from the surface. The loss in weight due to wear was calculated by weighing the pins before and after each test on a balance with an accuracy up to 0.1 mg. Two tests were done for each load condition. The specific wear rate was calculated by the expression:

$$w_s = w / (l L)$$



where 'w' is the wear mass, 'L' is the normal load and 'l' is the sliding distance. The sliding distance was calculated at the mean radius of the disc. Immediately after the end of each test, the wear track on the pins was examined using an optical or scanning electron microscope (SEM). The roughness of the pins, before and after wear test, was determined using a portable roughness measuring station (Make: Mahr; Model: Perthometer-M2).

### 3.3.6 Evaluation of corrosion resistance

The corrosion resistance of ED and EL Ni-B and Ni-B-Si<sub>3</sub>N<sub>4</sub> composite coatings in 3.5% sodium chloride solution was determined by potentiodynamic polarization and electrochemical impedance (EIS) studies using a potentiostat/galvanostat/frequency response analyzer (ACM INSTRUMENTS, UK). A conventional three-electrode set-up with platinum electrode and saturated calomel electrode (SCE) as the counter and reference electrodes, respectively, was used to evaluate the corrosion resistance. All coatings used for the evaluation of corrosion resistance have a thickness of 20  $\mu\text{m}$ . A flat cell (Wear and Friction Tech, Chennai, India), which enables the exposure of exactly 1  $\text{cm}^2$  area of the sample to the electrolyte solution, was specially fabricated and used for all the tests. The schematic of the flat cell is shown in **Fig. 3.3**. The corrosion potential ( $E_{\text{corr}}$ ) and corrosion current density ( $i_{\text{corr}}$ ) were determined from the polarization curves using the Tafel extrapolation method. The  $R_{\text{ct}}$  and  $C_{\text{dl}}$  values were determined from the Nyquist plot after fitting the data using Boukamp software.

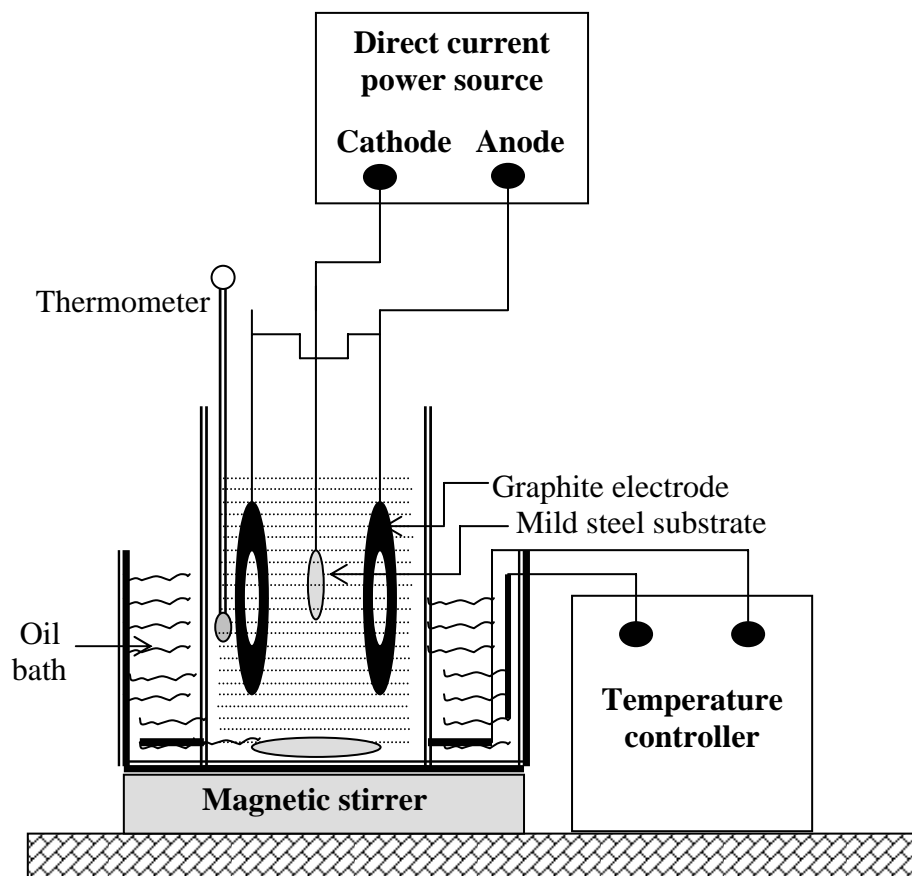


**Fig. 3.1 Schematic of the experimental setup used for electrodeposition of Ni-B and Ni-B-Si<sub>3</sub>N<sub>4</sub> composite coatings**

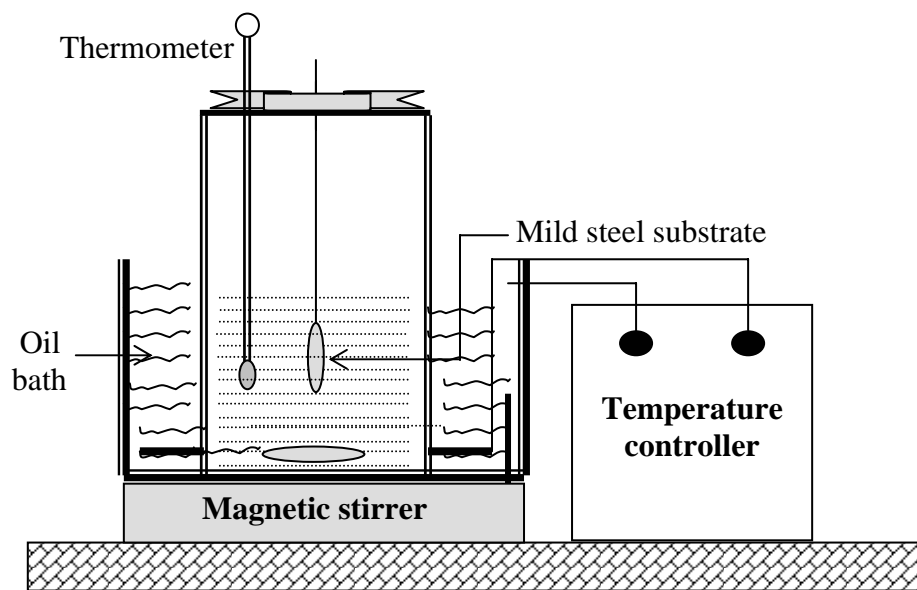


**Fig. 3.2 Schematic of the experimental setup used for Electroless deposition of Ni-B and Ni-B-Si<sub>3</sub>N<sub>4</sub> composite coatings**

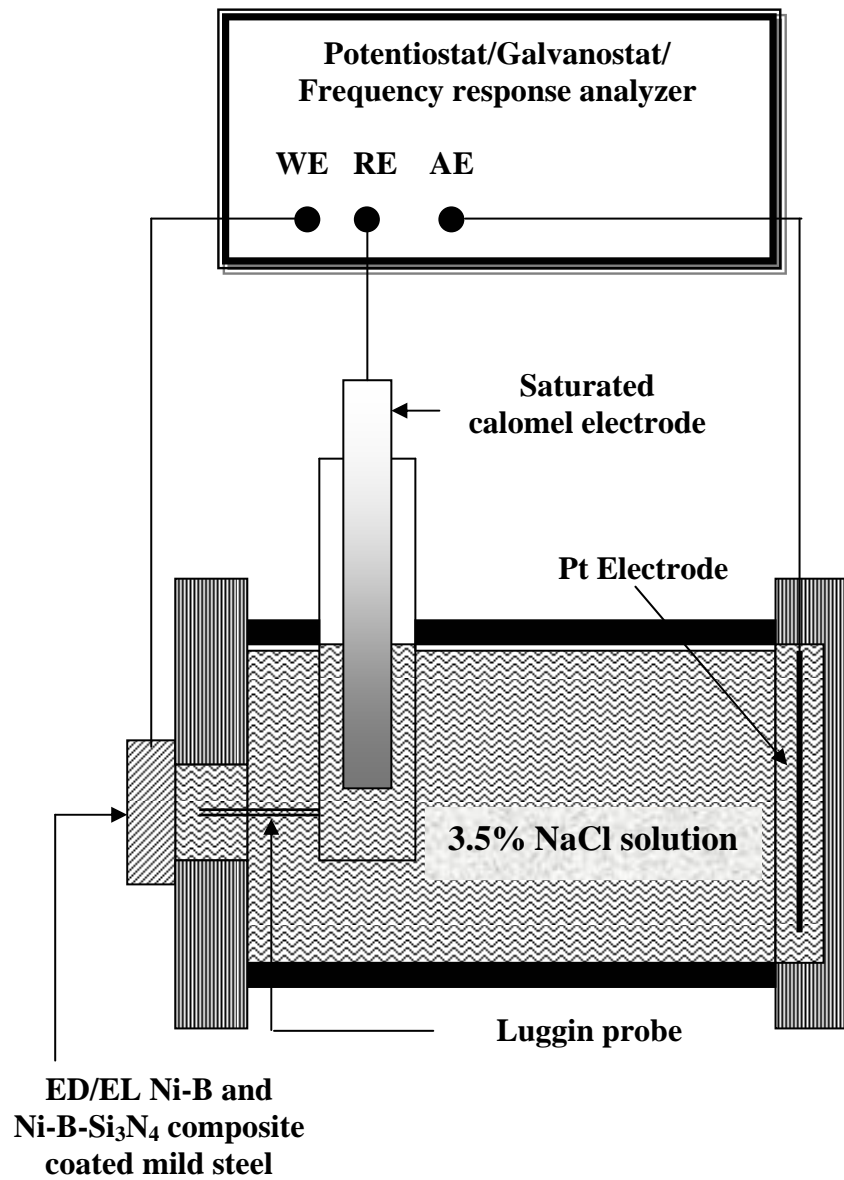


**Fig. 3.3 Schematic of the flat cell used for the evaluation of corrosion resistance of Ni-B and Ni-B-Si<sub>3</sub>N<sub>4</sub> composite coatings obtained by electro- and electroless deposition processes**

**Table 3.1 Properties of Silicon Nitride (Adapted from Ettmayer and Lengauer, 1991)**

Structure	Hexagonal
Melting point (°C)	1900
Density (g/cc)	3.4
Coefficient of thermal expansion	$2.75 \times 10^{-6}$
Thermal conductivity (Cal/sec/cm <sup>-2</sup> /°C/cm)	0.0035
Heat capacity (298-900°C)	$-16.83 + 23.6 \times 10^{-3} T$
Hardness (HV <sub>100</sub> )	
Reaction bonded	750
Hot pressed	1600 - 1800
Tensile strength (kg/mm <sup>2</sup> )	11.18
Modulus of rupture (kg/mm <sup>2</sup> ) (at room temperature - 1200°C)	11.25 - 14.06
Compressive strength (kg/mm <sup>2</sup> )	50.62 - 63.28
Resistivity (Ohm.cm)	$10^9$
Permittivity (1 MHz) at 25°C	10
Other properties	Good thermal shock resistance; good oxidation resistance up to 1200°C; Excellent compatibility with molten metal; Chemically and thermally very stable

**Table 3.2 Bath composition and operating conditions  
used to prepare electrodeposited Ni-B coatings**

<b>Bath Composition</b>	
Nickel sulphate hexahydrate	240 g/l
Nickel chloride hexahydrate	45 g/l
Boric acid	30 g/l
Dimethylamine borane	3 g/l
<b>Operating conditions</b>	
Temperature	$45 \pm 1^{\circ}\text{C}$
pH	3.5
Current density	$0.4 - 4 \text{ A/dm}^2$
Agitation	Mechanical – using magnetic stirrer at 600 rpm
Time	40 – 180 min.

**Table 3.3 Bath composition and operating conditions  
of the borohydride-reduced electroless nickel bath**

<b>Bath Composition</b>	
Nickel chloride hexahydrate	30 g/l
Ethylenediamine	90 g/l
Sodium hydroxide	90 g/l
Sodium borohydride	0.8 g/l
Thallium acetate	14 mg/l
<b>Operating Conditions</b>	
pH	14.0
Temperature	95 ± 1°C

## **CHAPTER IV**

### **RESULTS AND DISCUSSION**

#### **PART A - ELECTRO- AND ELECTROLESS DEPOSITED Ni-B COATINGS**

##### **4.1 ELECTRODEPOSITED Ni-B COATING**

###### **4.1.1 COATING SYNTHESIS**

The Ni-B alloy coating is electrodeposited (ED) on mild steel substrate using a dimethylamine borane (DMAB) modified Watt's nickel plating bath using the bath composition and operating conditions given in Table 3.2. DMAB is a well known reducing agent used in electroless plating baths. It has three active hydrogen atoms bonded to the boron atom and, therefore, should theoretically reduce three nickel ions for each DMAB molecule consumed (Mallory, 1971). Hence, it is essential to ascertain whether the DMAB added in the Watt's nickel plating bath could enable the formation of Ni-B coating also by an electroless deposition mechanism. Wehner et al. (2003) have observed an improvement in throwing power of the bright nickel plating bath containing 0.034 M DMAB at 40°C. They have suggested that the improvement in throwing power of the nickel plating bath containing DMAB could be due to the overlapping of deposition of nickel by electroless and electrochemical deposition mechanisms. To separate the contributions from electro- and electroless deposition mechanisms, they have used electrochemical quartz crystal microbalance (EQCM) study and identified that 5  $\mu\text{g}/\text{cm}^2$  is the critical mass density of nickel nuclei below which the deposition of nickel will not occur by electroless deposition mechanism. The hydrolysis reaction of DMAB suggests that there is a practical lower limit for the pH of the plating bath at



which DMAB could enable deposition by an electroless deposition mechanism. Above pH 5.0, the quantity of DMAB consumed by hydrolysis approaches a minimum almost asymptotically. Mallory (1971) has suggested that the pH of a DMAB reduced electroless nickel plating bath should be maintained above pH 5.0 to minimize DMAB hydrolysis and the preferred operating pH range is around 6-7. Hence, DMAB reduced electroless plating baths are operated at  $\text{pH} \geq 6$ . In the present study, the pH of the DMAB modified Watt's nickel plating bath is maintained at  $3.5 \pm 0.2$  (Table 3.2). Hence, the possibility of deposition of nickel by an electroless deposition mechanism is less likely. Visual examination of the DMAB modified Watt's nickel plating bath reveals neither the deposition of the coating nor the hydrogen evolution even after 60 minutes of immersion of the mild steel substrate in the plating bath in the absence of applied current density. Hence, it is evident that in the experimental conditions used in the present study, DMAB does not promote deposition of nickel by an electroless deposition mechanism and it serves only as the source of boron in the plating bath. Onada et al. (1998, 1999) have also used DMAB modified nickel plating baths to prepare ED Ni-B coatings.

The deposition rate of ED Ni-B coating increases with increase in applied current density in the range of 0.4-4 A/dm<sup>2</sup>. However, at higher current densities, the current efficiency is decreased due to the competition from hydrogen evolution reaction. The deposition rate of ED Ni-B alloy coating using the bath composition given in Table 3.2 at 1 A/dm<sup>2</sup> is 12  $\mu\text{m}/\text{hour}$ . The current density also influences the chemical composition of the ED Ni-B coating (**Table 4.1**). The boron content of the ED Ni-B coating is found to decrease with increase in current density in the range of 0.4-4 A/dm<sup>2</sup>.

The mechanism of alloying of boron in ED Ni-B coating is not yet fully understood. It is presumed that the boron gets incorporated in the ED Ni-B coating due to the adsorption of DMAB on the already formed nickel surface and its subsequent decomposition to elementary boron (Onada et al., 1998, 1999). Hence, the amount of boron co-deposited with nickel is determined by the distribution of DMAB, and the thickness of the diffusion layer at the cathode surface, regardless of the electrode potential. Since, the concentration of DMAB is kept constant in the bath at 3 g/l, the amount of boron co-deposited with nickel becomes constant, regardless of the applied current density whereas the amount of nickel increases with increase in current density. Hence, it is supposed that the boron content of the ED Ni-B alloy coating is determined by the ratio of rate of reduction of nickel and rate of decomposition of DMAB. An increase in this ratio with increase in current density could be accounted for the observed decrease in boron content of the ED Ni-B coating with increase in current density in the range of 0.4-4 A/dm<sup>2</sup>. Since the amount of boron in the ED Ni-B coating is relatively low, it will be of much interest to know how the boron content could influence the structural characteristics of the resultant coating.

#### **4.1.2 SURFACE MORPHOLOGY**

The surface morphology of the ED Ni-B coatings (**Fig. 4.1**) reveals the formation of well-crystallized, uniform and fine-grained deposits. The presence of cracks observed on coatings electrodeposited at different current densities in the range of 0.4 - 4 A/dm<sup>2</sup> indicates that the coatings are highly stressed due to the hydrogen evolution that occurs during electrolysis. Fissuring had occurred

in the high current density range because of the increasing internal stress following a decrease in the boron content of the coating. This could be expected since the DMAB modified Watts nickel bath of the present study does not contain any stress relieving additives. The formation of cracks in electrodeposited nickel due to stress was also observed earlier by Lantelme and Seghioer (1998), Cui and Lee (1995), Garcia et al. (2003) and Wehner et al. (2003). Energy dispersive X-ray analysis of the Ni-B coating electrodeposited at 1 A/dm<sup>2</sup> reveals the presence of nickel (**Fig. 4.2**) whereas the presence of boron could not be indexed with confidence due to the low atomic number of boron.

#### 4.1.3 STRUCTURAL CHARACTERISTICS

The X-ray diffraction pattern of Ni-B coatings electrodeposited in the current density range of 0.4-4 A/dm<sup>2</sup> exhibits the reflections from Ni (111), Ni (200) and Ni (220) planes (**Fig. 4.3**). However, Ni-B coatings electrodeposited at a current density of 0.4 A/dm<sup>2</sup> exhibit a broadening of the Ni (111) plane, suggesting a mixture of amorphous and crystalline nature of the coating. The amorphous nature decreases with increase in current density (1 A/dm<sup>2</sup>) and at higher current densities of the order of 4 A/dm<sup>2</sup>, the coating is predominantly crystalline. The grain size of ED Ni-B coatings is of the order of 10-13 nm. Selected area diffraction (SAD) pattern of the Ni-B coating electrodeposited at 1 A/dm<sup>2</sup> (**Fig. 4.4**) further confirms the results of XRD measurement. It has been established that the extent of segregation of the metalloid alloy (phosphorous or boron) in the coating determines its crystalline nature and is found to be applicable to both Ni-P and Ni-B alloy coatings

deposited either chemically or electrochemically (Riedel, 1991; Lewis and Marshall, 1996; Duncan and Arney, 1984; Saito et al., 1998; Onada et al. 1998, 1999). The reflections from Ni (111), Ni (200) and Ni (220) planes in XRD and SAD patterns of ED Ni-B coatings obtained in the current density range of 0.4-4 A/dm<sup>2</sup> suggest that the nucleation of nickel phase is not completely prevented since the boron segregation in the ED Ni-B coating is low (Table 4.1). In all the cases studied, the reflection from Ni (111) plane is the most intense one. This observation suggests that ED Ni-B coating obtained using the DMAB modified Watt's nickel plating bath has a (111) texture. Lewis and Marshall (1996) have also observed a preferred growth of (111) orientation, relative to the (200) orientation in ED Ni-P coatings.

The grain structure of relatively pure nickel coatings electrodeposited using a Watt's nickel plating bath has been studied previously and the results indicate that following the nucleation stage, preferential growth occurs on favorably oriented grains (Mohanty et al., 2002). The growth mechanism involves deposition on pyramidal grain surfaces resulting in surface roughening and loss of substrate surface character (Argyriou and Spyrellis, 1993). Comparison with the intensities with those of randomly oriented polycrystalline nickel confirms that the relatively pure nickel electrodeposited coatings have a definite orientation of (200) planes parallel to the surface, i.e., a highly preferred <100> growth direction (McCormack et al., 2003). Amblard et al. (1979) characterized the growth of nickel as, free mode with <100> preferred crystal orientation, and, as inhibited when <110>, <211>, <210> and/or <111> grains are formed. The <111> texture was not found for microcrystalline nickel deposited from sulphate, chloride, Watts plating bath

where mainly  $\langle 100 \rangle$ ,  $\langle 110 \rangle$  and  $\langle 211 \rangle$  orientations prevailed. Czerwinski and Szpunar (1999) have observed the  $\langle 111 \rangle$  orientation as the second texture component where the main orientation was  $\langle 100 \rangle$  in nanocrystalline nickel coatings. Kozlov and Peraldo Bicelli (2003) performed theoretical calculations of crystallization overvoltage and experiments with both nickel and copper depositions and proved that the initial texture axis of f.c.c. metals is always  $\langle 111 \rangle$ . Nickel changes its orientation from  $\langle 111 \rangle$  to  $\langle 100 \rangle$  with increasing layer thickness. Bozzini (2000) found an inverse correlation between the amounts of  $\langle 111 \rangle$  oriented grains and the cathodic current efficiency. Other orientations of nickel reported are  $\langle 311 \rangle$ ,  $\langle 411 \rangle$ ,  $\langle 221 \rangle$  and  $\langle 511 \rangle$ . According to Bozzini (2000), both Ni and Ni/SiC systems showed a preference for (111) grain growth; however, the volume density in the growth direction was always lower in the nickel samples containing embedded SiC compared to pure Ni. This reduction in the amount of (111) grains was compensated by (100) type growth ((200) in XRD). According to the relative peak intensities, the nickel (220) peak decreases, the Ni (200) increases with increase in the mean current density. This indicates a change from a (110) texture to a (100) texture with increase in mean current density. For mean current densities of  $10 \text{ mA/cm}^2$  and above the intensities of the nickel peaks show similar values (Fritz et al. 2002).

Argyriou and Spyrellis (1993) suggest that the Ni (200) orientation develops preferentially only when the growth of nickel crystal is uninhibited. Preferential growth mode in electrocrystallized nickel arises due to the inhibition of other growth modes. Amblard et al. (1977) observed a relationship between the texture and current density as well as pH of electroplated nickel

layers from Watts' electrolyte. The texture shift from (110) orientation at low current densities to (100) orientation at high current densities was explained by a mechanism of specific inhibition. At low current densities, the growth of nickel crystallites is inhibited by adsorbed hydrogen, while the (100) texture at high current densities is the result of uninhibited growth. Statistically oriented electrodeposited nickel was observed in cases where stronger inhibition processes like precipitation of nickel hydroxide overcome or disturb the mechanism of adsorbed hydrogen at low current densities (Amblard et al., 1979; Valles et al., 1993). The most common inhibitors to affect the growth process are hydrogen gas, adsorbed hydrogen atoms or nickel hydroxides at the electrolyte-substrate interface. Adsorbed hydrogen inhibits growth of all crystallographic directions except (110). Gaseous hydrogen favours the preferred (210) growth direction and nickel hydroxide facilitates (211) preferred growth. Besides adsorbed hydrogen and nickel hydroxides, many other factors are also found to influence the texture of electrodeposited nickel, which include plating time, current density, presence of organic additives, nature of alloying elements, presence of second phase particles etc. (Mohanty et al. 2002; Bozzini, 2000; Fritz et al., 2002). As texture seems to be strongly related to surface adsorption process, bath temperature and electrolyte stirring would exert a strong influence on texture. Also, organic compounds in traces are known to interact with adsorbed hydrogen as well as raise the pH in the double layer (Amblard et al. 1979).

Hu et al. (1996) suggest that the preferred orientation of nickel deposits obtained using Watts nickel bath is Ni (200) when the bath pH is  $\leq 5.0$ , while it is Ni (111) when the bath pH is  $>5.0$ . For shorter plating durations, the Ni (111)

intensity is higher than that of Ni (200). For longer plating times, the Ni (200) intensity is higher than that of Ni (111). A transition exists from substrate-induced texture to the texture typical of electrodeposited conditions. The intensity ratio for thinner deposits matches that of the substrate, while the one imposed by the bath and operating conditions sets in gradually; the intensity ratio inversion occurs at a deposit thickness of a few tens of micrometers, much higher than the values required for loss of epitaxy (typical of the order of 100 nm). Mass transport has an effect on the degree of perfection of the preferred orientation of electrodeposited nickel. The texture type is (211) strongly perturbed by (111); the (200) to (111) peak intensity ratio was used to quantify the degree of perfection of the texture (the lower the value, the higher the degree of (111) preferred orientation) (Bozzini, 2000). According to Mohanty et al. (2002), the addition of  $\text{Cd}^{2+}$  or  $\text{Cr}^{3+}$  ions is found to influence the crystallographic orientation of nickel films. Bonino et al. (1998) have observed changes in the relative intensities of Ni (111) and (200) orientations for nickel electrodeposited in presence of  $\text{Co}_3\text{O}_4$ . These authors have attributed the preferred orientation changes to proton or cation  $\{\text{Ni}[\text{B}(\text{OH})_4]^+ \text{ or } \text{Ni}^{2+}\}$  adsorption. McCormack et al. (2003) showed that yttria particles inhibit the normal  $\langle 100 \rangle$  growth mode associated with the growth in the  $\langle 111 \rangle$  direction. This could be because of proton adsorption on yttria particle surface precluding the occurrence of adsorbed hydrogen at the cathode or the formation of hydrogen gas and yttria particles surrounded by  $\text{Ni}[\text{B}(\text{OH})_4]^+$  or  $\text{Ni}^{2+}$  cations adsorbed on growth centers with a  $\langle 100 \rangle$  texture.

In the present work, the pH of the bath is maintained at 3.5 and the bath does not contain any other special additives. Under such conditions, Ni (200) is expected as the preferred orientation. On the contrary, the Ni-B coatings electrodeposited in the current density range of 0.4-4 A/dm<sup>2</sup> have resulted with a Ni (111) texture. Hence, it appears that the inhibition of normal <100> growth mode is due to incorporated boron atoms in the Ni-B matrix. When the Ni-B coatings are electrodeposited using DMAB modified Watt's nickel bath, the boron atom has to be accommodated within the unit cell of f.c.c. nickel. This would induce lattice strain in the resultant Ni-B coating. It is suggested that under these conditions the growth in the (111) orientation is preferred over the (200) orientation due to a lower homogeneous strain (Ng et al. 1988; Bestgen, 1985). If this attribute is valid then there should be a correlation between boron content of the deposit (which is a function of current density, assuming all other factors remaining constant) and the ratio of the relative intensities of the Ni (111) and Ni (200) to the sum of the intensities of Ni (111), Ni (200) and Ni (220) reflections. The variation in the intensity ratio of Ni (111) to the sum of the intensities of Ni (111), Ni (200) and Ni (220) reflections as a function of current density (**Fig. 4.5(a)**) shows the preference of Ni (111) orientation at low current densities of the order of 0.4 A/dm<sup>2</sup> where the boron content of the coating is relatively higher. With increase in current density and a consequent decrease in boron content of the coating, the preferred orientation is changed from Ni (111) to Ni (200) (**Fig. 4.5(b)**). Hence, it is evident that the Ni (111) texture of electrodeposited Ni-B coatings has resulted following the accommodation of boron within the unit cell of f.c.c. nickel.



Annealing of ED Ni-B coatings at 400°C for 1 hour results in an enhancement of the intensities of nickel diffraction lines and the formation of bct-Ni<sub>3</sub>B phase (**Fig. 4.6**), which is further confirmed by the SAD pattern (**Fig. 4.7**). The grain size of the ED Ni-B coatings is of the order of 17-20 nm. The extent of Ni<sub>3</sub>B phase formation is relatively higher for Ni-B coatings electrodeposited at 0.4 A/dm<sup>2</sup> than the one obtained at higher current densities, which is directly a function of the boron content of the coating. However, even for Ni-B coatings electrodeposited at 0.4 A/dm<sup>2</sup> and annealed at 400°C for 1 hour, the volume fraction of Ni<sub>3</sub>B (201) phase is less than that of Ni (111) phase, which suggests the predominance of crystalline nickel over the Ni<sub>3</sub>B phase. Moreover, the ED Ni-B coatings retain the (111) texture even after annealing at 400°C for 1 hour.

Electrodeposited metals and alloys, in general, are not in a state of equilibrium and are prone to substantial changes during heating to a high temperature. Texture is a very sensitive indicator of such structural changes that occur within deposits at elevated temperatures (Czerwinski et al., 1999). Czerwinski and Szpunar (1999) suggest that texture evolution during annealing depends strongly on the deposit microstructure and in particular on grain size and its distribution. According to them, deposits consisting of uniform grains, with no sub-micro or nano-size components, exhibit high texture stability at elevated temperatures and microcrystalline electrodeposits with coarse grains, due to the relatively low excess free energy, are expected to preserve their unique behavior of an as-deposited state even at elevated temperatures (Czerwinski and Szpunar, 1999). Recrystallization and/or grain growth are considered as the major factors responsible for the observed changes in texture

during annealing of electrodeposits. For ED nickel coatings with grains of the order of micrometers, the recrystallization temperature is rather high. Jacobson and Sliwa (1972) observed the beginning of the recrystallization of nickel electrodeposits with a grain size between 0.2 and 3  $\mu\text{m}$  at 400°C, while recrystallization was completed at 600°C. Lee (2001, 2002) suggests that the occurrence of recrystallization process is to reduce the stored energy, which includes energies due to vacancies, dislocations, grain boundaries, surface etc. The most important driving force for recrystallization is known to be the stored energy due to dislocations. However, dislocations cannot be related to the recrystallization texture, unless they give rise to some anisotropic characteristics. Lee (2001, 2002) has proposed the strain energy release maximization (SERM) model for the evolution of the recrystallization textures. According to this model, when the absolute maximum internal stress directions is the same as the minimum elastic modulus direction of the material concerned, the fabrication texture of the material does not change during annealing, whether it may be recovery or recrystallization. Hence, the observed (111) texture of the ED Ni-B coatings even after annealing at 400°C for 1 hour could be due to the uniform grain size in the range of 17-20 nm and according to the SERM model.

#### **4.1.4 THERMAL CHARACTERISTICS**

Electrodeposited Ni-B coatings undergo phase transformation upon heat-treatment, which is best characterized by differential scanning calorimetry (DSC). The DSC trace of ED Ni-B coating prepared at 0.4 and 4  $\text{A}/\text{dm}^2$ , in the temperature range from 200 to 500°C at heating rate of 10K/min., are shown in

**Fig. 4.8(a)** and **Fig. 4.8(b)**, respectively. Two distinct exothermic peaks are observed for Ni-B coatings electrodeposited at 0.4 and 4 A/dm<sup>2</sup>. For the Ni-B coating prepared at 0.4 A/dm<sup>2</sup>, the first exothermic peak occurs over a temperature range of 240 to 340°C with a peak temperature of 300.9°C whereas the second exothermic peak occurs over a temperature of 340 to 408°C with a peak temperature of 367.9°C. For the Ni-B coating prepared at 4 A/dm<sup>2</sup>, the first exothermic peak occurs over a temperature range of 292 to 415°C with a peak temperature of 370.9°C whereas the second exothermic peak occurs over a temperature of 415 to 500°C with a peak temperature of 459.1°C. It has been reported in the literature that phase transformation from an amorphous to crystalline structure occurs over a narrow temperature range of 30 to 50°C and broad exothermic peaks are characteristic of nanocrystalline materials (Allen and Vander Sande, 1982; Mahoney and Dynes, 1985; Hur et al., 1990; Balaraju, 2000; Keong et al., 2002a, 2002b; Guo et al., 2003; Balaraju et al., 2006; Baskaran et al. 2006a). The temperature range at which the phase transformation of Ni-B coatings occurs is quite large and indicates the nanocrystalline nature of the Ni-B coating, which is also confirmed by X-ray diffraction measurements (Fig. 4.2). The grain size of ED Ni-B coatings (10-13 nm) also confirms that they are nanocrystalline in nature. The exothermic peak gives a measure of the heat liberated during the phase transformation. The energy evolved during the exothermic transition, calculated from the area of the exothermic peaks is -81.4 and -23.68 J/g for the first and second peaks, respectively for Ni-B coatings electrodeposited at 0.4 A/dm<sup>2</sup>. The corresponding values for Ni-B coatings electrodeposited at 4 A/dm<sup>2</sup> are -64.3 and -33.84 J/g. The peak temperature of the ED Ni-B

coatings are comparable to the values obtained for similar deposits reported elsewhere (Lee, 2005).

Onada et al. (1998, 1999) and Lee et al. (2005) have found a correlation between the peak temperature and the boron content of the Ni-B coating. According to them, the Ni-B coatings with the smallest amount of boron (2-6 at.%) exhibit only a single exothermic peak with its peak temperature between 360 and 380°C. As the amount of boron in the Ni-B coating increases, a shift was observed in the exothermic peak towards lower temperatures and when the amount of boron exceeds a critical level (24.40 at.%), the exothermic peak splits into two peaks. As the amount of co-deposited boron increases, the crystallization temperature decreases. This trend ceases around 18 at% boron, which is the eutectic point on the Ni-B thermal equilibrium diagram, and the crystallization temperature rises again until the boron content reaches 25 at%. On the other hand, the exothermic energy increases linearly up to approximately 24 at% boron and increases sharply thereafter. When the amount of boron in the plated film is less than the eutectic composition of 18 at% boron, the fine nickel crystals which exist in the plated film grow with increase in heat-treatment temperature, resulting in exothermic peaks. Hence, the first exothermic peak observed at 300.9 and 370.9°C for Ni-B coatings electrodeposited at 0.4 and 4 A/dm<sup>2</sup>, respectively, can be attributed to the precipitation of metallic nickel phase and formation of orthorhombic Ni<sub>3</sub>B phase. The difference in peak temperature is due to the difference in boron content of these coatings which is also reflected in the amount of energy evolved during the phase transformation. The second exothermic peak observed at 367.9°C for Ni-B coatings electrodeposited at 0.4 A/dm<sup>2</sup> could be

due to splitting of the exothermic peak suggested by Onada et al. (1998, 1999). Splitting of exothermic peak is generally reported for hypoeutectic Ni-P alloy coatings (Rajam et al., 1993) due to the differences in activation energy for crystallization from partially crystallized matrix and amorphous matrix. Though such occurrence is not prevalent in eutectic Ni-P alloys, Rajam et al. (1993) and Balaraju (2000) suggest that these peaks too may show splitting. The second exothermic peak observed at 459.1°C for Ni-B coating electrodeposited at 4 A/dm<sup>2</sup> could be due to the recrystallization and growth of Ni<sub>3</sub>B phase.

#### 4.1.5 MICROHARDNESS

The microhardness of Ni-B coatings electrodeposited at 1 A/dm<sup>2</sup> is determined in both as-plated and heat-treated conditions (200, 300, 350, 400, 450 and 600°C for 1 hour). The microhardness of as-plated ED Ni-B coating is of the order of 609 ± 15 HV<sub>0.1</sub>, which is considerably high compared to that of bulk Ni (100-150 HV<sub>0.1</sub>) and ED Ni (250-350 HV<sub>0.1</sub>). The hardness increases to 817 ± 20 HV<sub>0.1</sub> when the coating is heat-treated at 400°C for 1 hour. **Fig. 4.9** shows the variation in hardness of ED Ni-B coatings as a function of heat-treatment temperature. Compared to the hardness of ED Ni-B coating in as plated condition, there is not much change in the hardness when the heat-treatment temperature is of the order of 200°C. With further increase in temperatures, however, the hardness increases rapidly, as the structure of the coatings begins to change. The hardness versus heat treatment temperature curve resembles that of a bell shape with its maximum at 400°C. Beyond 400°C, the hardness decreases. The increase in hardness is due to the

precipitation of nickel boride ( $\text{Ni}_3\text{B}$ ), which is confirmed by XRD measurement (Fig. 4.4). At temperatures above  $400^\circ\text{C}$ , the ED Ni-B coating begins to soften as a result of coarsening of the  $\text{Ni}_3\text{B}$  particles, which thereby reduces the number of hardening sites. Similar behaviour of change in hardness with heat treatment temperature was also observed for electroless Ni-P and Ni-B coatings (Balaraju and Seshadri, 1998, 1999; Balaraju, 2000; Gorbunova et al., 1973; Sankara Narayanan and Seshadri, 2004).

#### 4.1.6 WEAR RESISTANCE

The wear resistance of ED Ni-B coatings, both in as-plated and heat-treated ( $400^\circ\text{C}$  for 1 hour) conditions is studied using three different applied normal loads, namely, 8, 10 and 12 N. The specific wear rate, calculated using the loss in weight due to wear, is given in **Table 4.2**. The specific wear rate is a measure of the ability of the ED Ni-B coatings to offer wear resistance against the hard counterface material (hardened steel of EN 31). The increase in specific wear rate with increase in applied normal load from 8 to 12 N indicates a decrease in wear resistance at higher applied loads and this trend is common for both as-plated and heat-treated ED Ni-B coatings. The wear resistance is higher for heat-treated ED Ni-B coatings compared to those obtained in as-plated condition. The better wear resistance obtained for heat-treated ED Ni-B coatings is due to the formation of hard nickel boride ( $\text{Ni}_3\text{B}$ ) phase, which enables the ED Ni-B matrix to experience a lesser wear. Besides the hardness of the matrix, the mutual solubility of atoms of the mating surfaces (nickel and iron) could also influence the wear resistance. In as-plated condition, the high mutual solubility of iron (steel counterface) and nickel

(coated steel) could induce a substantial attractive force between the mating surfaces, resulting in lower wear resistance. Heat-treatment enables the formation of hard  $\text{Ni}_3\text{B}$  phase, which has a low mutual solubility with iron resulting in an incompatible surface with the steel counterface, thereby increasing the wear resistance.

The average friction coefficient,  $\mu_{av}$  of ED Ni-B coatings, both in as-plated and heat-treated conditions, is also given in Table 4.2. The average coefficient of friction is less for heat-treated ED Ni-B coatings compared to the as-plated ones. The low coefficient of friction obtained for ED Ni-B coatings subjected to heat treatment could be accounted to a combination of factors, namely, the formation of hard  $\text{Ni}_3\text{B}$  phase, the low mutual solubility between the iron and the borides and the formation of iron oxide film. As already explained, the presence of hard  $\text{Ni}_3\text{B}$  phase and the decrease in mutual solubility between the boride and iron has resulted in the decrease in coefficient of friction. Besides these, the buildup of oxides could act as a lubricant film at the interface and it might also decrease the coefficient of friction in the case of heat-treated coatings. Examination of the heat-treated ED Ni-B coatings after wear test using optical microscopy clearly reveals the presence of adherent iron oxide particles, confirming that the iron oxide film is also responsible for the decrease in coefficient of friction of heat treated ED Ni-B coatings (**Fig. 4.10**).

The mechanism of wear of ED Ni-B coating depends on the attractive force between the atoms of nickel from the coating and iron from the counter disk. The main wear mechanism of the ED Ni-B coating is severe shearing of the surface layers of the coating due to the ploughing action of the hard counter

disk (**Fig. 4.11(a) and 4.11(b)**) (hardened steel of EN 31) (Panagopoulos et al., 2000a, 2003). The transferred patches from the ED Ni-B coatings and the wear debris present on the surface of the counter disk clearly indicate that an adhesion between the Ni-B coated mild steel pins and the counter disk had occurred. The possibility of occurrence of adhesive wear under the experimental conditions used is also supported by the high mutual solubility of nickel and iron. Hence, adhesive wear appears to be the most likely mechanism during the wear process of ED Ni-B coatings in their as-plated condition. In contrast to the as-deposited coatings, heat-treated coatings, after wear, exhibit a bright and smooth finish with fine grooves along the sliding direction (**Fig. 4.11(c) and 4.11(d)**). The loose debris generated during the wear process gets displaced to the sides leading to the formation of grooves along the wear track. In a substantial portion of the wear tracks, no gross adhesion between the coated pins and the counter disk is observed. In support of the morphological features of the wear track pattern, the roughness of heat-treated ED Ni-B coating is low, compared to that of the as-plated coating. The  $R_a$  value of ED Ni-B coating after wear testing at a load of 12 N is 0.55  $\mu\text{m}$  in as-plated and 0.25  $\mu\text{m}$  in heat-treated conditions. The relatively lower  $R_a$  value obtained for heat treated ED Ni-B coatings compared to those of the as plated ones is due to the increase in hardness leading to glazing of these deposits against the counterface material and strongly support the above wear mechanism suggested for heat-treated coatings. Besides these features, the scanning electron micrographs (Fig. 4.11(c) and 4.11(d)) also exhibit the presence of some cracks, which could have been generated due to the brittleness of the heat-treated coating.



#### 4.1.7 CORROSION RESISTANCE

The potentiodynamic polarization curves of ED Ni-B coatings in 3.5% sodium chloride solution, both in as-plated and heat-treated (400°C for 1 hour) conditions, are shown in **Fig. 4.12(a)**. The corrosion potential ( $E_{\text{corr}}$ ) and corrosion current density ( $i_{\text{corr}}$ ), calculated using the Tafel extrapolation method are given in **Table 4.3**. The  $E_{\text{corr}}$  and  $i_{\text{corr}}$  of as-plated ED Ni-B coating are -584 mV vs. SCE and 12.31  $\mu\text{A}/\text{cm}^2$ , respectively. However, heat-treatment of the ED Ni-B coating at 400°C for 1 hour results in a shift in the  $E_{\text{corr}}$  value towards more negative values (from -584 to -680 mV vs. SCE) and an increase in the  $i_{\text{corr}}$  value from 12.31 to 24.10  $\mu\text{A}/\text{cm}^2$ . The decrease in the linear polarization resistance (LPR) value from 1120 to 562 ohms. $\text{cm}^2$  also suggests a decrease in corrosion resistance of heat-treated ED Ni-B coatings. To confirm this aspect further, the current-time transient curves of the ED Ni-B coatings, both in as-plated and heat-treated (400°C for 1 hour) conditions, is recorded (**Fig. 4.12(b)**). It has been established that reduction of oxygen and dissolution of nickel are the major reactions occurring during cathodic and anodic polarization, respectively. Hence, the increase in current should have been due to the dissolution of nickel from the coating. To compare the ability of the as-plated and heat-treated ED Ni-B coatings, the time to reach a steady state current of 0.1 mA/ $\text{cm}^2$  is taken as a failure criterion (Table 4.3). It is evident from Fig. 4.12(b) and Table 4.3 that the corrosion resistance of ED Ni-B coatings after heat-treatment is considerably decreased.

Several factors, which include, the composition of the coating, grain size, porosity, structure, surface features and heterogeneity of the coating, could influence the corrosion resistance of electro- and electroless plated deposits. The coating thickness of the ED Ni-B coatings used for corrosion study is 20  $\mu\text{m}$ . Hence, the contribution from the porosity factor is expected to be minimal. In as-plated condition, the ED Ni-B coating is nanocrystalline in nature and its grain size is 10-13 nm. However, after heat-treatment at 400°C for 1 hour, the ED Ni-B coating becomes crystalline with the formation of crystalline Ni and  $\text{Ni}_3\text{B}$  phases and, the grain size is increased to 17-20 nm. Scanning electron micrographs of the ED Ni-B coating indicate the presence of cracks (Fig. 4.3). Since the DMAB modified Watts nickel bath of the present study does not contain any stress relieving additives, it is understandable that the ED Ni-B coatings become highly stressed due to the hydrogen evolution that occurs during electrolysis. The internal stress is responsible for the cracks in these coatings. This type of surface feature could allow the transport of corrosive medium through them. Hence, it is evident that the nanocrystalline nature and presence of cracks are primarily responsible for the observed corrosion behaviour of the ED Ni-B coating in their as-plated condition. Heat-treatment induces crystallinity of the ED Ni-B coating, which in turn increases the grain boundaries which are the active sites for corrosion attack.

The Nyquist plots of ED Ni-B coatings in 3.5% sodium chloride solution, both in as-plated and heat-treated conditions (400°C for 1 hour) at their respective open circuit potentials is shown in **Fig. 4.13**. The  $R_{\text{ct}}$  and  $C_{\text{dl}}$  values, calculated after fitting the data using Boukamp software are given in Table 4.3. The  $R_{\text{ct}}$  and  $C_{\text{dl}}$  values of as-plated ED Ni-B coating are

2707 ohms.cm<sup>2</sup> and 129  $\mu\text{F}/\text{cm}^2$ , respectively. However, heat-treatment of the ED Ni-B coating at 400°C for 1 hour results in a decrease in  $R_{ct}$  value from 2707 to 1710 ohms.cm<sup>2</sup> and an increase in  $C_{dl}$  value from 129 to 184  $\mu\text{F}/\text{cm}^2$ . It has been established that high values of  $R_{ct}$  and low values of  $C_{dl}$  imply a better corrosion protective ability of coatings (Van der Kouwe, 1993). The  $C_{dl}$  value is related to the porosity of the coating (Growcock and Jasinski, 1989). The higher  $C_{dl}$  values of ED Ni-B coatings of the present study suggest that the cracks in the coating have allowed penetration of the electrolyte through them.

It is evident from Fig. 4.13 that ED Ni-B coatings, both in as-plated and heat-treated conditions (400°C for 1 hour), exhibit a semicircle in the high frequency region followed by a loop in the low frequency region. Though the curves in the Nyquist plot appear to be similar with respect to their shape, they differ considerably in their size. This indicates that the same fundamental processes must be occurring on both the as-plated and heat-treated ED Ni-B coatings but over a different effective area in each case. The formation of a single semicircle or a semicircle in the high frequency region followed by a low frequency loop is typical of metallic coatings. The semicircle at high frequency region represents the coating response, while the loop at low frequency region is associated with simultaneous physicochemical phenomena at the metal/coating/solution interface (Atkinson and Smart, 1988; Balaraju and Seshadri, 1998; Lo et al., 1995; Contreras et al., 2006). According to Mansfeld et al. (1982) the loop at the lower frequency region is associated with the double layer capacitance and/or diffusion phenomena of the oxidant chemical species through the porous coating.

In order to get a better insight about the coating response as well as the diffusion phenomenon, Bode plots ( $\text{Log } f$  vs.  $\text{Log } |Z|$  and  $\text{Log } f$  vs Phase angle) were constructed. The Bode plots of ED Ni-B coating, both in as-plated and heat-treated conditions ( $400^{\circ}\text{C}$  for 1 hour), indicate the presence of two phase angle maxima (**Fig. 4.14**), suggesting the involvement of two time constants. The two phase angle maxima could be related to the electrolyte/coating and the electrolyte/substrate interface. The occurrence of the second phase angle maximum clearly indicates that the electrolyte has penetrated via cracks in these coatings to create another interface, namely, the electrolyte/substrate. The surface morphology of the ED Ni-B coatings (Fig. 4.3) strongly supports this view. The cracks in the ED Ni-B coatings enable the electrolyte to penetrate through them. The Bode plots (Fig. 4.14) also indicate the involvement of a diffusion phenomenon in the low frequency region.

## 4.2 ELECTROLESS Ni-B COATINGS

### 4.2.1 COATING SYNTHESIS

The formulation of borohydride-reduced electroless (EL) nickel plating bath allows only a narrow window of opportunity. Since sodium borohydride readily hydrolyzes in acidic or neutral condition, the plating bath should be alkaline, preferably the pH should be higher than 12. This warrants the addition of higher concentration of alkali, which in turn necessitates the presence of an effective complexing agent in the bath. Ethylenediamine is the most preferred complexing agent for borohydride-reduced electroless nickel plating bath (Gorbunova et al., 1973). The selection of stabilizer is very critical. Although lead nitrate and mercaptobenzothiazole are good in stabilizing the plating bath, the plating rate is poor in these baths. The only choice to achieve better bath stability and higher deposition rate is the addition of thallium compounds as stabilizers. This is due to the ability of thallium ions, which not only stabilizes the plating bath but also increases the reduction efficiency of borohydride (Duncan and Arney, 1984). The rate of deposition of EL Ni-B coatings is found to be a function of molar ratio of ethylenediamine to nickel. The plating rate increases with increase in temperature whereas it decreases with increase in molar ratio of ethylenediamine to nickel. The rate of deposition of EL Ni-B coatings as a function of plating time is given in **Fig. 4.15**. The thickness of EL Ni-B coating increases with increase in plating time. However, the extent of increase in thickness is not linear throughout the entire duration of plating and it saturates after some time. This is due to the decrease in the concentration of borohydride and accumulation of oxidation product(s) of borohydride in the plating bath. The plating rate of EL Ni-B coatings obtained using the bath

composition and operating conditions given in Table 3.3 is 18-20  $\mu\text{m}/\text{hour}$ . The EL Ni-B coatings of the present investigation are matte in appearance and dark gray in colour. The EL Ni-B coating contains 93.2 wt.% nickel, 6.5 wt.% boron and 0.3 wt.% thallium. The incorporation of thallium along with nickel and boron is due to the use of thallium acetate as the stabilizer in the plating bath, which is also confirmed by other researchers (Duncan and Arney, 1984; Gorbunova et al., 1973; Baudrand, 1994; Delaunois and Lienard, 2002).

#### 4.2.2 SURFACE MORPHOLOGY

The scanning electron micrographs of EL Ni-B coatings obtained at 0.4 and 0.8 g/l of  $\text{NaBH}_4$  are shown in **Fig. 4.16 (a & b)** and **Fig. 4.16 (c & d)**, respectively. The EL Ni-B coatings are uniform. The morphology of EL Ni-B coatings resembles a typical cauliflower type feature, characteristic of electroless plated nickel coatings (Delaunois et al., 2000; Delaunois and Lienard, 2002). A comparison of the morphological features of the EL Ni-B coatings obtained using 0.4 and 0.8 g/l of  $\text{NaBH}_4$  reveals that the size of the nodules increases with increase in concentration of  $\text{NaBH}_4$ . An increase in the size of the nodules of the EL Ni-B coatings with increase in concentration of  $\text{NaBH}_4$  in the plating bath was also reported by Baskaran et al. (2006b). These nodules combined to form a granular type structure, which makes the EL Ni-B coatings naturally lubricious and enables them to achieve a higher wear resistance by reducing the surface contact (Delaunois et al., 2000; Delaunois and Lienard, 2002). Energy dispersive X-ray analysis of EL Ni-B coating reveals the presence of nickel and thallium (**Fig. 4.17**). The presence of boron could not be indexed with confidence due to the low atomic number of boron.

### 4.2.3 STRUCTURAL CHARACTERISTICS

X-ray diffraction (XRD) pattern of the EL Ni-B coating in its as-plated condition is shown in **Fig. 4.18**. The XRD pattern exhibits a single broad peak indicative of the amorphous nature of the coating. Theoretically, a disorder in arrangement of atoms manifests itself as a broad peak in XRD (Warren, 1969). In electroless deposition process, the extent of segregation of metalloid alloy in the coating determines its crystallinity. Since the required boron segregation (6.5 wt.%) is relatively large, nucleation of the nickel phase is prevented and this has resulted in an amorphous structure. The grain size of as-plated EL Ni-B coating is of the order of 2-3 nm. The microstructure of the EL Ni-B coating assessed by transmission electron microscope (TEM) confirms its amorphous nature in its as-plated condition. The selected area diffraction (SAD) pattern reveals the presence of diffused halo rings, which is a typical characteristic of amorphous structure (**Fig. 4.19(a)**). Watanabe and Tanabe (1983), Srivastava et al. (1992a, 1992b) and Evans and Schlesinger (1994) have also observed the amorphous nature of electroless Ni-B coatings in the same composition range. However, TEM analysis carried out at different regions, indicate the presence of micro cracks, which spreads throughout the film and their presence is more pronounced at the edges (**Fig. 4.19(b)**). Analysis performed at the cracks/boundary regions reveals the presence of nanometer-sized crystals, which are concentrated in these regions. The dark field image confirms the presence of very small crystallites (white spots), which are nanocrystalline in size (**Fig. 4.19(c)**). Hence, it can be inferred that the EL Ni-B coatings in their as-plated condition consist of two phases; the major part is amorphous whereas a small portion of it is nanocrystalline.

Heat-treatment of the EL Ni-B coating results in the transformation of the amorphous phase to crystalline nickel and nickel boride phases. XRD pattern of EL Ni-B coatings heat-treated at 325°C for 1 hour indicates the formation of crystalline nickel and Ni<sub>3</sub>B phases (**Fig. 4.20**) whereas those heat-treated at 450°C for 1 hour indicates the formation of crystalline nickel, Ni<sub>3</sub>B and Ni<sub>2</sub>B phases (**Fig. 4.21**). The grain size of EL Ni-B coating after heat-treatment at 450°C for 1 hour is of the order of 8-10 nm. The formation of nickel boride phases upon heat-treatment of EL Ni-B deposits was also shown by many researchers (Gorbunova et al., 1973; Duncan and Arney, 1984; Delaunois and Lienard, 2002; Baskaran et al., 2006b). Heat-treatment at temperatures higher than 450°C results in the growth of crystalline nickel and causes conversion of Ni<sub>2</sub>B phase to the more stable Ni<sub>3</sub>B phase. XRD pattern of EL Ni-B coating heat-treated at 600°C for 1 hour indicates the absence of Ni<sub>2</sub>B phase and presence of nickel and Ni<sub>3</sub>B phases, with nickel being the predominant phase (**Fig. 4.22**).

The bright field image of EL Ni-B coating heat-treated at 325°C for 1 hour indicates the formation of well-developed crystallites (**Fig. 4.23 (a)**). The regions which appear white in colour are due to the precipitation of crystalline nickel. The corresponding SAD pattern exhibits the characteristic features of crystalline nickel (**Fig. 4.23 (b)**). TEM micrograph of EL Ni-B coating heat-treated at 450°C for 1 hour reveals an increase in size of the nickel particles (**Fig. 4.24 (a)**). The SAD patterns taken at different regions reveal the presence of nickel and Ni+Ni<sub>3</sub>B phases (**Figs. 4.24 (b & c)**).



#### 4.2.4 THERMAL CHARACTERISTICS

EL Ni-B coatings undergo phase transformation upon heat-treatment, which is best characterized by differential scanning calorimetry (DSC). **Fig. 4.25** depicts the DSC trace of EL Ni-B coating in the temperature range from 50 to 550°C at heating rate of 10K/min. Two distinct exothermic peaks are evident; the first one is seen at 307.5°C whereas the second one is noticed at 418°C. Literature reports on the DSC traces obtained for electroless Ni-B deposits indicate that the number of exothermic peaks and the temperature range at which they occur is a function of the boron content of the film (Watanabe and Tanabe, 1983; Srivastava et al., 1992a). Accordingly, for EL Ni-B films with less than 6 at.% of boron, DSC curves hardly exhibit any thermal effects corresponding to phase formation. For films having 6-20 at.% boron, a single exothermic peak around 300-350°C is prevalent. The exact position of this exothermic peak in this temperature range depends on the boron content of the film; the higher the boron content, the earlier the occurrence of the peak. For films having higher than 20 at.% boron, besides the crystallization of nickel and Ni<sub>3</sub>B phase, the formation of Ni<sub>2</sub>B phase is evident at higher temperatures above 400°C. Thermograms of Ni-B films having boron content higher than 30 at.%, exhibit a single broad exothermic peak at 410-415°C. The chemical composition of the EL Ni-B coating of the present study reveals that the boron content is 6.5 wt.%, which falls in the range of 20-30 at.%. Hence, the exothermic peak that occurs at 307.5°C can be attributed to the precipitation of metallic nickel phase and formation of orthorhombic Ni<sub>3</sub>B phase. Similarly the exothermic peak that occurs at 418°C

would corroborate the formation of  $\text{Ni}_2\text{B}$  phase. XRD patterns of EL Ni-B coatings heat-treated at 325 and 450°C for 1 hour ascertain the formation of  $\text{Ni}_3\text{B}$  and  $\text{Ni}_2\text{B}$  phases, respectively, at these temperatures (Figs. 4.20 and 4.21).

The estimation of rate of liberation of hydrogen from the EL Ni-B coating during annealing is of great significance. Evolved gas analysis (EGA) performed using the EL Ni-B coating of the present study clearly reveals the liberation of hydrogen upon annealing (**Fig. 4.26**). It is obvious that the hydrogen occluded during plating should be liberated before the formation of new phases. It is evident from Fig. 4.26 that the rate of liberation of hydrogen is higher at two distinct regions: at temperatures just below the point at which  $\text{Ni}_3\text{B}$  and  $\text{Ni}_2\text{B}$  phase formation occurs, complementing the results obtained using DSC and XRD.

#### 4.2.5 MICROHARDNESS

The microhardness ( $\text{HV}_{0.1}$ ) of EL Ni-B coatings is determined in both as-plated and heat-treated conditions (200, 300, 350, 400, 450 and 600°C for 1 hour). The microhardness of EL Ni-B coating is of the order of  $570 \pm 14 \text{ HV}_{0.1}$  for as-plated coatings and  $908 \pm 17 \text{ HV}_{0.1}$  for coatings heat-treated at 450°C for 1 hour, which is comparable with the values reported in literature for similar coatings (Duncan and Arney, 1984; Gorbunova et al., 1973; Delaunois et al., 2002). **Fig. 4.27** shows the variation in the hardness of EL Ni-B coatings as a function of the heat treatment temperature. Compared to the hardness of the EL Ni-B coating in as plated condition, there is not much change in hardness at lower temperatures of the order of 200°C. With further

increase in temperatures, however, the hardness increases rapidly, as the structure of the coating begins to change. The hardness vs. heat treatment temperature curve exhibits two maxima, the first maximum occurs at 350°C whereas the second maximum occurs at 450°C. Beyond 450°C, the hardness decreases. The increase in hardness is due to the precipitation of nickel borides,  $\text{Ni}_3\text{B}$  and  $\text{Ni}_2\text{B}$ . The formation of these phases is confirmed by XRD measurement (Figs. 4.20 and 4.21). At temperatures above 450°C, the coating begins to soften as a result of coarsening of the  $\text{Ni}_3\text{B}$  particles, which thereby reduces the number of hardening sites. Gorbonova et al. (1973) have also observed a similar behaviour of change in hardness with heat treatment temperature for borohydride-reduced EL Ni-B coatings.

#### 4.2.6 WEAR RESISTANCE

The specific wear rate of EL Ni-B coatings, both in as-plated and heat treated conditions, obtained at different applied loads is given in **Table 4.4**. The specific wear rate increases with increase in applied load from 20 to 40 N and this trend is common for both as-plated and heat-treated EL Ni-B coatings. At all applied loads the specific wear rate is less for heat-treated EL Ni-B coatings compared to the as-plated ones. This is due to the formation of hard nickel boride phases following heat-treatment, which presents a virtually incompatible surface for the counterface material, as there exists very little solubility between iron and these hard phases. Besides, following heat treatment, there is a considerable increase in the hardness of the coatings. Hence, when the counterface material comes in contact with the matrix, because of the high hardness, the EL Ni-B matrix experiences lesser wear.

The coefficient of friction recorded simultaneously during the wear test clearly reveals the characteristics of the wear process. The average friction coefficient,  $\mu_{av}$  of EL Ni-B coatings in as-plated and heat-treated conditions, is given in Table 4.4. The coefficient of friction is less for heat-treated EL Ni-B coatings compared to that obtained for as-plated ones. As already mentioned, this is due to the ability of the heat-treated EL Ni-B coatings to present a virtually incompatible surface for the hard counterface material. The relationship between the coefficient of friction and the sliding distance of EL Ni-B coating, heat treated at 450°C for 1 hour, is shown in **Fig. 4.28**. The coefficient of friction though exhibit an initial abrupt increase, it stabilizes after some distance, which signifies the removal of coating and the onset of a friction process between the counter disc and the coated mild steel pins, perhaps with some coating particles entrapped in the contact.

The mechanism of wear of EL Ni-B coating depends on the attractive force that operates between the atoms of nickel from the coating and iron from the counter disk (hardened steel of EN 31 specification). The scanning electron micrographs of EL Ni-B coatings subjected to pin-on-disc wear test clearly indicate the presence of torn patches and, in some places even detachment of the coating, in their as-plated condition (**Fig. 4.29 (a & b)**). This type of morphological feature, commonly called as “prows” is reported for adhesive wear failure of EL Ni-P coatings, by several researchers (Staia et al., 1996; Gawne and Ma, 1987a, 1987b; Kanani, 1991; Dennis and Sagoo, 1991; Balaraju, 2000). The transferred patches from the EL Ni-B coatings and the wear debris are also observed on the surface of the counter disc, which clearly indicates that adhesion between the EL Ni-B coated mild steel pins and the

counter disc had occurred. The possibility of occurrence of adhesive wear under the experimental conditions used is also supported by the high mutual solubility of nickel and iron. Hence, adhesive wear appears to be the most likely mechanism during the wear process of EL Ni-B coatings in their as-plated condition. In contrast to the as-deposited coatings, heat-treated coatings after wear exhibit bright and smooth finish with fine grooves along the sliding direction (**Figs. 4.29 (c-f)**). In a substantial portion of the wear tracks, no gross adhesion between the coated pins and the counter disc is observed. In support of the morphological features of the wear track pattern, the  $R_a$  value is relatively less for heat treated EL Ni-B coatings. The  $R_a$  value of EL Ni-B coating after wear testing at a load of 40 N is 0.18  $\mu\text{m}$  in as-plated and 0.12  $\mu\text{m}$  in heat-treated conditions. The increase in coating hardness following heat-treatment increases the plastic resistance of the coating and decreases the true area of contact between the mating surfaces, supporting the observed decrease in friction coefficient in the case of these deposits. The loose debris generated during the wear process gets displaced to the sides leading to the formation of grooves along the wear track.

#### 4.2.7 CORROSION RESISTANCE

The potentiodynamic polarization curves of EL Ni-B coatings in 3.5% sodium chloride solution, both in as-plated and heat-treated (450°C for 1 hour) conditions, are shown in **Fig. 4.30(a)**. The corrosion potential ( $E_{\text{corr}}$ ) and corrosion current density ( $i_{\text{corr}}$ ), calculated using the Tafel extrapolation method are given in **Table 4.5**. The  $E_{\text{corr}}$  and  $i_{\text{corr}}$  of as-plated EL Ni-B coating are -506 mV vs. SCE and 8.41  $\mu\text{A}/\text{cm}^2$ , respectively. However, heat-treatment

of the EL Ni-B coating at 450°C for 1 hour results in a shift in the  $E_{\text{corr}}$  value towards more negative values (from -506 to -593 mV vs. SCE) and an increase in the  $i_{\text{corr}}$  value from 8.41 to 19.23  $\mu\text{A}/\text{cm}^2$ . The decrease in the linear polarization resistance (LPR) value from 2558 to 1025  $\text{ohms}\cdot\text{cm}^2$  also suggests a decrease in corrosion resistance of heat-treated EL Ni-B coatings. To confirm this aspect further, the current-time transient curves of the EL Ni-B coatings, both in as-plated and heat-treated (450°C for 1 hour) conditions, is recorded (**Fig. 4.30(b)**). It has been established that reduction of oxygen and dissolution of nickel are the major reactions occurring during cathodic and anodic polarization, respectively. Hence, the increase in current should have been due to the dissolution of nickel from the coating. To compare the ability of the as-plated and heat-treated EL Ni-B coatings, the time to reach a steady state current of 0.05  $\text{mA}/\text{cm}^2$  is taken as a failure criterion (Table 4.5). It is evident from Fig. 4.30(b) and Table 4.5 that the corrosion resistance of EL Ni-B coatings after heat-treatment is considerably decreased.

Several factors, which include, the composition of the coating, grain size, porosity, structure, surface features and heterogeneity of the coating, could influence the corrosion resistance of electro- and electroless plated deposits. The coating thickness of the EL Ni-B coatings used for the evaluation of corrosion resistance is 20  $\mu\text{m}$ . Hence, the contribution from the porosity factor is expected to be minimal. The codeposition of thallium along with nickel and boron could induce surface heterogeneity in EL Ni-B coatings. In as-plated condition, the EL Ni-B coating is amorphous and its grain size is of the order of 2-3 nm. However, after heat-treatment at 450°C for 1 hour, the

EL Ni-B coating becomes crystalline with the formation of crystalline Ni, Ni<sub>3</sub>B and Ni<sub>2</sub>B phases and, the grain size is increased to 8-10 nm. Scanning electron micrographs of the EL Ni-B coating confirms a nodular growth with a columnar structure. This type of surface feature could allow the transport of corrosive medium through them. Hence, it is evident that the surface heterogeneity and columnar structure are primarily responsible for the observed corrosion behaviour of the EL Ni-B coating in their as-plated condition. Heat-treatment induces crystallinity of the EL Ni-B coating and increases the grain boundaries, which are the active sites for corrosion attack.

The Nyquist plots of EL Ni-B coatings in 3.5% sodium chloride solution, both in as-plated and heat-treated conditions (450°C for 1 hour) at their respective open circuit potentials is shown in **Fig. 4.31**. The  $R_{ct}$  and  $C_{dl}$  values, calculated after fitting the data using Boukamp software are given in Table 4.5. The  $R_{ct}$  and  $C_{dl}$  values of as-plated EL Ni-B coating are 5163 ohms.cm<sup>2</sup> and 139  $\mu$ F/cm<sup>2</sup>, respectively. However, heat-treatment of the EL Ni-B coating at 450°C for 1 hour results in a decrease in  $R_{ct}$  value from 5163 to 3465 ohms.cm<sup>2</sup> and an increase in  $C_{dl}$  value from 139 to 165  $\mu$ F/cm<sup>2</sup>. It has been established that high values of  $R_{ct}$  and low values of  $C_{dl}$  imply a better corrosion protective ability of coatings (Van der Kouwe, 1993). The  $C_{dl}$  value is related to the porosity of the coating (Growcock and Jasinski, 1989). Zeller III (1991) reported a  $C_{dl}$  value of 28  $\mu$ F/cm<sup>2</sup> for 50-60  $\mu$ m thick EL Ni-P (10-11 wt.%) coating in 5% NaCl solution. Van Der Kouwe (1993) reported  $C_{dl}$  values of 30 and 42  $\mu$ F/cm<sup>2</sup> for 20  $\mu$ m thick EL Ni-high P coating in 3% NaCl solution. Lo et al. (1995) reported  $C_{dl}$  values in the range of 100 - 120  $\mu$ F/cm<sup>2</sup>

for EL Ni-P (11.8 - 12.8 wt.% P) in 1 N NaOH solution at -1.2 V. Balaraju et al. (2001) have reported the  $C_{dl}$  values of 11-17  $\mu\text{F}/\text{cm}^2$  for EL Ni-P and Ni-P composite coatings in 3.5% NaCl solution. The higher  $C_{dl}$  values of EL Ni-B coatings of the present study suggest that the columnar structure of the coating has allowed penetration of the electrolyte through them.

It is evident from Fig. 4.31 that EL Ni-B coatings, both in as-plated and heat-treated conditions (450°C for 1 hour), exhibit a semicircle in the high frequency region followed by a loop in the low frequency region. Though the curves in the Nyquist plot appear to be similar with respect to their shape, they differ considerably in their size. This indicates that same fundamental processes must be occurring on both the as-plated and heat-treated EL Ni-B coatings but over a different effective area in each case. The formation of a single semicircle or a semicircle in the high frequency region followed by a low frequency loop is typical of metallic coatings. The semicircle at high frequency region represents the coating response, while the loop at low frequency region is associated with simultaneous physicochemical phenomena at the metal/coating/solution interface (Atkinson and Smart, 1988; Balaraju and Seshadri, 1998; Lo et al., 1995; Contreras et al., 2006). Mansfeld et al. (1982) suggest that the low frequency loop is associated with the double layer capacitance and/or diffusion phenomena of the oxidant chemical species through the porous coating.

In order to understand the coating response as well as the diffusion phenomenon, Bode plots (Log  $f$  vs. Log  $|Z|$  and Log  $f$  vs. Phase angle) were constructed. The Bode plots of EL Ni-B coating, both in as-plated and heat-



treated conditions (450°C for 1 hour), indicate the presence of two phase angle maxima (**Fig. 4.32**), suggesting the involvement of two time constants. The two phase angle maxima could be related to the electrolyte/coating and the electrolyte/substrate interface. The occurrence of the second phase angle maximum clearly indicates that the electrolyte has penetrated via pores in these coatings to create another interface, namely, the electrolyte/substrate. The surface morphology of the EL Ni-B coatings (Fig. 4.16) strongly supports this view. The nodular growth with a columnar structure of the EL Ni-B coatings enables the electrolyte to penetrate through them. The Bode plot (Fig. 4.32) confirms the involvement of a diffusion phenomenon in the low frequency regions.

## **PART B - ELECTRO- AND ELECTROLESS DEPOSITED Ni-B-Si<sub>3</sub>N<sub>4</sub> COMPOSITE COATINGS**

### **4.3 ELECTRODEPOSITED Ni-B-Si<sub>3</sub>N<sub>4</sub> COMPOSITE COATINGS**

#### **4.3.1 COATING SYNTHESIS**

Electrodeposited (ED) Ni-B-Si<sub>3</sub>N<sub>4</sub> composite coatings are prepared using DMAB modified Watts nickel bath containing varying concentrations of silicon nitride particles (25-150 g/l). It has been established that several factors influence the level of incorporation of second phase particles in ED composite coatings which include, concentration of particles in the bath, current density, pH, temperature, particle size, particle shape and agitation of the bath (Ghouse et al., 1980). Among these, particle concentration in the bath and current density demonstrate the most pronounced effects. An increase in the concentration of particles in the bath yields higher level of incorporation in the electrodeposited metal matrix whereas an increase in the current density results in a decrease in the level of incorporation (Zimmerman et al. 2002a).

#### **(i) *Effect of concentration of Si<sub>3</sub>N<sub>4</sub> particles in the bath***

**Fig. 4.33** shows the level of incorporation of Si<sub>3</sub>N<sub>4</sub> particles in the ED Ni-B matrix as a function of the concentration of Si<sub>3</sub>N<sub>4</sub> particles in the bath (25-150 g/L) at 1 A/dm<sup>2</sup>. It is evident that the level of incorporation of Si<sub>3</sub>N<sub>4</sub> particles increases with increase in its concentration in the bath up to 50 g/L, beyond which it gets saturated. The maximum level of incorporation of Si<sub>3</sub>N<sub>4</sub> particles is 8 wt.% at a bath loading of 50 g/l. The observed trend is in agreement with the literature reports (Garcia et al., 2001; Berkh et al., 1995; Kim and Yoo, 1998; Ayyappa Raju et al., 1989; Joshi and Totalani, 1981). The

mechanism of incorporation of  $\text{Si}_3\text{N}_4$  particles in the ED Ni-B matrix can be explained based on the Gugliemi's model. According to this model, the first step is the adsorption of nickel ions present in the plating bath on the  $\text{Si}_3\text{N}_4$  particles. The next step is the diffusion of these particles with their "ionic cloud" towards the cathode via the diffusion layer. Subsequently, loose adsorption of the  $\text{Si}_3\text{N}_4$  particles occurs on the cathode surface. When the nickel ions are discharged at the cathode, the  $\text{Si}_3\text{N}_4$  particles are encapsulated and finally incorporated in the ED Ni-B matrix (Rajiv and Seshadri 1993).

The increase in the level of incorporation of  $\text{Si}_3\text{N}_4$  particles up to 50 g/L is due to the increase in the number of particles that are reaching and striking the cathode surface without interference. According to Yeh and Wan (1995), an increase in concentration of the particles in the bath would increase the quantity of loosely adsorbed particles on the cathode surface, which results in an increase in the level of incorporation of the particles in the matrix. The maximum level of incorporation attained at 50 g/l suggests that at this concentration, the rate of  $\text{Si}_3\text{N}_4$  particles reaching the cathode surface is equal to that of particle incorporated in the growing ED Ni-B deposit. Similar observation was also made earlier by Zahavi and Hazan (1983). The saturation in the level of incorporation of  $\text{Si}_3\text{N}_4$  particles beyond 50 g/L could be attributed to the insufficient agitation of the bath so as to keep all the  $\text{Si}_3\text{N}_4$  particles in suspension and also possibly to a greater degree of agglomeration of the  $\text{Si}_3\text{N}_4$  particles in the bath (Ayyappa Raju, 1989; Muller et al., 2002). Zahavi and Hazan (1983) have suggested that increase in the particle concentration beyond a critical value would probably cause the removal of already adsorbed particles on the cathode surface and a reduction in the number

of new particles adhering to the surface because of geometrical effects and collisions among the particles approaching the cathode. A similar effect could have also occurred during the formation of ED Ni-B-Si<sub>3</sub>N<sub>4</sub> composite coatings. Ramesh Bapu et al. (1990) have suggested that insufficient agitation of the bath to keep the particles in suspension could result in the formation of rough deposits. Lee et al. (1999) have found out that if the particle concentration is too high, then breakage of the coating layer would occur due to the shortage of nickel as bonding medium and this would generate stress between substrate and coated layer. Abdel Hamid and Ghayad (2002) reported that when the concentration of the particle in the bath is higher than the optimum level, the level of incorporation could also decrease slightly.

**(ii) *Effect of current density***

**Fig. 4.34** shows the level of incorporation of Si<sub>3</sub>N<sub>4</sub> particles (50 g/l) in the ED Ni-B matrix as a function of current density (0.4-4 A/dm<sup>2</sup>). It is evident that the level of incorporation of Si<sub>3</sub>N<sub>4</sub> particles increases with increase in current density and reaches a maximum at 1 A/dm<sup>2</sup>, beyond which it decreases. The maximum level of incorporation of Si<sub>3</sub>N<sub>4</sub> particles is 8 wt.% at a current density of 1 A/dm<sup>2</sup>. The observed trend is in agreement with the literature reports (Joshi and Totlani 1981, Ramesh et al., 1991, Balathandan and Seshadri, 1992b; Ramesh Babu, 1994, 1995; Pushpavanam et al. 1989; Pushpavanam and Natarajan, 1995; Aruna et al. 2006). Different explanations, based on adsorption of ions on the particles, activation and diffusion control of metal deposition, point of zero charge of the particle and fluid flow resistance for the particles, have been suggested to account for the level of incorporation

of second phase particle in a metal matrix as a function of current density (Kerr et al., 2000; Shrestha et al., 2001; Wang et al. 2002a, Muller et al., 2002).

The observed low level of incorporation of  $\text{Si}_3\text{N}_4$  particles in the ED Ni-B matrix at lower current densities can be explained based on the solvation and adsorption of  $\text{Ni}^{2+}$  ions on the  $\text{Si}_3\text{N}_4$  particles. The energy required to deposit  $\text{Ni}^{2+}$  ions that are solvated and adsorbed on the  $\text{Si}_3\text{N}_4$  particle surface is larger than that is needed to deposit freely solvated  $\text{Ni}^{2+}$  ions. Due to the difference in activation energy, deposition of free  $\text{Ni}^{2+}$  ions are preferred at low current densities and this results in a lower level of incorporation of  $\text{Si}_3\text{N}_4$  particles in the ED Ni-B matrix. With increase in current density from 0.4 to 1  $\text{A}/\text{dm}^2$ , this energy difference criterion becomes less important and hence, codeposition of  $\text{Si}_3\text{N}_4$  particles increases with increase in current density. However, at current densities beyond 1  $\text{A}/\text{dm}^2$ , loose adsorption of  $\text{Si}_3\text{N}_4$  particles at the cathode surface becomes the rate controlling step. Since this is always slower than the metal deposition rate, incorporation of the  $\text{Si}_3\text{N}_4$  particles decreases at higher current densities (Rajiv and Seshadri 1993; Wu et al., 2003). Hwang and Hwang (1993) have suggested that at low current densities, the particle co-deposition rates are determined mainly by the reduction of adsorbed  $\text{H}^+$  ion on the particle whereas at high current densities, reduction of both the metal ions as well as the  $\text{H}^+$  ions are important to the co-deposition rate of the particle.

With increase in current density from 0.4 to 1  $\text{A}/\text{dm}^2$ , the solution in the vicinity of the cathode becomes depleted of  $\text{Ni}^{2+}$  ions, which results in polarization and an increase in adsorption of the  $\text{Si}_3\text{N}_4$  particles on the cathode

and their level of incorporation in the ED Ni-B Matrix. The maximum level of incorporation of  $\text{Si}_3\text{N}_4$  particles observed at  $1 \text{ A/dm}^2$  suggests that at this current density, the rate of movement of  $\text{Ni}^{2+}$  ions and the  $\text{Si}_3\text{N}_4$  particles from the bulk solution to the cathode surface is equal to the rate of deposition. However, at higher current densities, nickel deposition is governed by charge transfer control. Hence, the amount of codeposition of  $\text{Si}_3\text{N}_4$  particles gradually decreases (Abdel Hamid and Ghayad, 2002).

Various models have been put forth to explain the mechanism of incorporation of second phase particles in the metal matrix. Guglielmi suggested that, at the first step, particles are adsorbed weakly at the cathode by the Vander Waals force and, at the second step, particles are adsorbed strongly on the cathode by the Coulomb force and consequently buried with depositing metals (Guglielmi, 1972). However, Kurozaki suggested that, at the first stage, particles are transported to the Helmholtz's double layer by mechanical agitation and, at the second stage, particles charged in the high potential gradient are transported to the cathode surface by electrophoresis and, at the third stage, particles are adsorbed at the cathode surface by the Coulomb force which exists between particles and adsorbed anions, and are buried by depositing metals (Kurozaki, 1979). Yeh and Wan (1994, 1997) have reported that at low current densities codeposition of SiC particles in ED Ni matrix follows Guglielmi's two-step adsorption model (i.e., particles are loosely adsorbed on the electrode surface initially and then the loose adsorption progresses to strong adsorption under the influence of the applied electric field) and results in a higher level of incorporation of SiC particles. At high current densities, nickel ions are transported faster than SiC particles transported by the

mechanical agitation and the codeposition of SiC particles becomes particle-transfer controlled. Besides, the SiC particles do not have enough time to be adsorbed loosely on the surface of the electrode and does not follow Guglielmi's model. This results in a lower level of incorporation of SiC. A similar explanation can also be made for the incorporation of  $\text{Si}_3\text{N}_4$  particles in the ED Ni-B matrix as a function of current density.

According to Wang et al. (2003a) particle migration is an electrophoretic process, which is dependent on the fluid flow resistance. The flow resistance of particles will be high at higher current densities. Besides, at higher current densities, the hydrogen bubbles generated at the cathode surface tend to attract the particles and prevent them from co-deposition in the metal matrix. These factors could have also contributed to the observed low level of incorporation of  $\text{Si}_3\text{N}_4$  particles at current densities beyond  $1 \text{ A/dm}^2$ . Banovic et al. (1996) reported  $1 \text{ A/dm}^2$  as the optimum current density for Ni- $\text{Al}_2\text{O}_3$  composite coating while Celis et al. (1987) reported  $2 \text{ A/dm}^2$  as the optimum current density for Cu- $\text{Al}_2\text{O}_3$  composite coating. Kim and Yoo (1998) reported that a maximum level of incorporation of SiC particles in the nickel matrix occurs at  $1\text{--}2 \text{ A/dm}^2$ . In the present study also the maximum level of incorporation is obtained at  $1 \text{ A/dm}^2$ . Hence, for further characterization studies, ED Ni-B- $\text{Si}_3\text{N}_4$  composite coatings obtained at  $1 \text{ A/dm}^2$  are used.

#### **4.3.2 PLATING RATE AND CHEMICAL COMPOSITION**

There is not much change in the rate of deposition of the ED Ni-B- $\text{Si}_3\text{N}_4$  composite coating when compared to that of ED Ni-B coatings. However, the incorporation of  $\text{Si}_3\text{N}_4$  particles in the ED Ni-B matrix causes a change in

chemical composition of the coating. The coating consists of 89.6 wt.% Ni; 2.4 wt.% B and 8 wt.%  $\text{Si}_3\text{N}_4$  particles.

### 4.3.3 SURFACE TOPOGRAPHY AND MORPHOLOGY

The metallic lustre of the coating is lost when the  $\text{Si}_3\text{N}_4$  particles are incorporated in the ED Ni-B matrix. Besides, the incorporation of  $\text{Si}_3\text{N}_4$  particles in the ED Ni-B matrix increases the roughness of the coating. In general, composite coatings are considered to be rougher than the particle-free coatings due to the entrapment of particles. Loss of metallic lustre and increase in surface roughness following incorporation of second phase particles in the metal matrix has also been reported by several researchers (Berkh et al. 1995; Balaraju, 2000; Muller et al. 2002; Novakovic, 2006). The three dimensional view of the surface topography and surface profile of ED Ni-B- $\text{Si}_3\text{N}_4$  composite coating assessed using laser scanning microscope are shown in **Figs. 4.35 and 4.36**, respectively. The surface profile indicates the presence of several peaks and very few valleys. Though majority of the  $\text{Si}_3\text{N}_4$  particles are believed to be engulfed by the ED Ni-B matrix, at the end of the electrodeposition process a small portion of  $\text{Si}_3\text{N}_4$  particles might stuck out of the matrix. The protrusion of the  $\text{Si}_3\text{N}_4$  particles in the ED Ni-B- $\text{Si}_3\text{N}_4$  composite coating could have caused unevenness in the surface profile. The average surface roughness ( $R_a$ ) of ED Ni-B- $\text{Si}_3\text{N}_4$  composite coating is of the order of  $1.17 \mu\text{m}$ .

The scanning electron micrographs of Ni-B- $\text{Si}_3\text{N}_4$  composite coatings electrodeposited at  $1 \text{ A/dm}^2$  is shown in **Fig. 4.37**. The morphology of ED Ni-B- $\text{Si}_3\text{N}_4$  composite coating consists of a homogeneous fine globular



structure with embedded  $\text{Si}_3\text{N}_4$  particles, which appears as white spots. From Fig. 4.37, it is evident that the  $\text{Si}_3\text{N}_4$  particles are distributed uniformly in the ED Ni-B matrix. The EDX line scan performed on a selected region (marked by arrow in Fig. 4.37(b)) on the surface of ED Ni-B- $\text{Si}_3\text{N}_4$  composite coating is shown in **Fig. 4.38**. The EDX line scanning also indicates the uniform distribution of  $\text{Si}_3\text{N}_4$  particles in the ED Ni-B matrix. The EDX pattern taken at different regions of ED Ni-B- $\text{Si}_3\text{N}_4$  composite coatings is shown in **Fig. 4.39**. The EDX pattern taken on the coating surface area that is predominantly the ED Ni-B matrix indicates the presence of nickel with some amount of  $\text{Si}_3\text{N}_4$  particles in it (Fig. 4.39(a)) whereas the EDX pattern taken on the coating surface area predominantly occupied by the  $\text{Si}_3\text{N}_4$  particles indicates that these areas are rich in silicon and nitrogen (Fig. 4.39(b)). The EDX pattern taken on the coating surface also indicates the presence of smaller quantities of boron and carbon that might have originated from the DMAB used in the plating bath (Fig. 4.39(c)). The X-ray elemental mapping of silicon, nickel and nitrogen along with the secondary electron image of the ED Ni-B- $\text{Si}_3\text{N}_4$  composite coating is shown in **Fig. 4.40**. The X-ray elemental mapping of silicon and nitrogen further confirms the uniform distribution of the  $\text{Si}_3\text{N}_4$  particles in the ED Ni-B matrix.

#### 4.3.4 STRUCTURAL CHARACTERISTICS

The XRD patterns of ED Ni-B- $\text{Si}_3\text{N}_4$  composite coating obtained at a bath loading of 0, 25, 50 and 75 g/l of  $\text{Si}_3\text{N}_4$ , in their as-plated condition, is shown in **Fig. 4.41**. It is evident from Fig. 4.4.1 that the incorporation of  $\text{Si}_3\text{N}_4$  particles causes a significant change in structure of the ED Ni-B- $\text{Si}_3\text{N}_4$

composite coatings. The absence of the reflection from Ni (200) plane and the change in intensity and broadening of the reflection from Ni (111) plane at higher particle loadings (50 and 75 g/l of  $\text{Si}_3\text{N}_4$ ) suggest a change in crystal orientation of the coating following incorporation of the  $\text{Si}_3\text{N}_4$  particles in the ED Ni-B matrix. The influence of incorporation of second phase particles on the crystal orientation of electro- and electroless deposited composite coatings has been studied by many researchers. Bozzini et al. (1999) have reported that incorporation of  $\text{B}_4\text{C}$  particles affects the orientation of nickel crystallites without influencing the crystallite dimensions. According to them, nickel tends to be less oriented in layers with  $\text{B}_4\text{C}$  particles. McCormack et al. (2003) have shown that addition of yttria particles to a Watt's nickel plating bath significantly changes the surface morphology and the preferred crystallographic orientation of the Ni-yttria composite coatings. Carac et al. (2004) have reported that the co-deposition of  $\text{CeO}_2$  particles leads to structural modification of the Ni-Co matrix. Qu et al. (2006) have reported that though the incorporation of  $\text{CeO}_2$  particles in ED Ni matrix does not change the preferred orientation of Ni (200), it causes a significant increase in the relative intensities of reflections of Ni (111) and Ni (220) orientations. Hence, it appears that the incorporation of  $\text{Si}_3\text{N}_4$  particles in the ED Ni-B matrix causes a change in crystal orientation. The XRD patterns of ED Ni-B- $\text{Si}_3\text{N}_4$  composite coating obtained using 0 and 50 g/l of  $\text{Si}_3\text{N}_4$ , after heat-treatment at  $400^\circ\text{C}$  for 1 hour is shown in **Fig. 4.42**. It is evident from Fig. 4.42 that the intensity of the reflection from Ni (111) plane of ED Ni-B- $\text{Si}_3\text{N}_4$  composite coating is relatively higher than that of ED Ni-B coating, further confirming the change in crystal orientation of the coating following incorporation of the  $\text{Si}_3\text{N}_4$  particles

in the ED Ni-B matrix. The grain size of ED Ni-B-Si<sub>3</sub>N<sub>4</sub> composite coatings is of the order of 6-8 nm and it increases to 12-14 nm after heat-treatment at 400°C for 1 hour.

#### 4.3.5 MICROHARDNESS

The microhardness of Ni-B-Si<sub>3</sub>N<sub>4</sub> composite coatings (8 wt.% Si<sub>3</sub>N<sub>4</sub>) electrodeposited at 1 A/dm<sup>2</sup> is determined in both as-plated and heat-treated conditions (200, 300, 350, 400, 500 and 600°C for 1 hour). The microhardness of as-plated ED Ni-B-Si<sub>3</sub>N<sub>4</sub> composite coating is of the order of  $640 \pm 16$  HV<sub>0.1</sub>, which is considerably high compared to that of bulk Ni (100-150 HV<sub>0.1</sub>) and ED Ni (250-350 HV<sub>0.1</sub>) and ED Ni-B coatings ( $609 \pm 15$  HV<sub>0.1</sub>). The hardness of ED Ni-B-Si<sub>3</sub>N<sub>4</sub> composite coating increases to  $955 \pm 24$  HV<sub>0.1</sub> when the coating is heat-treated at 400°C for 1 hour. **Fig. 4.43** shows the effect of heat treatment temperature on the hardness of ED Ni-B-Si<sub>3</sub>N<sub>4</sub> composite coatings. With increase in temperatures, the hardness increases rapidly. Compared to the hardness of ED Ni-B-Si<sub>3</sub>N<sub>4</sub> composite coating in as plated condition, there is not much change in the hardness when the heat-treatment temperature is of the order of 200°C. With further increase in temperatures, however, the hardness increases rapidly, as the structure of the coating begins to change. The hardness versus heat treatment temperature curve resembles that of a bell shape with its maximum at 400°C. Beyond 400°C, the hardness decreases. The increase in hardness is due to the precipitation of nickel boride (Ni<sub>3</sub>B), which is confirmed by XRD measurement (Fig. 4.9). At temperatures above 400°C, the ED Ni-B coating begins to soften as a result of coarsening of the Ni<sub>3</sub>B particles, which thereby reduces the number of hardening sites.

Similar behaviour of change in hardness with heat treatment temperature was also observed for electro- and electroless deposited Ni-P and Ni-B coatings and their composite counterparts (Gorbunova et al., 1973; Ramesh and Seshadri, 2003; Sankara Narayanan and Seshadri, 2004; Balaraju and Sheshadri, 1998, 1999, Balaraju, 2000). Although all these changes are believed to occur in both ED Ni-B and ED Ni-B-Si<sub>3</sub>N<sub>4</sub> composite coatings, the higher hardness obtained for the later coatings can be ascribed to the presence of Si<sub>3</sub>N<sub>4</sub> particle in the coating (Joshi and Totlani, 1981; Lausmann, 1984). The high hardness of the ED Ni-B-Si<sub>3</sub>N<sub>4</sub> composite coating is attributed due to the combined strengthening effect of solid solution hardening and dispersion hardening.

#### 4.3.6 WEAR RESISTANCE

The wear resistance of ED Ni-B-Si<sub>3</sub>N<sub>4</sub> composite coatings (8 wt.% Si<sub>3</sub>N<sub>4</sub>), both in as-plated and heat-treated (400°C for 1 hour) conditions is studied using three different applied normal loads, namely, 8, 10 and 12 N. The specific wear rate, calculated using the loss in weight due to wear, is given in **Table 4.6**. A comparison of Table 4.2 and Table 4.6 clearly reveals that the specific wear rate of ED Ni-B-Si<sub>3</sub>N<sub>4</sub> composite coatings is relatively lesser than that of ED Ni-B coating, both in as-plated and heat-treated conditions. Improvement in wear resistance following incorporation of hard second phase particles in electro- and electroless nickel matrix has also been observed by several researchers (Changgeng et al., 1988; Wu et al., 2000a, 2000b; Li, 1997; Staia et al., 1996, Balraju, 2000; Ramesh and Seshadri, 2003). The improvement in wear resistance offered by ED Ni-B-Si<sub>3</sub>N<sub>4</sub> composite coatings is due to (i) the characteristics of the Si<sub>3</sub>N<sub>4</sub> particles, such as high hardness,

high yield limit and high resistance to plastic deformation, which is superior to that of ED Ni-B alloy matrix; and (ii) the dispersion of the  $\text{Si}_3\text{N}_4$  particles in the ED Ni-B matrix. The uniform distribution of  $\text{Si}_3\text{N}_4$  particles in the ED Ni-B matrix could act as supporting points, further strengthening the ED Ni-B alloy matrix and enables an improvement in wear resistance. Similar observations was also made earlier by many researchers (Hou et al., 2002; Ramesh, 2003; Wu et al., 2003, Chang et al., 2006). The scanning electron micrograph of ED Ni-B- $\text{Si}_3\text{N}_4$  composite coatings confirms the uniform distribution of the  $\text{Si}_3\text{N}_4$  particles in the ED Ni-B matrix (Fig. 4.37) and supports the above view.

The specific wear rate is a measure of the ability of the ED Ni-B coatings to offer wear resistance against the hard counterface material (hardened steel of EN 31). The increase in specific wear rate with increase in applied normal load from 8 to 12 N indicates a decrease in wear resistance at higher applied loads and this trend is common for both as-plated and heat-treated ED Ni-B- $\text{Si}_3\text{N}_4$  composite coatings. At all applied loads, the specific wear rate is less for heat-treated ED Ni-B- $\text{Si}_3\text{N}_4$  composite coatings compared to that obtained for the as-plated ones. This is due to the formation of hard nickel boride phases following heat-treatment, which presents a virtually incompatible surface for the counterface material, as there exists very little solubility between iron and these hard nickel boride phases, leading to a decrease in specific wear rate of heat-treated coatings. Besides, following heat treatment, there is a considerable increase in the hardness of ED Ni-B- $\text{Si}_3\text{N}_4$  composite coatings due to the incorporation of  $\text{Si}_3\text{N}_4$  particles in the ED Ni-B matrix. The ED Ni-B- $\text{Si}_3\text{N}_4$  composite coating have a double strengthening effect - dispersion strengthening of the hard  $\text{Si}_3\text{N}_4$  particles and precipitation

strengthening of the ED Ni-B alloy matrix. Hence, when the counterface material comes in contact with the ED Ni-B-Si<sub>3</sub>N<sub>4</sub> composite matrix, the high hardness of the later enables it to experience a lesser wear.

The average friction coefficient,  $\mu_{av}$  of ED Ni-B-Si<sub>3</sub>N<sub>4</sub> composite coatings in as-plated and heat-treated conditions, is given in Table 4.6. The friction coefficient of ED Ni-B-Si<sub>3</sub>N<sub>4</sub> composite coatings is relatively high compared to ED Ni-B coating owing to their high surface roughness and high mechanical interlocking forces under similar loading and temperature conditions. Similar observations were also made earlier by Wu et al. (2003) and Grosjean et al. (2001). According to Grosjean et al. (2001), incorporation of SiC particles in EL Ni-P matrix leads to a gradual increase in friction coefficient due to the high hardness and abrasive properties of the particles themselves. The coefficient of friction of heat-treated ED Ni-B-Si<sub>3</sub>N<sub>4</sub> composite coatings is relatively less compared to that obtained for the as-plated ones. As already mentioned, this is due to the ability of the heat-treated ED Ni-B-Si<sub>3</sub>N<sub>4</sub> composite coatings to present a virtually incompatible surface for the hard counterface material. Besides, the build up of iron oxides at the interface could act as a lubricant film and might have also caused a decrease in the coefficient of friction in the case of heat-treated coatings.

The mechanism of wear of ED Ni-B-Si<sub>3</sub>N<sub>4</sub> composite coatings depends on the attractive force between the atoms of nickel from the coating and iron from the counter disk. Adhesive wear is most likely to occur under the present experimental conditions which induce a substantial attractive force between these mating surfaces, leading to a high mutual solubility of nickel and iron. At

the beginning of the friction and wear process, the  $\text{Si}_3\text{N}_4$  particles protruding in the ED Ni-B matrix act as the main sliding plane in the contacting surface and participate in the wear. However, as the wear continues, the ED Ni-B alloy matrix takes part in the wear process as the second plane just after the surface layer containing particles being worn out. The ED Ni-B alloy matrix can effectively sustain the  $\text{Si}_3\text{N}_4$  particles firmly, which enables the matrix a high strengthening effect. The scanning electron micrographs of wear track pattern of ED Ni-B- $\text{Si}_3\text{N}_4$  composite coatings subjected to pin-on-disc wear test clearly indicates severe shearing of the surface layers of the coating due to the ploughing action of the hard counter disk (**Fig. 4.44 (a & b)**) (hardened steel of EN 31) (Panagopoulos et al., 2000a, 2003). This type of morphological feature, commonly called as “prows” is reported for adhesive wear failure of EL Ni-P coatings, by several researchers (Statia et al., 1996; Gawne and Ma, 1987a, 1987b; Kannai, 1991; Dennis and Sagoo, 1991; Balaraju, 2000). The transferred patches from the ED Ni-B- $\text{Si}_3\text{N}_4$  composite coatings and the wear debris present on the surface of the counter disk clearly indicates that adhesion between the ED Ni-B- $\text{Si}_3\text{N}_4$  composite coated mild steel pins and the counter disk had occurred. The possibility of occurrence of adhesive wear under the experimental conditions used is also supported by the high mutual solubility of nickel and iron. Hence, adhesive wear appears to be the most likely mechanism during the wear process of ED Ni-B- $\text{Si}_3\text{N}_4$  composite coatings in their as-plated condition.

In contrast to the as-deposited coatings, heat-treated coatings after wear exhibit bright and smooth finish with fine grooves along the sliding direction (**Fig. 4.44 (c & d)**). The loose debris generated during the wear process gets

displaced to the sides leading to the formation of grooves along the wear track. In a substantial portion of the wear tracks, no gross adhesion between the coated pins and the counter disk is observed. In support of the morphological features of the wear track pattern, the  $R_a$  value is relatively less for heat treated ED Ni-B-Si<sub>3</sub>N<sub>4</sub> composite coatings. The  $R_a$  value of ED Ni-B-Si<sub>3</sub>N<sub>4</sub> composite coating after wear testing at a load of 12 N is 0.32  $\mu\text{m}$  in as-plated and 0.18  $\mu\text{m}$  in heat-treated conditions. The relatively lower  $R_a$  value obtained for heat-treated ED Ni-B-Si<sub>3</sub>N<sub>4</sub> composite coatings compared to those of the as plated ones is due to the increase in hardness leading to glazing of these deposits against the counterface material and strongly support the above wear mechanism suggested for heat-treated coatings.

Though the wear mechanism is quite similar for ED Ni-B and ED Ni-B-Si<sub>3</sub>N<sub>4</sub> composite coatings, the adverse effects due to wear is observed to be less in the case of ED Ni-B-Si<sub>3</sub>N<sub>4</sub> composite coatings. This can be ascribed to the presence of Si<sub>3</sub>N<sub>4</sub> particles in the ED Ni-B-Si<sub>3</sub>N<sub>4</sub> composite coatings, which decreases the available surface area for metal-to-metal contact, leading to a lesser degree of wear.

#### 4.3.7 CORROSION RESISTANCE

The potentiodynamic polarization curves of ED Ni-B-Si<sub>3</sub>N<sub>4</sub> composite coatings in 3.5% sodium chloride solution, both in as-plated and heat-treated (400°C for 1 hour) conditions, are shown in **Fig. 4.45(a)**. The corrosion potential ( $E_{\text{corr}}$ ) and corrosion current density ( $i_{\text{corr}}$ ), calculated using the Tafel extrapolation method are given in **Table 4.7**. The  $E_{\text{corr}}$  and  $i_{\text{corr}}$  of as-plated ED Ni-B-Si<sub>3</sub>N<sub>4</sub> composite coating are -560 mV vs. SCE and 10.92  $\mu\text{A}/\text{cm}^2$ ,



respectively. However, heat-treatment of the ED Ni-B-Si<sub>3</sub>N<sub>4</sub> composite coating at 400°C for 1 hour results in a shift in the  $E_{\text{corr}}$  value towards more negative values (from -560 to -665 mV vs. SCE) and an increase in the  $i_{\text{corr}}$  value from 10.92 to 21.98  $\mu\text{A}/\text{cm}^2$ . The decrease in the linear polarization resistance (LPR) value from 1416 to 597  $\text{ohms}\cdot\text{cm}^2$  also suggests a decrease in corrosion resistance of heat-treated ED Ni-B-Si<sub>3</sub>N<sub>4</sub> composite coatings. To confirm this aspect further, the current-time transient curves of the ED Ni-B-Si<sub>3</sub>N<sub>4</sub> composite coatings, both in as-plated and heat-treated (400°C for 1 hour) conditions, is recorded (**Fig. 4.45(b)**). It has been established that reduction of oxygen and dissolution of nickel are the major reactions occurring during cathodic and anodic polarization, respectively. Hence, the increase in current should have been due to the dissolution of nickel from the coating. To compare the ability of the as-plated and heat-treated ED Ni-B-Si<sub>3</sub>N<sub>4</sub> composite coatings, the time to reach a steady state current of 0.1  $\text{mA}/\text{cm}^2$  is taken as a failure criterion (Table 4.7). It is evident from Fig. 4.45(b) and Table 4.7 that the corrosion resistance of ED Ni-B-Si<sub>3</sub>N<sub>4</sub> composite coatings after heat-treatment is considerably decreased.

Several factors, which include, the composition of the coating, grain size, porosity, structure, surface features and heterogeneity of the coating, could influence the corrosion resistance of electro- and electroless plated deposits. The coating thickness of the ED Ni-B-Si<sub>3</sub>N<sub>4</sub> composite coatings used for corrosion study is 20  $\mu\text{m}$ . Hence, the contribution from the porosity factor is expected to be minimal. In as-plated condition, the ED Ni-B-Si<sub>3</sub>N<sub>4</sub> composite coating is nanocrystalline in nature and its grain size is of the order

of 6-8 nm. However, after heat-treatment at 400°C for 1 hour, the ED Ni-B-Si<sub>3</sub>N<sub>4</sub> composite coating becomes crystalline with the formation of crystalline Ni and Ni<sub>3</sub>B phases and, the grain size is increased to 12-14 nm. Scanning electron micrographs of the ED Ni-B-Si<sub>3</sub>N<sub>4</sub> composite coating indicate uniform distribution of the Si<sub>3</sub>N<sub>4</sub> particles in the ED Ni-B matrix and the cracks in the coating are considerably reduced (Fig. 4.37). This type of surface feature would significantly reduce the transport of corrosive medium through them. Hence, it is evident that the nanocrystalline nature is responsible for the observed corrosion behaviour of the ED Ni-B-Si<sub>3</sub>N<sub>4</sub> composite coating in their as-plated condition. Heat-treatment induces crystallinity of the ED Ni-B-Si<sub>3</sub>N<sub>4</sub> composite coating and increases the grain boundaries which are the active sites for corrosion attack.

The Nyquist plots of ED Ni-B-Si<sub>3</sub>N<sub>4</sub> composite coatings in 3.5% sodium chloride solution, both in as-plated and heat-treated conditions (400°C for 1 hour) at their respective open circuit potentials is shown in **Fig. 4.46**. The  $R_{ct}$  and  $C_{dl}$  values, calculated after fitting the data using Boukamp software are given in Table 4.7. The  $R_{ct}$  and  $C_{dl}$  values of as-plated ED Ni-B-Si<sub>3</sub>N<sub>4</sub> composite coating are 2992 ohms.cm<sup>2</sup> and 109 µF/cm<sup>2</sup>, respectively. However, heat-treatment of the ED Ni-B-Si<sub>3</sub>N<sub>4</sub> composite coating at 400°C for 1 hour results in a decrease in  $R_{ct}$  value from 2992 to 1935 ohms.cm<sup>2</sup> and an increase in  $C_{dl}$  value from 109 to 148 µF/cm<sup>2</sup>. It has been established that high values of  $R_{ct}$  and low values of  $C_{dl}$  imply a better corrosion protective ability of coatings (Van der Kouwe, 1993). The  $C_{dl}$  value is related to the porosity of the coating (Growcock and Jasinski, 1989). The higher  $C_{dl}$  values of ED Ni-B-Si<sub>3</sub>N<sub>4</sub>

composite coatings suggest the penetration of the electrolyte through micropores in the coating.

It is evident from Fig. 4.46 that ED Ni-B-Si<sub>3</sub>N<sub>4</sub> composite coatings, both in as-plated and heat-treated conditions (400°C for 1 hour), exhibit a semicircle in the high frequency region followed by a loop in the low frequency region. Though the curves in the Nyquist plot appear to be similar with respect to their shape, they differ considerably in their size. This indicates that same fundamental processes must be occurring on both the as-plated and heat-treated ED Ni-B-Si<sub>3</sub>N<sub>4</sub> composite coatings but over a different effective area in each case. The formation of a single semicircle or a semicircle in the high frequency region followed by a low frequency loop is typical of metallic coatings. The semicircle at high frequency region represents the coating response, while the loop at low frequency region is associated with simultaneous physicochemical phenomena at the metal/coating/solution interface (Atkinson and Smart, 1988; Balaraju and Seshadri, 1998; Lo et al., 1995; Contreras et al., 2006). According to Mansfeld et al. (1982) the loop at the lower frequency region is associated with the double layer capacitance and/or diffusion phenomena of the oxidant chemical species through the porous coating.

In order to get a better insight about the coating response as well as the diffusion phenomenon, Bode plots (Log f vs. Log |Z| and Log f vs. Phase angle) were constructed. The Bode plots of ED Ni-B-Si<sub>3</sub>N<sub>4</sub> composite coating, both in as-plated and heat-treated conditions (400°C for 1 hour), indicate the presence of two phase angle maxima (**Fig. 4.47**) suggesting the involvement of two time constants. The two phase angle maxima could be related to the

electrolyte/coating and the electrolyte/ substrate interface. The occurrence of the second phase angle maximum clearly indicates that the electrolyte has penetrated via the micropores in these coatings to create another interface, namely, the electrolyte/substrate. The Bode plots (Fig. 4.47) also indicate the involvement of a diffusion phenomenon in the low frequency regions.

A comparison of the corrosion behaviour of ED Ni-B and ED Ni-B-Si<sub>3</sub>N<sub>4</sub> composite coatings (Figs. 4.12-4.14 and Table 4.3 with Figs. 4.45-4.47 and Table 4.7) clearly reveals that the corrosion resistance of ED Ni-B-Si<sub>3</sub>N<sub>4</sub> composite coating is relatively higher than ED Ni-B coatings, both in as-plated and heat-treated conditions. Corrosion resistance of ED and EL composite coatings has been a debatable issue in the published literature (Table 1.8). The improvement or impairment of corrosion resistance of ED and EL composite coatings depends on the chemical stability of the particle, effective metallic area prone to corrosion, structural state or microstructural feature of the coating, porosity or defect size of the coating, ability to prevent diffusion of chloride ions along the interface between the metal and the particle, the ability of the particle to prevent the corrosive pits from growing up, etc. The Si<sub>3</sub>N<sub>4</sub> particles are chemically stable in 3.5% sodium chloride solution. It is obvious to expect that the incorporation of Si<sub>3</sub>N<sub>4</sub> particles in the ED Ni-B matrix would decrease the effective metallic area prone to corrosion. Besides, the incorporation of Si<sub>3</sub>N<sub>4</sub> particles in the ED Ni-B matrix enables a change in microstructural feature, which is evidenced by the scanning electron micrographs (Fig. 4.37). The change in microstructural feature of the ED Ni-B-Si<sub>3</sub>N<sub>4</sub> composite coating reduces the defects such as cracks and voids in the coating and imparts a better chemical stability. These factors, in turn,

enable the ED Ni-B-Si<sub>3</sub>N<sub>4</sub> composite coatings to decrease the penetration of the chloride ions across the metal-solution interface and offer them a better corrosion resistance compared to ED Ni-B coatings.

## 4.4 ELECTROLESS Ni-B-Si<sub>3</sub>N<sub>4</sub> COMPOSITE COATING

### 4.4.1 COATING SYNTHESIS

Electroless (EL) Ni-B-Si<sub>3</sub>N<sub>4</sub> composite coatings are prepared using the alkaline borohydride-reduced electroless nickel plating bath containing varying concentrations of silicon nitride particles (2-25 g/l). It has been established that several factors influence the incorporation of second phase particles in electroless nickel matrix which include, the size, shape and specific gravity of particles, particle charge, inertness of the particle, concentration of particles in the plating bath, method and degree of agitation, the deposition rate, compatibility of the particle with the matrix, and the orientation of the part being plated (Sharp, 1975).

#### *Effect of concentration of Si<sub>3</sub>N<sub>4</sub> particles in the bath*

**Fig. 4.48** shows the level of incorporation of Si<sub>3</sub>N<sub>4</sub> particles in the EL Ni-B matrix as a function of the concentration of Si<sub>3</sub>N<sub>4</sub> particles in the bath (2- 25 g/L). It is evident that the level of incorporation of Si<sub>3</sub>N<sub>4</sub> particles increases with increase in its concentration in the bath up to 10 g/L, beyond which it gets saturated in spite of a continuous increase in their concentration up to 25 g/l. The maximum level of incorporation of Si<sub>3</sub>N<sub>4</sub> particles in the EL Ni-B matrix obtained at a bath loading of 10 g/l is 2 wt.%. Several researchers have also observed a similar trend of saturation in the level of incorporation of second phase particles, beyond a critical level of these particles in the bath (Pushpavanam et al. 1977; Dennis et al. 1981; Izzard and Dennis, 1987; Xinguo and Naichao 1990; Pushpavanam, 1992; Balaraju 2000; Balaraju and Seshadri 1998, 2003). Although incorporation of various second

phase particles has been studied, their critical concentration in the bath at which these particles exhibit saturation in incorporation level is not very different. Based on the observations of the present study and literature reports, it can be construed that the particle flux at the interface available for impingement at the surface and the holding time of these particles at the surface determines their level of incorporation rather than the type and nature of second phase particles added to the electroless plating bath. The impingement of the particle on the substrate is determined by the flux of the particle at the interface. The particle flux at the interface, in turn, is determined by the concentration, size and density of the particle. The holding time is a function of mode of agitation, speed, and particle shape (Balaraju, 2000).

The observed increase in incorporation of  $\text{Si}_3\text{N}_4$  particles in the EL Ni-B matrix up to a concentration of 10 g/l can be ascribed to the increased flux of these particles adjacent to the electrode surface. However, beyond this concentration, there is a possibility of grouping or agglomeration of  $\text{Si}_3\text{N}_4$  particles due to the decrease in the mean distance between them, resulting in settlement of these particles. Such an effect will lead to a leveling off in the flux of the  $\text{Si}_3\text{N}_4$  particles that are available at the interface for incorporation in the deposit, causing either a saturation or slight decrease in the level of incorporation.

The maximum level of incorporation of  $\text{Si}_3\text{N}_4$  particles in the EL Ni-B matrix obtained at a bath loading of 10 g/l is only of the order of 2 wt.%. However, Balaraju (2000) have obtained a maximum of 8-10 wt.% incorporation of  $\text{Si}_3\text{N}_4$  particles for a similar bath loading in EL Ni-P matrix from an acidic

hypophosphite-reduced electroless plating bath. The  $\text{Si}_3\text{N}_4$  particles used in the present study as well used by Balaraju (2000) have similar characteristics; the particle size is in the range of 20% 8-10  $\mu\text{m}$ ; 40% 6-8  $\mu\text{m}$ ; 10% 3-4  $\mu\text{m}$ ; 20% 2-3  $\mu\text{m}$ ; remaining 10% 16-28  $\mu\text{m}$ . The  $\text{Si}_3\text{N}_4$  particles used in the present has a  $d_{10}$ ,  $d_{50}$  and  $d_{80}$  of 0.08, 0.39 and 0.92  $\mu\text{m}$ , respectively, with a mean diameter of 0.80  $\mu\text{m}$  and the density is 3.44  $\text{g/cm}^3$ . The observed lower level of incorporation of  $\text{Si}_3\text{N}_4$  particles in the EL Ni-B matrix could be attributed to the decrease in holding time of the particles on the substrate surface. Sodium borohydride is a very powerful reducing agent and it can provide up to eight electrons for the reduction of some metals (Duncan and Arney, 1984). The plating rate of EL Ni-B coating using the bath composition and operating conditions given in Table 3.3 is 18-20  $\mu\text{m/hour}$ . Deposition of EL Ni-B coating is accompanied by a heavy hydrogen evolution. The heavy hydrogen evolution which occurs on the surface of the substrate tends to push the  $\text{Si}_3\text{N}_4$  particles away from the substrate, thus decreasing the particle flux at the interface and making it less amenable for incorporation. Heavy hydrogen evolution is also suggested as a reason for the observed lower level of incorporation of various second phase particles in ED Cr matrix (Narayanan and Seshadri, 2001).

#### 4.4.2 PLATING RATE AND CHEMICAL COMPOSITION

There is not much change in the rate of deposition of the EL Ni-B- $\text{Si}_3\text{N}_4$  composite coating when compared to that of EL Ni-B coatings. However, the incorporation of  $\text{Si}_3\text{N}_4$  particles in the EL Ni-B matrix causes a



change in chemical composition of the coating. The coating consists of 91.7 wt.% Ni; 6.0 wt.% B; 0.3 wt.% Ti and 2 wt.%  $\text{Si}_3\text{N}_4$  particles.

#### 4.4.3 SURFACE FINISH AND SURFACE MORPHOLOGY

The incorporation of  $\text{Si}_3\text{N}_4$  particles in EL Ni-B matrix does not change its dark colour and matte finish. However, the incorporation of  $\text{Si}_3\text{N}_4$  particles increases the roughness of the EL Ni-B matrix. In general, composite coatings are considered to be rougher than the particle-free coatings due to the entrapment of particles. Increase in surface roughness following incorporation of second phase particles in the metal matrix has also been reported by several researchers (Balaraju, 2000; Balaraju et al., 2003). The average surface roughness ( $R_a$ ) of EL Ni-B- $\text{Si}_3\text{N}_4$  composite coatings is of the order of 0.92  $\mu\text{m}$ . The surface morphology of EL Ni-B- $\text{Si}_3\text{N}_4$  composite coating is shown in **Fig. 4.49**. It is evident from Fig. 4.49 that the  $\text{Si}_3\text{N}_4$  particles are uniformly distributed in the EL Ni-B matrix. The presence of Si peaks in the EDX pattern taken on the surface of the EL Ni-B- $\text{Si}_3\text{N}_4$  composite coating confirms the incorporation of  $\text{Si}_3\text{N}_4$  particles in the EL Ni-B matrix (**Fig. 4.50**).

#### 4.4.4 STRUCTURAL CHARACTERISTICS

The X-ray diffraction pattern obtained for EL Ni-B- $\text{Si}_3\text{N}_4$  composite coating is very similar to those obtained for EL Ni-B coating, both in as plated and heat treated conditions (Refer Figs. 4.18-4.20 in section 4.2.3). This observation suggests that the incorporated  $\text{Si}_3\text{N}_4$  particles have very little influence on the structure of EL Ni-B matrix. Hansen and Moller (1990), Balaraju (2000), Balaraju and Seshadri (1999), Balaraju et al. (2006b) and Das

et al. (2006) have reported that the incorporation of TiC, Si<sub>3</sub>N<sub>4</sub>, CeO<sub>2</sub> and TiO<sub>2</sub> particles does not alter the structure of the electroless Ni-P matrix. The grain size of EL Ni-B-Si<sub>3</sub>N<sub>4</sub> composite coatings is of the same order as that of EL Ni-B coatings; 2-3 nm in as-plated condition and 8-10 nm after heat-treatment at 450°C for 1 hour.

#### 4.4.5 MICROHARDNESS

The microhardness (HV<sub>0.1</sub>) of EL Ni-B-2 wt.% Si<sub>3</sub>N<sub>4</sub> composite coatings is determined in both as-plated and heat-treated conditions. The microhardness for as-plated electroless Ni-B-Si<sub>3</sub>N<sub>4</sub> composite coatings is of the order of  $670 \pm 17$  HV<sub>0.1</sub>. The microhardness of electroless Ni-B-Si<sub>3</sub>N<sub>4</sub> composite coatings after heat-treatment at 350 and 450°C for 1 hour is of the order of  $946 \pm 18$  HV<sub>0.1</sub> and  $1012 \pm 17$  HV<sub>0.1</sub>, respectively. **Fig. 4.51** shows the variation in hardness of EL Ni-B-Si<sub>3</sub>N<sub>4</sub> composite coating as a function of heat-treatment temperature. The hardness vs. heat treatment temperature curve exhibits two maxima. The first maximum is observed at 350°C whereas the second one is observed at 450°C. Beyond 450°C, the hardness of EL Ni-B-Si<sub>3</sub>N<sub>4</sub> composite coating decreases. The observed trend in variation of hardness as a function of heat-treatment temperature is quite similar for EL Ni-B and EL Ni-B-Si<sub>3</sub>N<sub>4</sub> composite coating (Figs. 4.27 and 4.51). The increase in hardness with increase in heat-treatment temperature up to 450°C is due to the precipitation of nickel borides (Ni<sub>3</sub>B and Ni<sub>2</sub>B). The formation of these phases is confirmed by XRD measurement (Figs. 4.20 and 4.21). At temperatures above 450°C, the coating begins to soften as a result of coarsening of the Ni<sub>3</sub>B particles, which reduces the number of hardening sites.

These changes occur on the EL Ni-B matrix and they are common for both EL Ni-B and EL Ni-B-Si<sub>3</sub>N<sub>4</sub> composite coatings.

Though the trend in variation of hardness as a function of heat-treatment temperature is quite similar for both EL Ni-B and EL Ni-B-Si<sub>3</sub>N<sub>4</sub> composite coating, the hardness of the later type of coating is relatively higher at all temperatures studied. This is due to the fact that the Si<sub>3</sub>N<sub>4</sub> particles that is incorporated firmly in the EL Ni-B matrix and distributed uniformly throughout the matrix increase the resistance to plastic deformation of the EL Ni-B matrix. The EL Ni-B-Si<sub>3</sub>N<sub>4</sub> composite coating have a double strengthening effect - dispersion strengthening of the hard Si<sub>3</sub>N<sub>4</sub> particles and precipitation strengthening of the EL Ni-B alloy matrix.

#### **4.4.6 WEAR RESISTANCE**

The wear resistance of EL Ni-B-2 wt.% Si<sub>3</sub>N<sub>4</sub> composite coatings, both in as-plated and heat-treated (450°C for 1 hour) conditions, is studied using three different applied normal loads, namely, 20, 30 and 40 N. The specific wear rate, calculated using the loss in weight due to wear, is given in **Table 4.8**. A comparison of Table 4.4 and Table 4.8 clearly reveals that the specific wear rate of EL Ni-B-Si<sub>3</sub>N<sub>4</sub> composite coatings is relatively lesser than that of EL Ni-B coating, both in as-plated and heat-treated conditions. Improvement in wear resistance following incorporation of hard second particles in electroless nickel matrix has also been observed by several researchers (Changgeng et al., 1988; Staia et al., 1996, 2002; Li, 1997; Wu et al., 2000a, 2000b; Balaraju, 2000). The improvement in wear resistance offered by EL Ni-B-Si<sub>3</sub>N<sub>4</sub> composite coatings is due to (i) the characteristics of the Si<sub>3</sub>N<sub>4</sub> particles, such

as high hardness, high yield limit and high resistance to plastic deformation, which is superior to that of EL Ni-B alloy matrix; and (ii) the dispersion of the  $\text{Si}_3\text{N}_4$  particles in the EL Ni-B matrix. The uniform distribution of  $\text{Si}_3\text{N}_4$  particles in the EL Ni-B matrix could act as supporting points, further strengthening the EL Ni-B alloy matrix and enables an improvement in wear resistance. Similar observations were also made earlier by many researchers (Changgeng et al., 1988; Staia et al., 1996, 2002; Li, 1997; Wu et al., 2000a, 2000b; Balaraju, 2000). The scanning electron micrograph of the EL Ni-B- $\text{Si}_3\text{N}_4$  composite coatings confirms the uniform distribution of the  $\text{Si}_3\text{N}_4$  particles in the EL Ni-B matrix (Fig. 4.49) and supports the above view.

The specific wear rate is a measure of the ability of the EL Ni-B- $\text{Si}_3\text{N}_4$  composite coatings to offer wear resistance against the hard counterface material (hardened steel of EN 31). The increase in specific wear rate with increase in applied normal load from 20 to 40 N indicates a decrease in wear resistance at higher applied loads and this trend is common for both as-plated and heat-treated EL Ni-B- $\text{Si}_3\text{N}_4$  composite coatings. At all applied loads, the specific wear rate is less for heat-treated EL Ni-B- $\text{Si}_3\text{N}_4$  composite coatings compared to that obtained for the as-plated ones. This is due to the formation of hard nickel boride phases following heat-treatment, which presents a virtually incompatible surface for the counterface material, as there exists very little solubility between iron and these hard nickel boride phases, leading to a decrease in specific wear rate of heat-treated coatings. Besides, following heat treatment, there is considerable increase in the hardness of EL Ni-B- $\text{Si}_3\text{N}_4$  composite coatings due to the incorporation of  $\text{Si}_3\text{N}_4$  particles in the EL Ni-B matrix. The EL Ni-B- $\text{Si}_3\text{N}_4$  composite coating have a double strengthening

effect - dispersion strengthening of the hard  $\text{Si}_3\text{N}_4$  particles and precipitation strengthening of Ni-B alloy matrix. Hence, when the counterface material comes in contact with the EL Ni-B- $\text{Si}_3\text{N}_4$  composite matrix, the high hardness of the later enables it to experience a lesser wear.

The average friction coefficient,  $\mu_{av}$  of EL Ni-B- $\text{Si}_3\text{N}_4$  composite coatings in as-plated and heat-treated conditions, is also given in Table 4.8. The friction coefficient of EL Ni-B- $\text{Si}_3\text{N}_4$  composite coatings is relatively high compared to EL Ni-B coating owing to their higher surface roughness and high mechanical interlocking forces under similar loading and temperature conditions. Similar observations were also made earlier by Wu et al. (2000a, 2000b) and Grosjean et al. (2001). According to Grosjean et al. (2001), incorporation of SiC particles in EL Ni-P matrix leads to a gradual increase in friction coefficient due to the high hardness and abrasive properties of the particles themselves. The coefficient of friction of heat-treated EL Ni-B- $\text{Si}_3\text{N}_4$  composite coatings is relatively less compared to that obtained for the as-plated ones. As already mentioned, this is due to the ability of the heat-treated EL Ni-B- $\text{Si}_3\text{N}_4$  composite coatings to present a virtually incompatible surface for the hard counterface material.

The mechanism of wear of EL Ni-B- $\text{Si}_3\text{N}_4$  composite coatings depends on the attractive force that operates between the atoms of nickel from the coating and iron from the counter disk ((hardened steel of EN 31 specification). Adhesive wear is most likely to occur under the present experimental conditions which induce a substantial attractive force between these mating surfaces, leading to a high mutual solubility of nickel and iron. At the

beginning of the friction and wear process, the  $\text{Si}_3\text{N}_4$  particles protruding in the EL Ni-B matrix act as the main sliding plane in the contacting surface and participate in the wear. However, as the wear continues, the EL Ni-B alloy matrix takes part in the wear process as the second plane just after the surface layer containing particles being worn out. The EL Ni-B alloy matrix with good strengthening effect can effectively sustain the  $\text{Si}_3\text{N}_4$  particles firmly, which enables the matrix a high strengthening effect. The scanning electron micrographs of wear track pattern of EL Ni-B- $\text{Si}_3\text{N}_4$  composite coatings subjected to pin-on-disc wear test clearly indicate the presence of torn patches and, in some places even detachment of the coating, in their as-plated condition (**Fig. 4.52 (a)**). This type of morphological feature, commonly called as “prows” is reported for adhesive wear failure of EL Ni-P coatings, by several researchers (Statia et al., 1996; Gawne and Ma, 1987a, 1987b; Kanani, 1991; Dennis and Sagoo, 1991; Balaraju, 2000). The transferred patches from the EL Ni-B- $\text{Si}_3\text{N}_4$  composite coatings and the wear debris are also observed on the surface of the counter disc, which clearly indicates that adhesion between the EL Ni-B coated mild steel pins and the counter disc had occurred. The possibility of occurrence of adhesive wear under the experimental conditions used is also supported by the high mutual solubility of nickel and iron. Hence, adhesive wear appears to be the most likely mechanism during the wear process of EL Ni-B- $\text{Si}_3\text{N}_4$  composite coatings in their as-plated condition.

In contrast to the as-deposited coatings, heat-treated coatings after wear exhibit bright and smooth finish with fine grooves along the sliding direction (**Figs. 4.52 (b & c)**). In a substantial portion of the wear tracks, no gross adhesion between the coated pins and the counter disc is observed. The

increase in coating hardness following heat-treatment increases the plastic resistance of the coating and decreases the true area of contact between the mating surfaces, supporting the observed decrease in friction coefficient in the case of these deposits. The loose debris generated during the wear process gets displaced to the sides leading to the formation of grooves along the wear track. In support of the morphological features of the wear track pattern, the  $R_a$  value is relatively less for heat treated EL Ni-B-Si<sub>3</sub>N<sub>4</sub> composite coatings. The  $R_a$  value of EL Ni-B-Si<sub>3</sub>N<sub>4</sub> composite coating after wear testing at a load of 40 N is 0.11  $\mu\text{m}$  in as-plated and 0.08  $\mu\text{m}$  in heat-treated conditions.

Though the wear mechanism is quite similar for EL Ni-B and EL Ni-B-Si<sub>3</sub>N<sub>4</sub> composite coatings, the adverse effects due to wear is observed to be less in the case of EL Ni-B-Si<sub>3</sub>N<sub>4</sub> composite coatings. This can be ascribed to the presence of Si<sub>3</sub>N<sub>4</sub> particles in the EL Ni-B-Si<sub>3</sub>N<sub>4</sub> composite coatings, which decreases the available surface area for metal-to-metal contact, leading to a lesser degree of wear.

#### 4.4.7 CORROSION RESISTANCE

The potentiodynamic polarization curves of EL Ni-B-Si<sub>3</sub>N<sub>4</sub> composite coatings in 3.5% sodium chloride solution, both in as-plated and heat-treated (450°C for 1 hour) conditions, are shown in **Fig. 4.53(a)**. The corrosion potential ( $E_{\text{corr}}$ ) and corrosion current density ( $i_{\text{corr}}$ ), calculated using the Tafel extrapolation method are given in **Table 4.9**. The  $E_{\text{corr}}$  and  $i_{\text{corr}}$  of as-plated EL Ni-B-Si<sub>3</sub>N<sub>4</sub> composite coating are -476 mV vs. SCE and 4.42  $\mu\text{A}/\text{cm}^2$ , respectively. However, heat-treatment of the EL Ni-B-Si<sub>3</sub>N<sub>4</sub> composite coating at 450°C for 1 hour results in a shift in the  $E_{\text{corr}}$  value towards more negative

values (from -476 to -555 mV vs. SCE) and an increase in the  $i_{\text{corr}}$  value from 4.42 to 9.57  $\mu\text{A}/\text{cm}^2$ . The decrease in the linear polarization resistance (LPR) value from 5398 to 1795  $\text{ohms}\cdot\text{cm}^2$  also suggests a decrease in corrosion resistance of heat-treated EL Ni-B-Si<sub>3</sub>N<sub>4</sub> composite coatings. To confirm this aspect further, the current-time transient curves of the EL Ni-B-Si<sub>3</sub>N<sub>4</sub> composite coatings, both in as-plated and heat-treated (450°C for 1 hour) conditions, is recorded (**Fig. 4.53(b)**). It has been established that reduction of oxygen and dissolution of nickel are the major reactions occurring during cathodic and anodic polarization, respectively. Hence, the increase in current should have been due to the dissolution of nickel from the coating. To compare the ability of the as-plated and heat-treated EL Ni-B-Si<sub>3</sub>N<sub>4</sub> composite coatings, the time to reach a steady state current of 0.02 mA/cm<sup>2</sup> is taken as a failure criterion (Table 4.9). It is evident from Fig. 4.53(b) and Table 4.9 that the corrosion resistance of EL Ni-B-Si<sub>3</sub>N<sub>4</sub> composite coatings after heat-treatment is considerably decreased.

Several factors, which include, the composition of the coating, grain size, porosity, structure, surface features and heterogeneity of the coating, could influence the corrosion resistance of electro- and electroless plated deposits. The coating thickness of the EL Ni-B-Si<sub>3</sub>N<sub>4</sub> composite coatings used for the evaluation of corrosion resistance is 20  $\mu\text{m}$ . Hence, the contribution from the porosity factor is expected to be minimal. The codeposition of thallium along with nickel and boron could induce surface heterogeneity in EL Ni-B-Si<sub>3</sub>N<sub>4</sub> composite coatings. Besides, the distribution of Si<sub>3</sub>N<sub>4</sub> particles in the EL Ni-B matrix also influences the corrosion resistance. In as-plated condition, the EL Ni-B-Si<sub>3</sub>N<sub>4</sub> composite coating is amorphous and its grain size



is of the order of 2-3 nm. However, after heat-treatment at 450°C for 1 hour, the EL Ni-B-Si<sub>3</sub>N<sub>4</sub> composite coating becomes crystalline with the formation of crystalline Ni, Ni<sub>3</sub>B and Ni<sub>2</sub>B phases and, the grain size is increased to 8-10 nm. Scanning electron micrograph of the EL Ni-B-Si<sub>3</sub>N<sub>4</sub> composite coatings reveals a nodular growth with a columnar structure in which the Si<sub>3</sub>N<sub>4</sub> particles are distributed uniformly (Fig. 4.49). This type of surface feature could allow the transport of corrosive medium through them. Hence, it is evident that the surface heterogeneity and columnar structure are primarily responsible for the observed corrosion behaviour of the EL Ni-B-Si<sub>3</sub>N<sub>4</sub> composite coating in their as-plated condition. Heat-treatment induces crystallinity of the EL Ni-B-Si<sub>3</sub>N<sub>4</sub> composite coating and increases the grain boundaries, which are the active sites for corrosion attack.

The Nyquist plots of EL Ni-B-Si<sub>3</sub>N<sub>4</sub> composite coatings in 3.5% sodium chloride solution, both in as-plated and heat-treated conditions (450°C for 1 hour) at their respective open circuit potentials is shown in **Fig. 4.54**. The  $R_{ct}$  and  $C_{dl}$  values, calculated after fitting the data using Boukamp software are given in Table 4.9. The  $R_{ct}$  and  $C_{dl}$  values of as-plated EL Ni-B-Si<sub>3</sub>N<sub>4</sub> composite coating are 5525 ohms.cm<sup>2</sup> and 124 μF/cm<sup>2</sup>, respectively. However, heat-treatment of the EL Ni-B-Si<sub>3</sub>N<sub>4</sub> composite coating at 450°C for 1 hour results in a decrease in  $R_{ct}$  value from 5525 to 4024 ohms.cm<sup>2</sup> and an increase in  $C_{dl}$  value from 124 to 154 μF/cm<sup>2</sup>. It has been established that high values of  $R_{ct}$  and low values of  $C_{dl}$  imply a better corrosion protective ability of coatings (Van der Kouwe, 1993). The  $C_{dl}$  value is related to the porosity of the coating (Growcock and Jasinski, 1989). Zeller III (1991) reported a  $C_{dl}$  value of

28  $\mu\text{F}/\text{cm}^2$  for 50-60  $\mu\text{m}$  thick EL Ni-P (10 - 11 wt.%) coating in 5% NaCl solution. Van Der Kouwe (1993) reported  $C_{dl}$  values of 30 and 42  $\mu\text{F}/\text{cm}^2$  for 20  $\mu\text{m}$  thick EL Ni-high P coatings in 3% NaCl solution. Lo et al. (1995) reported the  $C_{dl}$  values in the range of 100 - 120  $\mu\text{F}/\text{cm}^2$  for electroless Ni-P (11.8 - 12.8 wt.% P) in 1 N NaOH solution at -1.2 V. Balaraju et al (2001) have reported the  $C_{dl}$  values in the range of 11-17  $\mu\text{F}/\text{cm}^2$  for electroless Ni-P and Ni-P composite coatings in 3.5% NaCl solution. The higher  $C_{dl}$  values of EL Ni-B-Si<sub>3</sub>N<sub>4</sub> composite coatings of the present study suggest that the columnar structure of the coating has allowed penetration of the electrolyte through them.

It is evident from Fig. 4.54 that EL Ni-B-Si<sub>3</sub>N<sub>4</sub> composite coatings, both in as-plated and heat-treated conditions (450°C for 1 hour), exhibit a semicircle in the high frequency region followed by a loop in the low frequency region. Though the curves in the Nyquist plot appear to be similar with respect to their shape, they differ considerably in their size. This indicates that same fundamental processes must be occurring on both the as-plated and heat-treated EL Ni-B-Si<sub>3</sub>N<sub>4</sub> composite coatings but over a different effective area in each case. The formation of a single semicircle or a semicircle in the high frequency region followed by a low frequency loop is typical of metallic coatings. The semicircle at high frequency region represents the coating response, while the loop at low frequency region is associated with simultaneous physicochemical phenomena at the metal/coating/solution interface (Atkinson and Smart, 1988; Balaraju and Seshadri, 1998; Lo et al., 1995; Contreras et al., 2006). Mansfeld et al. (1982) suggest that the low frequency loop is associated with the double

layer capacitance and/or diffusion phenomena of the oxidant chemical species through the porous coating.

In order to get a better insight about the coating response as well as the diffusion phenomenon, Bode plots (Log  $f$  vs. Log  $|Z|$  and Log  $f$  vs Phase angle) are constructed. The Bode plots of EL Ni-B-Si<sub>3</sub>N<sub>4</sub> composite coatings, both in as-plated and heat-treated conditions (450°C for 1 hour), indicate the presence of two phase angle maxima (**Fig. 4.55**) suggesting the involvement of two time constants. The two phase angle maxima could be related to the electrolyte/coating and the electrolyte/ substrate interface. The occurrence of the second phase angle maximum clearly indicates that the electrolyte has penetrated via pores in these coatings to create another interface, namely, the electrolyte/substrate. The surface morphology of the EL Ni-B-Si<sub>3</sub>N<sub>4</sub> composite coatings (Fig. 4.49) strongly supports this view. The nodular growth with a columnar structure of the EL Ni-B-Si<sub>3</sub>N<sub>4</sub> composite coatings enables the electrolyte to penetrate through them. The Bode plot (Fig. 4.55) confirms the involvement of a diffusion phenomenon in the low frequency regions.

A comparison of the corrosion behaviour of EL Ni-B and Ni-B-Si<sub>3</sub>N<sub>4</sub> composite coatings (Figs. 4.30-4.32 and Table 4.5 with Figs.4.53-4.55 and Table 4.7) clearly reveals that the corrosion resistance of EL Ni-B-Si<sub>3</sub>N<sub>4</sub> composite coating is relatively higher than EL Ni-B coatings, both in as-plated and heat-treated conditions. Corrosion resistance of ED and EL composite coatings has been a debatable issue in the published literature (Table 1.8). The improvement or impairment of corrosion resistance of ED and EL composite coatings depends on the chemical stability of the particle, effective metallic

area prone to corrosion, structural state or microstructural feature of the coating, porosity or defect size of the coating, ability to prevent diffusion of chloride ions along the interface between the metal and the particle, the ability of the particle to prevent the corrosive pits from growing up, etc. The  $\text{Si}_3\text{N}_4$  particles are chemically stable in 3.5% sodium chloride solution. It is obvious to expect that the incorporation of  $\text{Si}_3\text{N}_4$  particles in the EL Ni-B matrix would decrease the effective metallic area prone to corrosion. Besides, the incorporation of  $\text{Si}_3\text{N}_4$  particles in the EL Ni-B matrix enables a change in microstructure and decreases the columnar size which is evidenced by the scanning electron micrographs (Fig. 4.49). The change in microstructural feature of the EL Ni-B- $\text{Si}_3\text{N}_4$  composite coating enables them to decrease the penetration of the chloride ions across the metal-solution interface and offer a better corrosion resistance compared to EL Ni-B coatings.

## **PART C – DUPLEX, MULTILAYER AND GRADED COATINGS**

### **4.5 ELECTROLESS Ni-P/Ni-B DUPLEX COATINGS**

#### **4.5.1 COATING SYNTHESIS**

The electroless (EL) Ni-P/Ni-B duplex coatings having both Ni-P and Ni-B coatings as inner and outer layers are prepared by sequential treatment in both the hypophosphite- and borohydride-reduced electroless nickel plating baths (**Tables 4.10 and 4.11**). Two types of duplex coatings are prepared; the first type having Ni-P as the outer layer and Ni-B as the inner layer whereas the second type having Ni-B as the outer layer and Ni-P as the inner layer. The thickness of each individual layer is kept as 10  $\mu\text{m}$  and the total coating thickness in all the cases is kept constant as 20  $\mu\text{m}$ . The performance of the two types of duplex coatings is compared with that of EL Ni-P and Ni-B coatings having a similar thickness.

#### **4.5.2 PLATING RATE AND CHEMICAL COMPOSITION**

It is essential to study the characteristics of the hypophosphite- and borohydride reduced EL plating baths and the resultant Ni-P and Ni-B coatings so as to use these baths to prepare the duplex coatings and to evaluate their performance. The plating rate of EL Ni-P and Ni-B coatings from their respective baths as a function of time is determined by measuring the gain in weight after plating and using the density of the coating (**Fig. 4.56**). It is evident that the thickness of EL Ni-P and Ni-B coatings increases with increase in plating time. However, the extent of increase in thickness is not linear throughout the entire duration of plating and it saturates after some time. This

is due to the decrease in the concentration of reducing agents and accumulation of oxidation products of hypophosphite and borohydride in their respective baths. The plot of thickness of the deposit versus plating time (Fig. 4.56) is used to prepare EL Ni-P/Ni-B duplex coatings having different layer thickness (10  $\mu\text{m}$  each). The chemical composition of the EL Ni-P and Ni-B coatings is given in **Table 4.12**. The EL Ni-P coating contains 9 wt.% phosphorous and 91 wt.% nickel, whereas the EL Ni-B coating contains 6.5 wt.% boron, 93.2 wt.% nickel and 0.3 wt.% thallium. The incorporation of thallium in the EL Ni-B coating is unavoidable since thallium acetate is used as the stabilizer and without the addition of thallium acetate it is not easy to prepare EL Ni-B coating with higher coating thickness.

### 4.5.3 STRUCTURAL CHARACTERISTICS

The XRD patterns of EL Ni-P and EL Ni-B coatings, both in as-plated and heat-treated (450°C for 1 hour) conditions are shown in **Figs. 4.57 and 4.58**, respectively. In as-plated condition, only a single broad peak around  $45^\circ 2\theta$  is observed for both EL Ni-P and EL Ni-B coatings (Figs. 4.57(a) and 4.58(a)). Theoretically, a disorder in arrangement of atoms manifests itself as a broad peak in X-ray diffractograms (Warren, 1969). The XRD patterns of as-plated EL Ni-P and Ni-B coatings can be explained based on the mechanism of formation of these coatings. During electroless deposition, phosphorous or boron atoms are randomly captured on the nickel atoms and the rate of segregation of nickel and phosphorous/boron atoms determines the crystallinity of the resultant coating. The rate of diffusion of phosphorous or boron is relatively small compared to that of nickel (Szasz et al., 1988). Hence, if the

coating contains higher amount of phosphorous/boron, then a larger number of phosphorous/boron atoms must be moved from a given area per unit time during deposition to achieve segregation of nickel and phosphorous/boron (Allen and Vander Sande, 1982). Chemical analysis reveals that the phosphorus and boron content of the EL Ni-P and EL Ni-B coatings are 9 and 6.5 wt.%, respectively. As the required phosphorous or boron segregation is very large, the nucleation of f.c.c nickel phase is prevented and this has resulted in an amorphous structure.

The XRD patterns of EL Ni-P and EL Ni-B coatings, after heat treatment at 450°C for 1 hour are shown in Figs. 4.57(b) and 4.58(b), respectively. In contrast to the single broad peak in their as-plated condition, several sharp peaks are observed after heat-treatment. These peaks, upon indexing indicate the presence of  $\text{Ni}_3\text{P}$  and Ni in case of EL Ni-P coatings (Fig. 4.57(b)) and Ni,  $\text{Ni}_3\text{B}$  and  $\text{Ni}_2\text{B}$  in case of EL Ni-B coatings (Fig. 4.58(b)). During heat treatment, the EL Ni-P and Ni-B coatings are transformed from a disordered structure to an ordered arrangement.

Obviously, one would expect the formation of both nickel phosphide and nickel boride phases along with nickel when the EL Ni-P/Ni-B duplex coatings are subjected to heat-treatment. The XRD pattern of EL Ni-P/Ni-B duplex coating heat-treated at 450°C for 1 hour confirms the presence of Ni,  $\text{Ni}_3\text{P}$  and  $\text{Ni}_3\text{B}$  phases (**Fig. 4.59**). The formation of both  $\text{Ni}_3\text{P}$  and  $\text{Ni}_3\text{B}$  phases in duplex coatings suggests that it is possible to impart the qualities of both Ni-P and Ni-B coatings in the duplex coating.

The scanning electron micrographs of the cross-section of EL Ni-P/Ni-B and Ni-B/Ni-P duplex coatings in their as-plated conditions are shown in **Figs. 4.60(a) and 4.61(a)**, respectively. It is evident from these figures that these duplex coatings are uniform and the compatibility between the EL Ni-P and EL Ni-B layers is good. The compatibility between these layers is found to be good even after heat-treatment at 450°C for 1 hour (**Figs. 4.60(b) and 4.61(b)**). However, some cracks are formed in heat-treated duplex coatings due to the brittleness of the EL Ni-B coating (Fig. 4.60(b)).

#### 4.5.4 MICROHARDNESS

The microhardness of EL Ni-P, EL Ni-B and the duplex coatings, both in as-plated and heat-treated (450°C for 1 hour) conditions, is given in **Table 4.13**. For all the coatings studied, the microhardness is higher for coatings subjected to heat-treatment (450°C for 1 hour) than those in as-plated condition. This is due to the formation of hard nickel phosphide phase ( $\text{Ni}_3\text{P}$ ) in EL Ni-P coating, nickel boride phase ( $\text{Ni}_3\text{B}$ ) in EL Ni-B coating and both nickel phosphide and nickel boride phases ( $\text{Ni}_3\text{P}$  and  $\text{Ni}_3\text{B}$ ) in duplex coatings. The formation of such phases is confirmed by XRD measurements (Figs. 4.57(b), 4.58(b) and 4.59). The microhardness of duplex coatings is higher than that of EL Ni-P and EL Ni-B coatings of similar thickness, both in as-plated and heat-treated (450°C for 1 hour) conditions. Between the two types of duplex coatings, the coating having EL Ni-B outer layer exhibits a higher hardness. The difference in microhardness between these duplex coatings will have a definite impact on the wear resistance of these coatings.



#### 4.5.5 WEAR RESISTANCE

The specific wear rate of EL Ni-P, EL Ni-B and the duplex coatings, of similar thickness, at an applied load of 40 N, both in as-plated and heat-treated (450°C for 1 hour) conditions, is given in **Table 4.14**. A comparison of the specific wear rate of all the coatings studied reveals that coatings that are heat-treated offer better wear resistance than the as-plated ones. The formation of hard  $\text{Ni}_3\text{P}$  and  $\text{Ni}_3\text{B}$  phases following heat-treatment, presents a virtually incompatible surface for the counterface material as there exists very little solubility between iron and these hard phases, leading to a decrease in specific wear rate. Besides, following heat-treatment, there is a considerable increase in the hardness of the coatings. Hence, when the counterface material comes in contact with the matrix, because of the high hardness, the matrix experiences lesser wear. The specific wear rate of duplex coatings is lesser than that of EL Ni-P and EL Ni-B coatings of similar thickness, both in as-plated and heat-treated (450°C for 1 hour) conditions. Between the two types of duplex coatings, the coating having EL Ni-B outer layer exhibits a lower specific wear rate. This could be attributed to the higher hardness of EL Ni-B coating, which facilitates the coating to experience lesser wear.

The mechanism of wear of EL Ni-P, EL Ni-B and the duplex coatings depends on the attractive force that operates between the atoms of nickel from the coating and iron from the counter disk (hardened steel of EN 31 specification). Adhesive wear is most likely to occur under the experimental conditions used, which induce a substantial attractive force between the mating surfaces, leading to a high mutual solubility of nickel and iron. The optical

micrographs of EL Ni-P, Ni-B and the two types of duplex coatings subjected to pin-on-disc wear test clearly indicate the presence of torn patches and, in some places even detachment of the coating, in their as-plated condition (**Figs. 4.62(a)-4.62(d)**). This type of morphological feature, commonly called as "prows" is reported for adhesive wear failure of EL Ni-P coatings, by several researchers (Statia et al., 1996; Gawne and Ma, 1987a, 1987b; Kannai, 1991; Dennis and Sagoo, 1991; Balaraju, 2000). Hence, adhesive wear appears to be the most likely mechanism during the wear process of EL Ni-P, EL Ni-B and the duplex coatings in their as-plated condition. Though the wear mechanism is the same, the adverse effects due to wear is observed to be less in the case of duplex coatings (Figs. 4.62(c) and 4.62(d)). Between the two types of duplex coatings, coating that has EL Ni-B as the outer layer exhibits lesser wear due to the higher microhardness of the EL Ni-B coating (Fig. 4.62(d)). In contrast to the as-deposited coatings, heat-treated coatings after wear, exhibit a bright and smooth finish with fine grooves along the sliding direction (**Figs. 4.63(a) - 4.63(d)**). Though this trend is common for EL Ni-P, EL Ni-B and the duplex coatings, the extent of adhesive wear is less pronounced in the case of duplex coatings (Fig. 4.63(c) and 4.63(d)).

#### 4.5.6 CORROSION RESISTANCE

The electrochemical parameters derived from potentiodynamic polarization and electrochemical impedance studies, such as, corrosion potential ( $E_{\text{corr}}$ ), corrosion current density ( $i_{\text{corr}}$ ), charge transfer resistance ( $R_{\text{ct}}$ ) and double layer capacitance ( $C_{\text{dl}}$ ), for all the coating systems studied, both in as-plated and heat-treated conditions, are presented in **Table 4.15**. There

appears to be a significant decrease in corrosion current density and increase in charge transfer resistance for EL Ni-P/Ni-B and EL Ni-B/Ni-P duplex coatings, compared to those obtained for EL Ni-P and EL Ni-B coatings. The loss in protective ability of the coatings upon heat-treatment at 450°C for 1 hour is clearly evident from the low values of charge transfer resistance, higher corrosion current densities and the cathodic shift in the corrosion potential.

The polarization curve of EL Ni-P/Ni-B duplex coating heat-treated at 450°C for 1 hour and the Nyquist plot of EL Ni-B/Ni-P duplex coating in its as-plated condition, at their respective open circuit potentials, are given in **Figs. 4.64 and 4.65**, respectively. The Nyquist plots of EL Ni-P, EL Ni-P/Ni-B and EL Ni-B/Ni-P duplex coatings, both in as-plated and heat-treated conditions, at their respective open circuit potentials, in 3.5% sodium chloride solution exhibit a single semicircle in the high frequency region whereas the Nyquist plot of EL Ni-B coatings, both in as-plated and heat-treated conditions, at their respective open circuit potentials, in 3.5% sodium chloride solution exhibit a semicircle in the high frequency region followed by a loop in the low frequency region (Fig. 4.31).

The corrosion behaviour of EL Ni-P/Ni-B and Ni-B/Ni-P duplex coatings, at their respective open circuit potentials, can be accounted using the equivalent electrical circuit model consisting of solution resistance, double layer capacitance and charge transfer resistance, in which the  $C_{dl}$  and  $R_{ct}$  are parallel to each other. Lo et al. (1995) and Balaraju et al. (2001) have also used a similar model to study the electrochemical impedance behavior of electroless Ni-P coatings in 1 M NaOH at -1.2 V vs. SCE and in 3.5% NaCl solution at

-0.32 V vs. SCE, respectively. The occurrence of a single semicircle in the Nyquist plots indicates that the corrosion process of EL Ni-P/Ni-B and EL Ni-B/Ni-P duplex coatings involves a single time constant. The appearance of a single inflection point in the plot of  $\log f$  versus  $\log Z$  and a single phase angle maximum in the plot of  $\log f$  versus phase angle (figure not shown), further confirms that the process involves only a single time constant. Hence, it is evident that the coating-solution interface of EL Ni-P/Ni-B and EL Ni-B/Ni-P deposits exhibit charge transfer behaviour.

The observed difference in the corrosion resistance of the two types of duplex coatings is due the difference in the corrosion behaviour of EL Ni-P and EL Ni-B coatings (Table 4.15). Since borohydride-reduced electroless nickel coating is not totally amorphous, the passivation films that form on its surface are not as glassy or protective as those that form on EL Ni-high-P coatings. The phase boundaries present in EL Ni-B coatings also produce passivation film discontinuities, which are preferred sites for corrosion attack to begin. Also, the inhomogeneous distribution of boron and thallium throughout the coating would create areas of different corrosion potential, leading to the formation of minute active/passive corrosion cells and accelerate the corrosion attack. Hence, in duplex coating systems, when EL Ni-B coating is used as the outer layer, the corrosion resistance is decreased (Table 4.15). On the other hand, when EL Ni-P coating is used as the outer layer, the ability of the EL Ni-P coating to impart passivity helps to increase the corrosion resistance significantly (Table 4.15).

## 4.6 MULTILAYER COATINGS

Metallic multilayer coatings are an emerging area of research, which offer the possibility to manipulate the desirable characteristics so as to meet the demands for a specific industrial application (Panagopoulos et al., 2000b). Electrodeposition is a viable method to prepare multilayer coatings. Panagopoulos et al. (2000b) have explored the possibility of producing Ni-P-W multilayered alloy coatings consisting of alternate layers having low and high tungsten content, by pulsed current electrodeposition. Chen et al. (2006b) have studied the utility of multi-layered EL Ni-P coatings to improve the corrosion resistance of powder-sintered Nd-Fe-B permanent magnet. Gu et al. (2005a, 2005b) have studied the role of multilayer coatings consisting of different layers of Ni-P and Ni on steel obtained by electro- and electroless deposition processes, respectively and multilayered EL Ni-P coatings on AZ 91D Mg alloy to improve their corrosion resistance.

Electrodeposition of multilayers can be carried out using either a single bath or dual baths. In dual bath technique, the substrate is successively transferred between two separate plating baths and each layer is deposited alternatively to laminate the sub-layer from the relevant bath. Dual bath technique has the disadvantage that it is susceptible to the formation of oxide layer on the substrate during the transfer between the baths. Such an oxide layer can deteriorate the quality of the multilayers. In the single bath technique, an electrolyte containing two or more metals can be used. Deposition of multilayers from a single bath is normally carried out by periodically varying the current density owing to the difference in the reduction potential of the

metal ions present in the electrolyte. This technique was effectively used to produce Cu-Ni, Cu-Co, Cu-Co-P, Cu-Ag and Cr-Ni multilayers.

The mechanism of deposition of Ni-B coatings by electrodeposition process (section 4.1) clearly indicates that coatings deposited at  $0.4 \text{ A/dm}^2$  has a higher boron content whereas those deposited at  $4 \text{ A/dm}^2$  has a very low boron content. XRD studies also confirm that the structure of the Ni-B coating electrodeposited at  $4 \text{ A/dm}^2$  is fully crystalline whereas the crystallinity of the Ni-B coating is considerably decreased when electrodeposited at  $0.4 \text{ A/dm}^2$ . The microhardness of Ni-B coating electrodeposited at  $4 \text{ A/dm}^2$  is relatively lower whereas those electrodeposited at  $0.4 \text{ A/dm}^2$  is relatively higher. Similarly, a considerable variation in other properties of the coating, such as wear resistance, corrosion resistance, etc. following the variation in the boron content as a function of current density can be expected. The variation in structure, hardness and other properties suggest that ED Ni-B multilayer coatings having an alternate layers of Ni-high B and Ni-low B can be prepared by alternatively varying the current density between  $0.4$  and  $4 \text{ A/dm}^2$ .

In the present investigation, the Ni-B multilayer coatings were prepared by electrodeposition technique using a dimethylamine borane (DMAB) modified Watts' nickel bath, with DMAB as the source of boron. It is essential to determine the rate of deposition of Ni-B coatings as a function of current density so that thickness of the individual layers in the multilayer coatings can be properly controlled. The time required to build a 10 micron thick Ni-B coating as a function of current density is shown in **Fig. 4.66**. The Ni-B multilayer coating, having a periodicity of 10 microns, is prepared by

alternatively varying the current density between 0.4 and 4 A/dm<sup>2</sup> for 90 and 14 minutes, respectively. Anodic etching at a very low current density of 0.2 A/dm<sup>2</sup> is given after electrodeposition of each individual layer to improve the quality as well as the uniformity of the coating. The plating bath is replenished after deposition of every period. Optical micrograph of the ED Ni-B multilayer coating (**Fig. 4.67**) reveals that the coating is uniform and the compatibility between the layers is good. The microhardness of the Ni-B multilayer coating, tested at every 10 micron thickness, indicate a variation in the hardness, which is of the order of 654 HV<sub>0.1</sub> at the 10 micron layer prepared at 0.4 A/dm<sup>2</sup> and 340 HV<sub>0.1</sub> for the 10 micron layer prepared at 4 A/dm<sup>2</sup>, due to the variation in the boron content in these layers.

The ED Ni-B multilayer coatings prepared by alternatively varying the current density between 0.4 and 4 A/dm<sup>2</sup> suggest that it is possible to manipulate the ED Ni-B multilayer coatings with the desirable characteristics, by suitably modifying the bath composition and/or operating conditions.

#### **4.7 GRADED COATINGS**

Graded coatings have received considerable attention in recent years. Graded coatings have been produced by various methods such as thermal plasma spray, physical vapour deposition, chemical vapour deposition, and electro-deposition. Process limitations such as restrictions on size or shape of the component to be coated as well as process economics are the major constraint of the first three methods. Electrodeposition, however, is a relatively simple and cost-effective technique that allows deposition of coatings on complex shapes and large sized components without much difficulty.

Wang et al. (2002b) have reported that by suitably varying the bath temperature and the current density during electrodeposition it is possible to prepare ED nanostructured Ni-W gradient coating. The formation of ED Ni-P gradient coatings by gradual variation in the applied current density is also reported by Wang et al (2006a). According to them, functionally graded ED Ni-P coatings exhibit much better adhesive strength and high wear resistance compared to un-graded ED Ni-P coatings. Wang et al. (2006b) have also reported the formation of nanocrystalline Ni-Co alloys with continuous gradation in composition and structure by electrodeposition. They have suggested that with continuous changes in composition and structure of the ED Ni-Co alloys, the internal stress generated during the electrodeposition process is decreased to approximately the minimum level and the resultant coatings are found to possess better tribological properties. Sankara Narayanan et al. (2006) have reported the formation of EL Ni-P graded coatings having a gradation in the phosphorus content by sequential immersion in three different hypophosphite-reduced electroless plating baths. The EL Ni-P graded coating offer better corrosion resistance than un-graded EL Ni-P coatings and among the graded coatings those with EL Ni-high P outer layer is much superior in this respect. Banovic et al. (1999) have shown that by proper manipulation of the process variables, discretely graded electro-composites, with layers of varying volume percent of alumina could be prepared. Kim and Yoo (1998) have reported the formation of a bilayer ED Ni-SiC composite coating from a single bath in a single run by varying the current density and deposition time. They have suggested that by proper manipulation of process variables, bilayer electro-composites, with layers of varying vol.% of SiC can be produced. By



employing a current density of  $10 \text{ A/dm}^2$  for 30 minutes and  $1 \text{ A/dm}^2$  for 5 hours, they have obtained a variation in the level of incorporation of SiC of 5.4 and 24.6 vol.%, in the ED Ni matrix.

The possibility of preparing ED Ni-B graded coating having a gradation in the boron content throughout the thickness of the coating is explored. The two possible approaches to prepare ED Ni-B graded coatings are: (i) by varying the concentration of dimethylamine borane (DMAB) in the Watt's nickel plating bath; and (ii) by varying the current density. In the present investigation, variation in DMAB concentration is not attempted since excess concentration of DMAB could destabilize the plating bath and use of higher concentration of DMAB is not economical. The ED Ni-B graded coatings are prepared by continuously varying the current density between  $0.4$  and  $4 \text{ A/dm}^2$ . Based on the plating rate at each current density and the time required to coat a 10 micron thick coating (Fig. 4.66), the ED Ni-B graded coating is prepared. At each current density a 10 micron thick Ni-B coating is deposited. During plating, the plating bath was continuously filtered and replenished at regular intervals.

The ED Ni-B coatings prepared at  $0.4 \text{ A/dm}^2$  has relatively higher boron content than those prepared at  $4 \text{ A/dm}^2$  (Table 4.1). ED Ni-B coatings with higher boron content are expected to possess higher hardness, better wear and corrosion resistance. However, the time required to prepare a 10 micron thick ED Ni-B coating at  $0.4 \text{ A/dm}^2$  is about 90 minutes, which is practically not viable whereas the Ni-B coating of similar thickness can be electrodeposited in about 12 minutes at  $4 \text{ A/dm}^2$ . Hence, the formation of a Ni-B graded coating by

continuously decreasing the current density from 4 to 0.4 A/dm<sup>2</sup> assumes significance in terms of saving the time as well as to impart the desirable characteristics in the coating. The prepared ED Ni-B graded coating has a total thickness of 60 microns. The cross sectional optical micrograph of the ED Ni-B graded coating is shown in **Fig. 4.68**. In order to understand the gradation in the ED Ni-B coating, the microhardness of the coated layer is evaluated at every 10 micron interval. The hardness profile as a function of coating thickness is shown in **Fig. 4.69**. It is evident that with increase in coating thickness (decrease in current density) the hardness of the coating is increased. The ED Ni-B graded coating with a relatively hard outer layer is expected to offer a better wear resistance. Much remains to be explored on ED Ni-B graded coatings.

#### **4.8 COMPARISON OF THE IMPORTANT CHARACTERISTICS OF Ni-B AND Ni-B-Si<sub>3</sub>N<sub>4</sub> COMPOSITE COATINGS**

A comparison of the important characteristics of Ni-B coatings obtained by electro- and electroless deposition processes is given in **Table 4.16** and a similar comparison of ED and EL Ni-B-Si<sub>3</sub>N<sub>4</sub> composite coatings is given in **Table 4.17**. The rate of deposition is higher for EL Ni-B coatings. The hardness of ED and EL Ni-B coatings is comparable. EL Ni-B coatings offer a better resistance to wear and corrosion. The level of incorporation of Si<sub>3</sub>N<sub>4</sub> particles is relatively higher in ED Ni-B-Si<sub>3</sub>N<sub>4</sub> composite coatings. The hardness of ED and EL Ni-B-Si<sub>3</sub>N<sub>4</sub> composite coatings is comparable. The EL Ni-B-Si<sub>3</sub>N<sub>4</sub> composite coatings offer a better resistance to wear and corrosion.

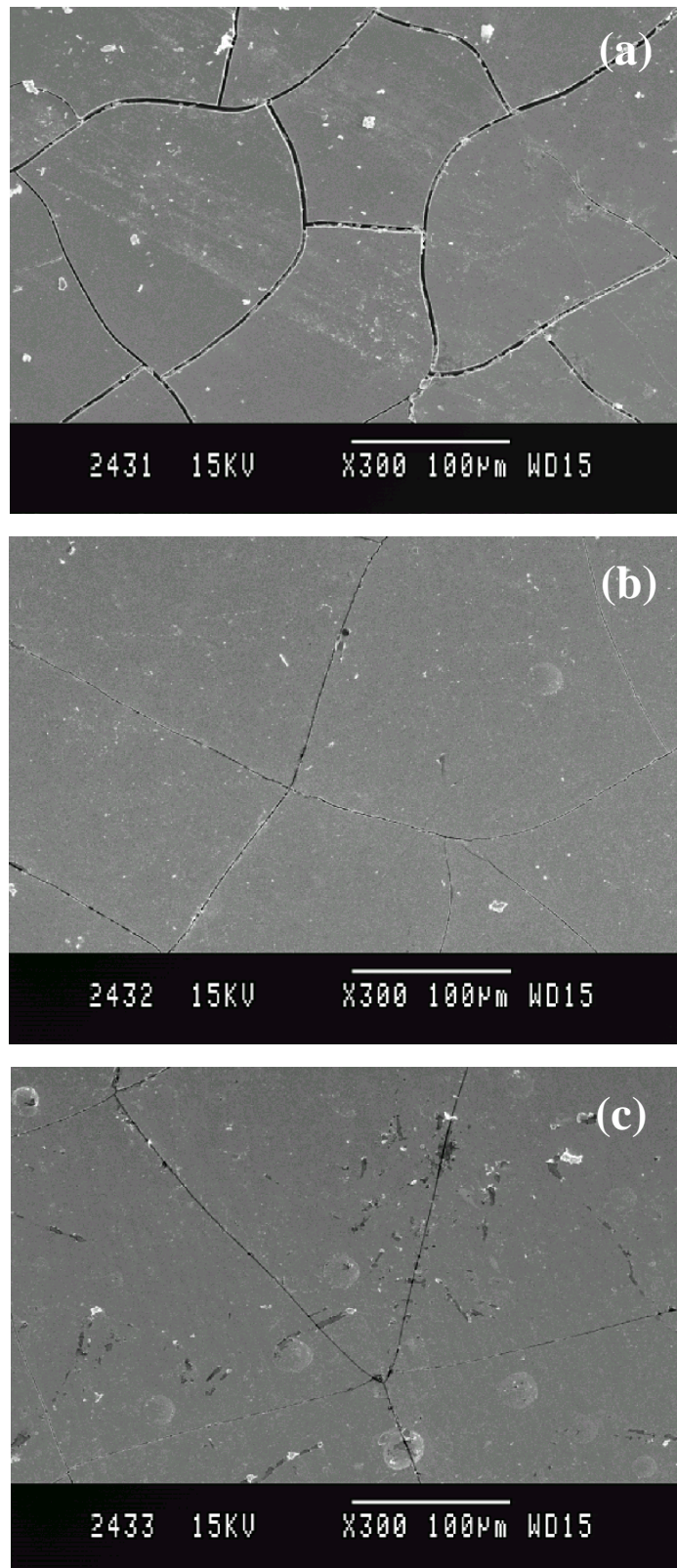


**Fig. 4.1 Surface morphology of Ni-B coatings electrodeposited at various current densities: (a)  $0.4 \text{ A/dm}^2$ ; (b)  $1 \text{ A/dm}^2$ ; and (c)  $4 \text{ A/dm}^2$**

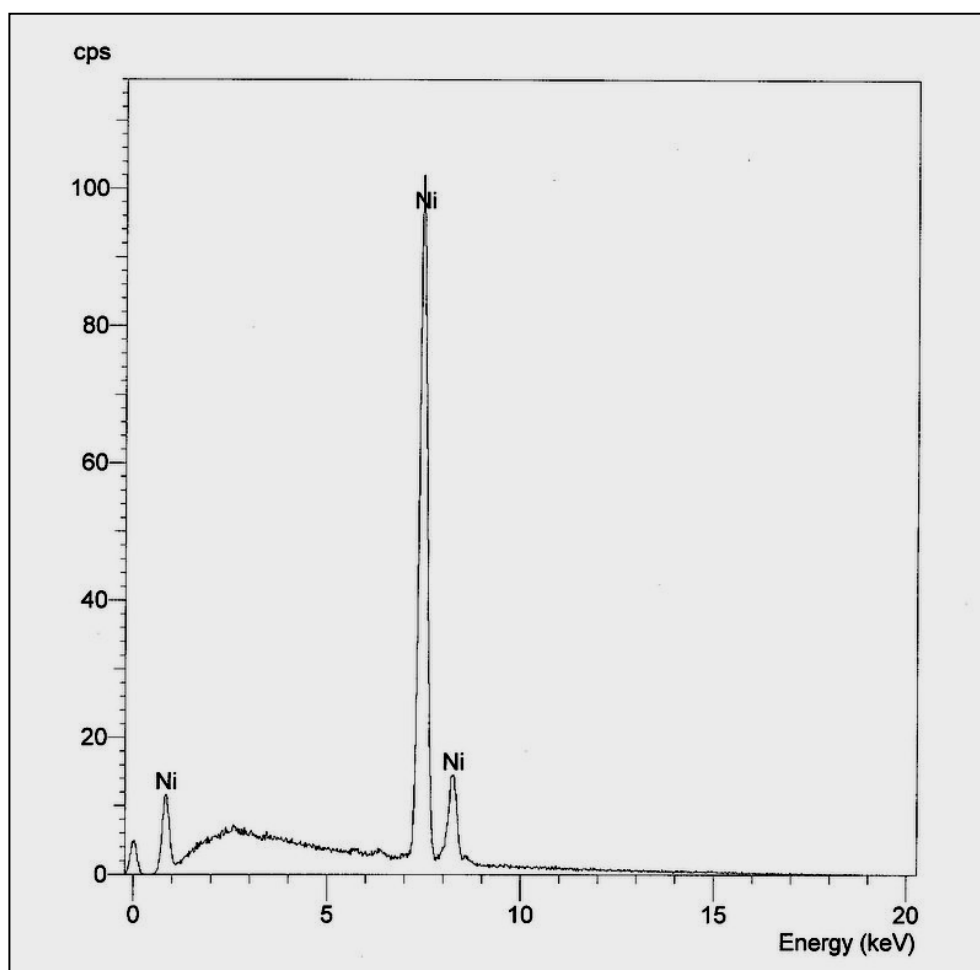


**Fig. 4.2 EDX spectrum of Ni-B coating electrodeposited at 1 A/dm<sup>2</sup>**

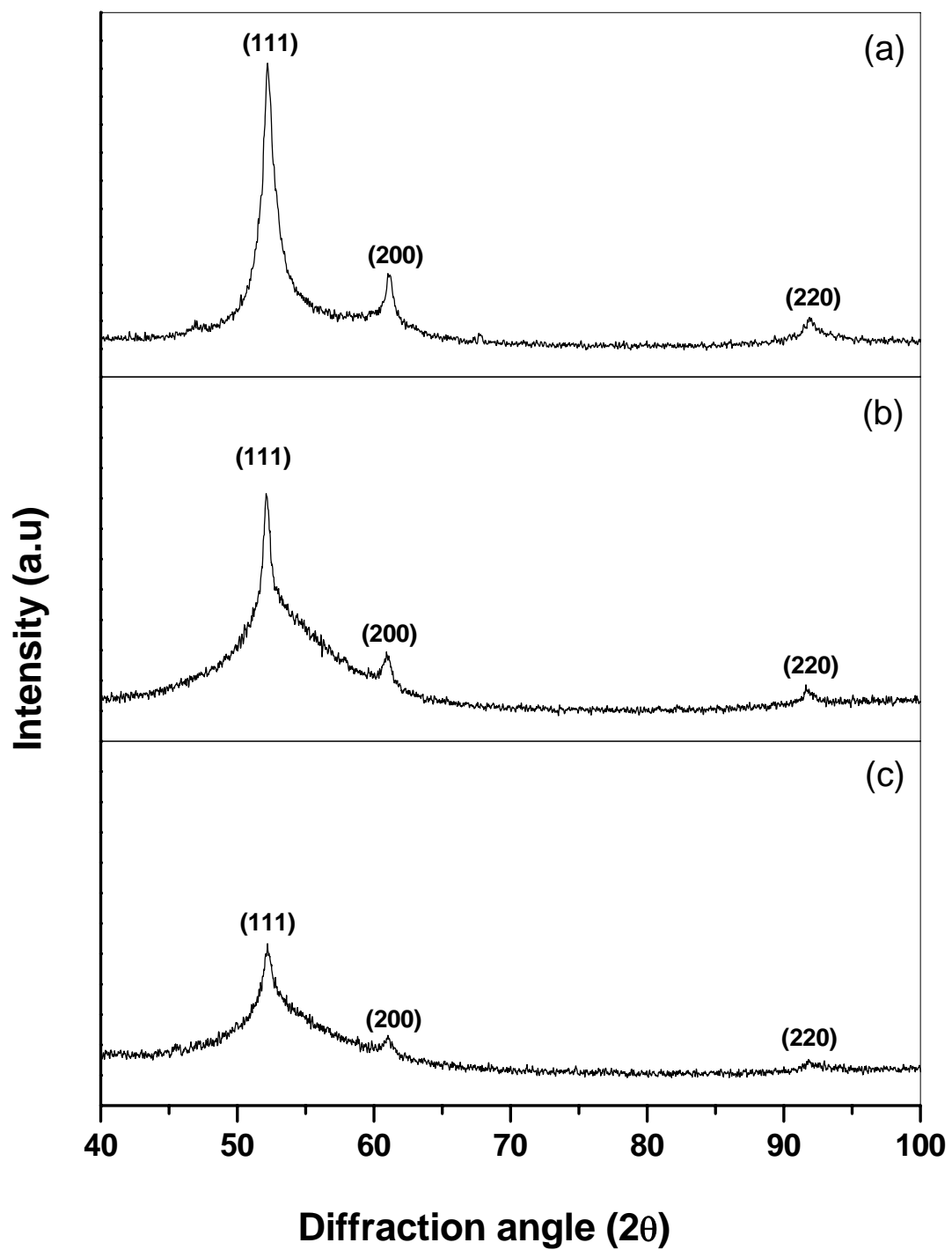


**Fig. 4.3 X-ray diffraction pattern of Ni-B coatings electrodeposited at various current densities in their as-plated condition:**  
(a) 4 A/dm<sup>2</sup>; (b) 1 A/dm<sup>2</sup>; (c) 0.4 A/dm<sup>2</sup>

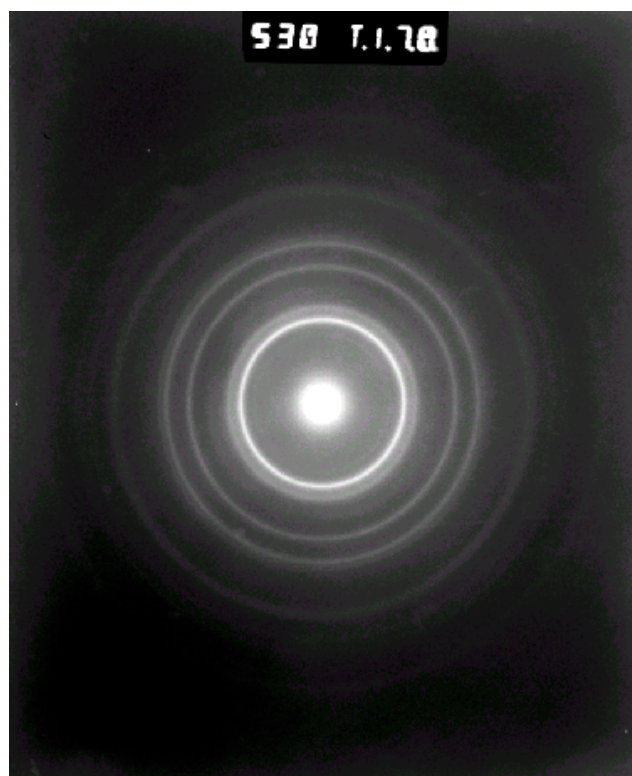


**Fig. 4.4** Selected area diffraction pattern of Ni-B coating electrodeposited at  $1 \text{ A/dm}^2$  in its as-plated condition (530 mm)

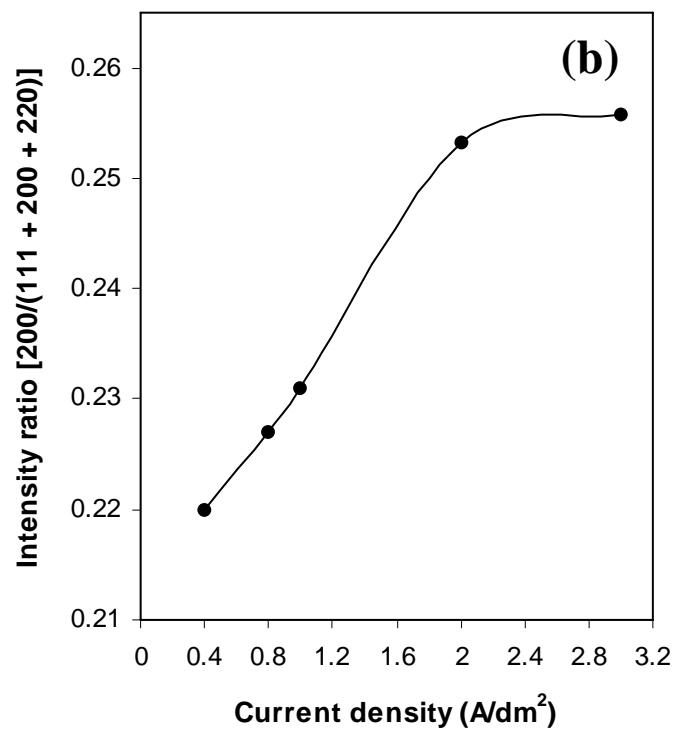
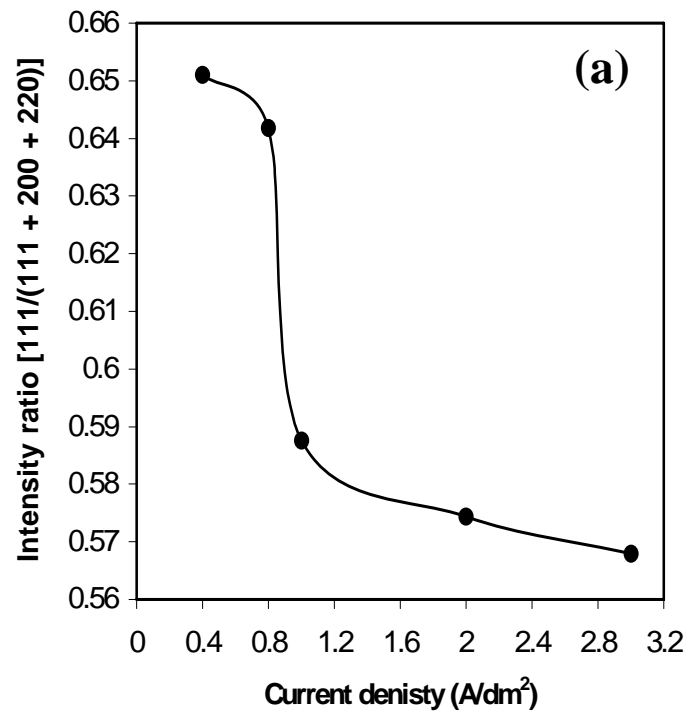


**Fig. 4.5 Variation in the intensity ratio of Ni (111) or Ni (200) to the sum of the intensities of Ni (111 + 200 + 220), as a function of current density (a) Ni (111)/ Ni (111 + 200 + 220); and (b) Ni (200)/ Ni (111 + 200 + 220)**

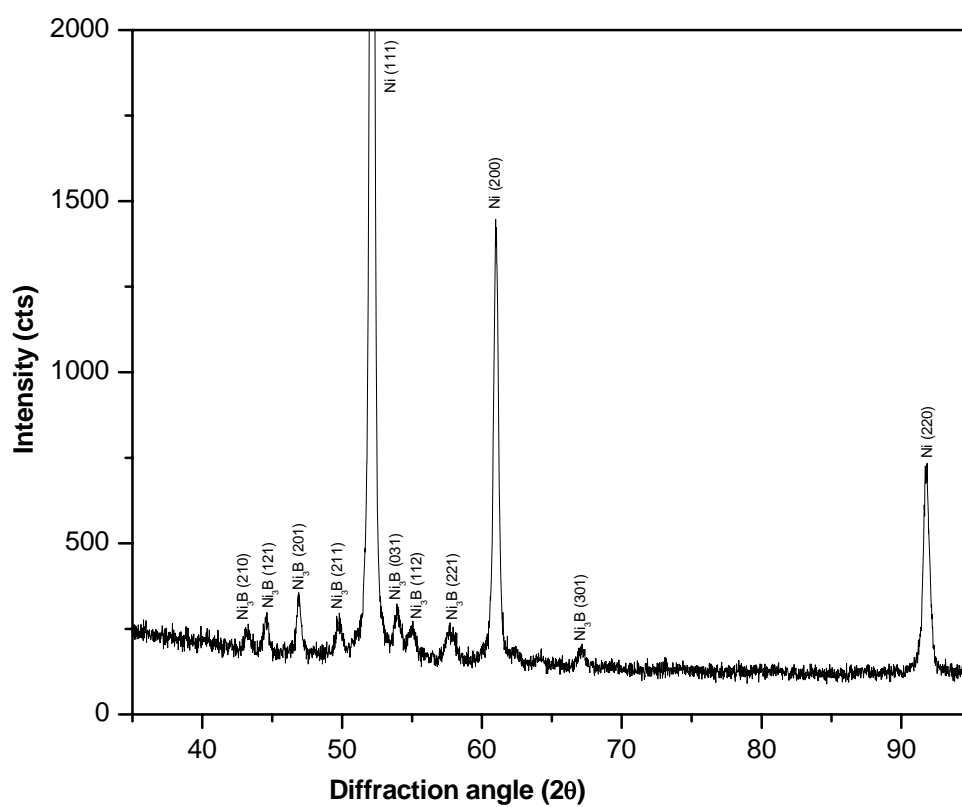


**Fig. 4.6 X-ray diffraction pattern of Ni-B coating electrodeposited at 0.4 A/dm<sup>2</sup> after heat-treatment at 400°C for 1 hour**



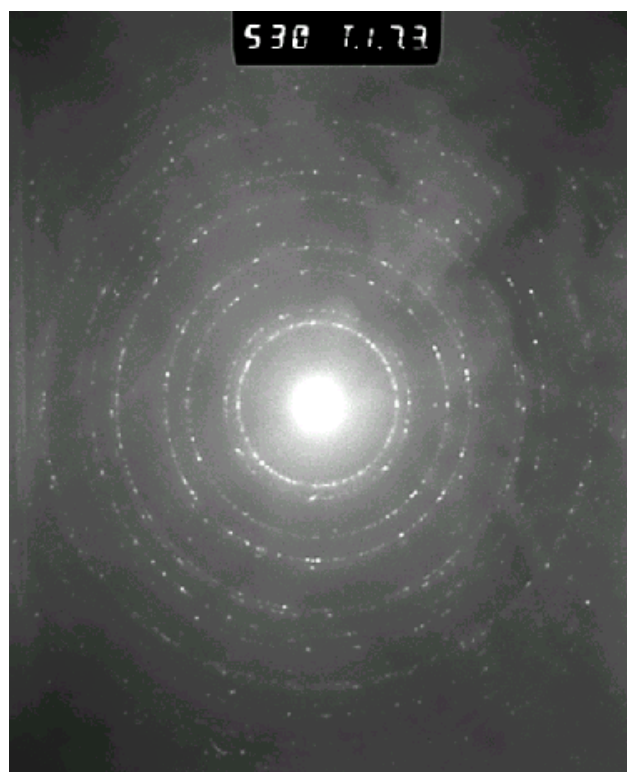


**Fig. 4.7** Selected area diffraction pattern of Ni-B coating electrodeposited at  $1 \text{ A/dm}^2$  after heat-treatment at  $400^\circ\text{C}$  for 1 hour (530 mm)

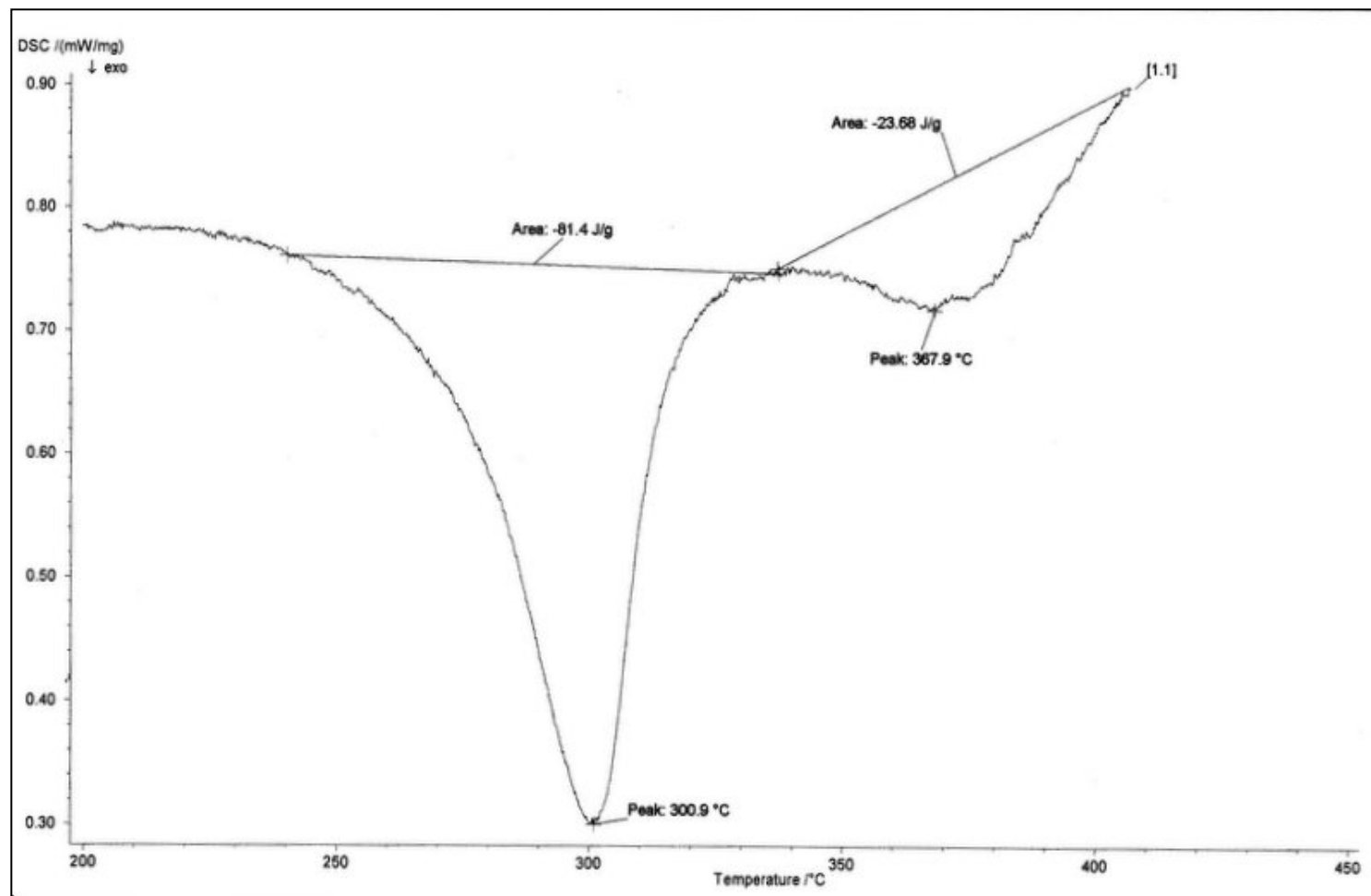
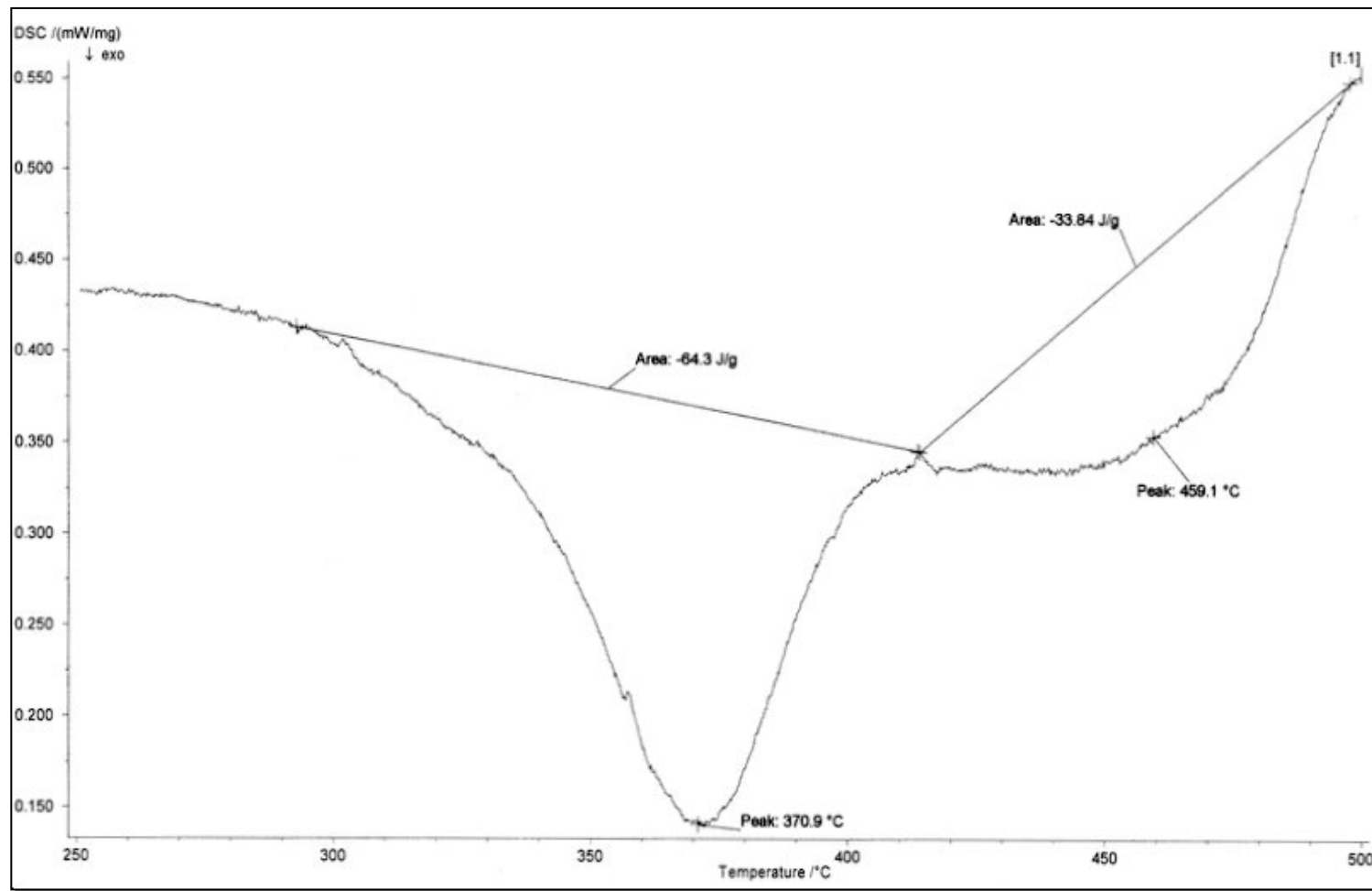
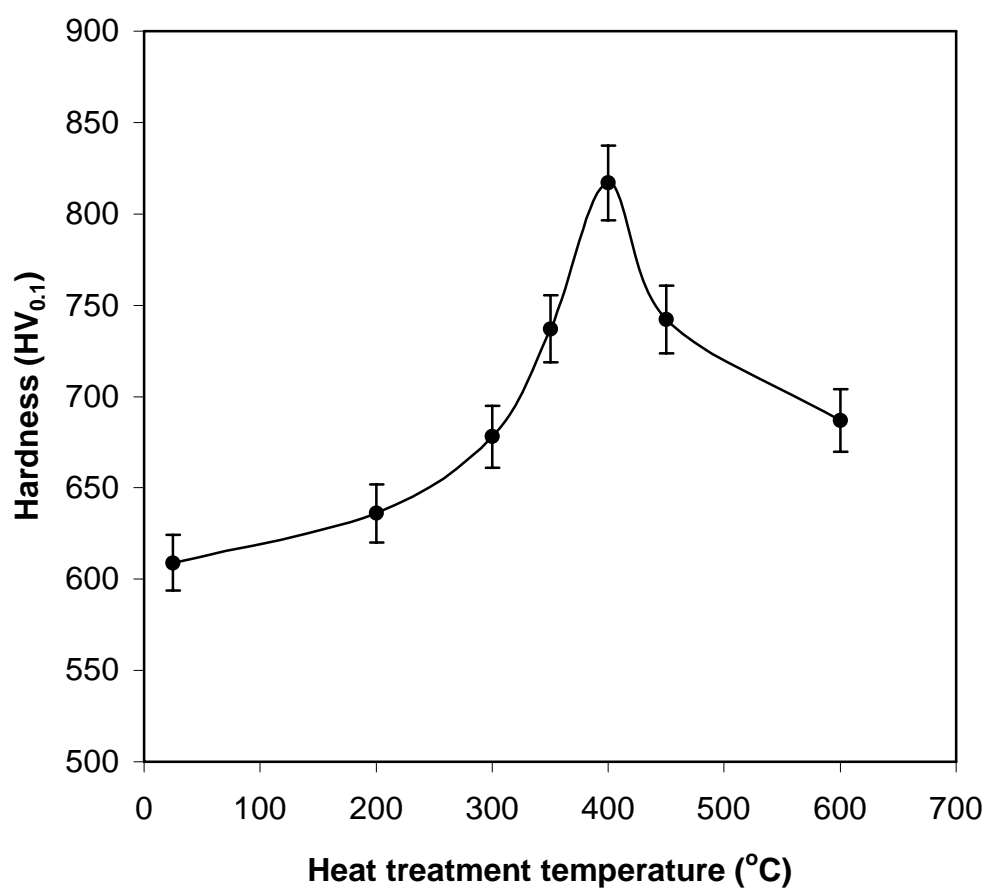


Fig. 4.8(a) DSC trace of Ni-B coating electrodeposited at  $0.4 \text{ A/dm}^2$  recorded at a heating rate of  $10\text{K/min}$ .



**Fig. 4.8(b)** DSC trace of Ni-B coating electrodeposited at 4 A/dm<sup>2</sup> recorded at a heating rate of 10K/min.



**Fig. 4.9 Variation in the hardness of Ni-B coating electrodeposited at 1 A/dm<sup>2</sup> as a function of heat-treatment temperature**

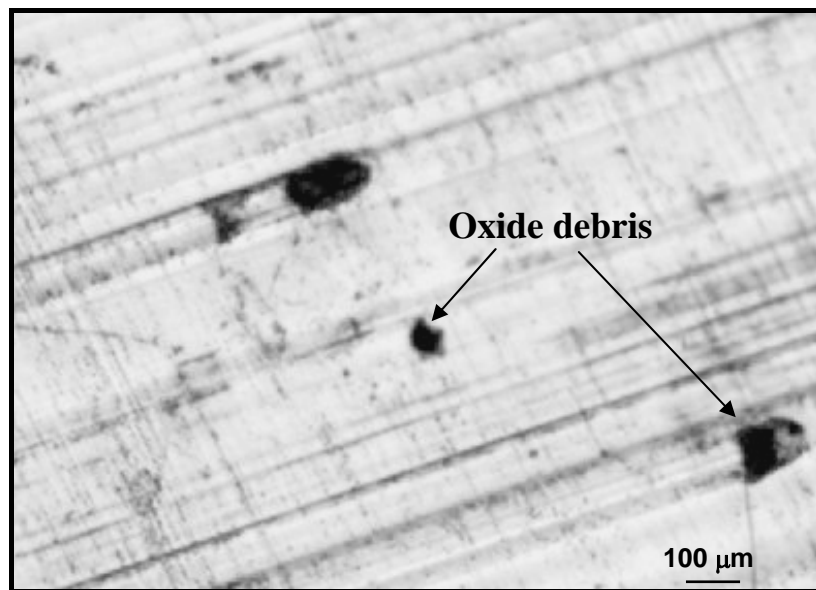


**Fig. 4.10 Optical micrograph of the wear track pattern of Ni-B coating electrodeposited at  $1 \text{ A/dm}^2$  after heat-treatment at  $400^\circ\text{C}$  for 1 hour (Applied load: 8 N; Sliding distance: 900 m).**

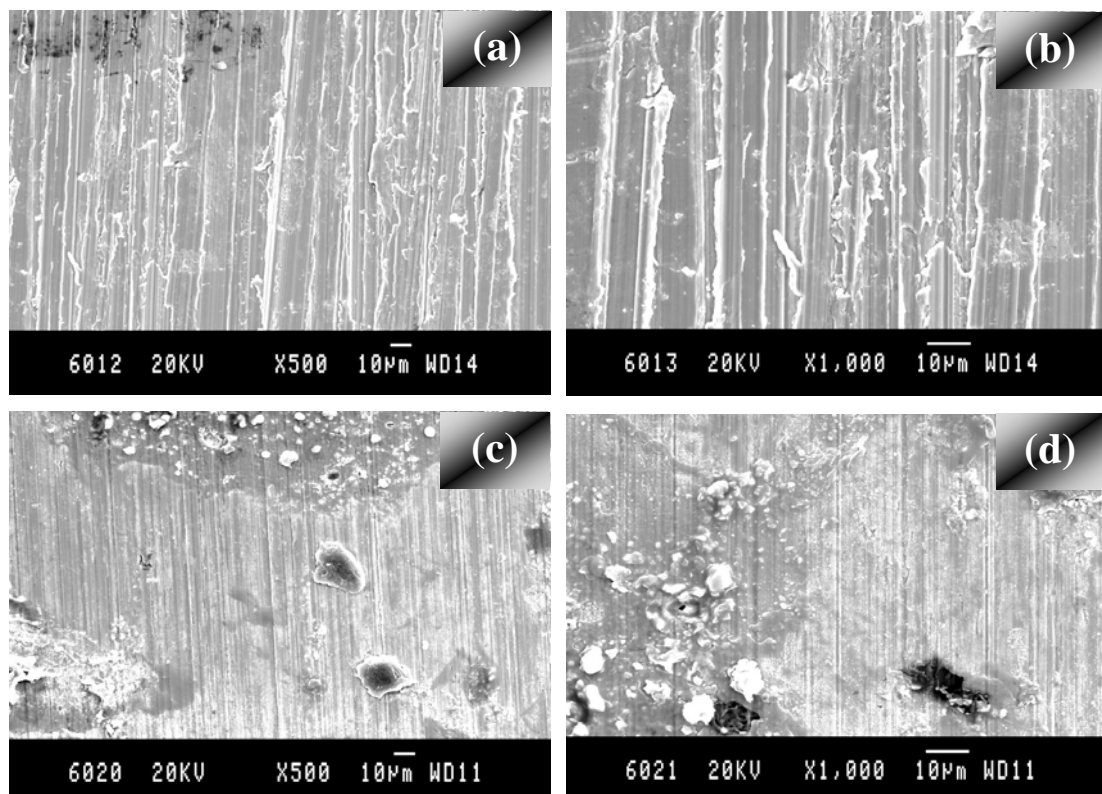


**Fig. 4.11 Wear track pattern of electrodeposited Ni-B coatings in as-plated and heat-treated conditions: (a and b) - As-plated; (c and d) - Heat-treated at 400°C for 1 hour (Applied load: 10 N; Sliding distance: 1800 m)**

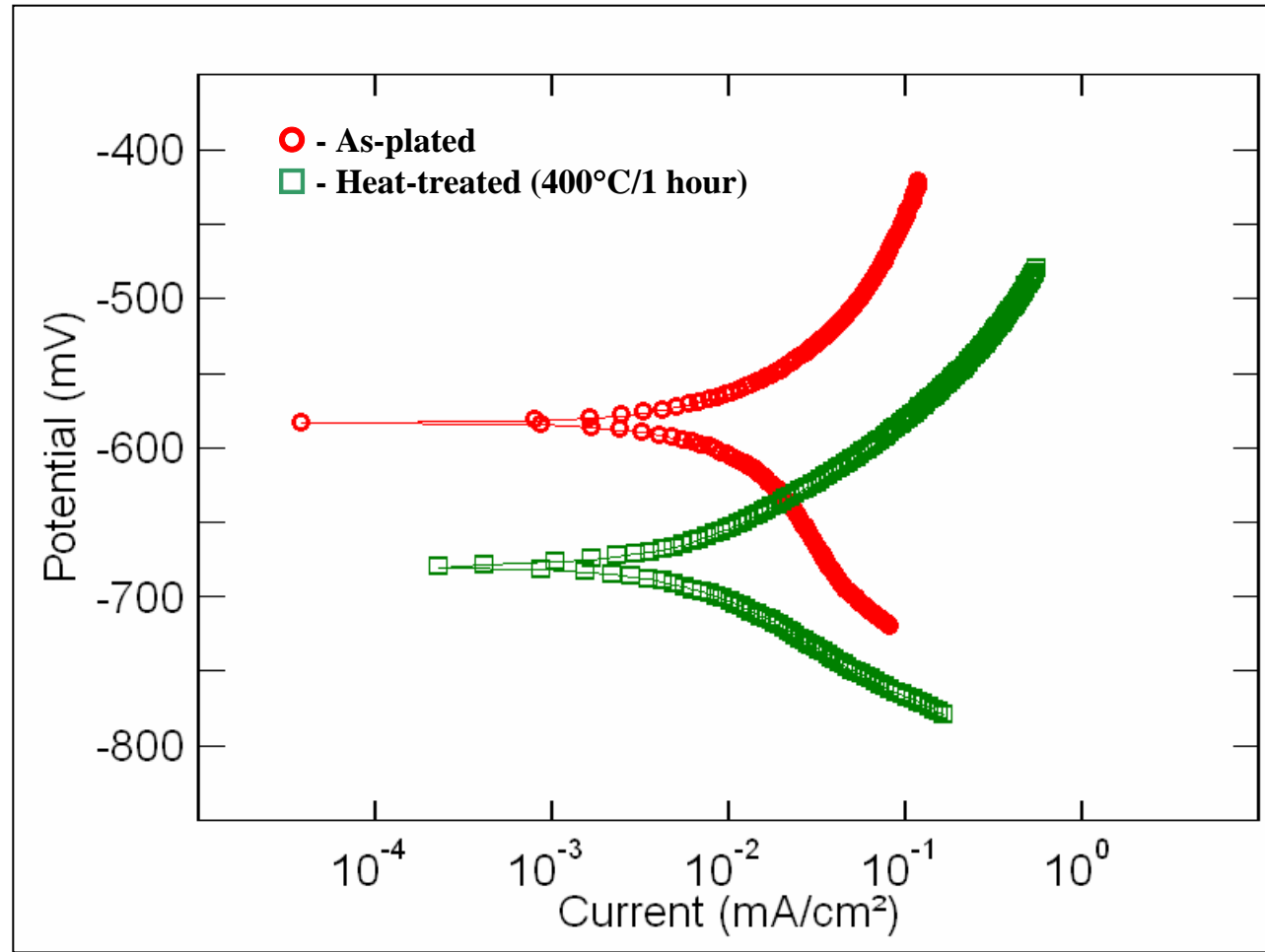


**Fig. 4.12(a) Polarization curve of ED Ni-B coating in 3.5% sodium chloride solution in its as-plated and heat-treated (400°C for 1 hour) conditions (potential in mV vs. SCE)**

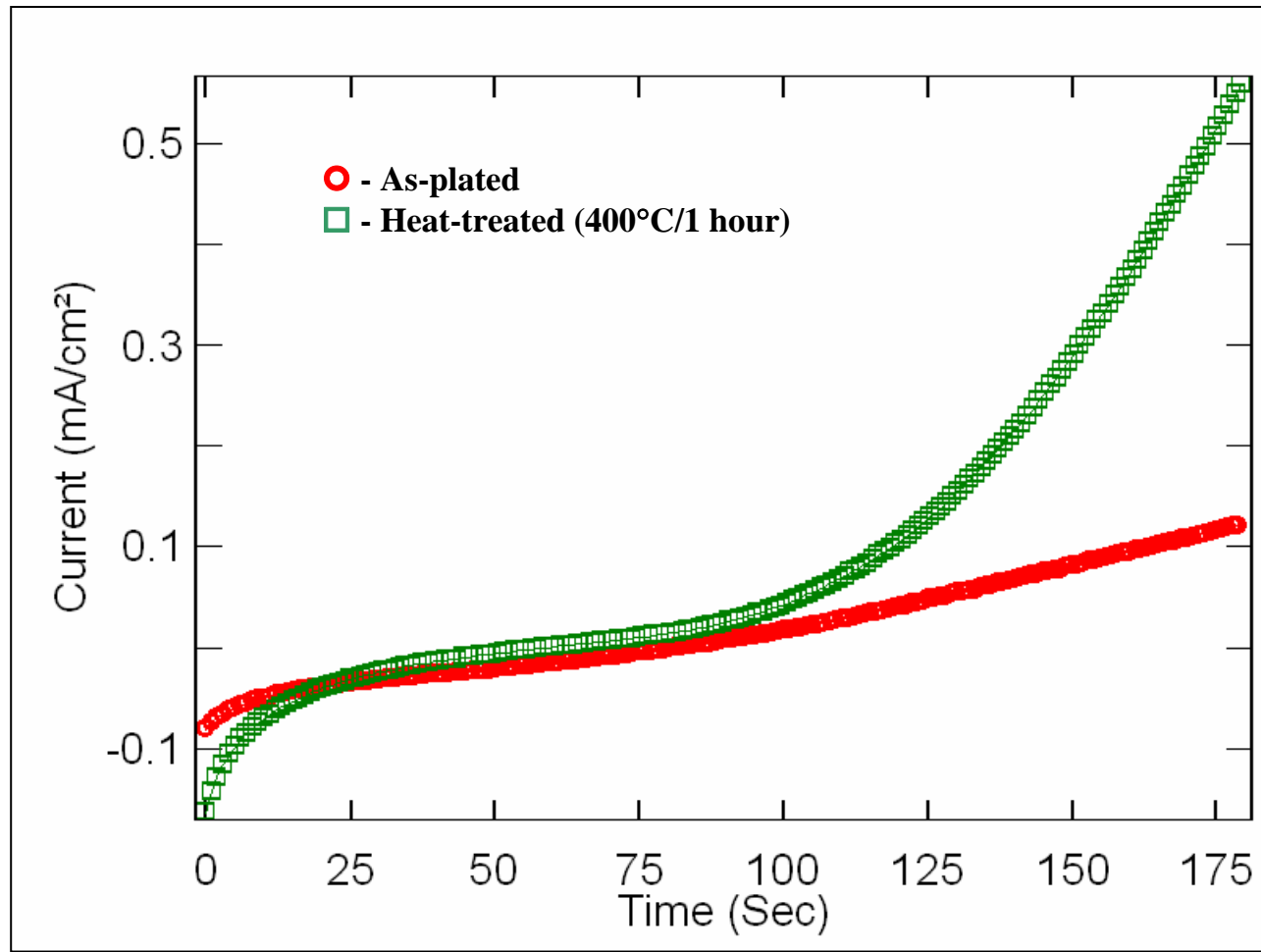


**Fig. 4.12(b)** Current-time transient curves of ED Ni-B coating in 3.5% sodium chloride solution in its as-plated and heat-treated (400°C for 1 hour) conditions



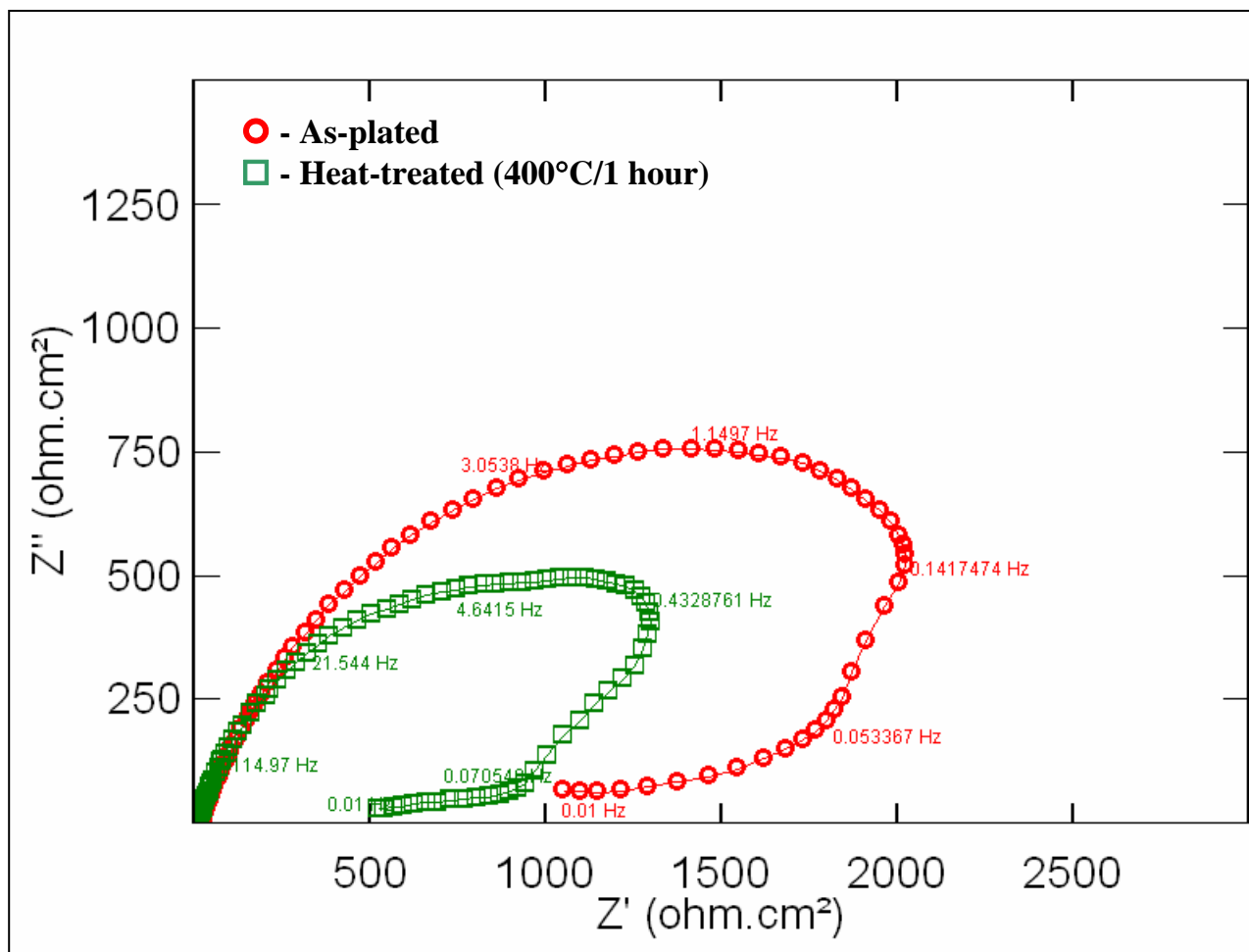


**Fig. 4.13 Nyquist plot of ED Ni-B coating in 3.5% sodium chloride solution in its as-plated and heat-treated (400°C for 1 hour) conditions**

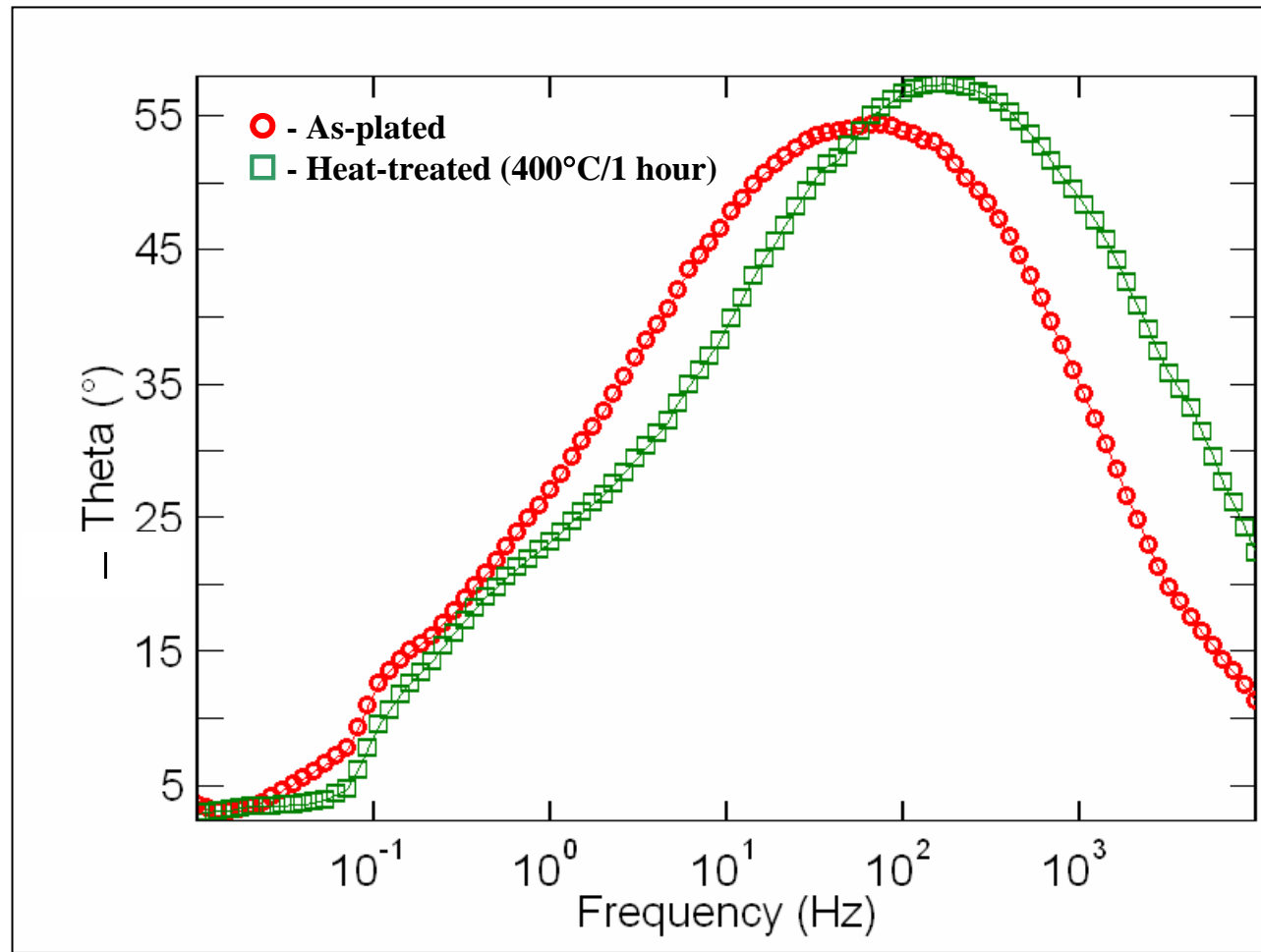


**Fig. 4.14 Bode plot of ED Ni-B coating in 3.5% sodium chloride solution in its as-plated and heat-treated (400°C for 1 hour) conditions**

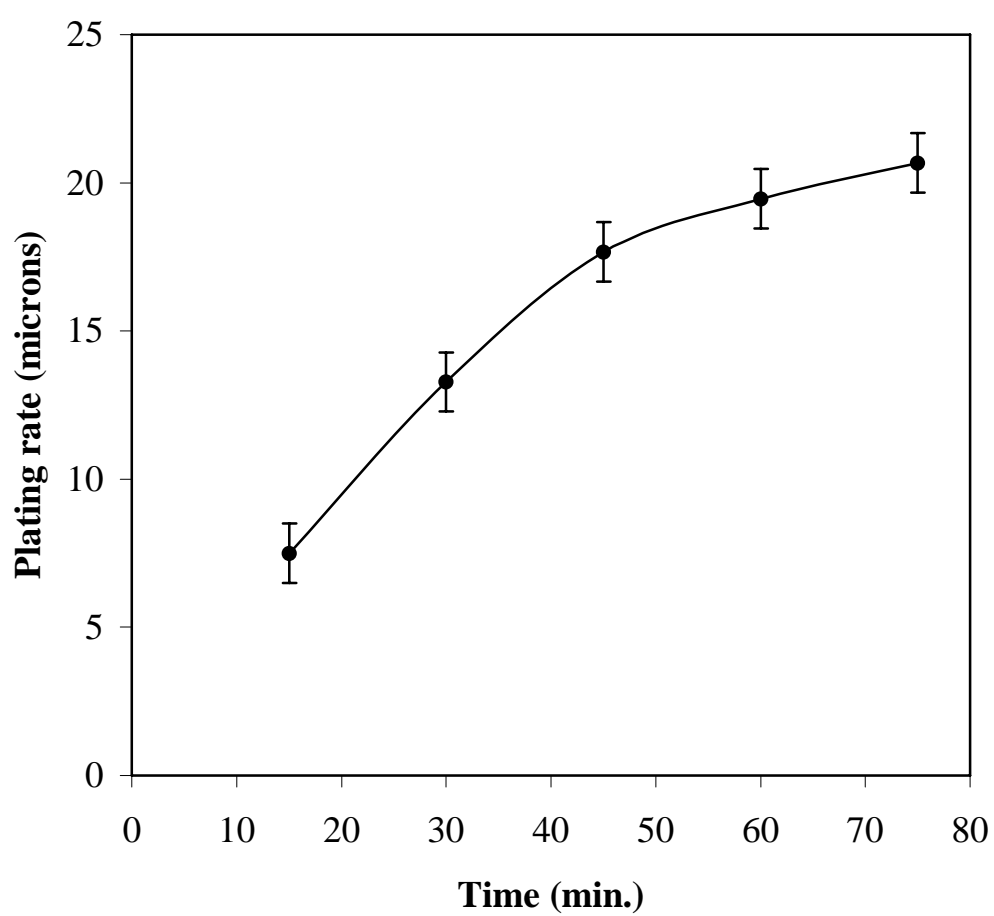


**Fig. 4.15 plating rate of electroless Ni-B coating as a function of time**

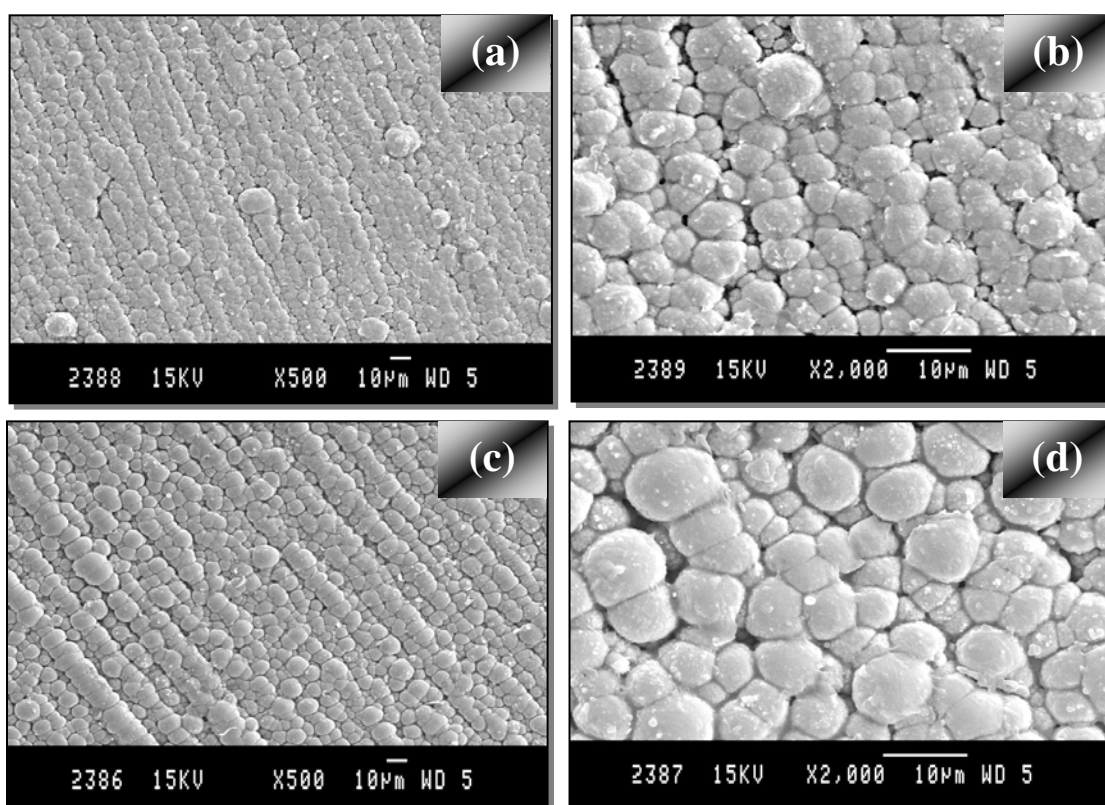


**Fig. 4.16** Scanning electron micrographs of EL Ni-B coatings obtained using varying concentrations of NaBH<sub>4</sub> : (a and b) 0.4 g/l; (c and d) 0.8 g/l

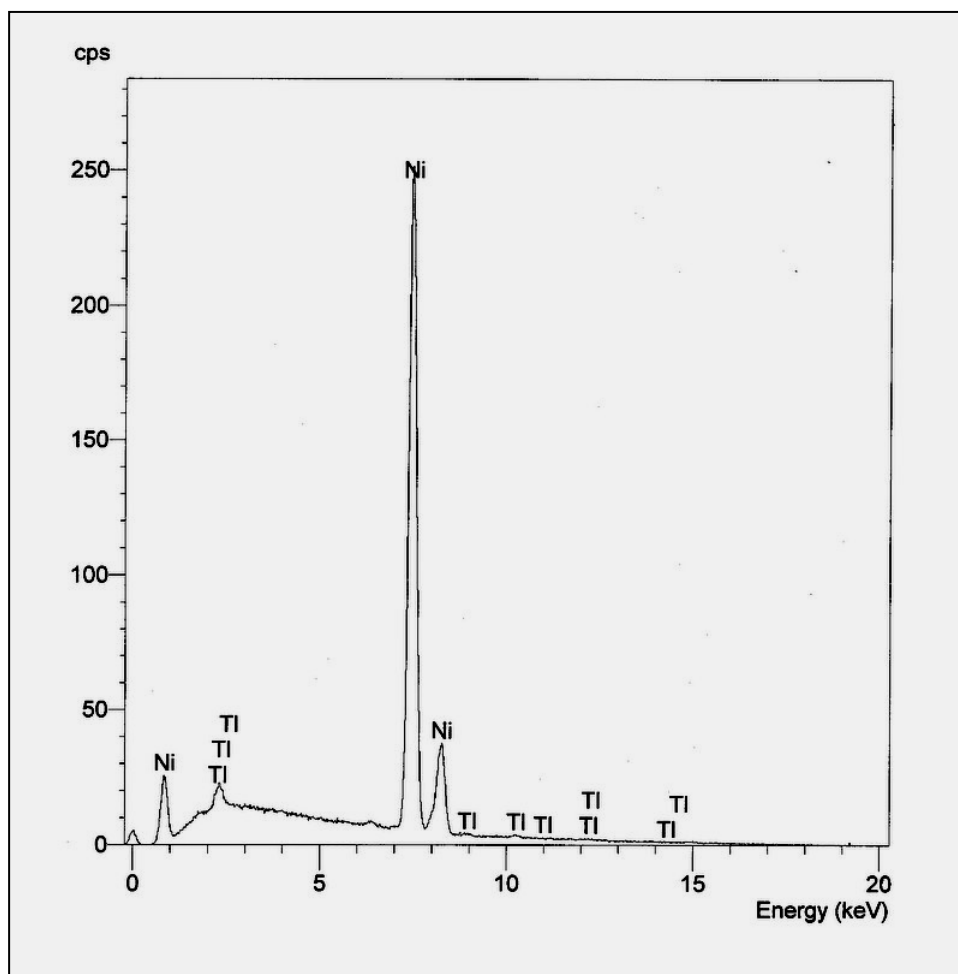


**Fig. 4.17** Energy dispersive X-ray pattern of EL Ni-B coating

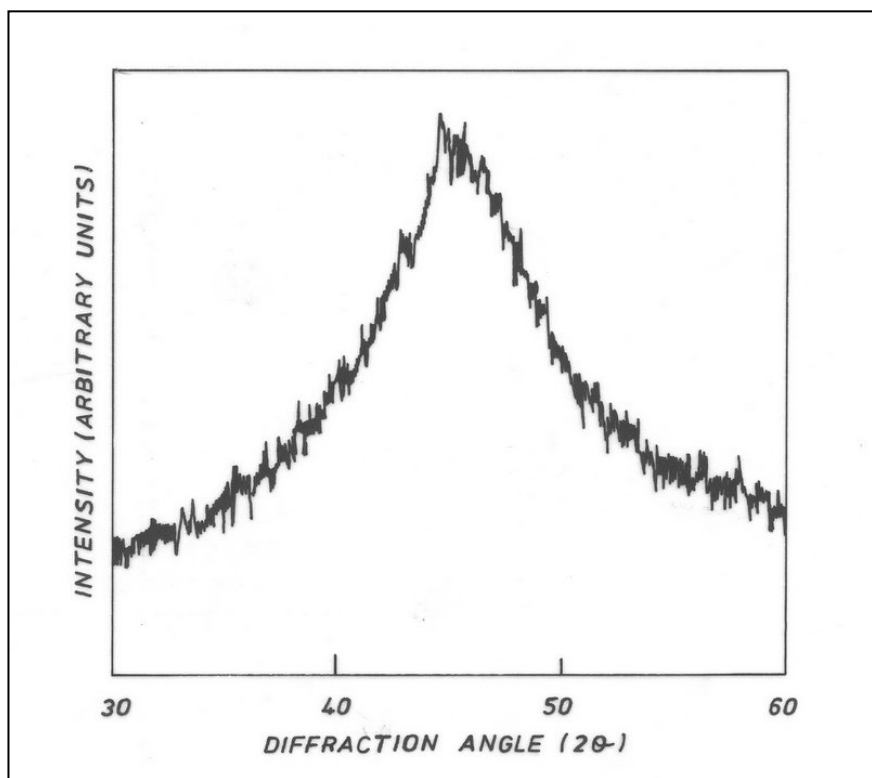


**Fig. 4.18 X-ray diffraction pattern of the electroless Ni-B coating in its as-plated condition**

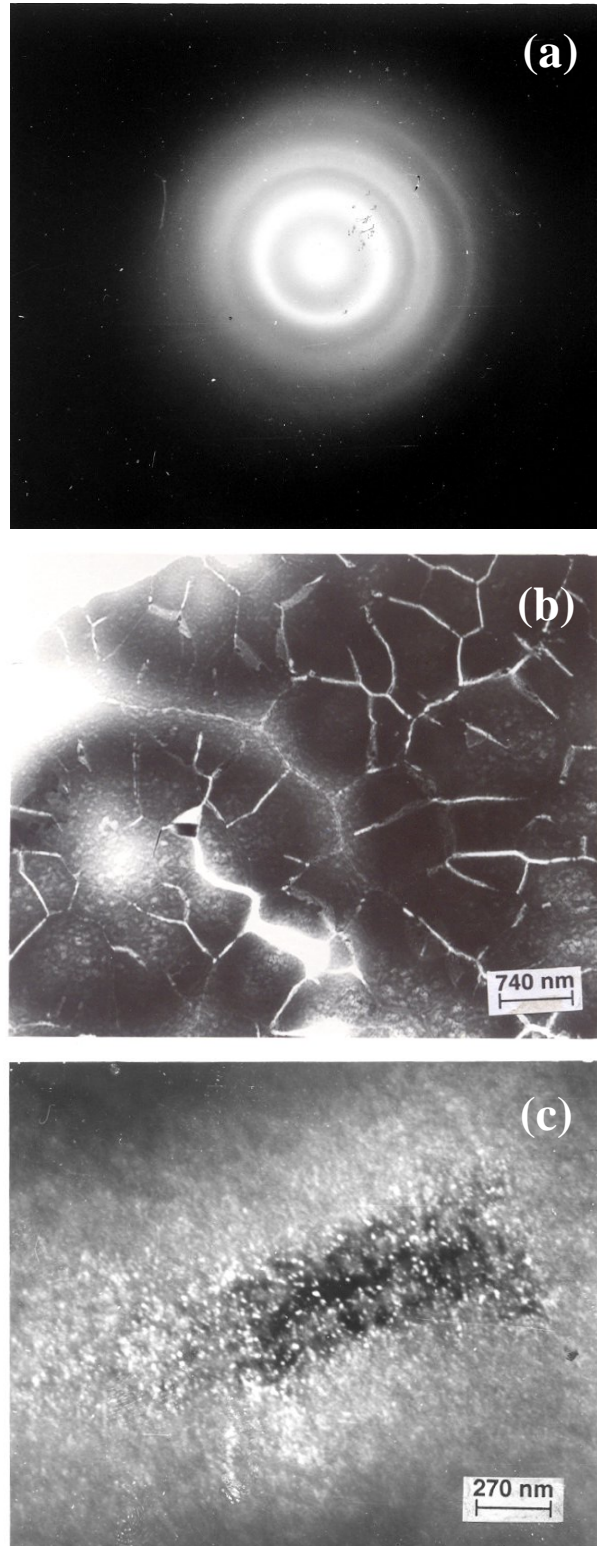


**Fig. 4.19** Selected area diffraction pattern (155 mm) (a); TEM microstructure (b); and dark field image at the crack/boundary region (c) of the electroless Ni-B coating in its as-plated condition

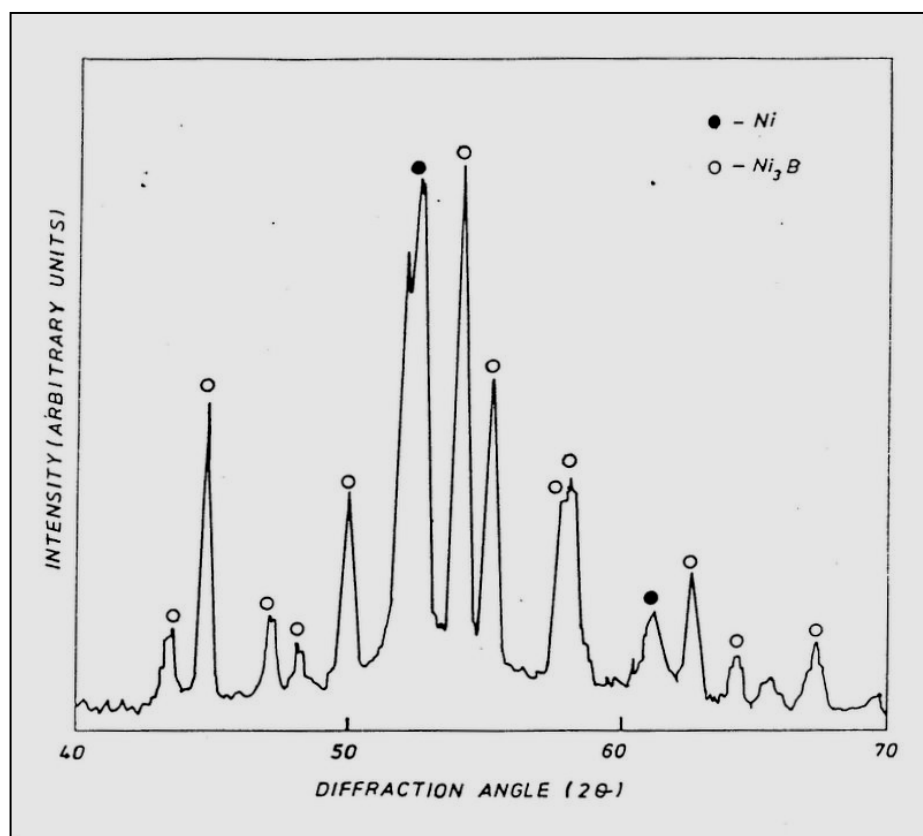


**Fig. 4.20 XRD pattern of the electroless Ni-B coating heat-treated at 325°C for 1 hour**



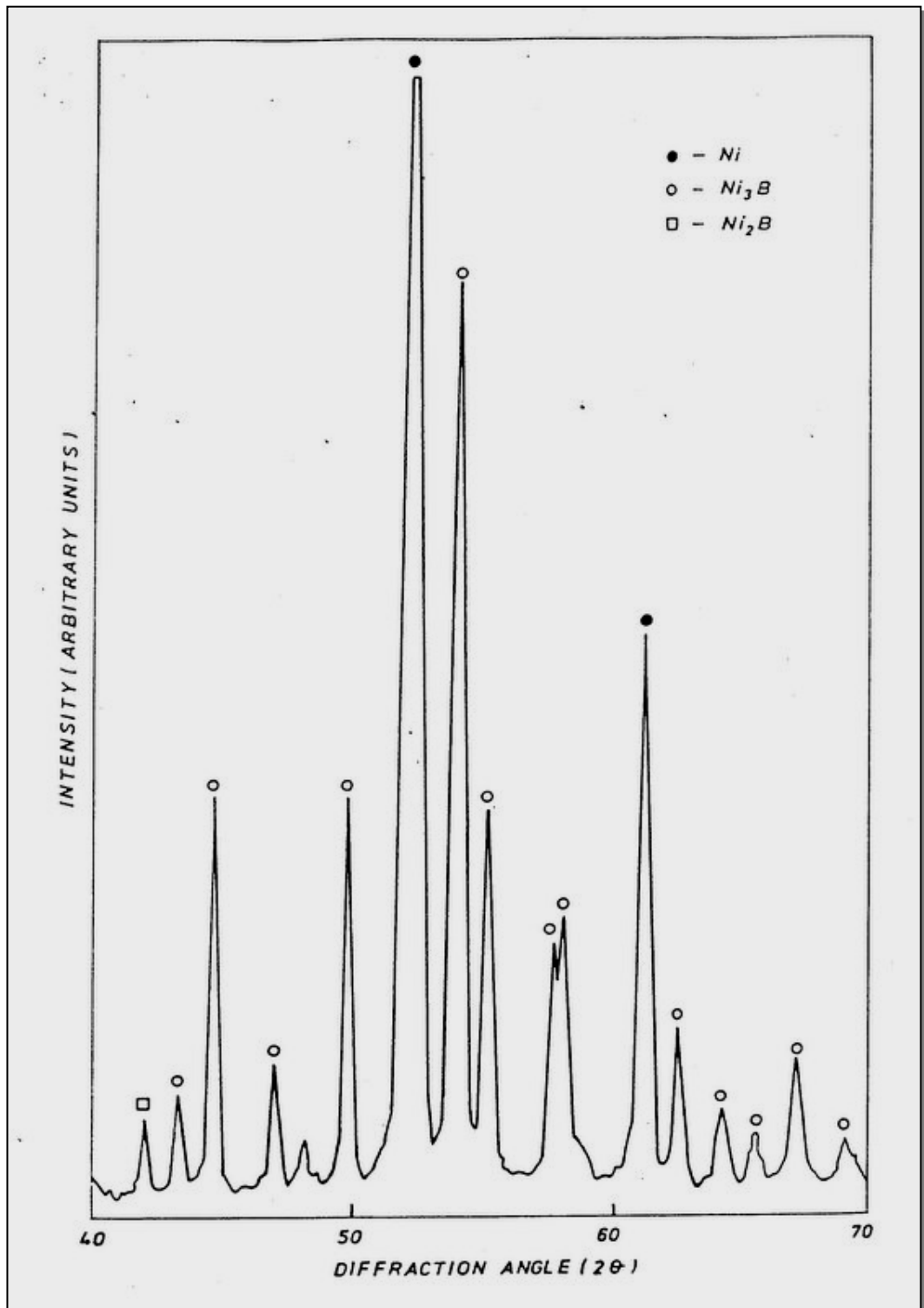


**Fig. 4.21 XRD pattern of the electroless Ni-B coating  
heat-treated at 450°C for 1 hour**

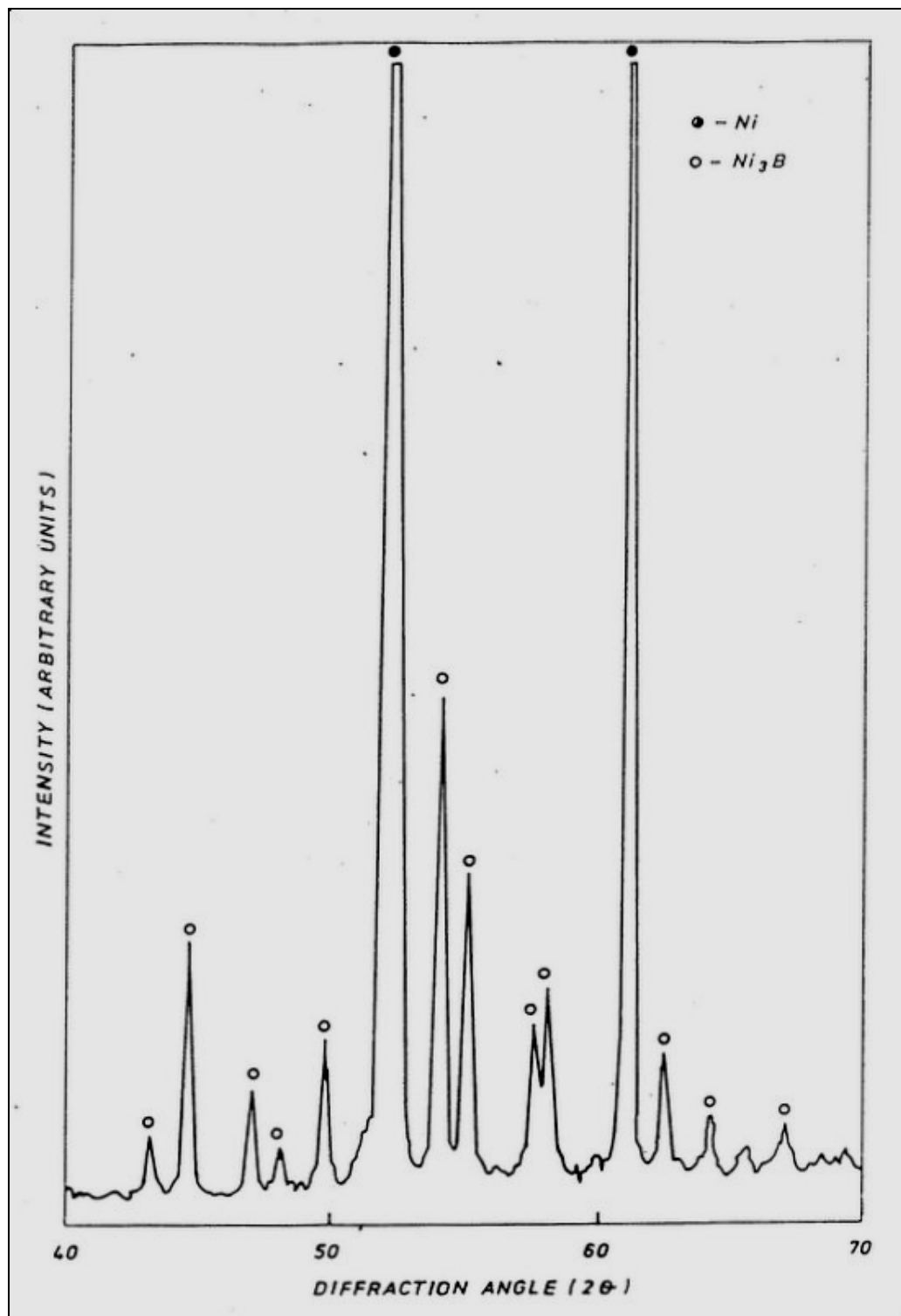


**Fig. 4.22 XRD pattern of the electroless Ni-B coating heat-treated at 600°C for 1 hour**

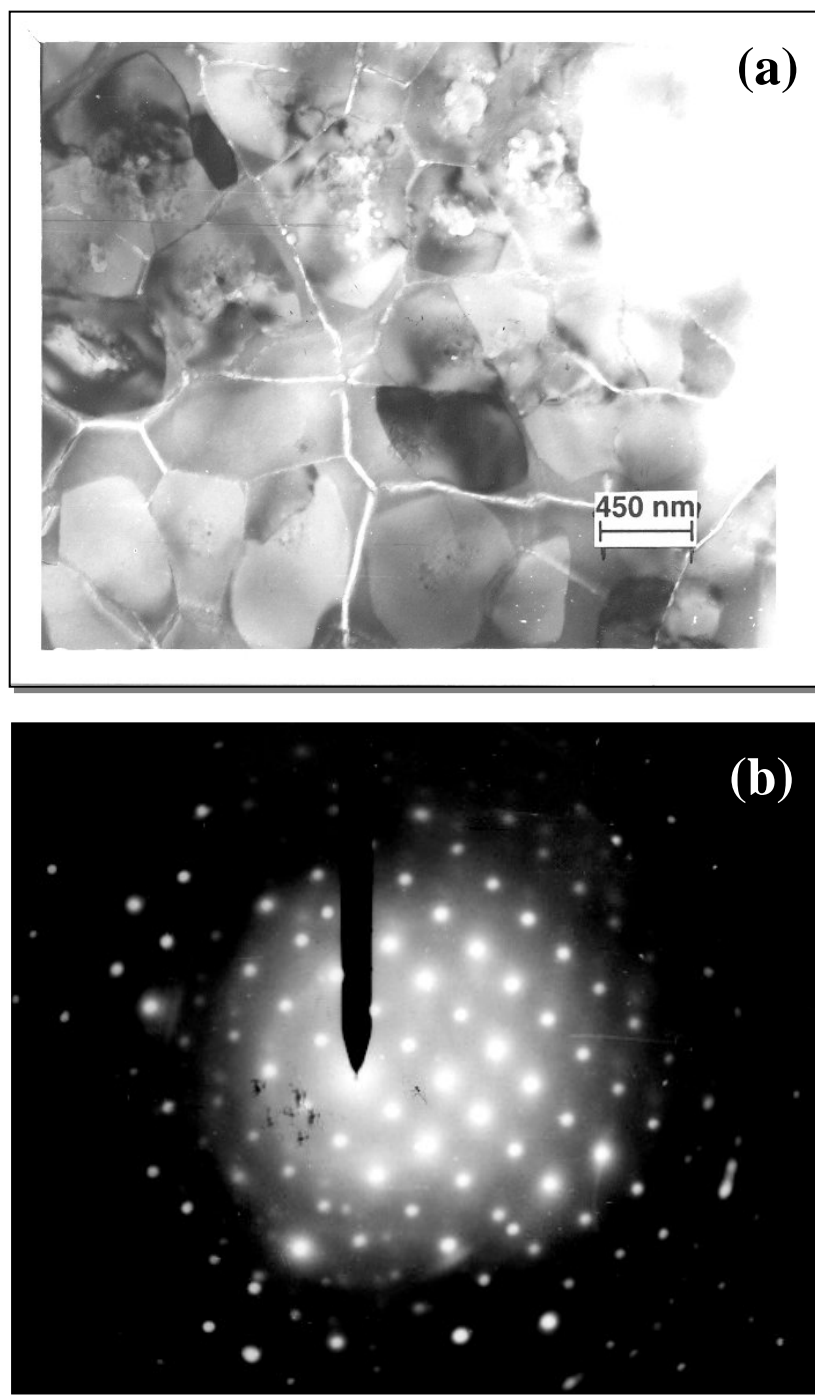


**Fig. 4.23 (a) Bright field image of the electroless Ni-B coating heat-treated at 325°C for 1 hour; and (b) selected area diffraction pattern obtained at the white regions (155 nm)**

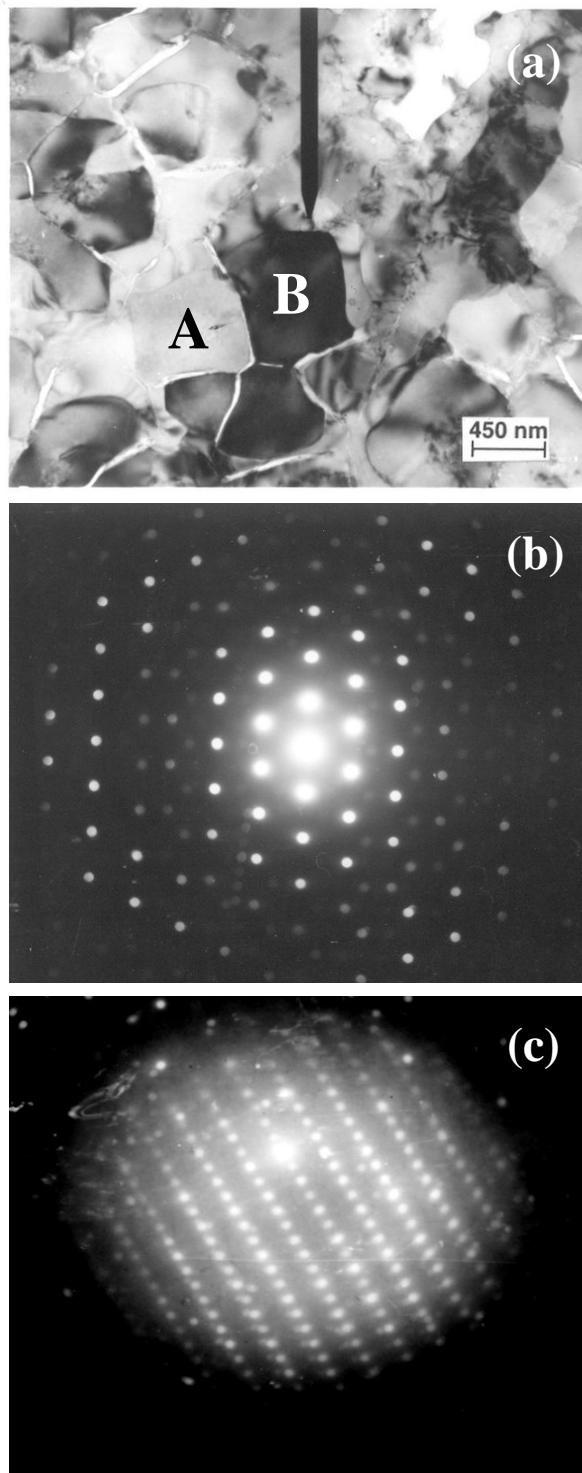


**Fig. 4.24 (a) TEM micrograph of the electroless Ni-B coating heat-treated at 450°C for 1 hour; (b) SAD pattern obtained at region 'A' (155 mm); and (c) SAD pattern obtained at region 'B' (155 mm)**

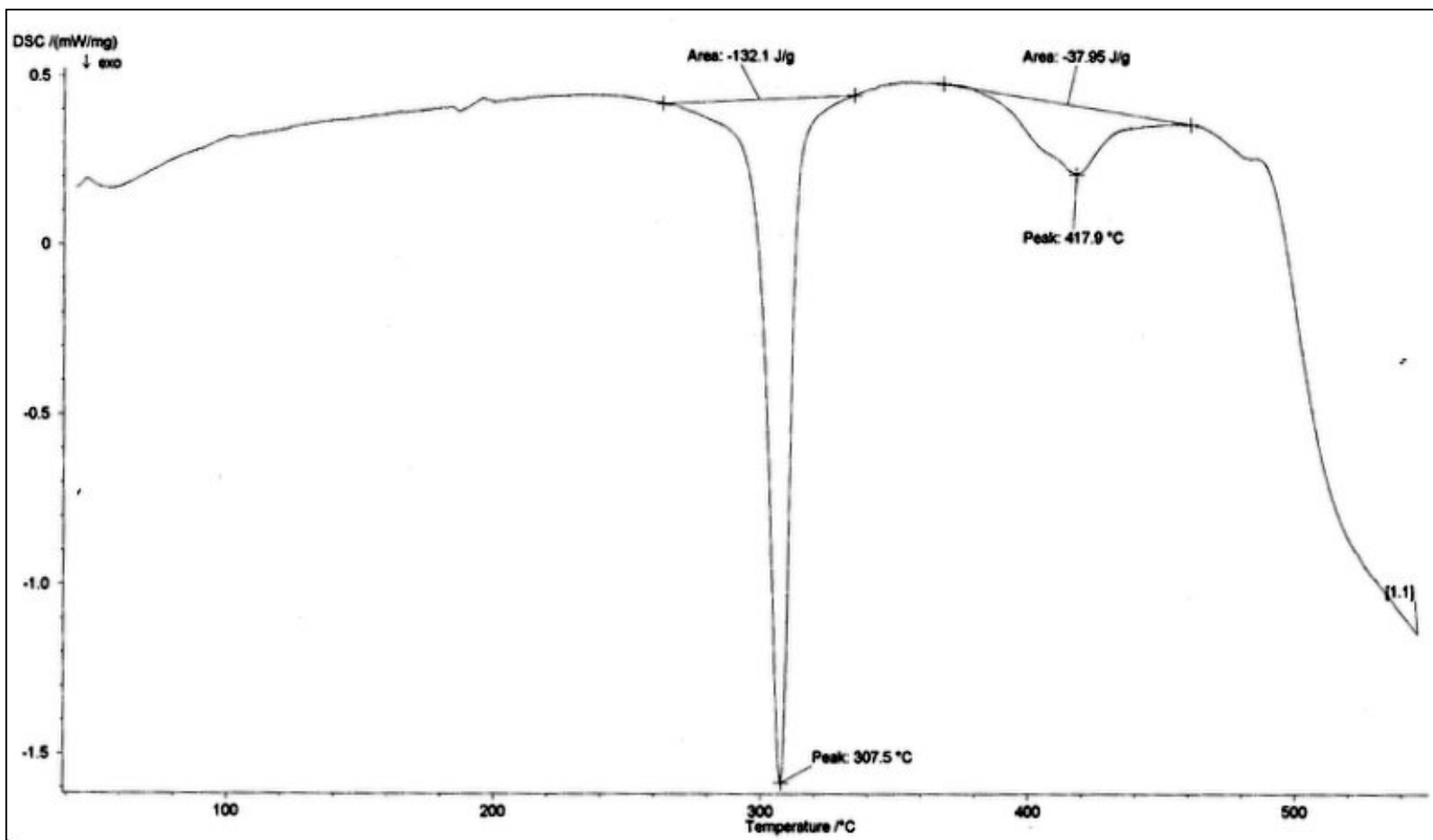
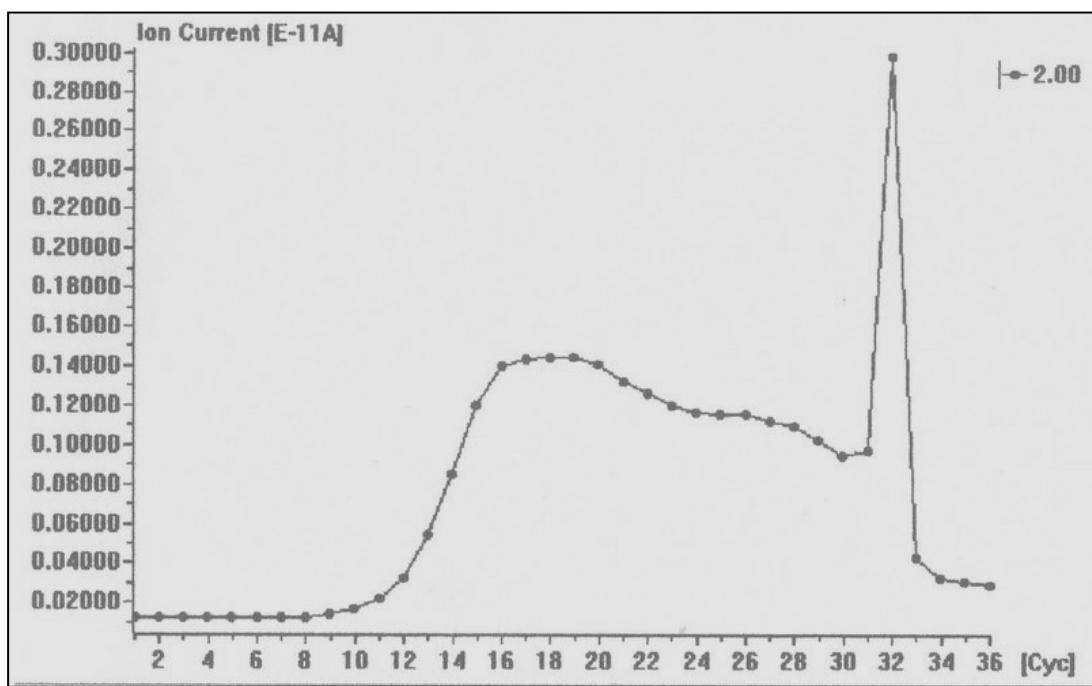
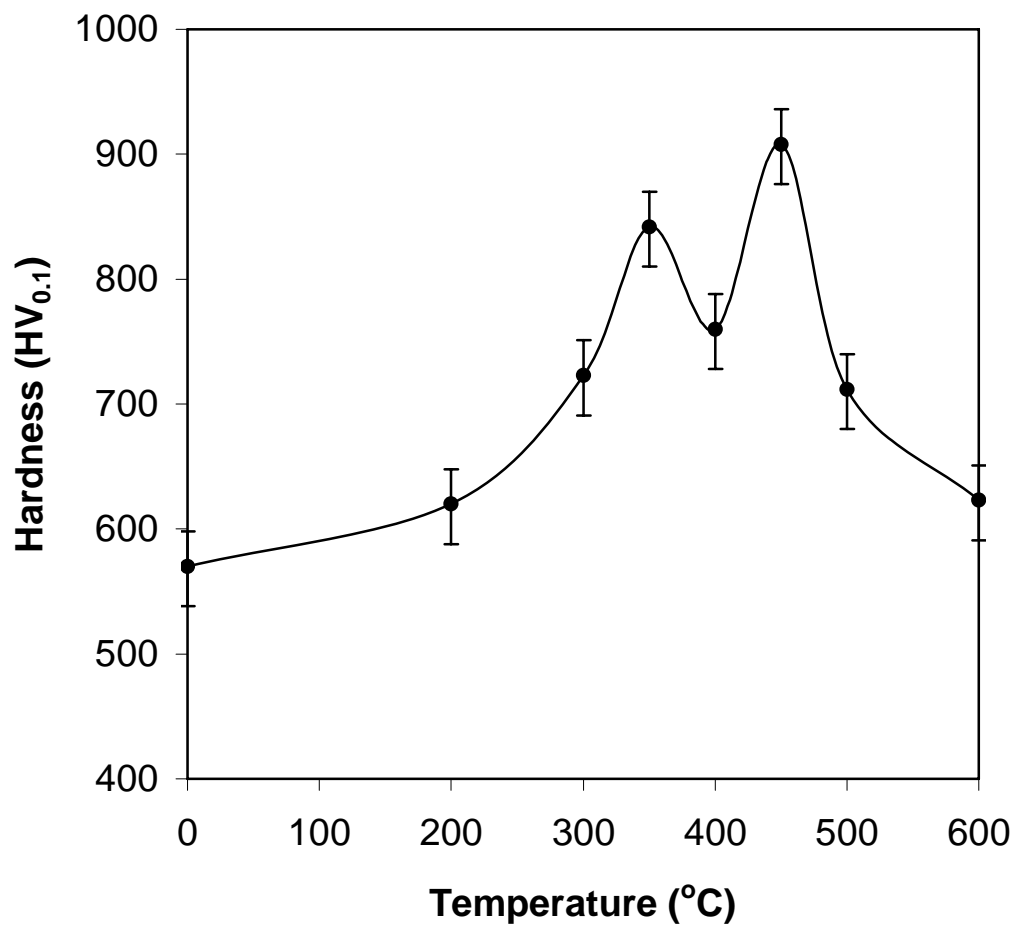


Fig. 4.25 DSC trace of the electroless Ni-B coating obtained at heating rate of 10K/min.



**Fig. 4.26 Evolved gas analysis of the EL Ni-B coating**



**Fig. 4.27** Variation in hardness of the EL Ni-B coating as a function of heat-treatment temperature

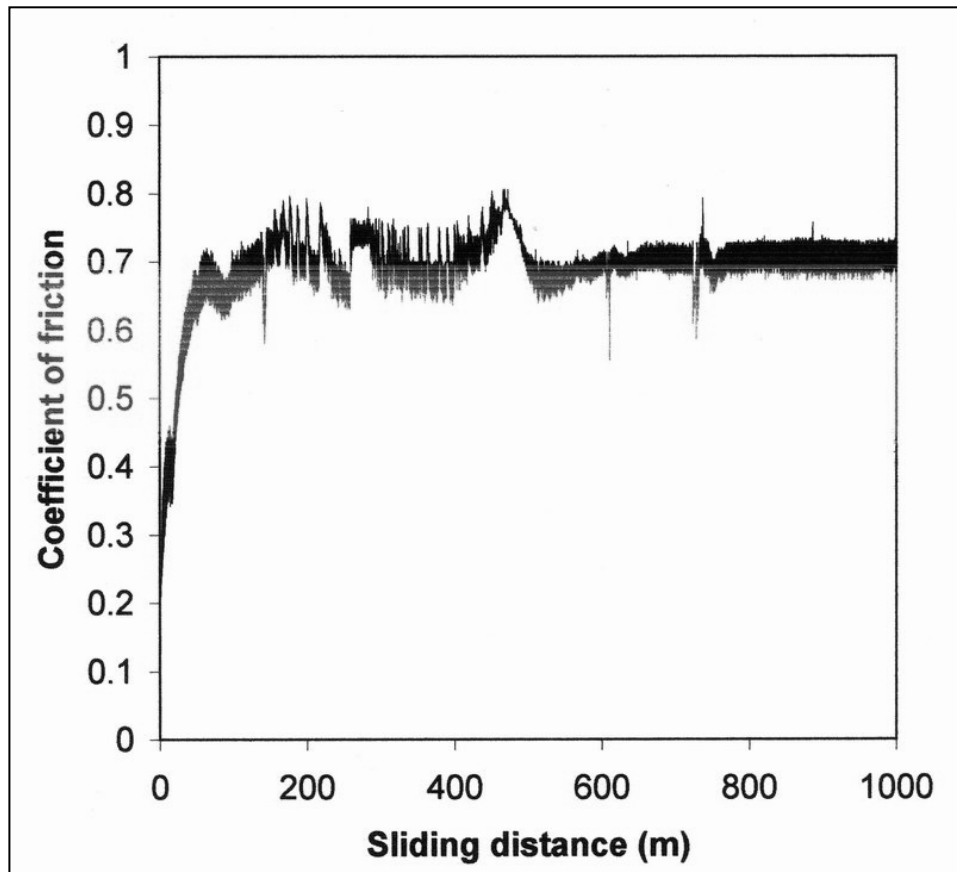


**Fig. 4.28 Coefficient of friction of the EL Ni-B coating heat-treated at 450°C for 1 hour as a function of sliding distance**



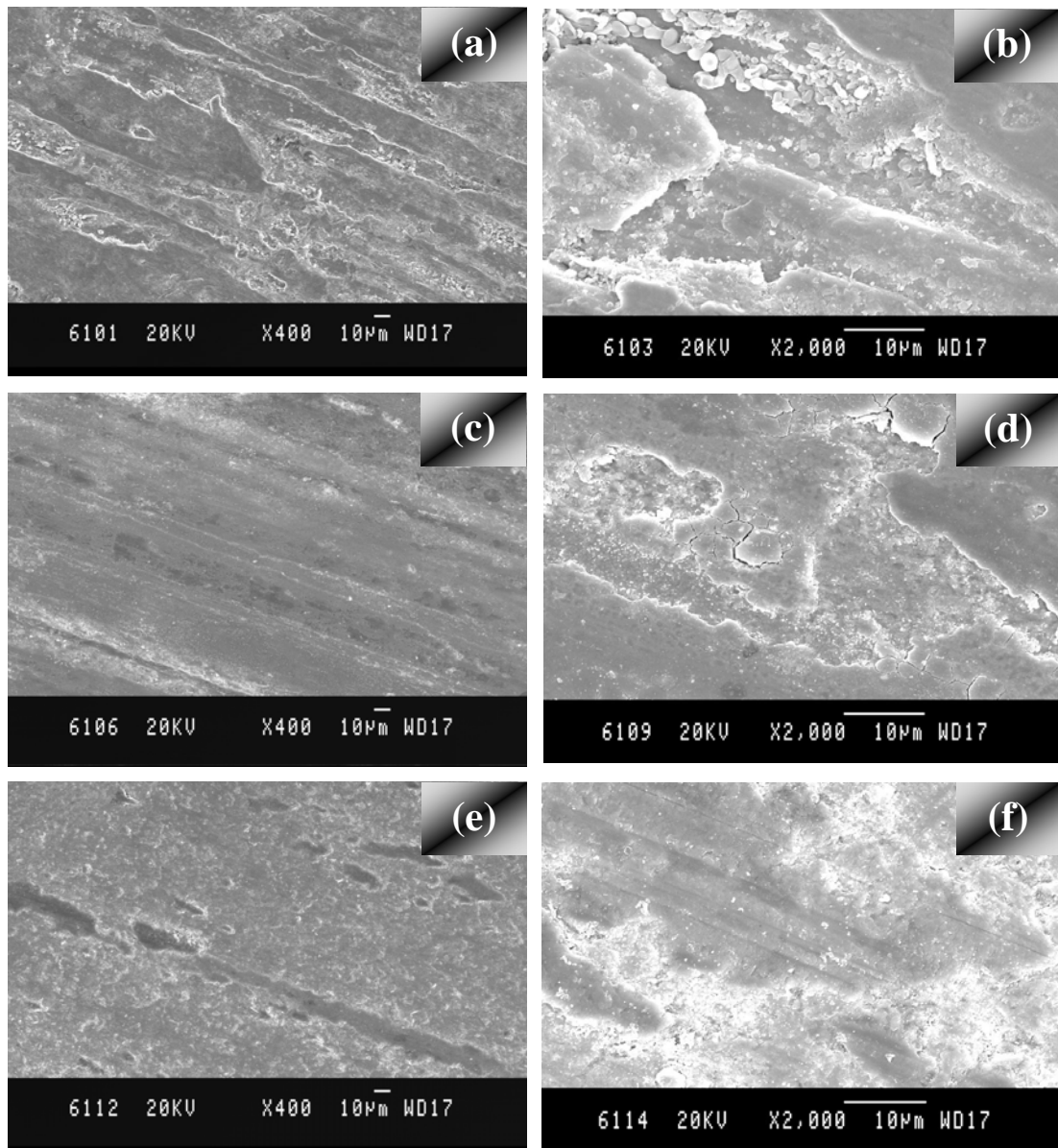


**Fig. 4.29** Wear track pattern of the EL Ni-B coatings in their as-plated (a and b), heat-treated at 350°C (c and d) and 450°C (e and f) for 1 hour (Applied load: 40 N; Sliding distance: 2700 m)

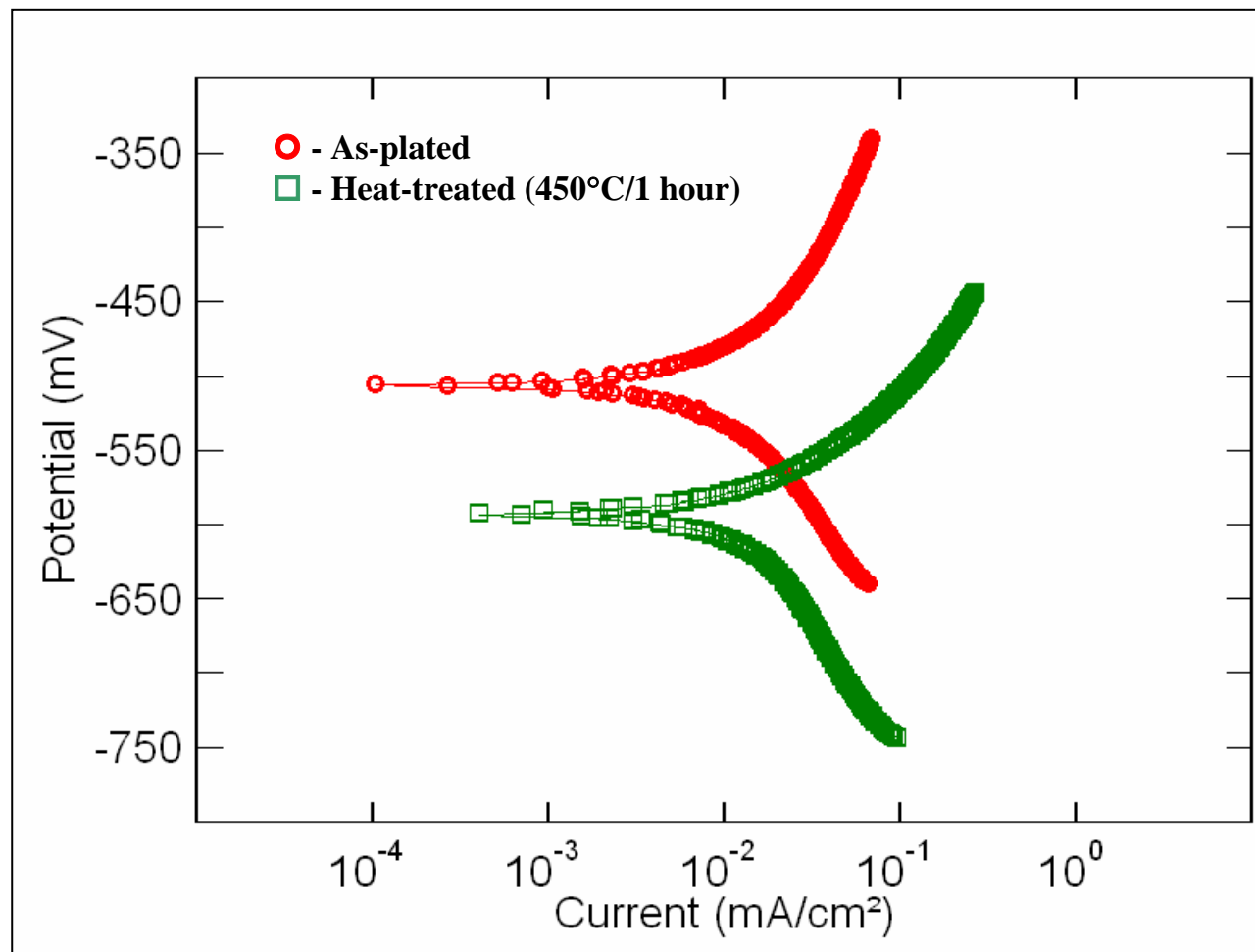


**Fig. 4.30(a) Polarization curve of EL Ni-B coating in 3.5% sodium chloride solution in its as-plated and heat-treated (450°C for 1 hour) conditions (potential in mV vs. SCE)**

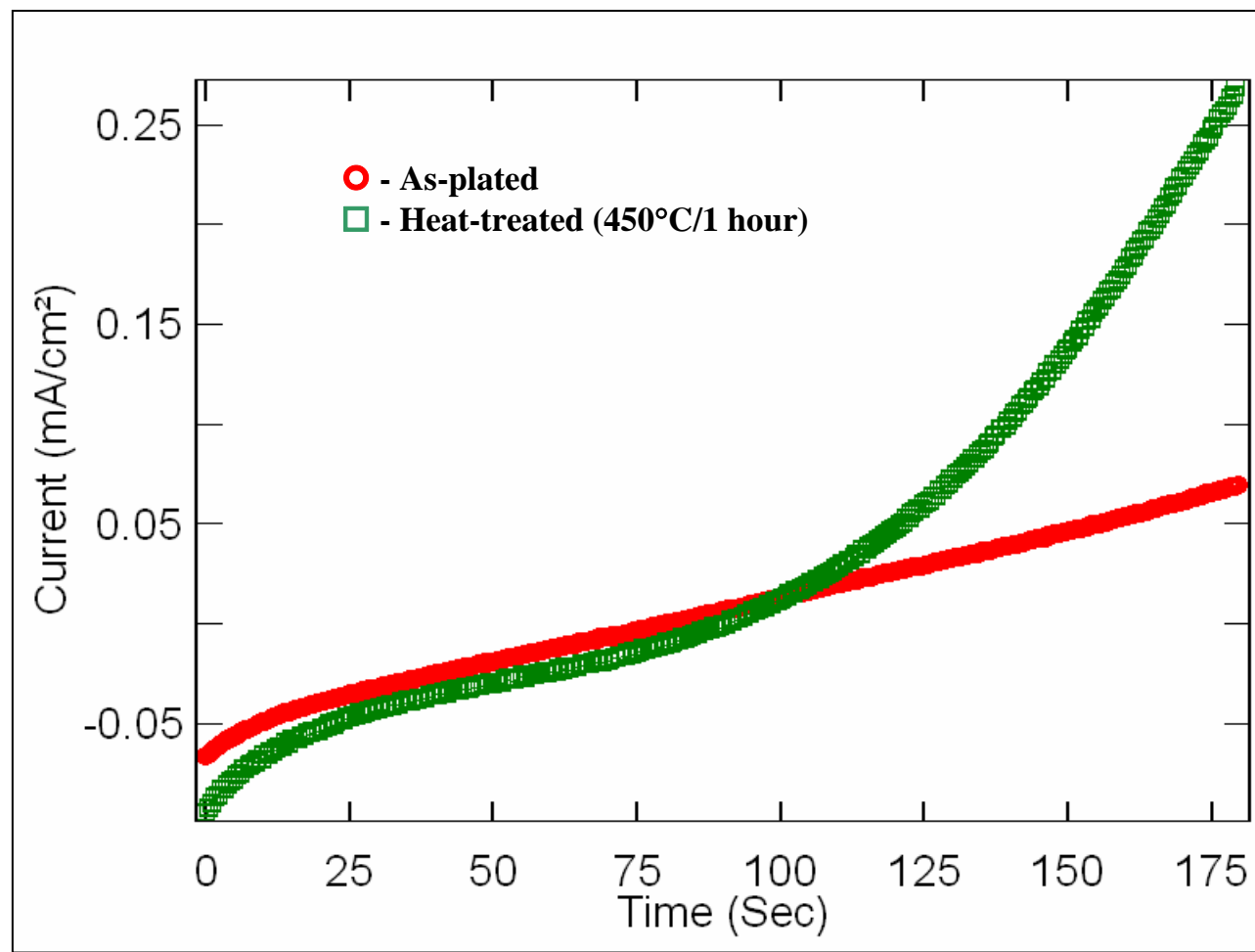


**Fig. 4.30(b)** Current-time transient curves of EL Ni-B coating in 3.5% sodium chloride solution in its as-plated and heat-treated (450°C for 1 hour) conditions

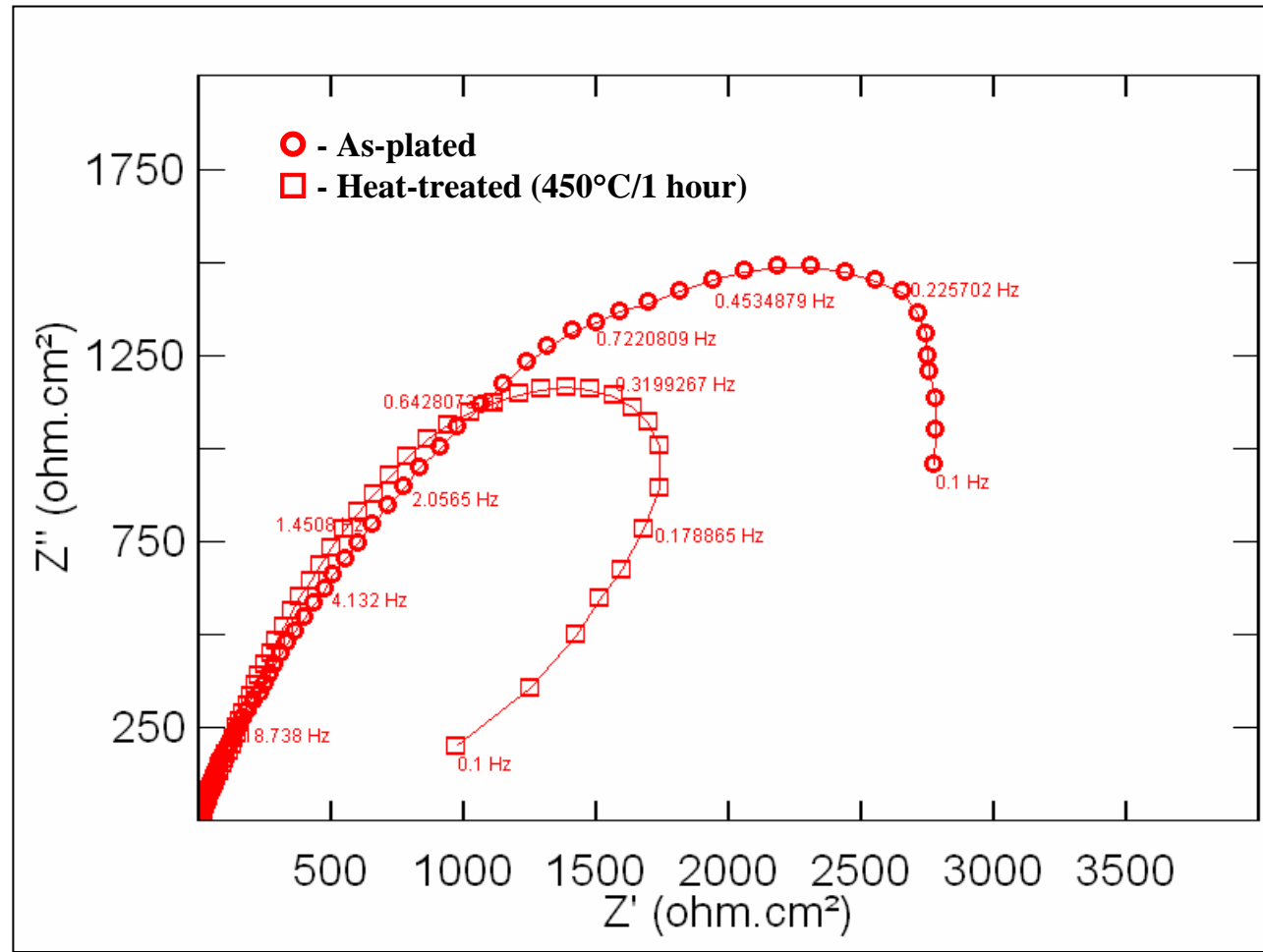


**Fig. 4.31 Nyquist plot of EL Ni-B coating in 3.5% sodium chloride solution in its as-plated and heat-treated (450°C for 1 hour) conditions**

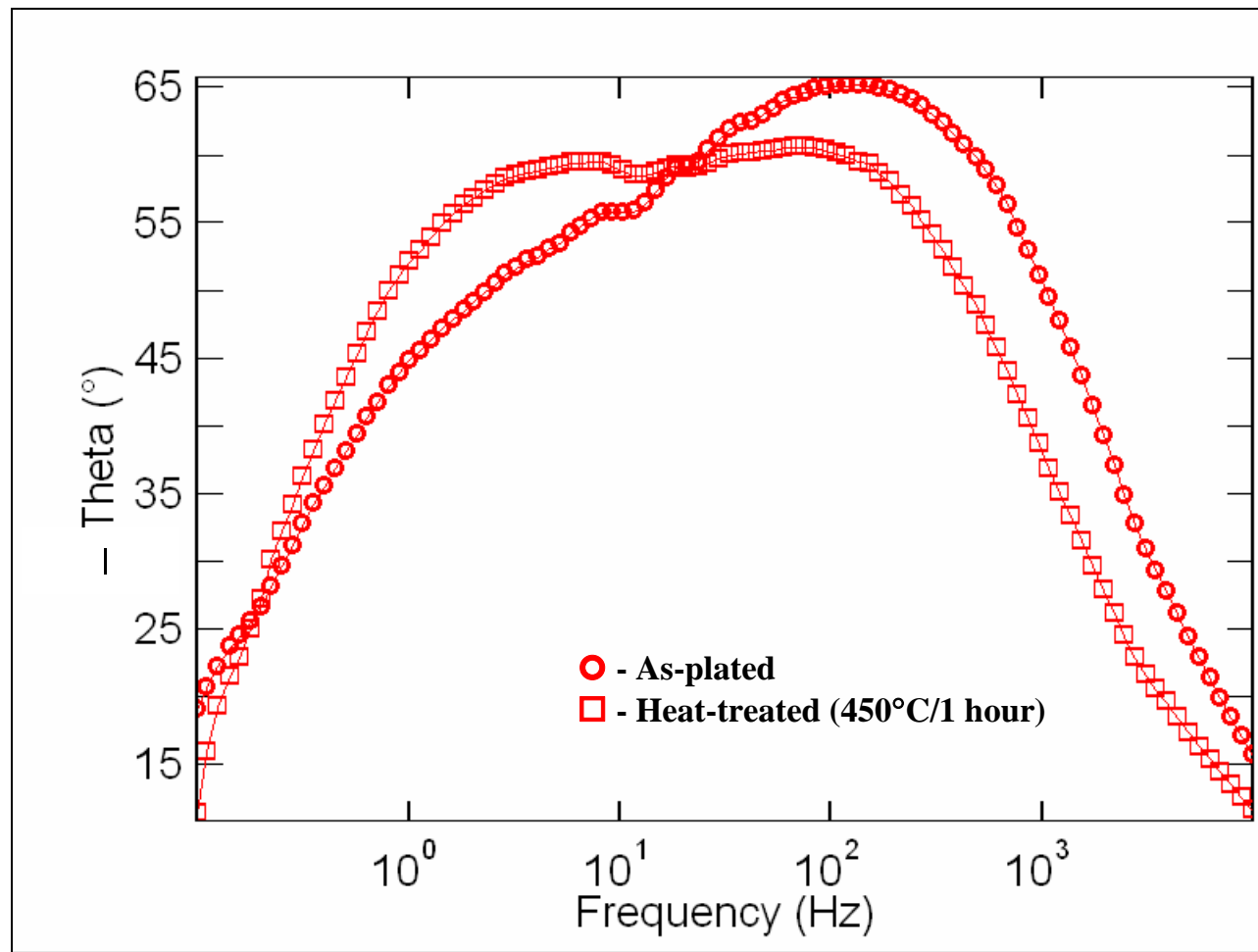


**Fig. 4.32 Bode plot of EL Ni-B coating in 3.5% sodium chloride solution in its as-plated and heat-treated (450°C for 1 hour) conditions**

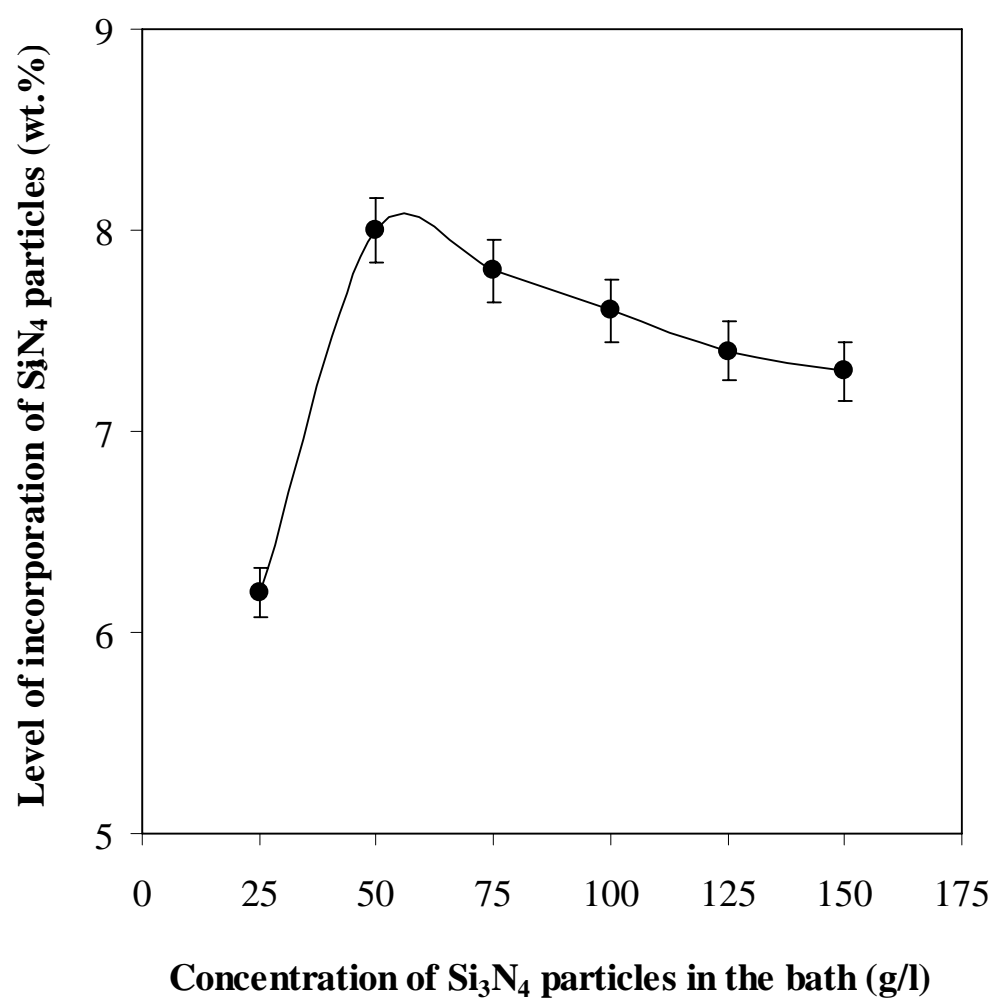


**Fig. 4.33 Variation in the level of incorporation of  $\text{Si}_3\text{N}_4$  particles in the ED Ni-B matrix as a function of their concentration in the plating bath (Current density:  $1 \text{ A/dm}^2$ )**

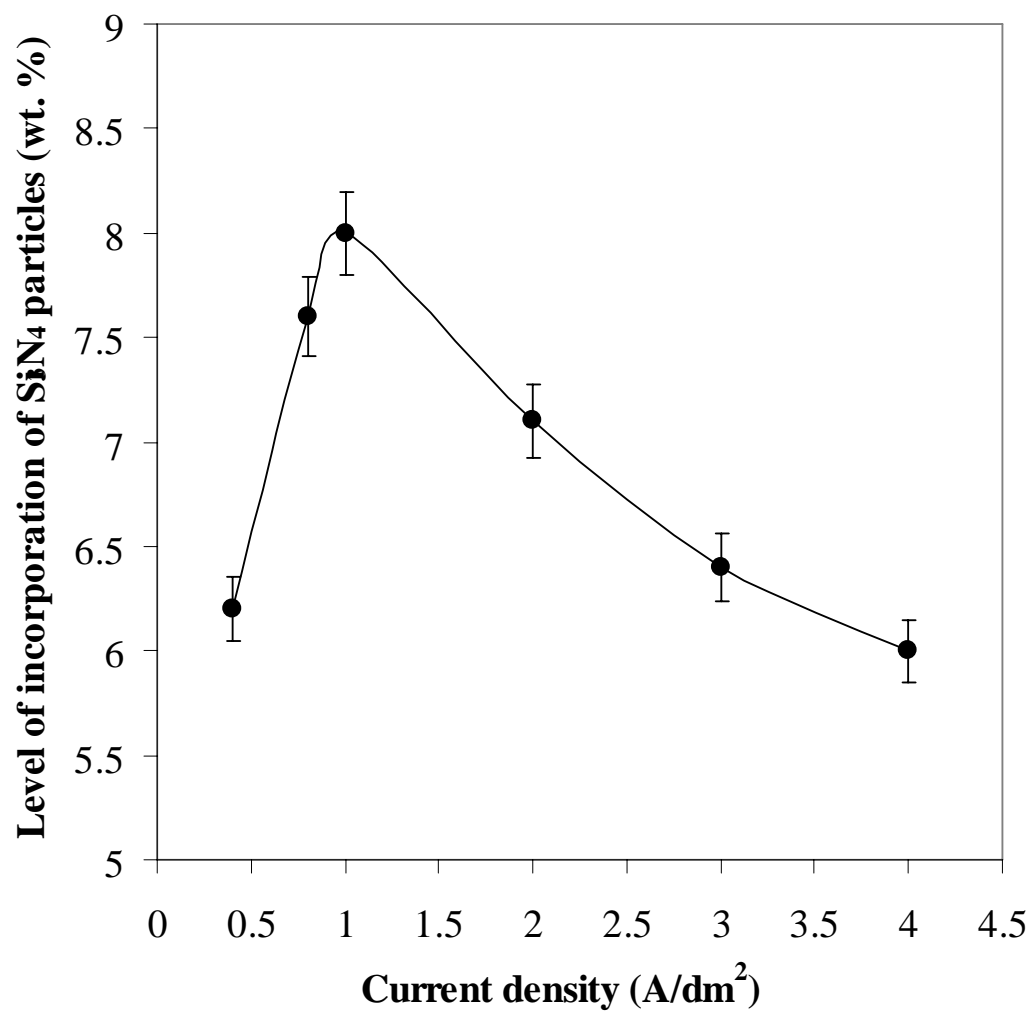


**Fig. 4.34** Variation in the level of incorporation of  $\text{Si}_3\text{N}_4$  particles as a function of current density (Concentration of  $\text{Si}_3\text{N}_4$  in the bath: 50 g/l)

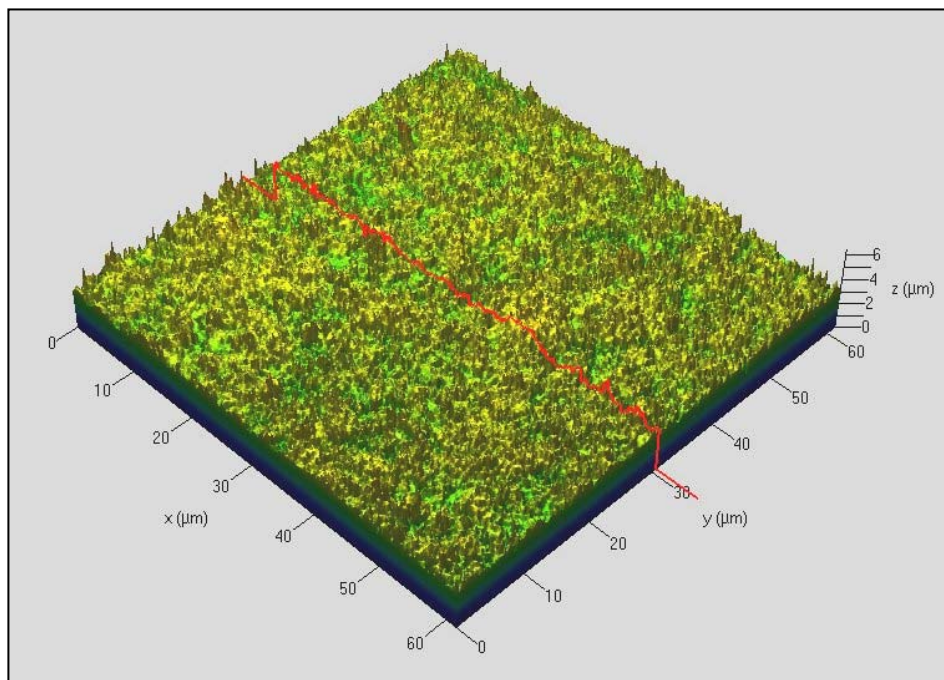


**Fig. 4.35 3-Dimensional view of the surface topography of Ni-B-Si<sub>3</sub>N<sub>4</sub> composite coating electrodeposited at 1 A/dm<sup>2</sup> assessed using a laser scanning microscope**



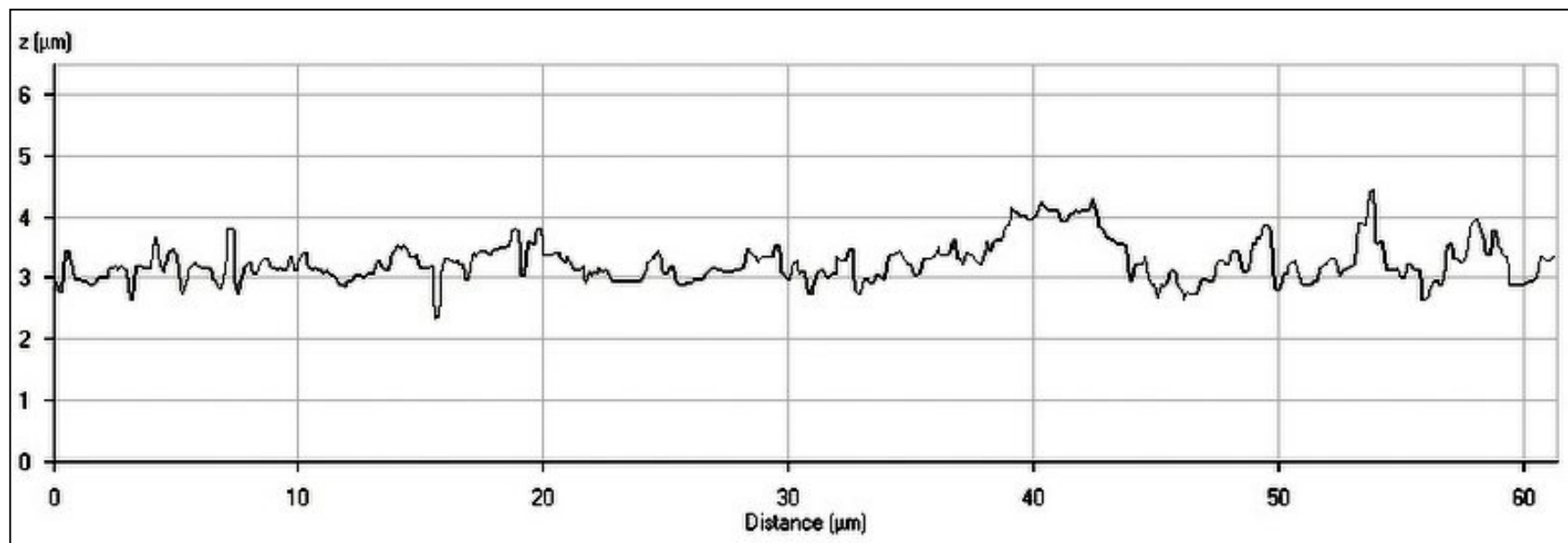


**Fig. 4.36 Surface profile of the Ni-B-Si<sub>3</sub>N<sub>4</sub> composite coating electrodeposited at 1 A/dm<sup>2</sup> assessed using a laser scanning microscope**

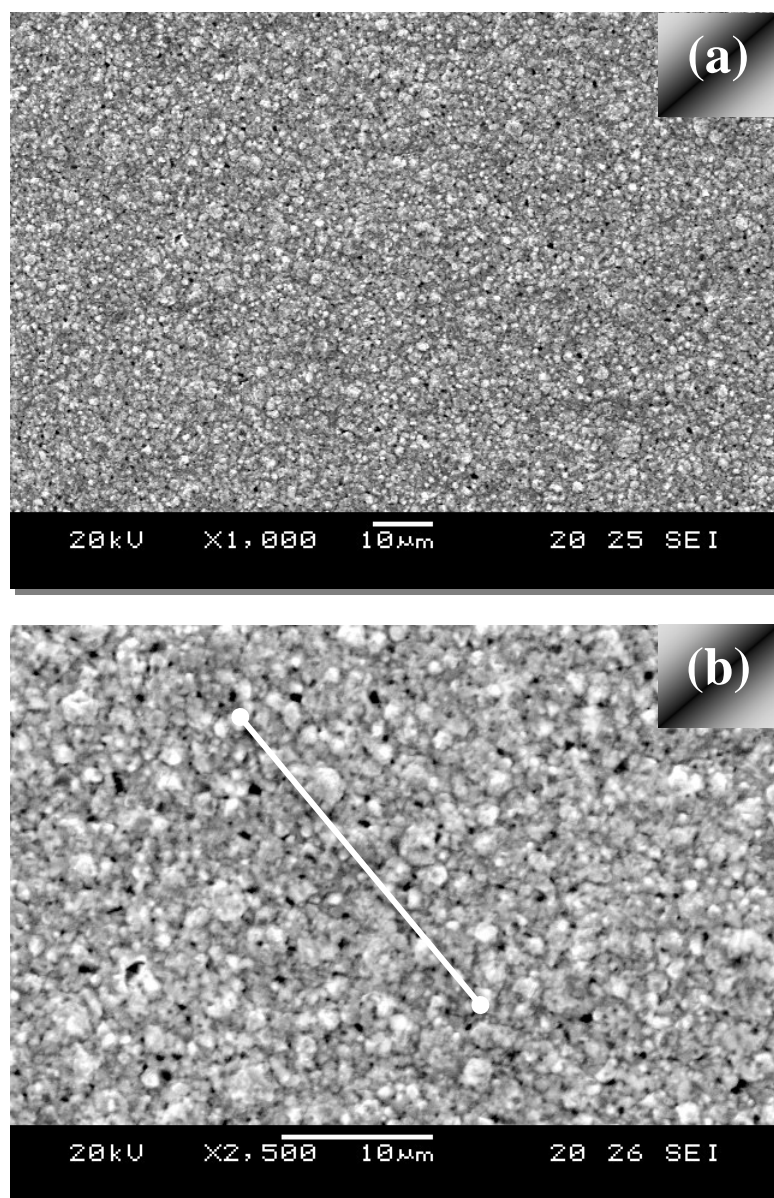


**Fig. 4.37 Scanning electron micrographs of Ni-B-Si<sub>3</sub>N<sub>4</sub> composite coatings electrodeposited at 1 A/dm<sup>2</sup>**  
**(The arrow mark indicates the region at which the EDX line scan is performed)**

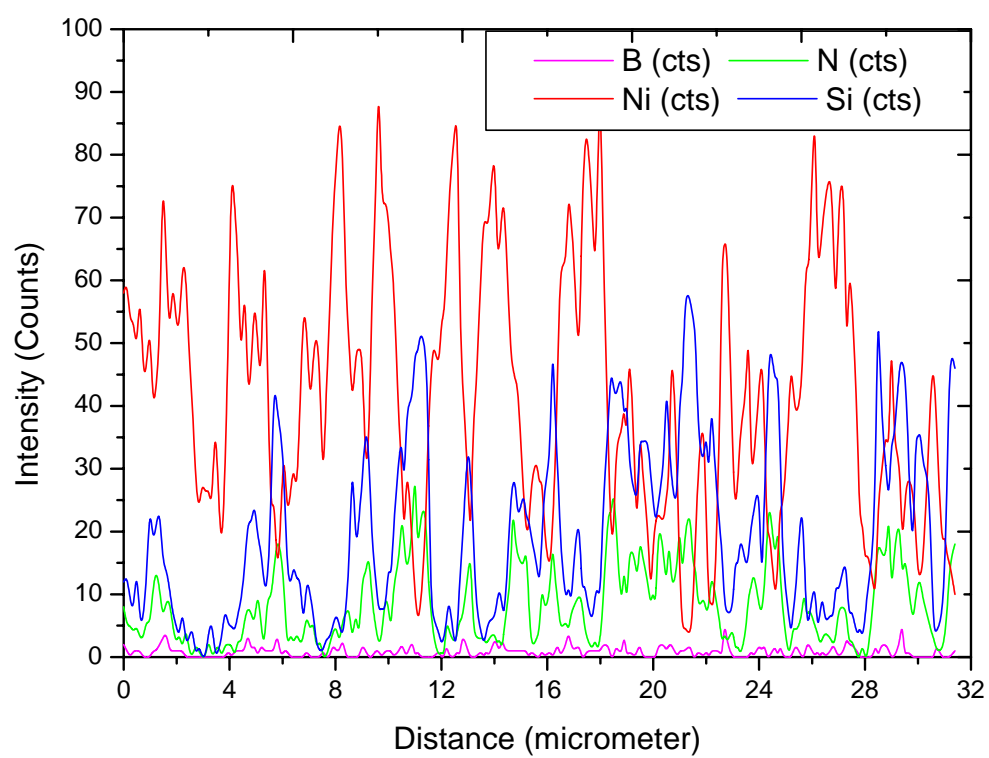


**Fig. 4.38** EDX line scan performed on a selected region (marked by arrow in Fig. 4.37(b)) on the surface of the ED Ni-B-Si<sub>3</sub>N<sub>4</sub> composite coating

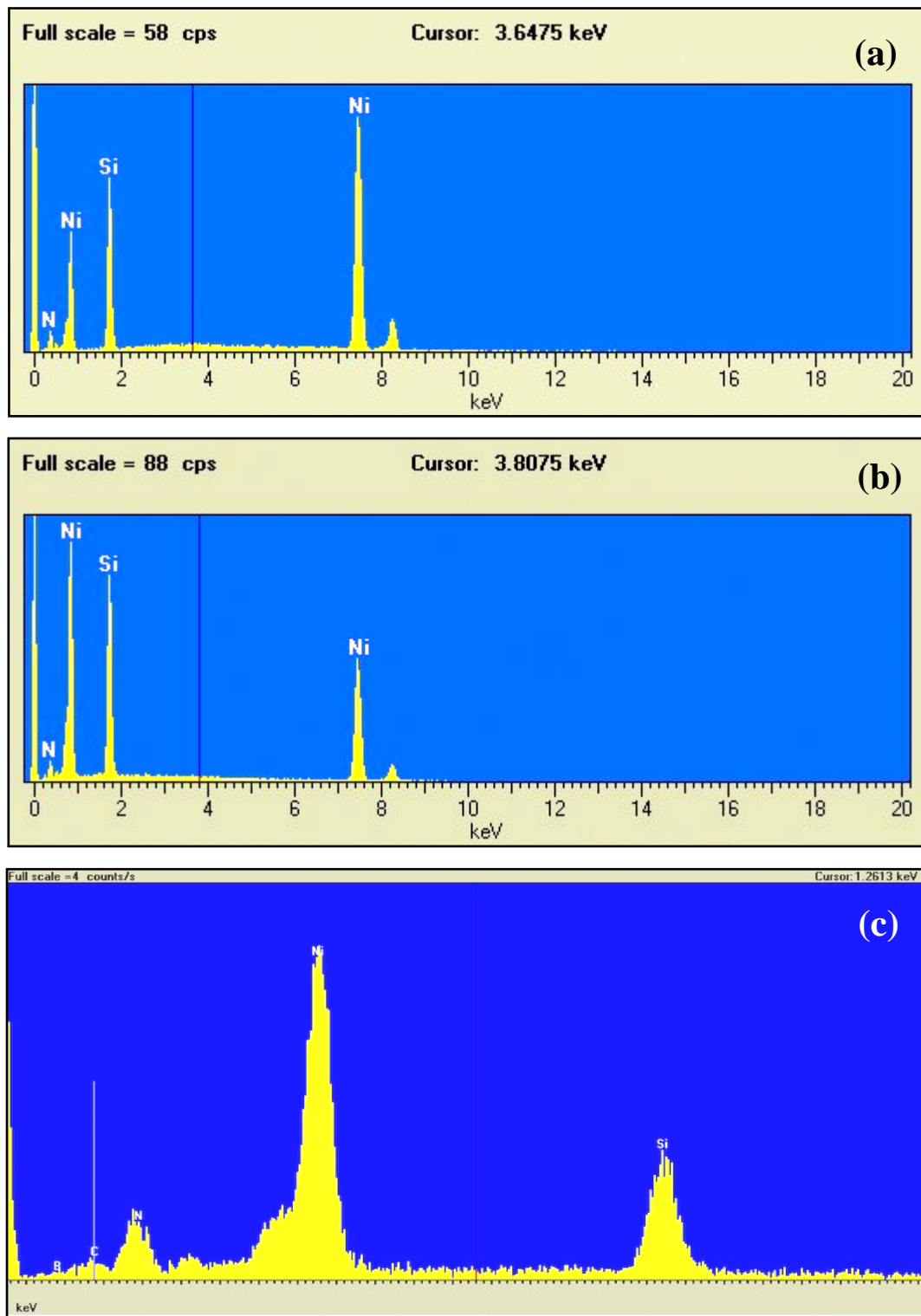


**Fig. 4.39** Energy dispersive X-ray spectral pattern taken at different regions of ED Ni-B-Si<sub>3</sub>N<sub>4</sub> composite coating: (a) on the coating surface area that is predominantly ED Ni-B matrix; (b) on the coating surface area predominantly occupied by Si<sub>3</sub>N<sub>4</sub> particles; and (c) on the coating surface showing the presence of smaller quantities of B and C that might have originated from DMAB

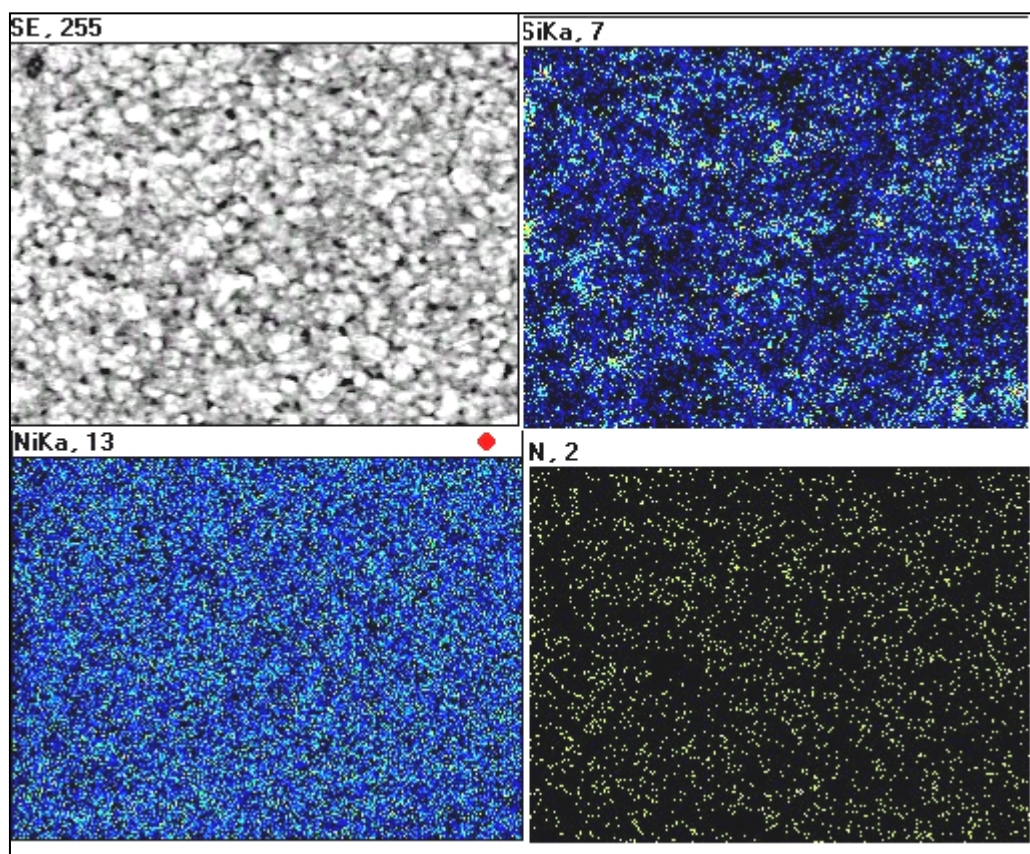


**Fig. 4.40** Secondary electron image of the coating (a) and X-ray elemental mapping of the surface of ED Ni-B-Si<sub>3</sub>N<sub>4</sub> composite coating: (b) Si map; (c) Ni map; and (d) N map.

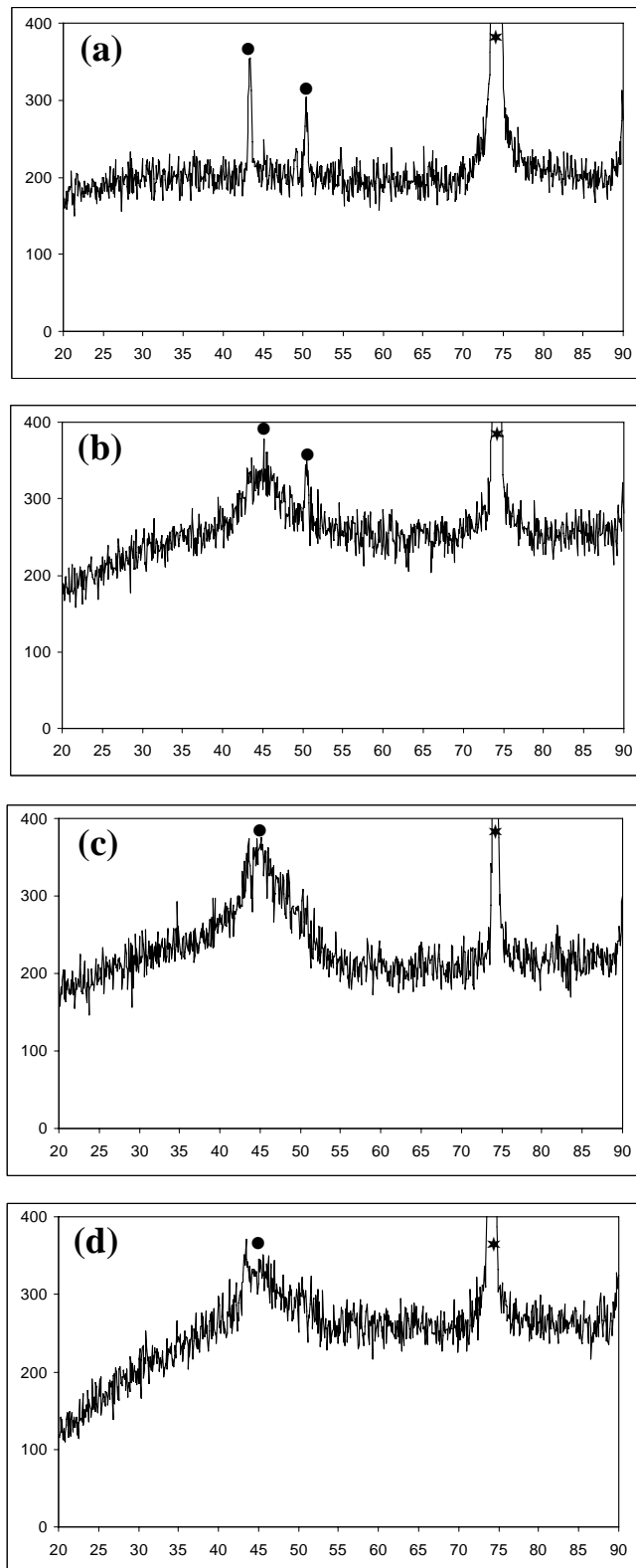


**Fig. 4.41 Comparison of the X-ray diffraction patterns of ED Ni-B-Si<sub>3</sub>N<sub>4</sub> composite coatings obtained in presence of varying concentration of Si<sub>3</sub>N<sub>4</sub> particles in their as-plated condition:**  
**(a) 0 g/l Si<sub>3</sub>N<sub>4</sub>; (b) 25 g/l Si<sub>3</sub>N<sub>4</sub>; (c) 50 g/l Si<sub>3</sub>N<sub>4</sub>; and (d) 75 g/l Si<sub>3</sub>N<sub>4</sub>**

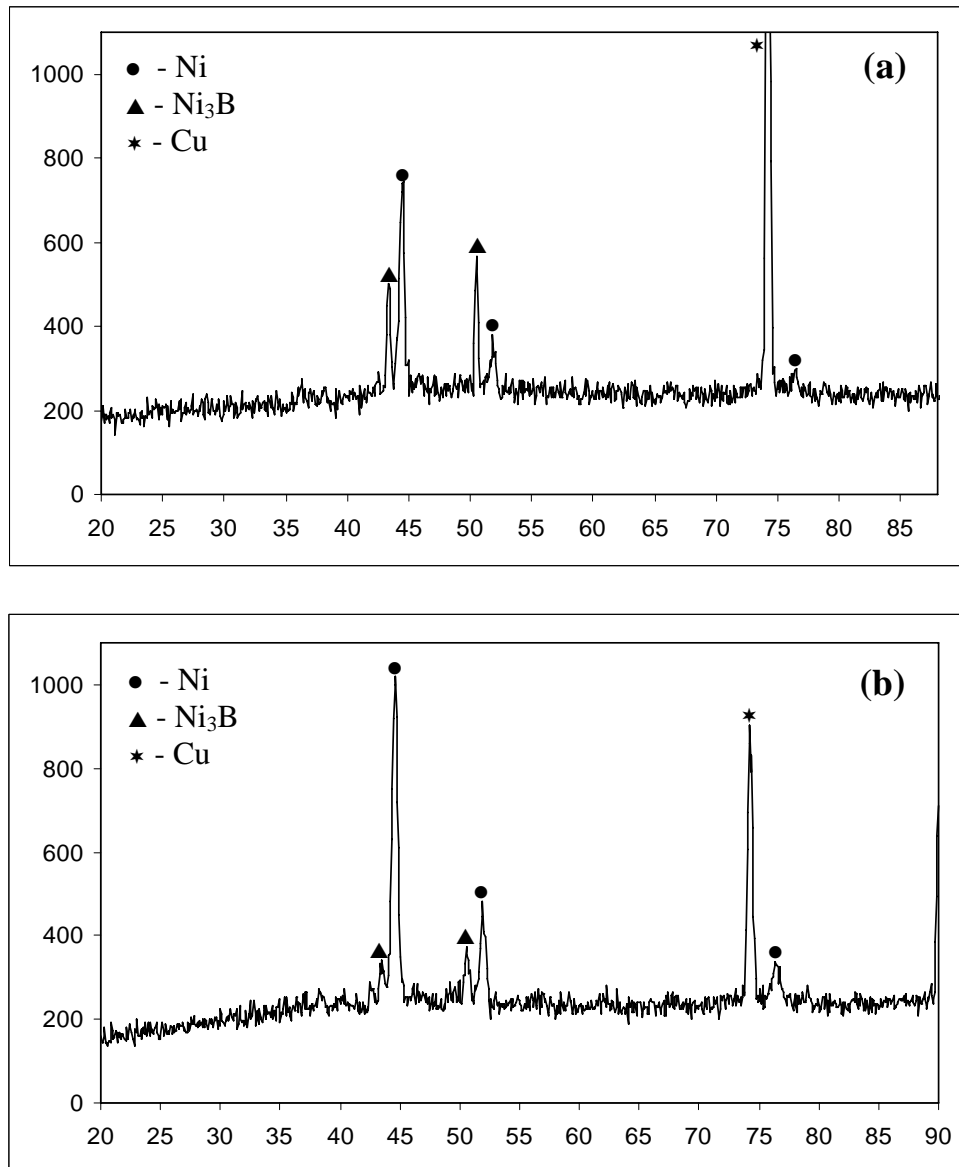


**Fig. 4.42 Comparison of the X-ray diffraction patterns of ED Ni-B-Si<sub>3</sub>N<sub>4</sub> composite coatings obtained in presence of varying concentration of Si<sub>3</sub>N<sub>4</sub> particles after heat-treatment at 400°C for 1 hour:  
(a) 0 g/l Si<sub>3</sub>N<sub>4</sub>; and (b) 50 g/l Si<sub>3</sub>N<sub>4</sub>**

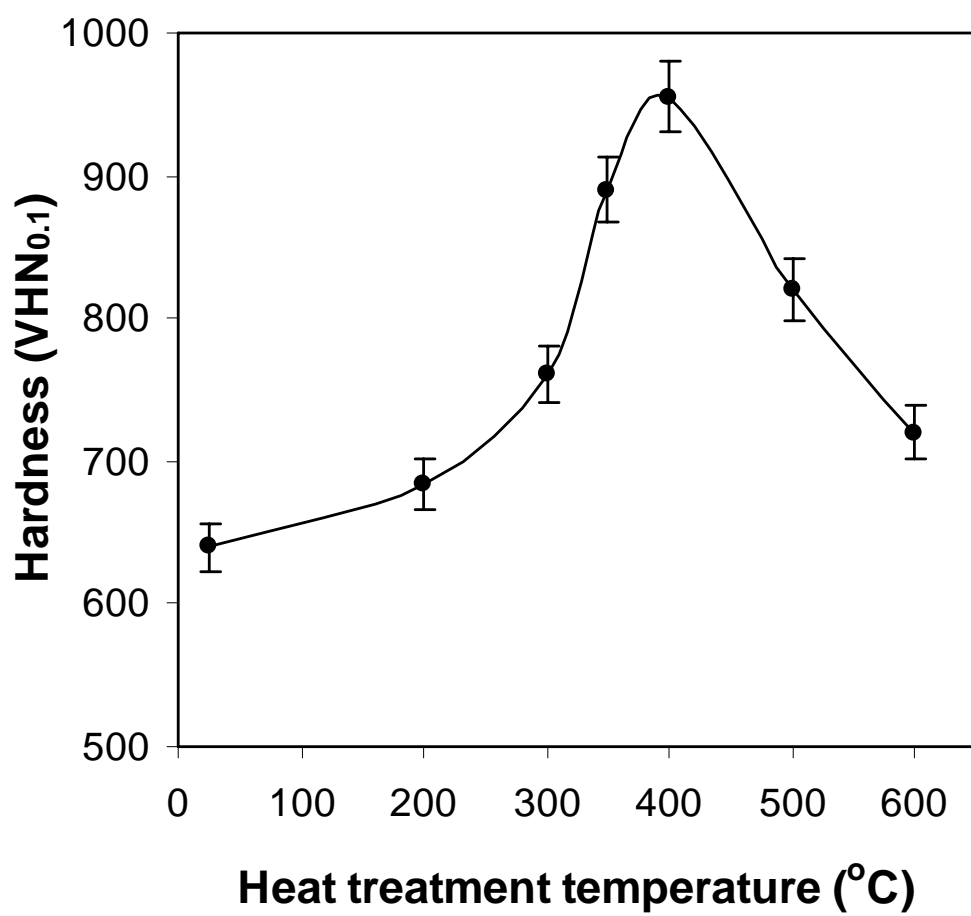


**Fig. 4.43** Variation in hardness of Ni-B-Si<sub>3</sub>N<sub>4</sub> coating electrodeposited at 1 A/dm<sup>2</sup> as a function of heat-treatment temperature



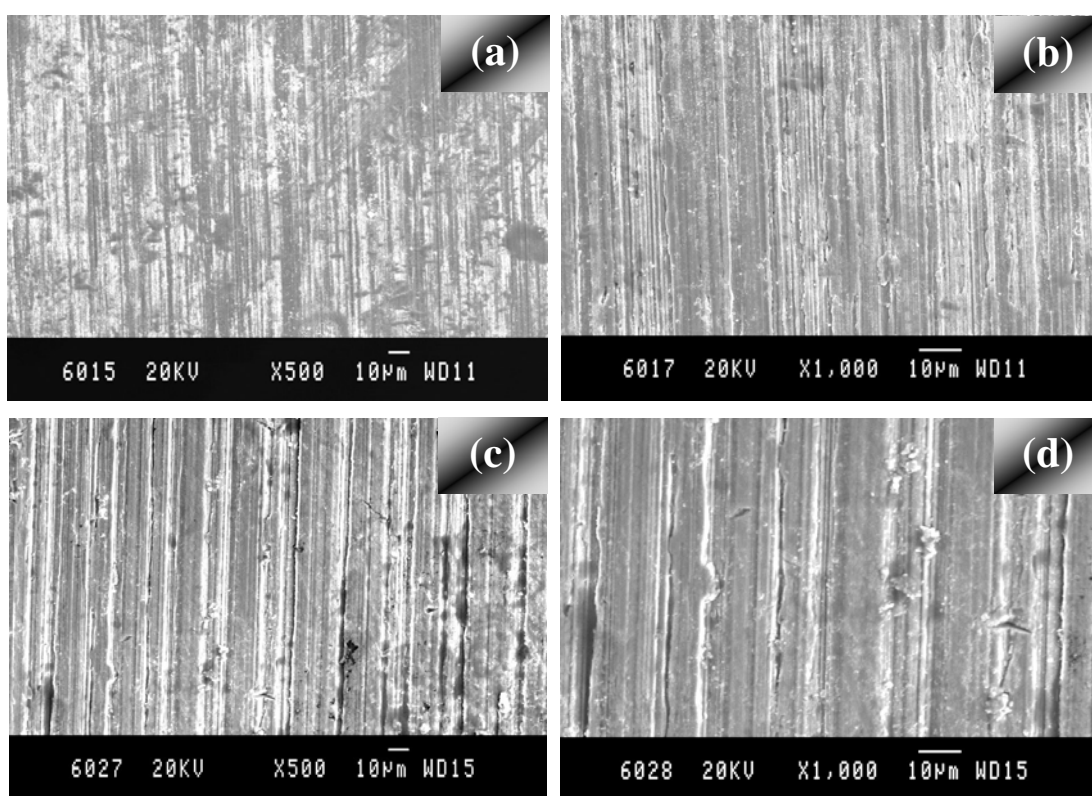


**Fig. 4.44 Wear track pattern of Ni-B-Si<sub>3</sub>N<sub>4</sub> composite coatings electrodeposited at 1 A/dm<sup>2</sup> in its as-plated and heat-treated conditions: (a and b) - As-plated; (c and d) - Heat-treated at 400°C for 1 hour (Applied load: 10 N; Sliding distance: 1800 m)**

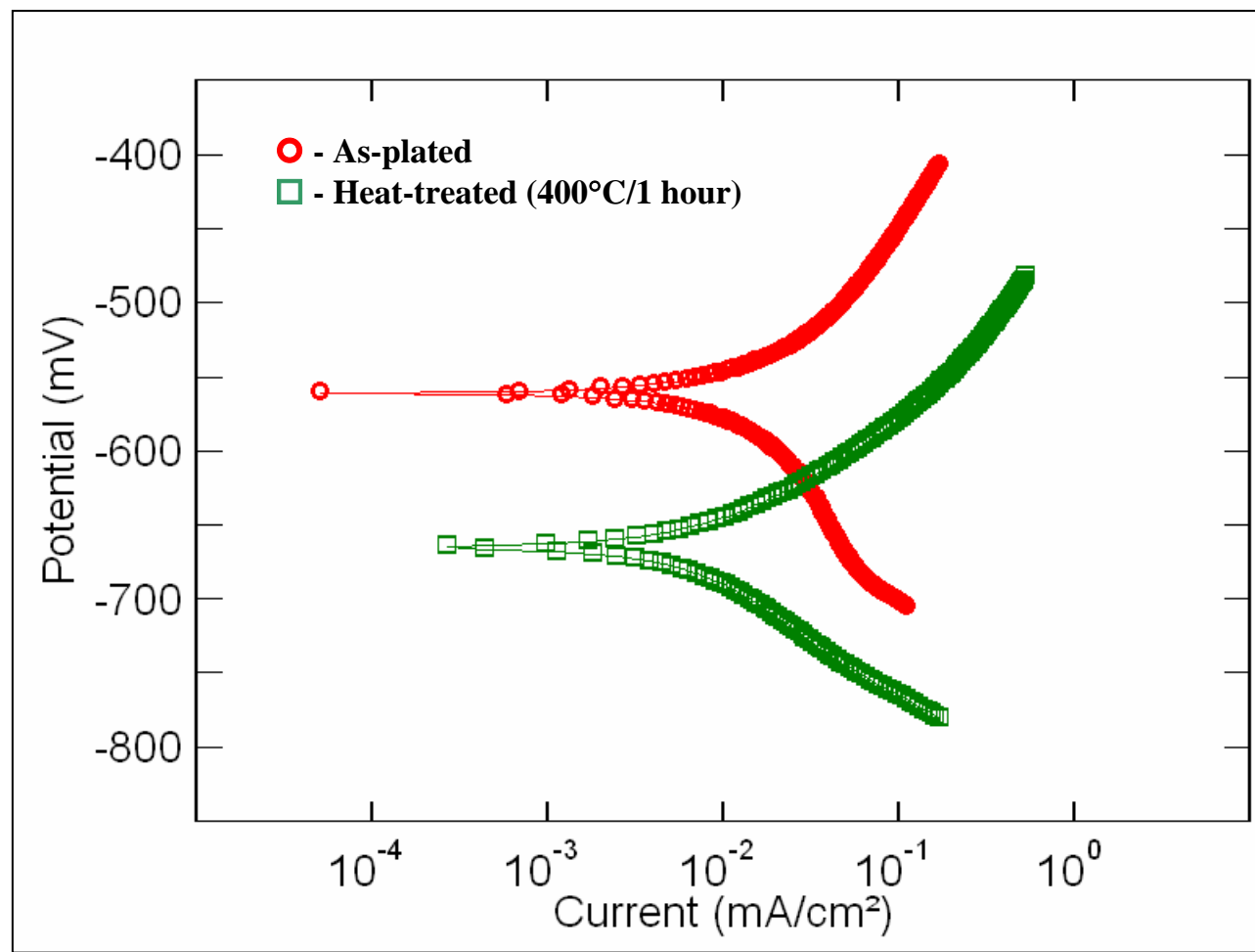


**Fig. 4.45(a) Polarization curve of ED Ni-B-Si<sub>3</sub>N<sub>4</sub> composite coating in 3.5% sodium chloride solution in its as-plated and heat-treated (400°C for 1 hour) conditions (potential in mV vs. SCE)**

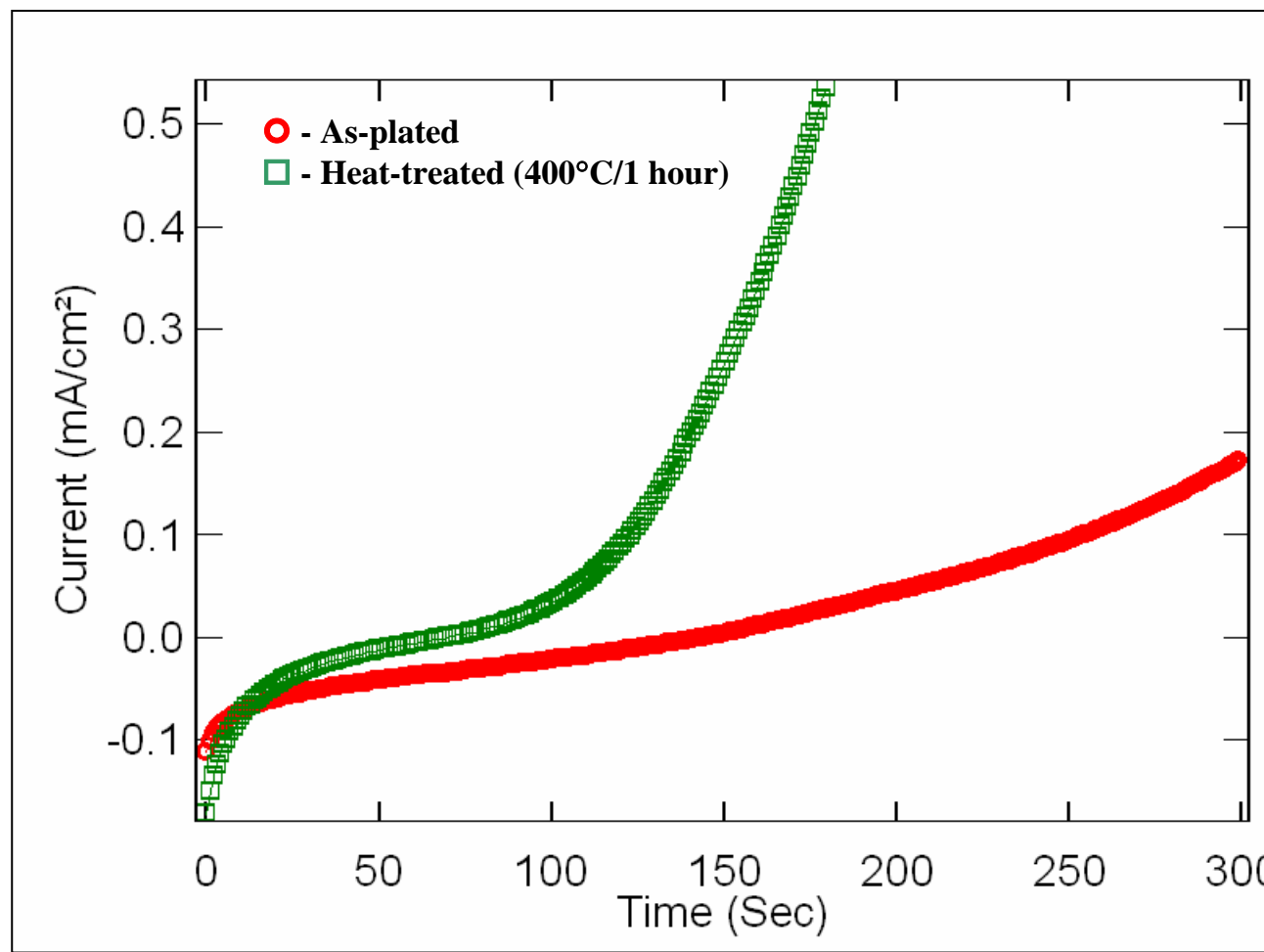


**Fig. 4.45(b)** Current-time transient curves of ED Ni-B-Si<sub>3</sub>N<sub>4</sub> composite coating in 3.5% sodium chloride solution in its as-plated and heat-treated (400°C for 1 hour) conditions

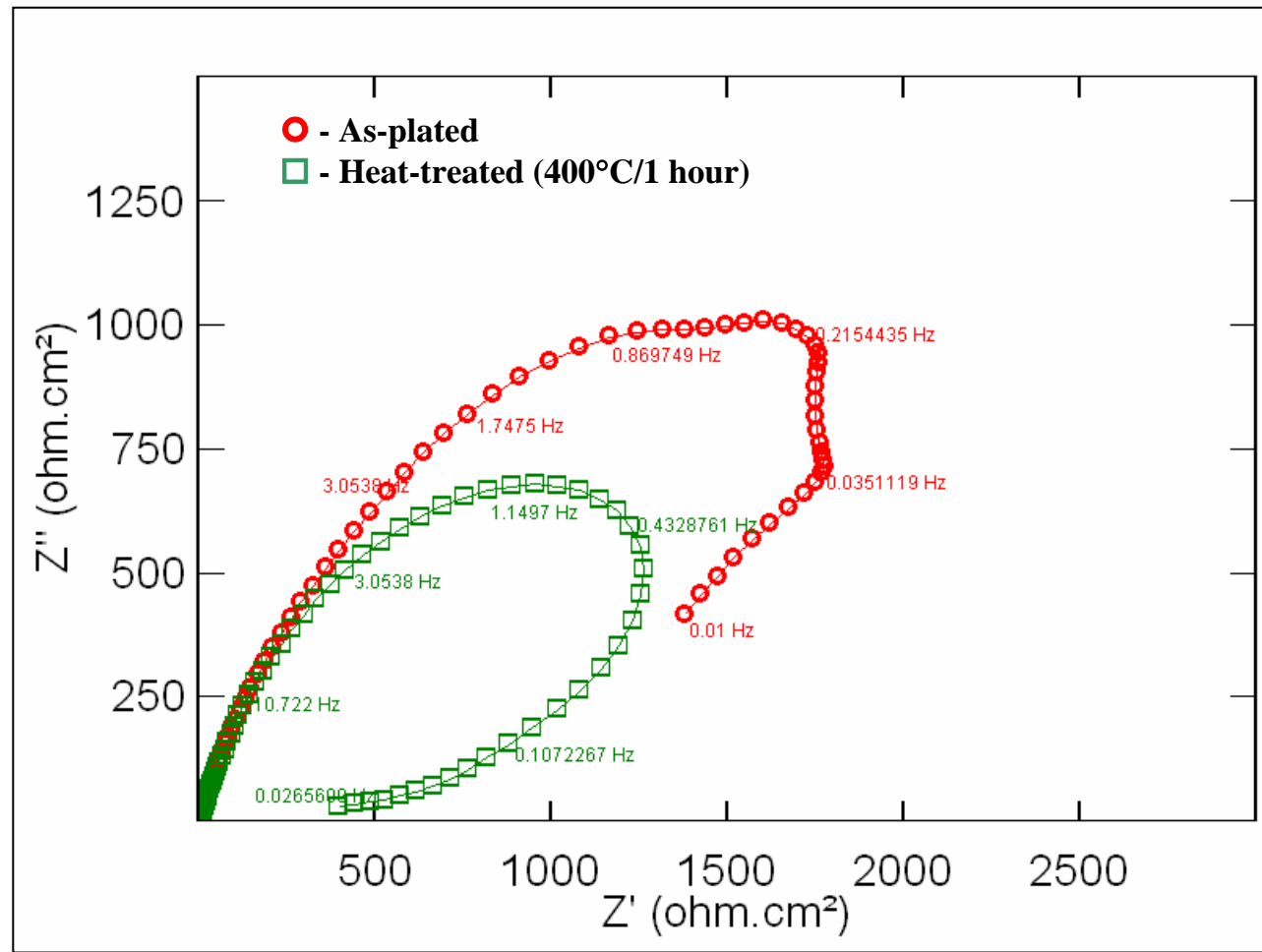


**Fig. 4.46 Nyquist plot of ED Ni-B-Si<sub>3</sub>N<sub>4</sub> composite coating in 3.5% sodium chloride solution in its as-plated and heat-treated (400°C for 1 hour) conditions**

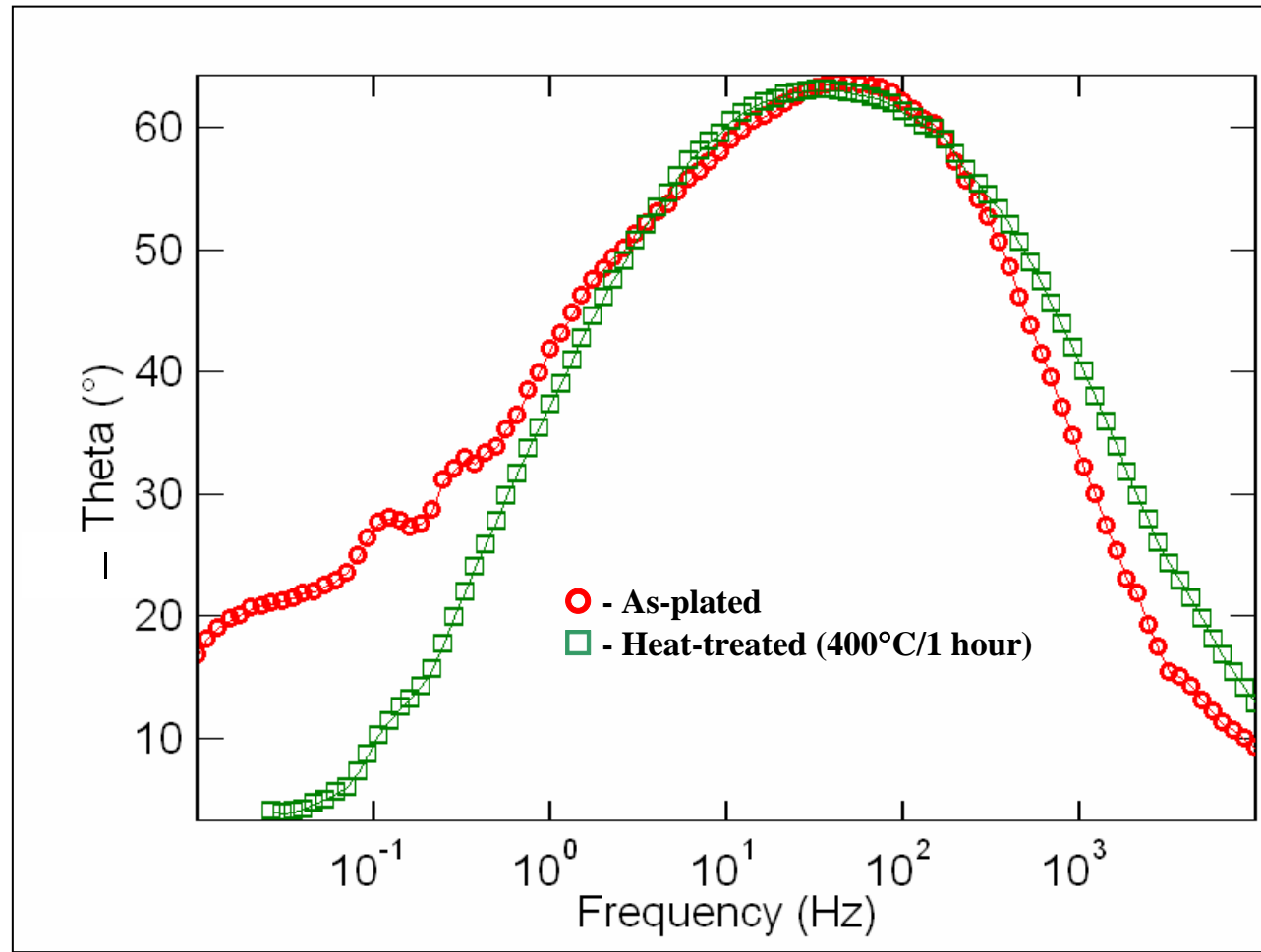


**Fig. 4.47** Bode plot of ED Ni-B-Si<sub>3</sub>N<sub>4</sub> composite coating in 3.5% sodium chloride solution in its as-plated and heat-treated (400°C for 1 hour) conditions

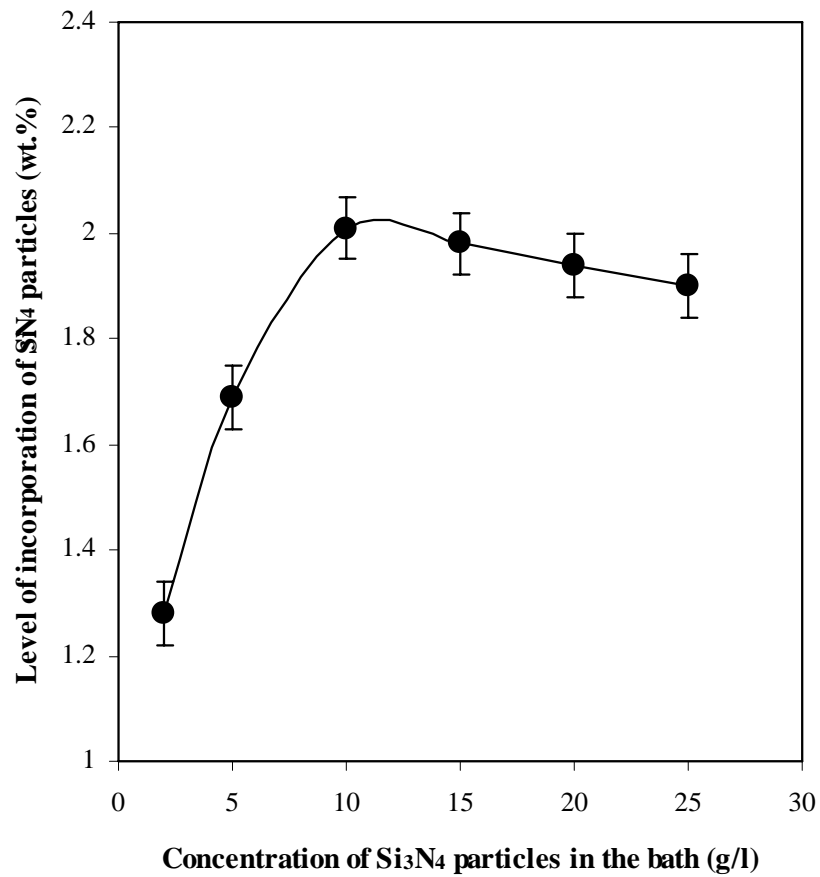


**Fig. 4.48** Variation in the level of incorporation of  $\text{Si}_3\text{N}_4$  particles in the EL Ni-B matrix as a function of their concentration in the plating bath

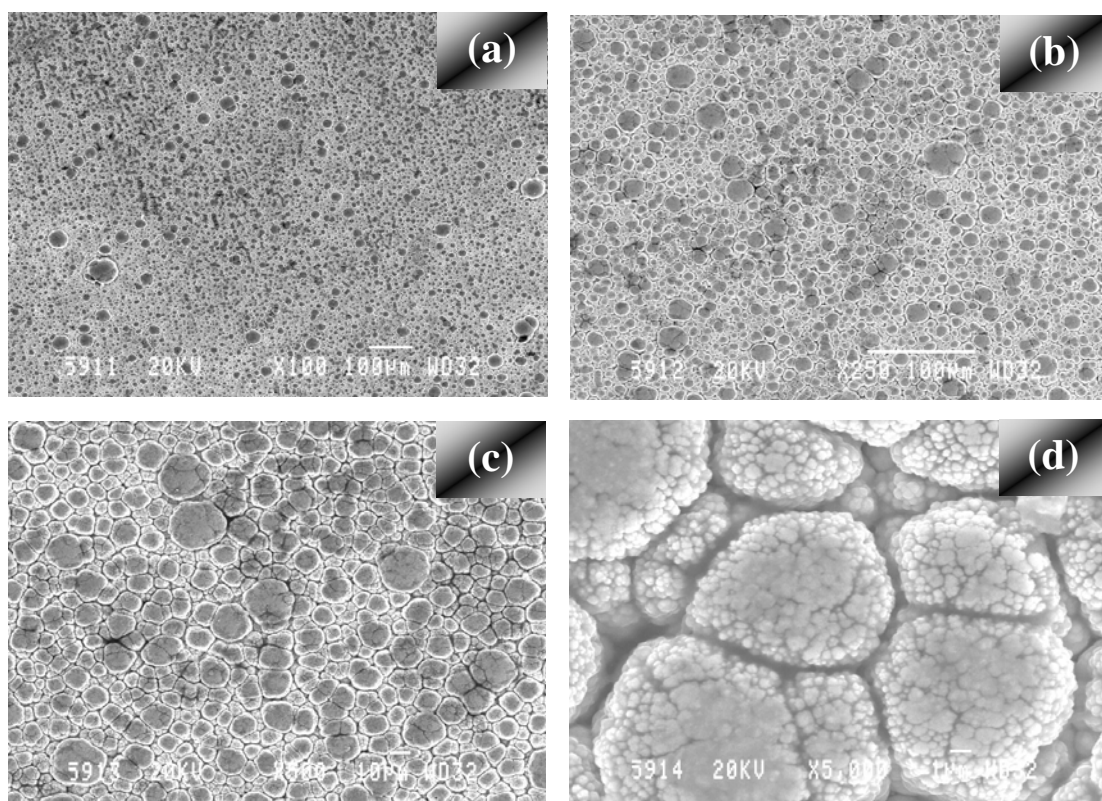


**Fig. 4.49 Scanning electron micrographs of the EL Ni-B-Si<sub>3</sub>N<sub>4</sub> composite coatings at different magnifications: (a) X 100; (b) X 250; (c) X 500; and (d) X 5000**

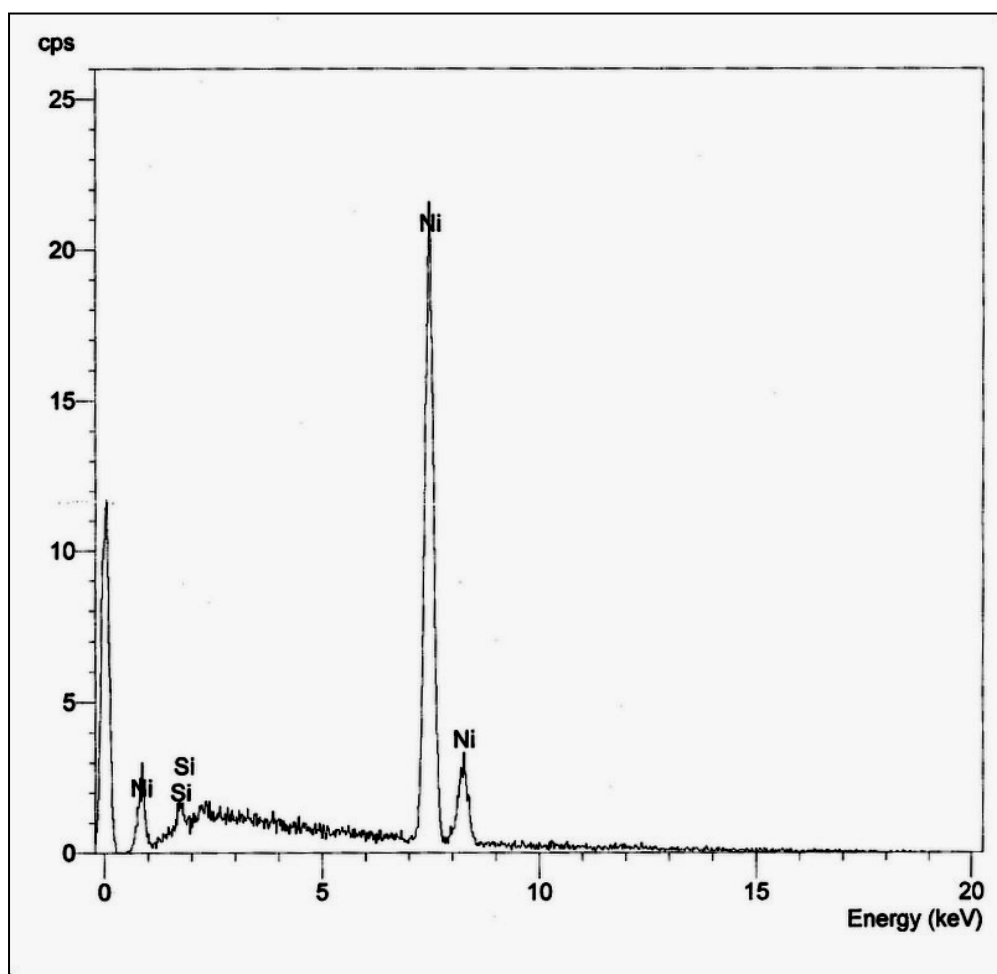


**Fig. 4.50 Energy dispersive X-ray pattern  
of EL Ni-B-Si<sub>3</sub>N<sub>4</sub> composite coating**



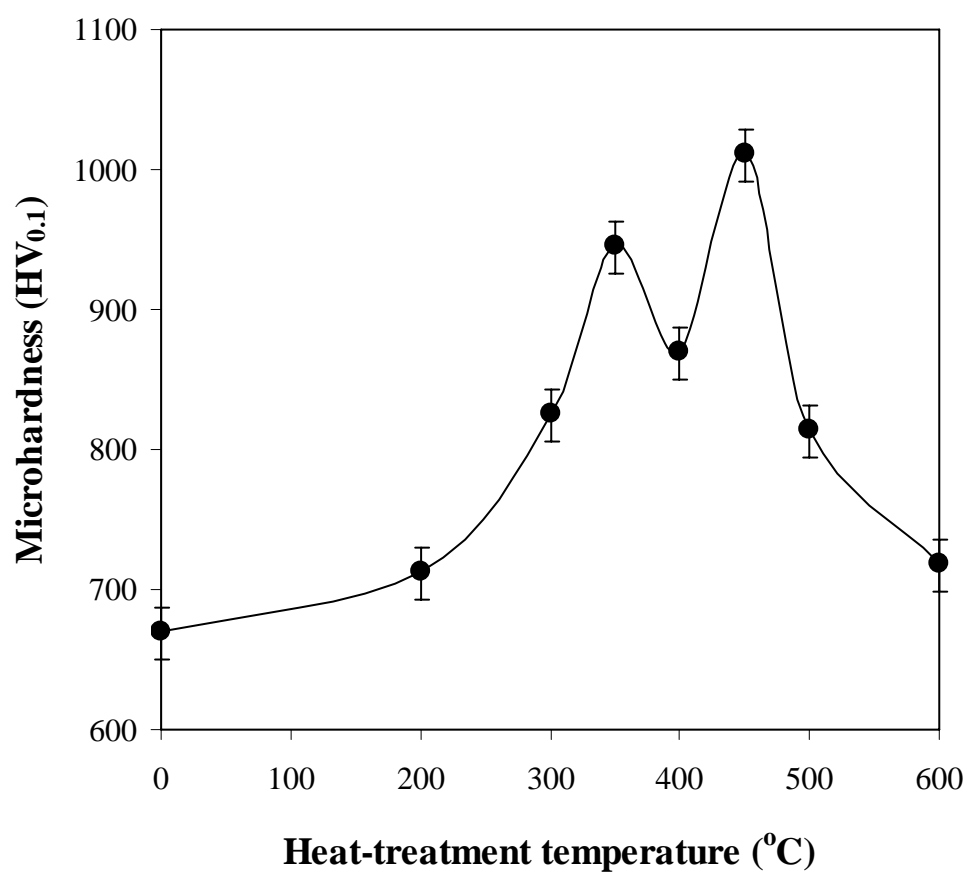


**Fig. 4.51 Variation in hardness of EL Ni-B-Si<sub>3</sub>N<sub>4</sub> composite coating as a function of heat-treatment temperature**

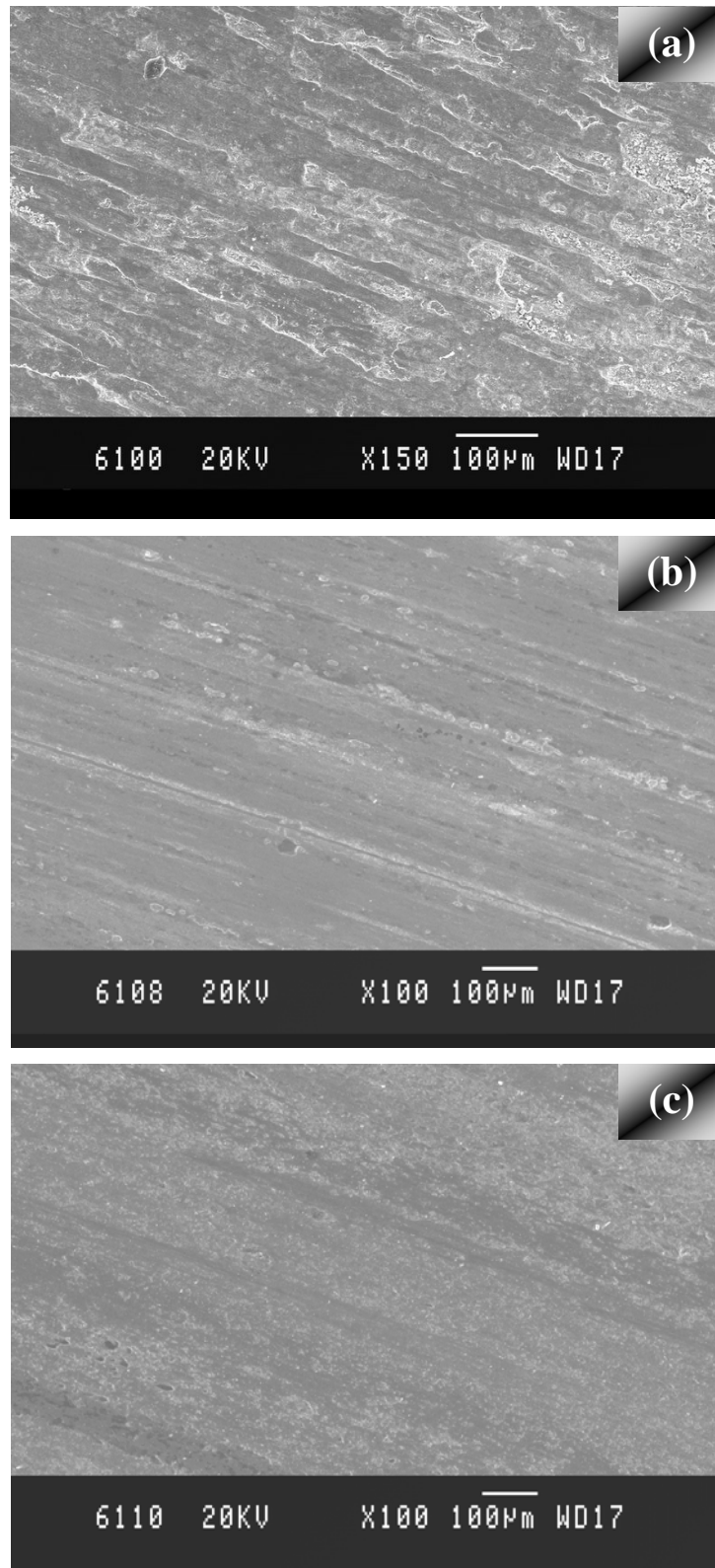


**Fig. 4.52 Wear track pattern of electroless Ni-B-Si<sub>3</sub>N<sub>4</sub> composite coating (a) as-plated; (b) heat-treated at 350°C for 1 hour; and (c) heat-treated at 450°C for 1 hour (Applied load: 40 N; Sliding distance: 2700 m)**

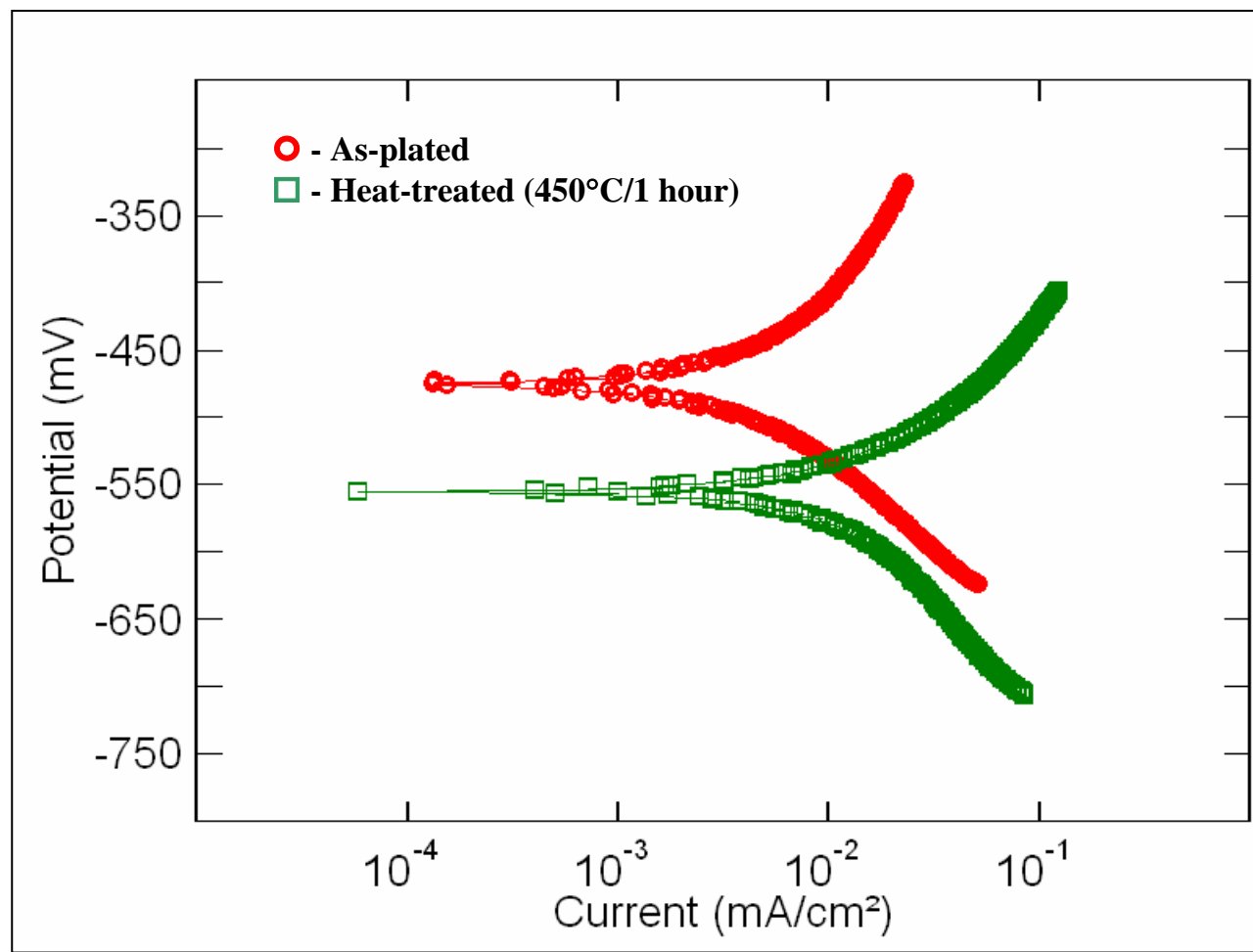


**Fig. 4.53(a) Polarization curve of EL Ni-B-Si<sub>3</sub>N<sub>4</sub> composite coating in 3.5% sodium chloride solution in its as-plated and heat-treated (450°C for 1 hour) conditions (potential in mV vs. SCE)**

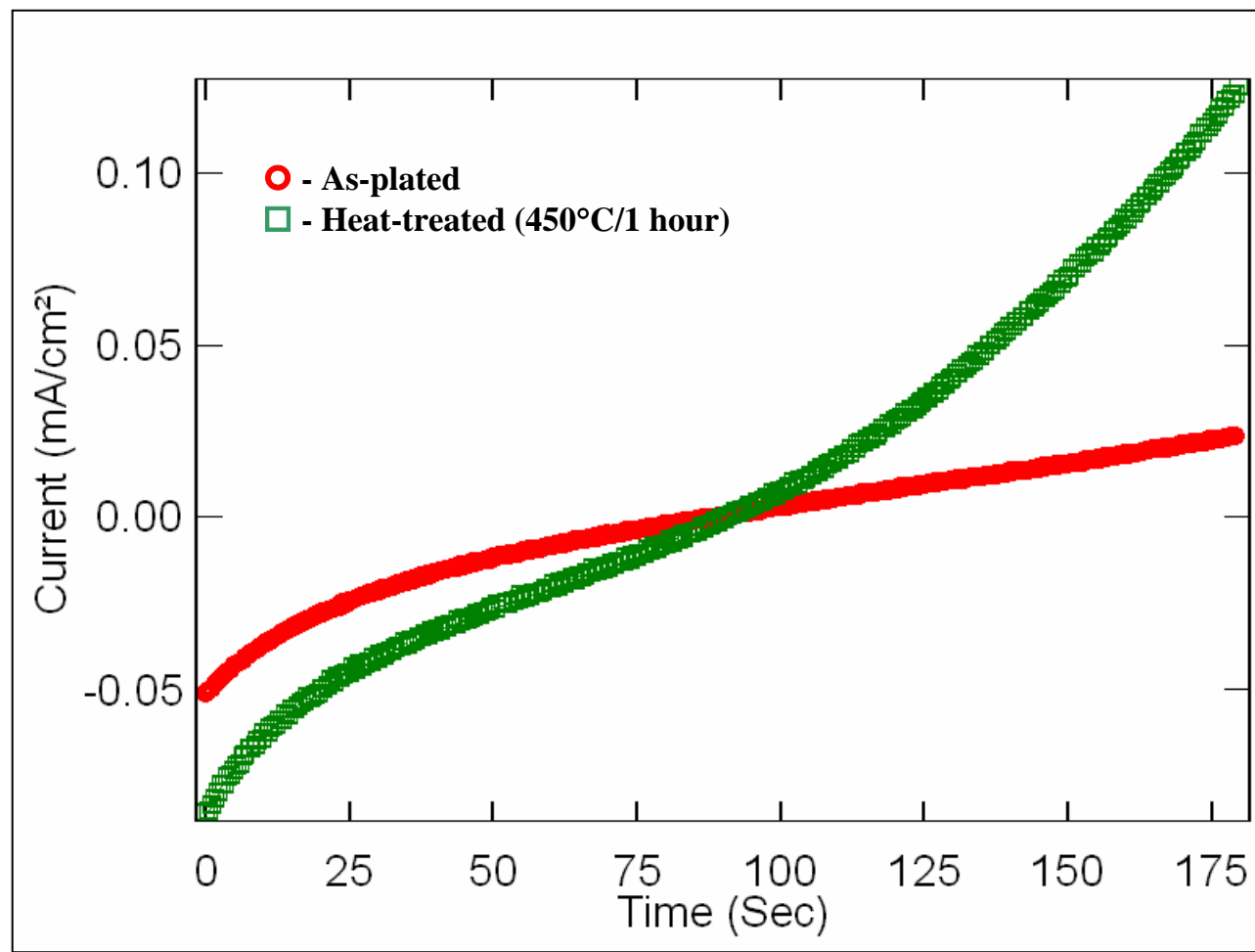


**Fig. 4.53(b) Current-time transient curves of EL Ni-B-Si<sub>3</sub>N<sub>4</sub> composite coating in 3.5% sodium chloride solution in its as-plated and heat-treated (450°C for 1 hour) conditions**

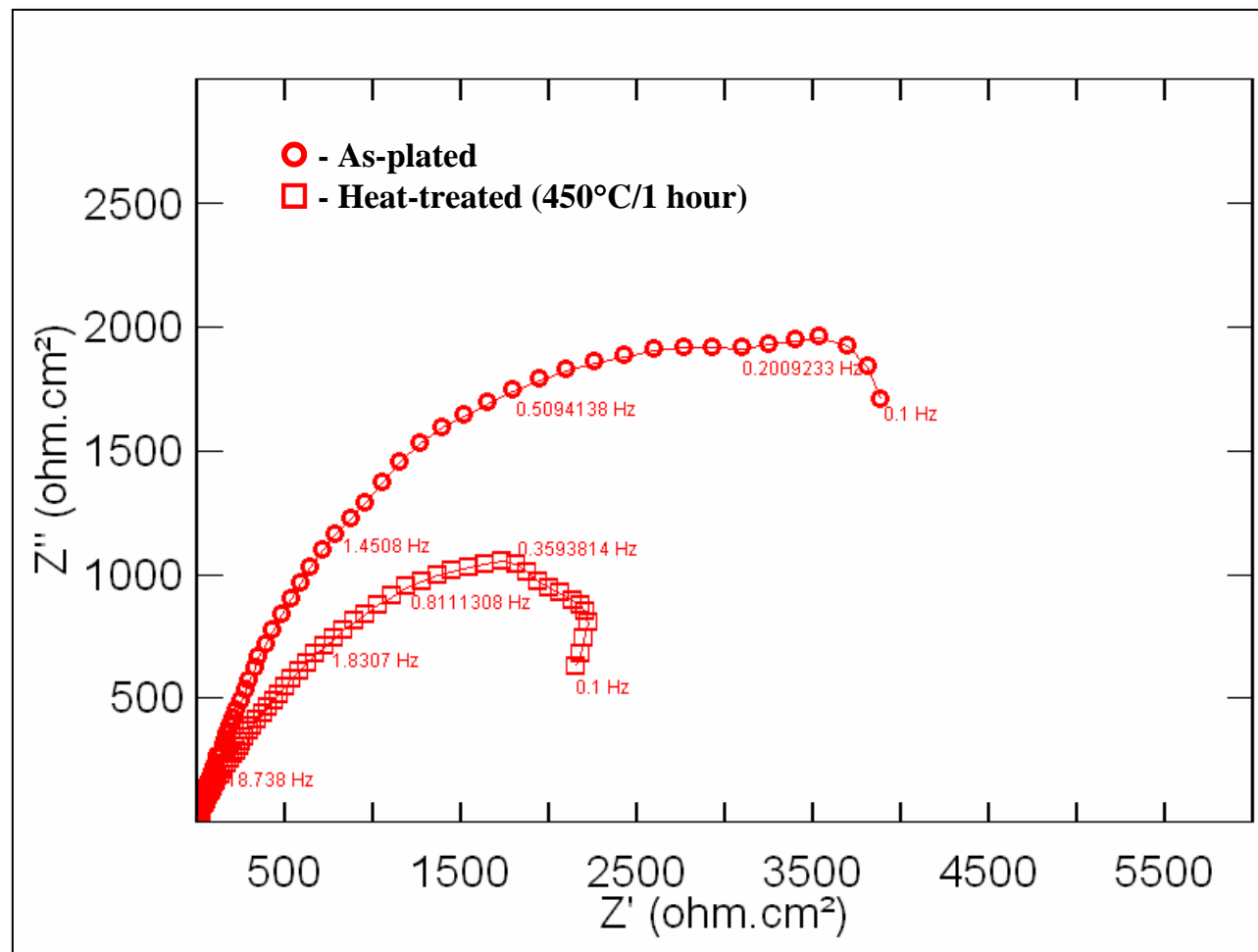


**Fig. 4.54** Nyquist plot of EL Ni-B-Si<sub>3</sub>N<sub>4</sub> composite coating in 3.5% sodium chloride solution in its as-plated and heat-treated (450°C for 1 hour) conditions

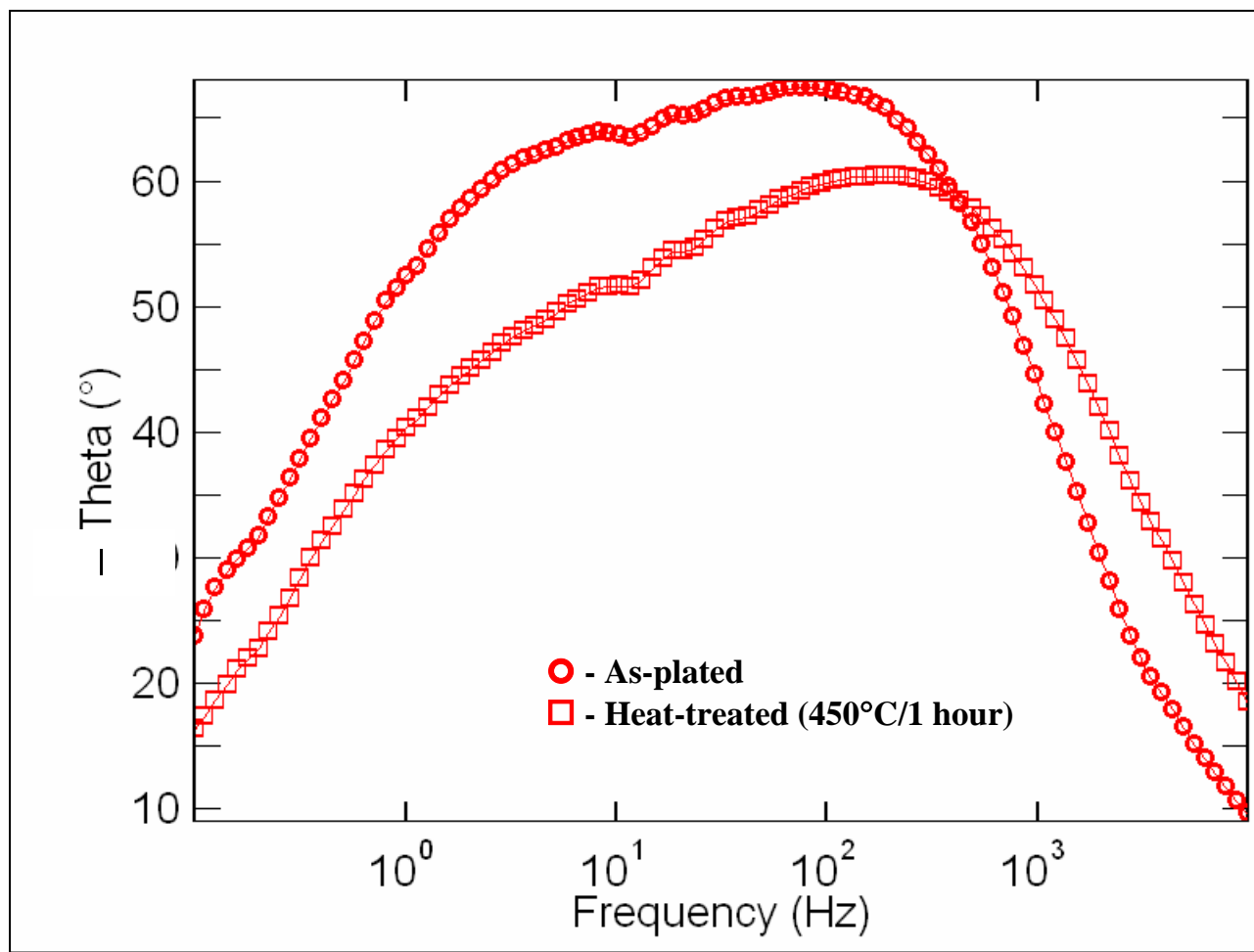


**Fig. 4.55** Bode plot of EL Ni-B-Si<sub>3</sub>N<sub>4</sub> composite coating in 3.5% sodium chloride solution in its as-plated and heat-treated (450°C for 1 hour) conditions

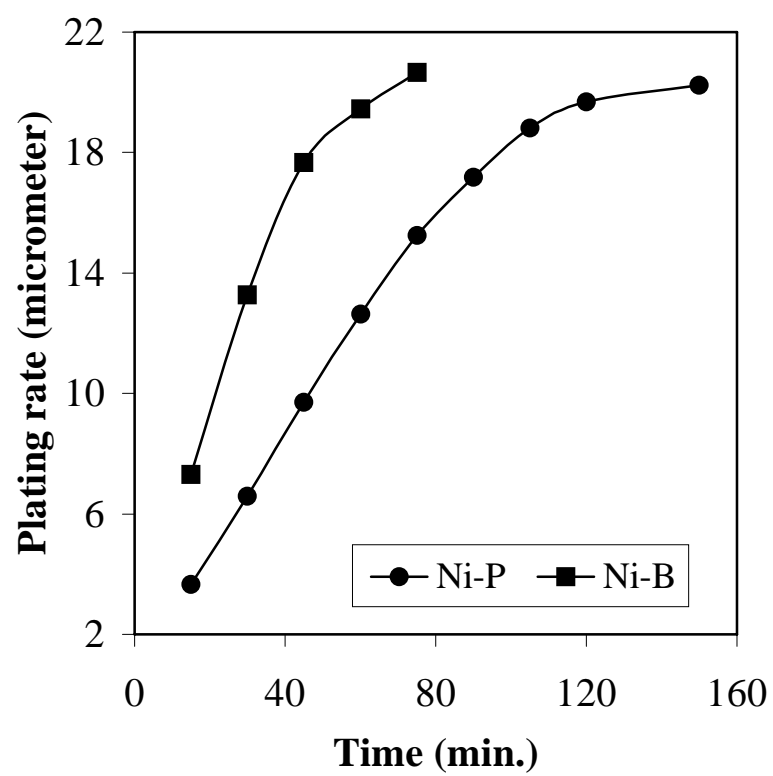


**Fig. 4.56** Plating rate of EL Ni-P and Ni-B coatings as a function of time

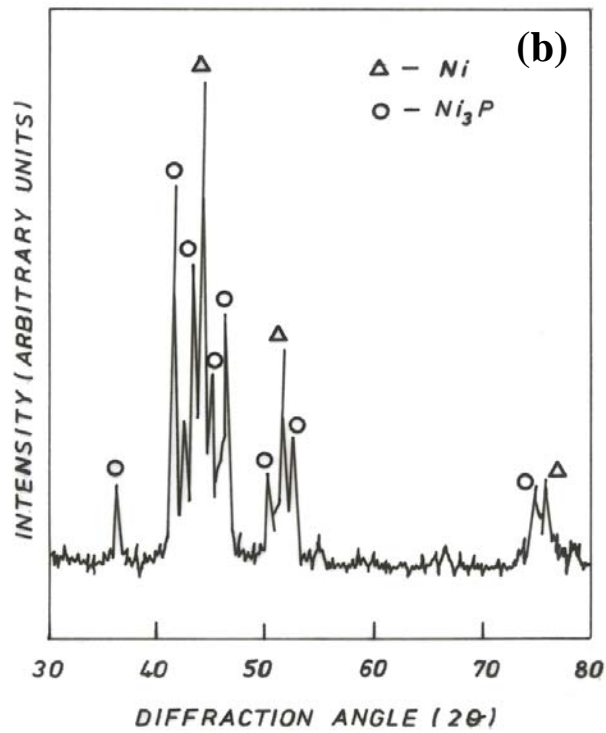
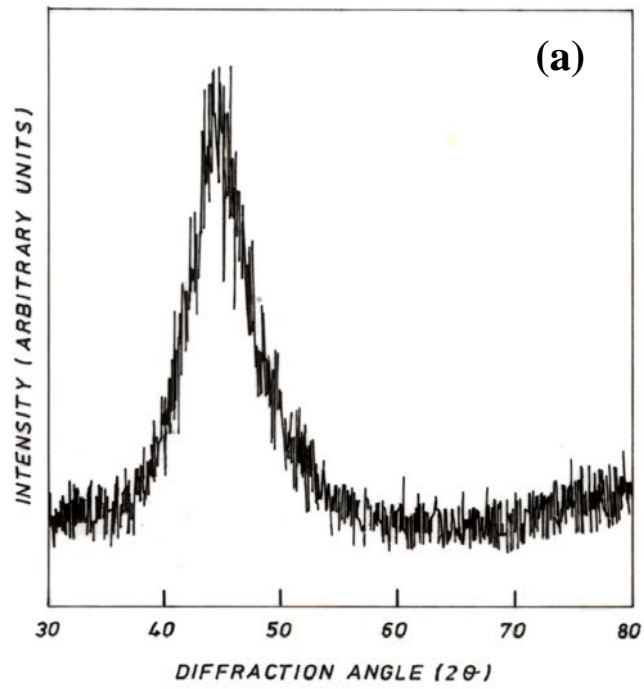


**Fig. 4.57** X-ray diffraction pattern of electroless Ni-P coating in its (a) as-plated and (b) heat-treated ( $450^\circ\text{C}$  for 1 hour) conditions



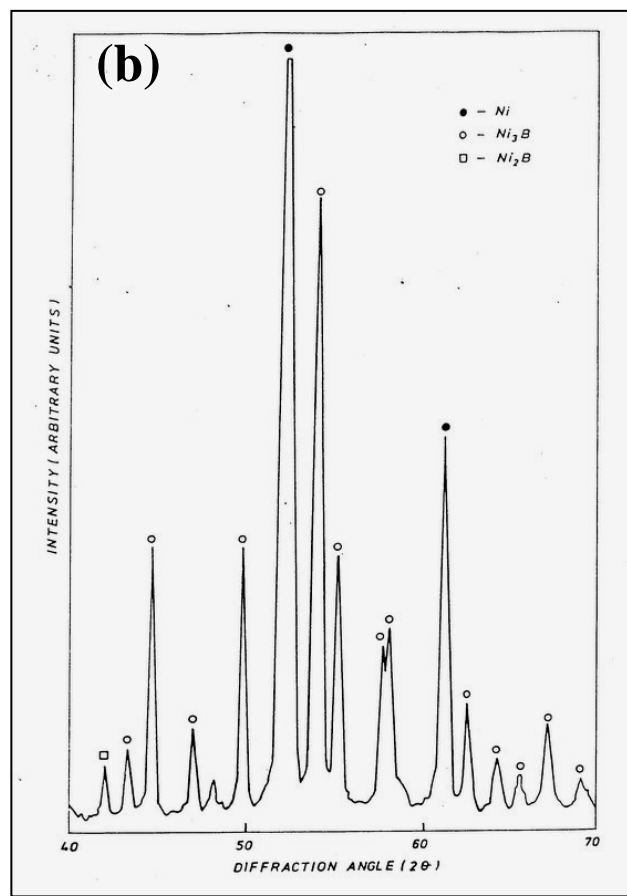
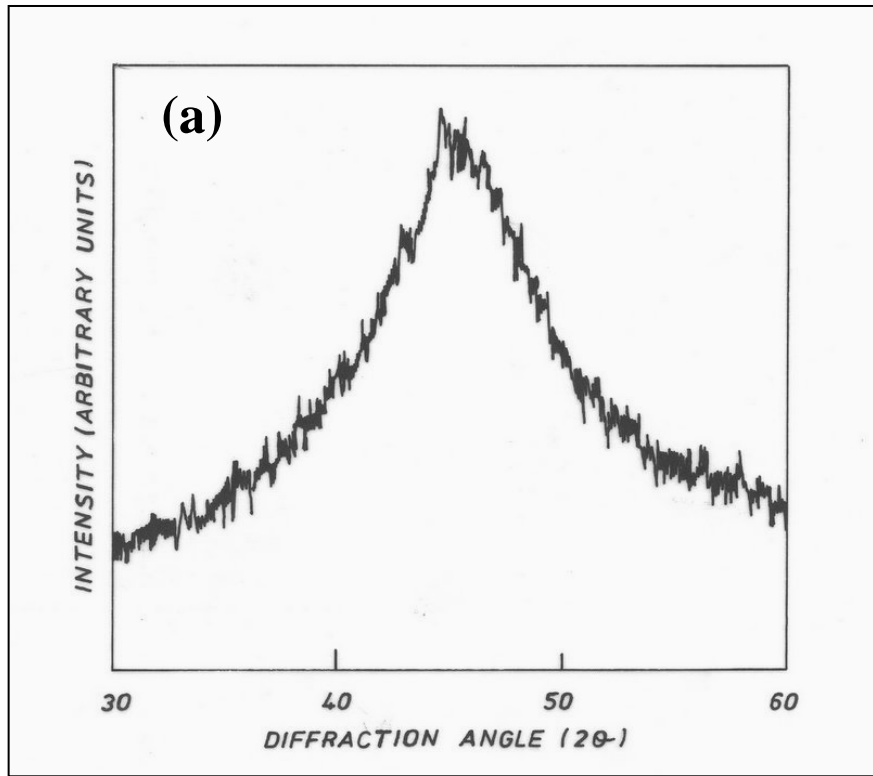


**Fig. 4.58** X-ray diffraction pattern of EL Ni-B coating in its (a) as-plated; and (b) heat-treated (450°C for 1 hour) conditions

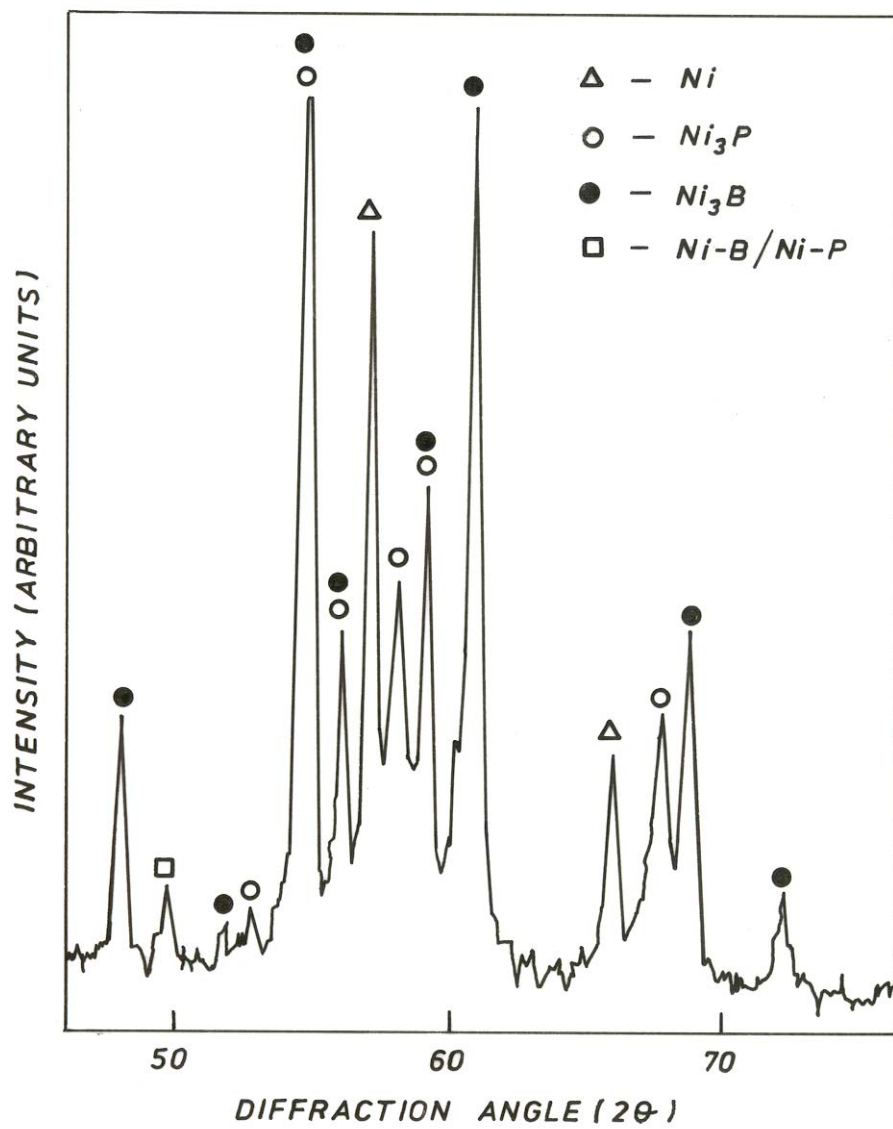


**Fig.4.59 XRD pattern electroless Ni-P/Ni-B duplex coating heat-treated at 450°C for 1 hour**

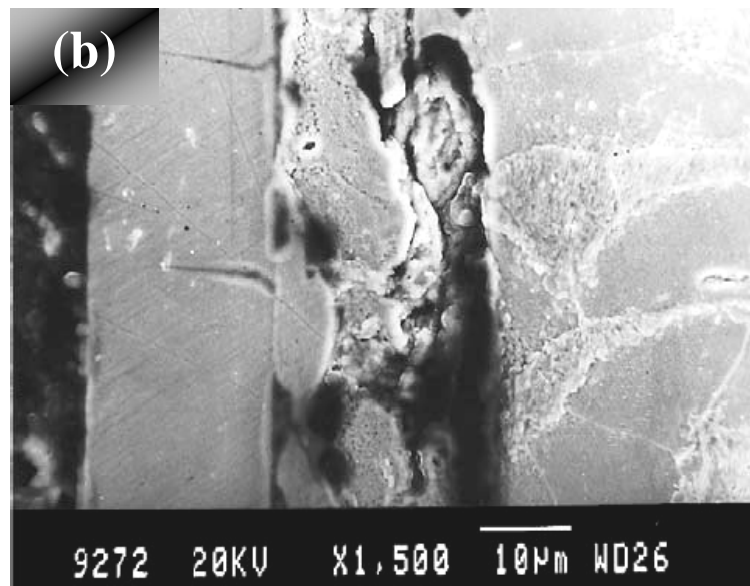
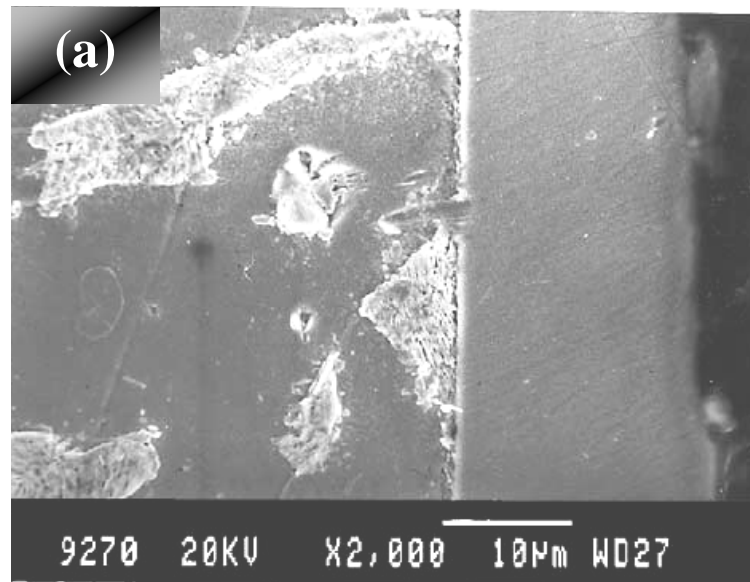


**Fig. 4.60 Scanning electron micrographs of the cross-section of EL Ni-P/Ni-B duplex coatings: (a) as-plated; and (b) heat-treated at 450°C for 1 hour**

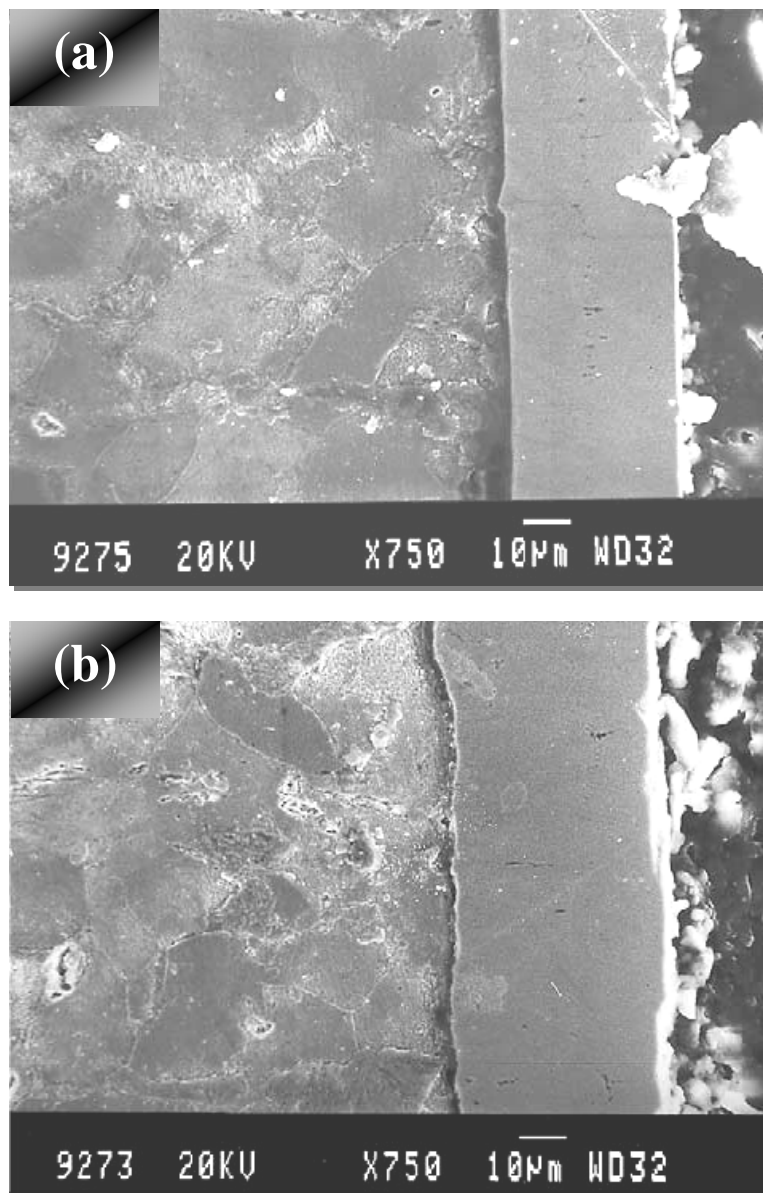


**Fig. 4.61 Scanning electron micrographs of the cross-section of EL Ni-B/Ni-P duplex coatings: (a) as-plated; and (b) heat-treated at 450°C for 1 hour**

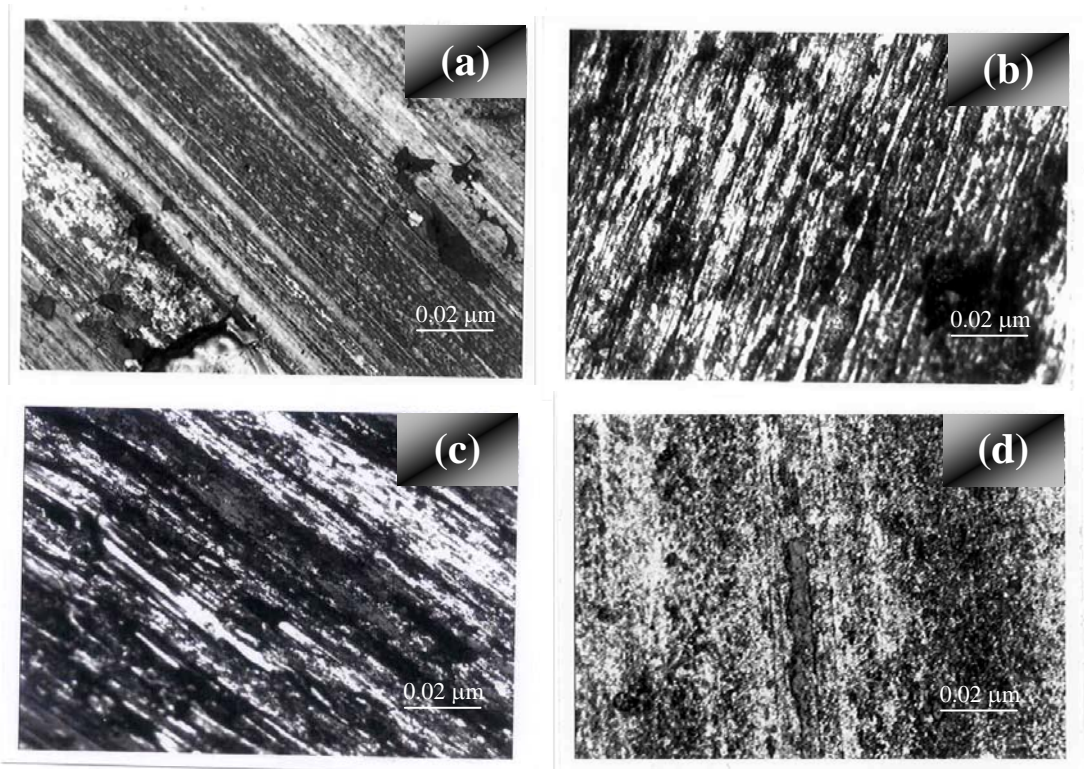


**Fig. 4.62 Optical micrographs of the wear track pattern of EL Ni-P, Ni-B and duplex coatings in their as-deposited condition**  
 (a) EL Ni-P coating; (b) EL Ni-B coating;  
 (c) EL Ni-P/Ni-B coating; and (d) EL Ni-B/Ni-P coating.

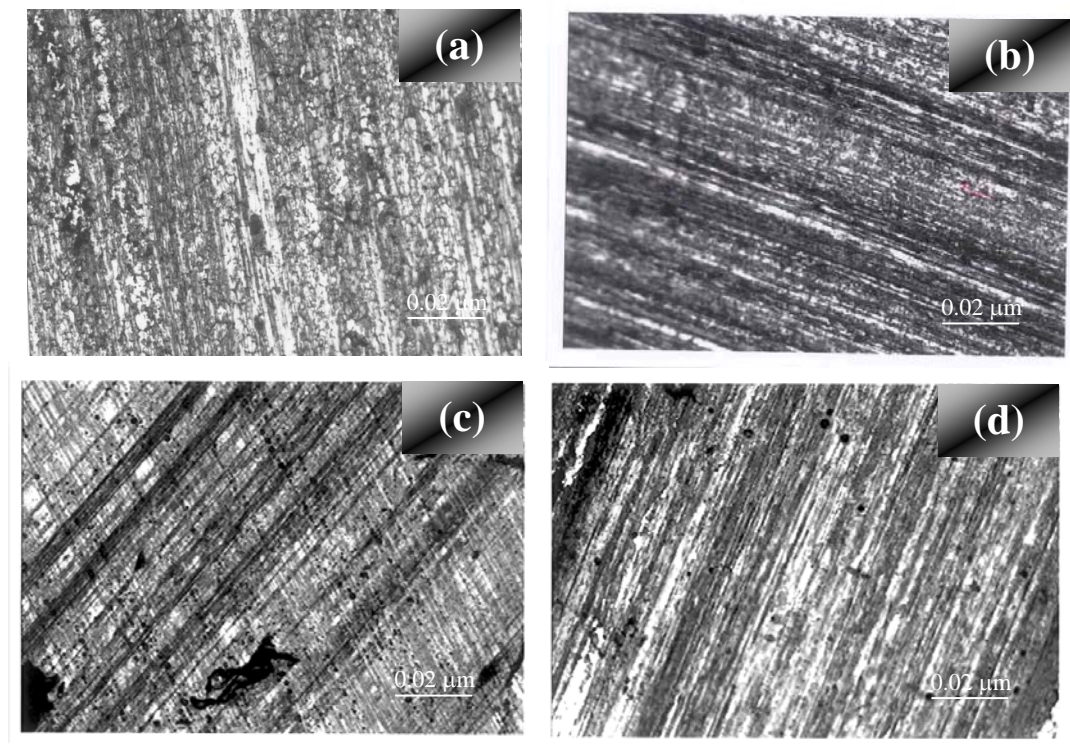


**Fig. 4.63 Optical micrographs of the wear track pattern of EL Ni-P, EL Ni-B and duplex coatings in their heat-treated condition:**  
**(a) EL Ni-P coating; (b) EL Ni-B coating;**  
**(c) EL Ni-P/Ni-B coating; and (d) EL Ni-B/Ni-P coating**

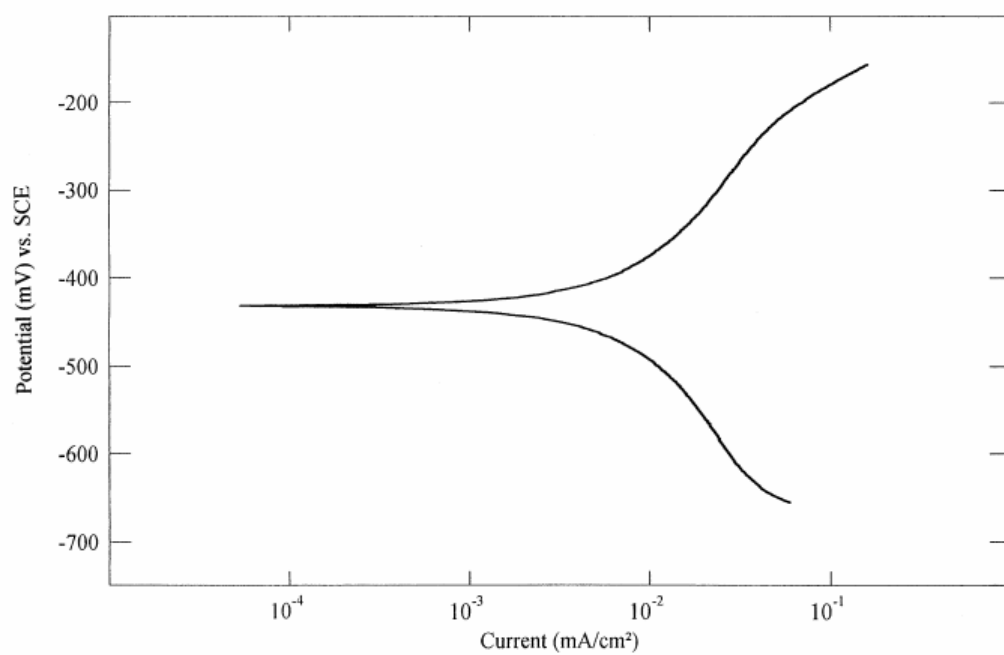


**Fig. 4.64 Polarization curve of EL Ni-P/Ni-B duplex coating heat-treated at 450°C for 1 hour in 3.5% sodium chloride solution**

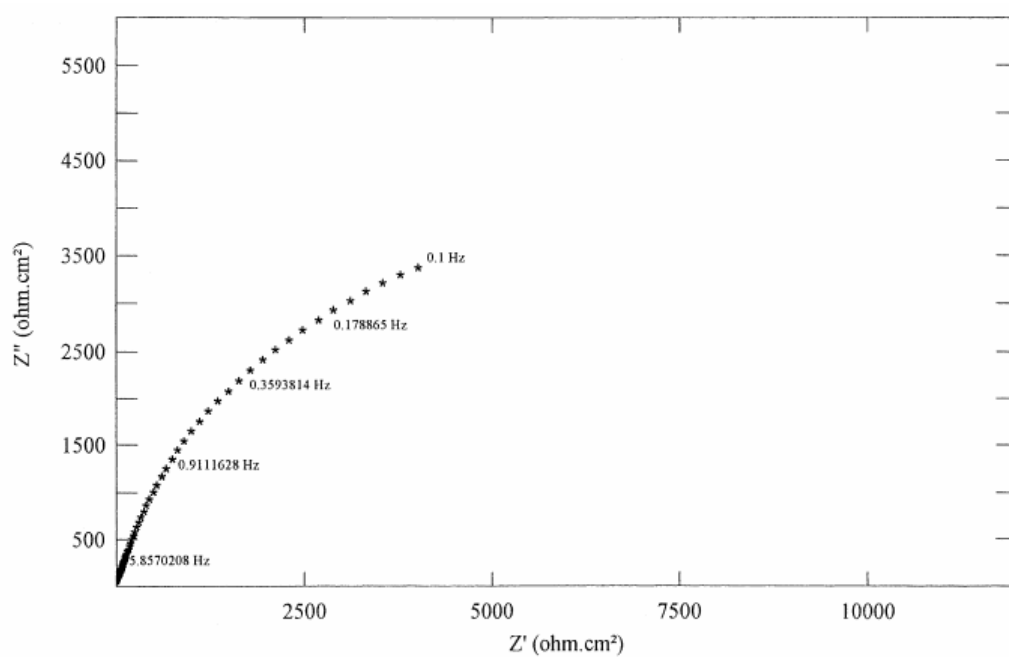


**Fig. 4.65 Nyquist plot of EL Ni-B/Ni-P duplex coating in as-plated condition in 3.5% sodium chloride solution**



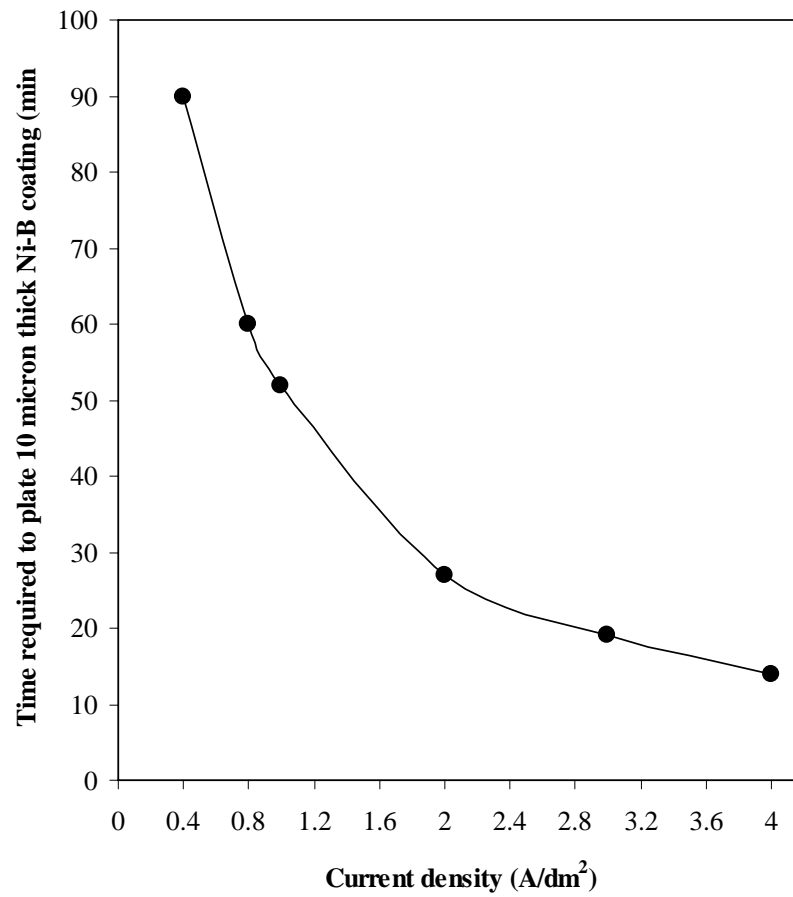


**Fig. 4.66 Time required to deposit a 10 micron thick ED Ni-B coating as a function of current density**

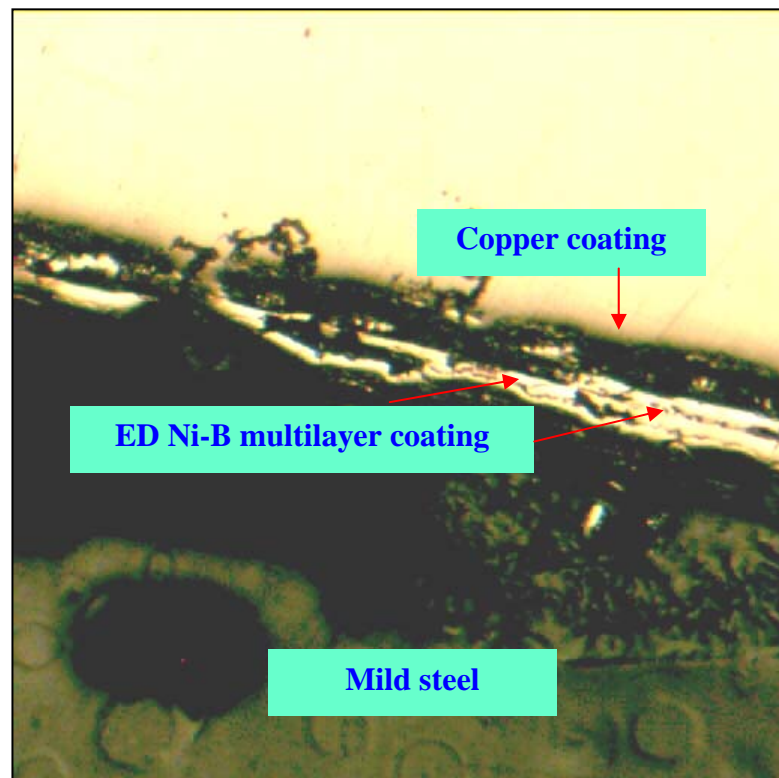


**Fig. 4.67 Optical micrograph of the ED Ni-B multilayer coating**

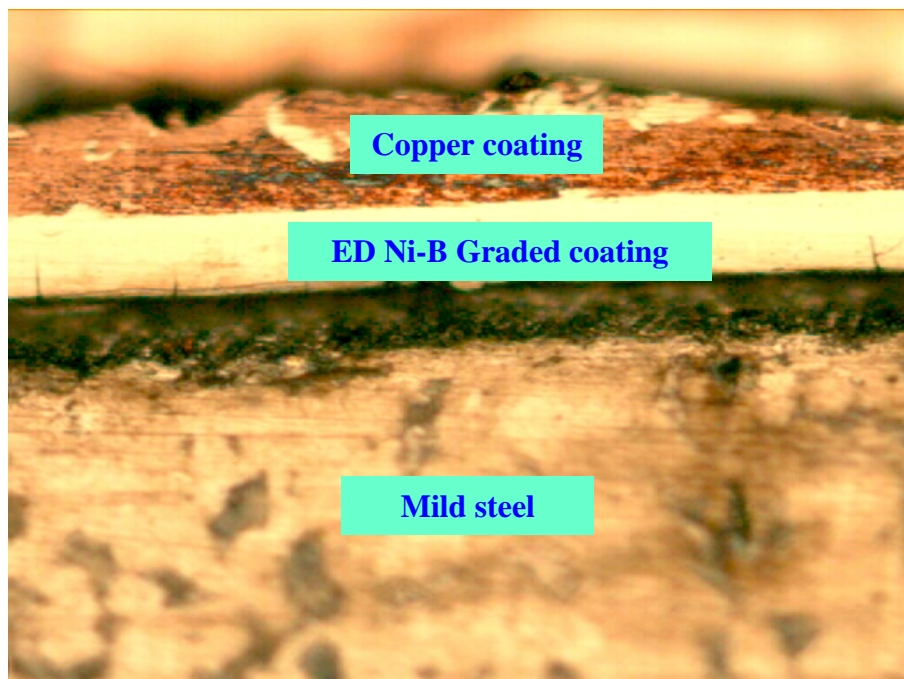


**Fig. 4.68 Optical micrograph of the cross section of the ED Ni-B graded coating**

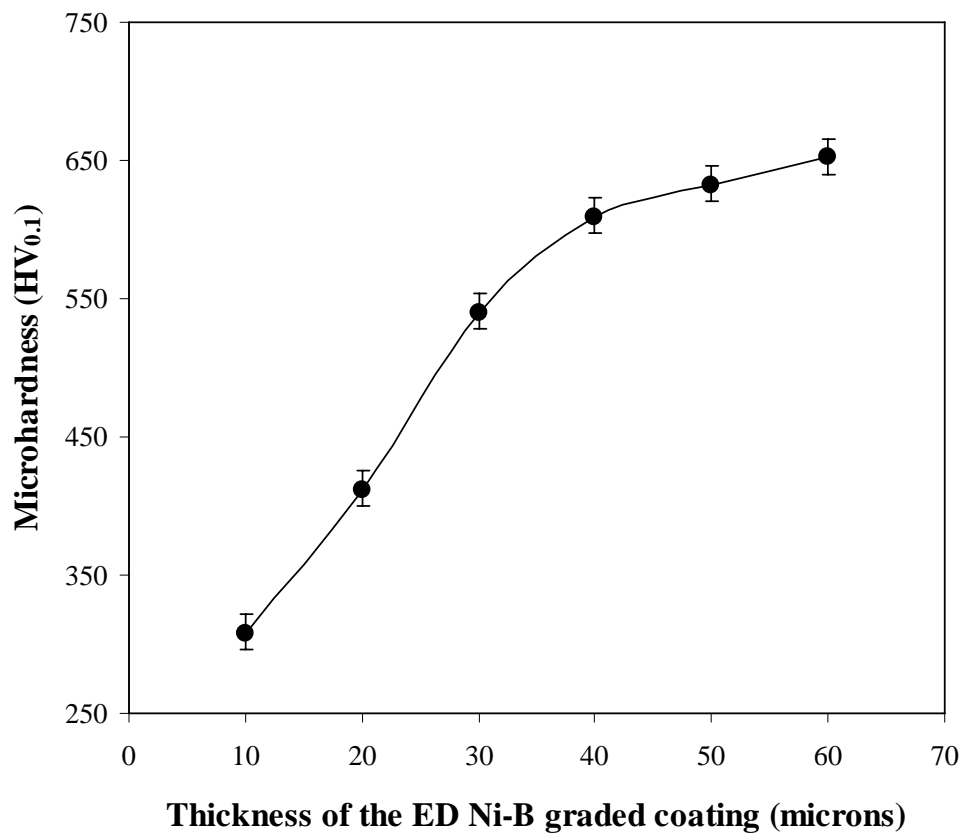


**Fig. 4.69 Variation in the microhardness of the ED Ni-B graded coating as a function of its thickness**

**Table 4.1 Chemical composition of the Ni-B coatings electrodeposited at various current densities**

<b>Current density (A/dm<sup>2</sup>)</b>	<b>Nickel content (wt.%)</b>	<b>Boron content (wt.%)</b>
1	97.0	3.0
2	98.8	1.2
3	99.2	0.8
4	99.4	0.6

**Table 4.2 Specific wear rate and average coefficient of friction of Ni-B coating electrodeposited at 1 A/dm<sup>2</sup> in their as-plated and heat-treated conditions obtained at different applied loads after a sliding distance of 1800 m**

Applied load (N)	Specific wear rate* (kg.N <sup>-1</sup> .m <sup>-1</sup> x 10 <sup>-10</sup> )		Average Coefficient of Friction (μ <sub>av</sub> )	
	As-plated	Heat treated at 400°C/1 hour	As-plated	Heat treated at 400°C/1 hour
8	6.41	4.89	0.65	0.61
10	7.30	5.97	0.67	0.64
12	8.44	7.14	0.69	0.66

\*Average of two determinations.

**Table 4.3 Corrosion resistance of ED Ni-B coatings in their as-plated and heat-treated conditions in 3.5% sodium chloride solution evaluated by potentiodynamic polarization and electrochemical impedance studies**

<b>System studied</b>	<b><math>E_{\text{corr}}</math> (mV vs. SCE)</b>	<b><math>i_{\text{corr}}</math> (<math>\mu\text{A}/\text{cm}^2</math>)</b>	<b>LPR (<math>\text{Ohm.cm}^2</math>)</b>	<b>Time taken to reach <math>0.1 \text{ mA}/\text{cm}^2</math>* (seconds)</b>	<b><math>R_{\text{ct}}</math> (<math>\text{Ohms.cm}^2</math>)</b>	<b><math>C_{\text{dl}}</math> (<math>\mu\text{F}/\text{cm}^2</math>)</b>
ED Ni-B coating as-plated	-584	12.31	1120	164	2707	129
ED Ni-B coating heat-treated at 400°C for 1 hour	-680	24.10	562	119	1710	184

\* - Calculated using current-time transient curves.

**Table 4.4 Specific wear rate and average coefficient of friction of EL Ni-B coatings in their as-plated and heat-treated conditions obtained at different applied loads after a sliding distance of 2700 m**

Applied load (N)	Specific wear rate* (kg.N <sup>-1</sup> .m <sup>-1</sup> x 10 <sup>-10</sup> )			Average Coefficient of Friction (μ <sub>av</sub> )		
	As-plated	Heat treated at 350°C/1 hour	Heat treated at 450°C/1 hour	As-plated	Heat treated at 350°C/1 hour	Heat treated at 450°C/1 hour
20	0.52	0.39	0.30	0.74	0.71	0.68
30	1.36	0.68	0.59	0.77	0.73	0.70
40	2.46	1.72	1.04	0.78	0.75	0.71

\*Average of two determinations.



**Table 4.5 Corrosion resistance of EL Ni-B coatings in their as-plated and heat-treated conditions in 3.5% sodium chloride solution evaluated by potentiodynamic polarization and electrochemical impedance studies**

<b>System studied</b>	<b>E<sub>corr</sub> (mV vs. SCE)</b>	<b>i<sub>corr</sub> (<math>\mu\text{A}/\text{cm}^2</math>)</b>	<b>LPR (<math>\text{Ohm}.\text{cm}^2</math>)</b>	<b>Time taken to reach 0.05 mA/cm<sup>2</sup>* (seconds)</b>	<b>R<sub>ct</sub> (<math>\text{Ohms}.\text{cm}^2</math>)</b>	<b>C<sub>dl</sub> (<math>\mu\text{F}/\text{cm}^2</math>)</b>
EL Ni-B coating as-plated	-506	8.41	2558	156	5163	139
EL Ni-B coating heat-treated at 450°C for 1 hour	-593	19.23	1025	121	3465	165

\* - Calculated using current-time transient curves.

**Table 4.6 Specific wear rate and average coefficient of friction of Ni-B-Si<sub>3</sub>N<sub>4</sub> composite coating electrodeposited at 1 A/dm<sup>2</sup> in their as-plated and heat-treated conditions obtained at different applied loads after a sliding distance of 1800 m**

Applied load (N)	Specific wear rate* (kg.N <sup>-1</sup> .m <sup>-1</sup> x 10 <sup>-10</sup> )		Average Coefficient of Friction (μ <sub>av</sub> )	
	As-plated	Heat treated at 400°C/1 hour	As-plated	Heat treated at 400°C/1 hour
8	5.32	3.53	0.69	0.63
10	6.21	4.43	0.73	0.67
12	7.12	5.56	0.78	0.70

\*Average of two determinations.

**Table 4.7 Corrosion resistance of ED Ni-B-Si<sub>3</sub>N<sub>4</sub> composite coatings in their as-plated and heat-treated conditions in 3.5% sodium chloride solution evaluated by potentiodynamic polarization and electrochemical impedance studies**

<b>System studied</b>	<b>E<sub>corr</sub> (mV vs. SCE)</b>	<b>i<sub>corr</sub> (μA/cm<sup>2</sup>)</b>	<b>LPR (Ohm.cm<sup>2</sup>)</b>	<b>Time taken to reach 0.1 mA/cm<sup>2</sup>* (seconds)</b>	<b>R<sub>ct</sub> (Ohms.cm<sup>2</sup>)</b>	<b>C<sub>dl</sub> (μF/cm<sup>2</sup>)</b>
ED Ni-B-Si <sub>3</sub> N <sub>4</sub> composite coating as-plated	-560	10.92	1416	255	2992	109
ED Ni-B-Si <sub>3</sub> N <sub>4</sub> composite coating heat-treated at 400°C for 1 hour	-665	21.98	597	123	1935	148

\* - Calculated using current-time transient curves.

**Table 4.8 Specific wear rate and average coefficient of friction of EL Ni-B-Si<sub>3</sub>N<sub>4</sub> composite coatings in their as-plated and heat-treated conditions obtained at different applied loads after a sliding distance of 2700 m**

Applied load (N)	Specific wear rate* (kg.N <sup>-1</sup> .m <sup>-1</sup> x 10 <sup>-10</sup> )			Average Coefficient of Friction (μ <sub>av</sub> )		
	As-plated	Heat treated at 350°C/1 hour	Heat treated at 450°C/ 1 hour	As-plated	Heat treated at 350°C/1 hour	Heat treated at 450°C/1 hour
20	0.30	0.19	0.12	0.79	0.77	0.73
30	1.08	0.45	0.37	0.81	0.79	0.75
40	2.18	1.49	0.86	0.85	0.82	0.79

\*Average of two determinations.

**Table 4.9 Corrosion resistance of EL Ni-B-Si<sub>3</sub>N<sub>4</sub> composite coatings in their as-plated and heat-treated conditions in 3.5% sodium chloride solution evaluated by potentiodynamic polarization and electrochemical impedance studies**

<b>System studied</b>	<b>E<sub>corr</sub> (mV vs. SCE)</b>	<b>i<sub>corr</sub> (μA/cm<sup>2</sup>)</b>	<b>LPR (Ohm.cm<sup>2</sup>)</b>	<b>Time taken to reach 0.02 mA/cm<sup>2</sup>* (seconds)</b>	<b>R<sub>ct</sub> (Ohms.cm<sup>2</sup>)</b>	<b>C<sub>dl</sub> (μF/cm<sup>2</sup>)</b>
EL Ni-B-Si <sub>3</sub> N <sub>4</sub> composite coating as-plated	-476	4.42	5398	168	5525	124
EL Ni-B-Si <sub>3</sub> N <sub>4</sub> composite coating heat-treated at 450°C for 1 hour	-555	9.57	1795	113	4024	154

\* - Calculated using current-time transient curves.

**Table 4.10 Bath composition and operating conditions  
of the hypophosphite-reduced electroless nickel bath**

<b>Bath Composition</b>	
Nickel sulphate hexahydrate	21 g/l
Sodium hypophosphite monohydrate	24 g/l
Lactic acid	28 g/l
Propionic acid	2.2 g/l
<b>Operating Conditions</b>	
pH	4.5
Temperature	90 ± 1°C

**Table 4.11 Bath composition and operating conditions  
of the borohydride-reduced electroless nickel bath**

<b>Bath Composition</b>	
Nickel chloride hexahydrate	30 g/l
Ethylenediamine	90 g/l
Sodium hydroxide	90 g/l
Sodium borohydride	0.8 g/l
Thallium acetate	14 mg/l
<b>Operating Conditions</b>	
pH	14.0
Temperature	95 ± 1°C

**Table 4.12 Chemical composition of the EL Ni-P and Ni-B coatings**

<b>Type of coating</b>	<b>Nickel content (wt.%)</b>	<b>Phosphorous content (wt.%)</b>	<b>Boron content (wt.%)</b>	<b>Thallium content (wt.%)</b>
Ni-P	91.0	9.0	-	-
Ni-B	93.2	-	6.5	0.3



**Table 4.13 Microhardness of EL Ni-P, Ni-B and duplex coatings in their as-plated and heat-treated conditions**

Type of coating	Thickness ( $\mu\text{m}$ )	Treatment condition	Microhardness* ( $\text{HV}_{0.1}$ )
Ni-P	20	As-plated	$497 \pm 22$
Ni-B	20	As-plated	$570 \pm 18$
Ni-B/Ni-P	10 + 10	As-plated	$596 \pm 24$
Ni-P/Ni-B	10 + 10	As-plated	$652 \pm 27$
Ni-P	20	Heat-treated 450°C/1 hour	$770 \pm 21$
Ni-B	20	Heat-treated 450°C/1 hour	$908 \pm 19$
Ni-B/Ni-P	10 + 10	Heat-treated 450°C/1 hour	$945 \pm 27$
Ni-P/Ni-B	10 + 10	Heat-treated 450°C/1 hour	$1062 \pm 22$

\*Average of five determinations.

**Table 4.14 Specific wear rate of EL Ni-P, Ni-B and duplex coatings in their as-plated and heat-treated conditions at an applied load of 40N**

Type of coating	Thickness (μm)	Treatment condition	Specific wear rate* (kg.N <sup>-1</sup> .m <sup>-1</sup> x 10 <sup>-10</sup> )
Ni-P	20	As-plated	4.60
Ni-B	20	As-plated	2.46
Ni-B/Ni-P	10 + 10	As-plated	1.93
Ni-P/Ni-B	10 + 10	As-plated	1.74
Ni-P	20	Heat-treated 450°C/1 hour	1.62
Ni-B	20	Heat-treated 450°C/1 hour	1.04
Ni-B/Ni-P	10 + 10	Heat-treated 450°C/1 hour	0.58
Ni-P/Ni-B	10 + 10	Heat-treated 450°C/1 hour	0.44

\*Average of two determinations.

**Table 4.15 Corrosion resistance of EL Ni-P, Ni-B and duplex Coatings in their as-plated and heat-treated conditions in 3.5% sodium chloride solution evaluated by potentiodynamic polarization and electrochemical impedance studies**

Type of coating	Thickness ( $\mu\text{m}$ )	$E_{\text{corr}}$ (mV vs. SCE)	$i_{\text{corr}}$ ( $\mu\text{A}/\text{cm}^2$ )	$R_{\text{ct}}$ (Ohms. $\text{cm}^2$ )	$C_{\text{dl}}$ ( $\mu\text{F}/\text{cm}^2$ )
<b>Single layer coatings</b>					
EL Ni-P as-plated	20	-354	3.62	7960	185
EL Ni-P heat-treated at 450°C for 1 hour	20	-492	6.89	6498	236
EL Ni-B as-plated	20	-506	8.41	5163	139
EL Ni-B heat-treated at 450°C for 1 hour	20	-593	19.43	3465	165
<b>Duplex coatings</b>					
EL Ni-P/Ni-B as-plated	10 + 10	-386	3.86	7638	189
EL Ni-P/Ni-B heat-treated at 450°C for 1 hour	10 + 10	-432	4.93	5339	244
EL Ni-B/Ni-P as-plated	10 + 10	-311	2.46	10130	112
EL Ni-B/Ni-P heat-treated at 450°C for 1 hour	10 + 10	-356	3.24	7024	123

**Table 4.16 Comparison of the important characteristics  
of ED Ni-B and EL Ni-B coatings**

<b>Characteristic</b>	<b>ED Ni-B coating</b>	<b>EL Ni-B coating</b>
Appearance	Semi-bright	Matt gray
Type of bath	Acidic Watts' nickel bath	Alkaline borohydride-reduced bath
Source of boron	DMAB - 3 g/l	NaBH <sub>4</sub> - 0.8 g/l
Operating problems	To be operated at less than 60°C and at pH 3.5 to prevent simultaneous electroless deposition	Deposition effective only at 95°C and at pH 14; vigorous alkaline vapours; Thallium is toxic
Current density	1 A/dm <sup>2</sup>	-
Pretreatment of the substrate	Anodic etching in the plating bath at 0.2 A/dm <sup>2</sup>	Nickel strike using Watts' nickel bath
Plating rate	12 µm/h at 1 A/dm <sup>2</sup>	20 µm/h at 0.8 g/l NaBH <sub>4</sub>
Post-finishing	Necessary	Mostly not required
Composition	Ni: 97 wt.%; B: 3 wt.%	Ni: 93.2 wt.%; B: 6.5 wt.%; Ti: 0.3 wt.%
Structure	Crystalline	Amorphous
Grain size	10-13 nm (as-plated) 17-20 nm (heat-treated)	2-3 nm (as-plated) 8-10 nm (heat-treated)
Morphology	Uniform	Nodular
Bath stability	Relatively more stable	Less stable; Presence of stabilizers is essential
Heat-treatment	Ni and Ni <sub>3</sub> B at 400°C	Ni and Ni <sub>3</sub> B at 350°C and Ni, Ni <sub>3</sub> B and Ni <sub>2</sub> B- 450°C
Microhardness	609 HV <sub>0.1</sub> (as-plated) 817 HV <sub>0.1</sub> (heat-treated)	570 HV <sub>0.1</sub> (as-plated) 908 HV <sub>0.1</sub> (heat-treated)
Wear resistance	Better at 8-12 N Specific wear rate at 8 N (kg/N/m x 10 <sup>-10</sup> ) 6.41 (as-plated) 4.89 (heat-treated) Coefficient of friction at 8 N 0.65 (as-plated) 0.61 (heat-treated)	Better even at 20-40 N Specific wear rate at 20 N (kg/N/m x 10 <sup>-10</sup> ) 0.52 (as-plated) 0.30 (heat-treated) Coefficient of friction at 20N 0.74 (as-plated) 0.68 (heat-treated)
Corrosion resistance	R <sub>ct</sub> : 2707 ohms.cm <sup>2</sup> C <sub>dl</sub> : 129 µF/cm <sup>2</sup> E <sub>corr</sub> : -584 mV vs.SCE I <sub>corr</sub> : 12.31 µA/cm <sup>2</sup>	R <sub>ct</sub> : 5163 ohms.cm <sup>2</sup> C <sub>dl</sub> : 139 µF/cm <sup>2</sup> E <sub>corr</sub> : - 506 mV vs.SCE I <sub>corr</sub> : 8.41 µA/cm <sup>2</sup>

**Table 4.17 Comparison of the important characteristics of ED Ni-B-Si<sub>3</sub>N<sub>4</sub> and EL Ni-B-Si<sub>3</sub>N<sub>4</sub> composite coatings**

<b>Characteristic</b>	<b>ED Ni-B-Si<sub>3</sub>N<sub>4</sub> composite coating</b>	<b>EL Ni-B-Si<sub>3</sub>N<sub>4</sub> composite coating</b>
Type of bath	Acidic Watts' nickel bath	Alkaline borohydride-reduced bath
Operating problems	Filtration of the bath is essential to remove the impurities	Heavy hydrogen evolution limits the level of incorporation
Bath stability	Relatively more stable	Less stable; Presence of stabilizers is essential
Current density	1 A/dm <sup>2</sup>	-
Bath loading	High: 25-100g/l	Relatively low: 2-25 g/l
Incorporation level	8 wt.% at 50 g/l	2 wt.% at 10 g/l
Particle distribution in the matrix	Uniform	Uniform
Structure	Change in crystal orientation	No significant change in structure
Microhardness	640 HV <sub>0.1</sub> (as-plated) 955 HV <sub>0.1</sub> (heat-treated) Higher than its plain counterpart	670 HV <sub>0.1</sub> (as-plated) 1012 HV <sub>0.1</sub> (heat-treated) Higher than its plain counterpart
Wear resistance	Better at 8-12 N Specific wear rate at 8 N (kg/N/m x 10 <sup>-10</sup> ) 5.32 (as-plated) 3.53 (heat-treated) Better than its plain counterpart Coefficient of friction at 8 N 0.69 (as-plated) 0.63 (heat-treated)	Better even at 20-40 N Specific wear rate at 20 N (kg/N/m x 10 <sup>-10</sup> ) 0.30 (as-plated) 0.12 (heat-treated) Better than its plain counterpart Coefficient of friction at 20N 0.79 (as-plated) 0.73 (heat-treated)
Corrosion resistance	R <sub>ct</sub> : 2992 ohms.cm <sup>2</sup> C <sub>dl</sub> : 109 μF/cm <sup>2</sup> E <sub>corr</sub> : -560 mV vs. SCE I <sub>corr</sub> : 10.92 μA/cm <sup>2</sup> Better than its plain counterpart	R <sub>ct</sub> : 5525 ohms.cm <sup>2</sup> C <sub>dl</sub> : 124 μF/cm <sup>2</sup> E <sub>corr</sub> : - 476 mV vs. SCE I <sub>corr</sub> : 4.42 μA/cm <sup>2</sup> Better than its plain counterpart

## CHAPTER V

### SUMMARY AND CONCLUSIONS

The formation of Ni-B and Ni-B-Si<sub>3</sub>N<sub>4</sub> composite coatings by electro- and electroless deposition processes and evaluation of their characteristic properties are reported in the present investigation. The Ni-B and Ni-B-Si<sub>3</sub>N<sub>4</sub> composite coatings are deposited on mild steel substrate. The ED Ni-B coatings are prepared using a dimethylamine borane (DMAB) modified Watt's nickel plating bath whereas the EL Ni-B coatings are prepared using an alkaline borohydride-reduced electroless plating bath. The ED and EL Ni-B-Si<sub>3</sub>N<sub>4</sub> composite coatings are prepared using the corresponding plating baths with the addition of Si<sub>3</sub>N<sub>4</sub> particles in them. The Ni-B and Ni-B-Si<sub>3</sub>N<sub>4</sub> composite coatings prepared by electro- and electroless deposition processes are evaluated for their plating rate, surface morphology, structural characteristics, thermal characteristics, microhardness, wear resistance and corrosion resistance. Besides, some studies on EL Ni-P/Ni-B duplex coatings, ED Ni-B multilayer and ED Ni-B graded coatings are also carried out. The EL Ni-P/Ni-B duplex coatings having both Ni-P and Ni-B coatings as inner and outer layers are prepared by sequential treatment in both the hypophosphite- and borohydride-reduced electroless nickel plating baths. The characteristic properties of the duplex coatings are evaluated and compared with that of single layer coatings of similar thickness. The ED Ni-B multilayer coatings are prepared by alternatively varying the current density between 0.4 and 4 A/dm<sup>2</sup>. The ED Ni-B graded coatings are prepared by continuously varying the current density between 0.4 and 4 A/dm<sup>2</sup>. The study leads to the following conclusions:

- ❖ The deposition rate of ED Ni-B alloy coatings increases with increase in current density whereas the boron content decreases with increase in applied current density. The plating rate of ED Ni-B coating at  $1 \text{ A/dm}^2$  is  $12 \text{ }\mu\text{m/hour}$ . The resultant ED Ni-B coating contains 97 wt.% nickel and 3 wt.% boron.
- ❖ The surface morphology of the ED Ni-B coatings reveals the formation of well-crystallized, uniform and fine-grained deposits, with some cracks which emerged due to the stress in the coatings.
- ❖ XRD pattern of ED Ni-B coatings indicates that the nucleation of the nickel phase is not completely prevented since the required boron segregation is relatively low. Alloying of boron with nickel causes a change in the preferred orientation of the Ni-B coating; Ni (111) being the most intense reflection. Heat-treatment increases the crystallinity and enables the formation of  $\text{Ni}_3\text{B}$  phase; the Ni (111) texture is retained even after heat-treatment. SAD pattern further confirms the structural characteristics observed by XRD.
- ❖ The grain size of ED Ni-B coatings is 10-13 nm in as-plated condition and it increases to 17-20 nm after heat-treatment at  $400^\circ\text{C}$  for 1 hour.
- ❖ The temperature range at which the phase transformation of ED Ni-B coatings occurs is quite large and indicates its nanocrystalline nature.
- ❖ The microhardness of as-plated ED Ni-B coating is  $609 \text{ HV}_{0.1}$ , which increases to  $817 \text{ HV}_{0.1}$  when the coating is heat-treated at  $400^\circ\text{C}$  for 1 hour.

- ❖ The wear resistance is higher for heat-treated ED Ni-B coatings compared to those obtained in as-plated condition. The mechanism of wear in ED Ni-B coatings is intensive plastic deformation of the coating due to the ploughing action of the hard counter disk.
- ❖ The nanocrystalline nature and presence of cracks are primarily responsible for the corrosion behaviour of the ED Ni-B coating in their as-plated condition. The corrosion resistance decreases further up on heat-treatment due to the crystallization of the coating, increase in the grain boundary region and formation of nickel boride phases. EIS studies indicate that the electrolyte has penetrated via cracks in the ED Ni-B coatings.
- ❖ The rate of deposition of EL Ni-B coating increases with increase in plating time. The plating rate of EL Ni-B coatings is 18-20  $\mu\text{m}/\text{hour}$ . The EL Ni-B coating contains 93.2 wt.% nickel, 6.5 wt.% boron and 0.3 wt.% thallium.
- ❖ The morphology of EL Ni-B coatings resembles a typical cauliflower type feature, characteristic of electroless plated nickel coatings.
- ❖ The EL Ni-B coating is amorphous in the as-plated condition whereas it becomes crystalline upon heat-treatment, with the formation of Ni,  $\text{Ni}_3\text{B}$  phases at  $350^\circ\text{C}$  and Ni,  $\text{Ni}_3\text{B}$  and  $\text{Ni}_2\text{B}$  phases at  $450^\circ\text{C}$ . Heat-treatment at  $600^\circ\text{C}$  for 1 hour causes conversion of the  $\text{Ni}_2\text{B}$  phase in to the more stable  $\text{Ni}_3\text{B}$  phase.
- ❖ The grain size of EL Ni-B coatings is 2-3 nm in as-plated condition and it increases to 8-10 nm after heat-treatment at  $450^\circ\text{C}$  for 1 hour.



- ❖ The TEM microstructure and SAD pattern confirms the amorphous nature of the EL Ni-B coating in its as-plated condition.
- ❖ DSC trace indicates two distinct exothermic peaks, at 307.5 and 418°C, suggesting precipitation of metallic nickel and formation of Ni<sub>3</sub>B phase at 307.5°C and the formation of Ni<sub>2</sub>B phase at 418°C, which is further confirmed by XRD measurements.
- ❖ The microhardness of EL Ni-B coating is 570 HV<sub>0.1</sub> for as-plated coatings and 908 HV<sub>0.1</sub> for coatings heat-treated at 450°C for 1 hour.
- ❖ The wear resistance of heat-treated EL Ni-B coating is relatively higher than that of the as-plated coatings. Adhesive wear appears to be the most likely mechanism during the wear process of EL Ni-B coatings.
- ❖ Surface heterogeneity and columnar structure are primarily responsible for the lower corrosion resistance of EL Ni-B coatings in their as-plated condition. The corrosion resistance decreases further up on heat-treatment due to the crystallization of the coating, increase in the grain boundary region and formation of nickel boride phases. EIS studies indicate that the electrolyte has penetrated through the pores in the EL Ni-B coating.
- ❖ The level of incorporation of Si<sub>3</sub>N<sub>4</sub> particles in ED Ni-B matrix increases with increase in its concentration in the bath up to 50 g/L, beyond which it gets saturated. The level of incorporation of Si<sub>3</sub>N<sub>4</sub> particles in ED Ni-B matrix increases with increase in current density and reaches a maximum at 1 A/dm<sup>2</sup>, beyond which it decreases. The maximum level of incorporation

of  $\text{Si}_3\text{N}_4$  particles in ED Ni-B matrix is 8 wt.% at a bath loading of 50 g/l and at a current density of  $1 \text{ A/dm}^2$ . The above composite coating contains 89.6 wt.% Ni; 2.4 wt.% B and 8 wt.%  $\text{Si}_3\text{N}_4$  particles.

- ❖ The incorporation of  $\text{Si}_3\text{N}_4$  particles in the ED Ni-B matrix increases the surface roughness of the coatings. The average surface roughness ( $R_a$ ) is of the order of  $1.17 \text{ }\mu\text{m}$ . The surface morphology shows the uniform distribution of  $\text{Si}_3\text{N}_4$  particles in the ED Ni-B matrix.
- ❖ Incorporation of  $\text{Si}_3\text{N}_4$  particles in the ED Ni-B matrix causes a change in crystal orientation. The grain size of ED Ni-B- $\text{Si}_3\text{N}_4$  composite coating is 6-8 nm in as-plated condition and it increases to 12-14 nm after heat-treatment at  $400^\circ\text{C}$  for 1 hour.
- ❖ The microhardness of as-plated ED Ni-B- $\text{Si}_3\text{N}_4$  composite coating is  $640 \text{ HV}_{0.1}$  and it increases to  $955 \text{ HV}_{0.1}$  when heat-treated at  $400^\circ\text{C}$  for 1 hour. The microhardness of ED Ni-B- $\text{Si}_3\text{N}_4$  composite coatings is relatively higher than that of ED Ni-B coatings, due to the combination strengthening of solid solution hardening of the matrix and dispersion hardening induced by particle incorporation.
- ❖ The wear resistance is higher for heat-treated ED Ni-B- $\text{Si}_3\text{N}_4$  composite coatings compared to those obtained in as-plated condition. The wear resistance of ED Ni-B- $\text{Si}_3\text{N}_4$  composite coatings is relatively higher than that of ED Ni-B coatings, both in as-plated and heat-treated conditions due to the double strengthening effect of the hard  $\text{Si}_3\text{N}_4$  particles and precipitation strengthening of the Ni-B alloy matrix. The wear mechanism

of ED Ni-B-Si<sub>3</sub>N<sub>4</sub> composite coatings is also similar to that of ED Ni-B coatings - intensive plastic deformation of the coating due to the ploughing action of the hard counter disk.

- ❖ The nanocrystalline nature is primarily responsible for the corrosion behaviour of ED Ni-B-Si<sub>3</sub>N<sub>4</sub> composite coatings in their as-plated condition. The corrosion resistance decreases further up on heat-treatment due to the crystallization of the coating, increase in the grain boundary region and formation of nickel boride phases. EIS studies indicate that the electrolyte has penetrated via micropores in the ED Ni-B-Si<sub>3</sub>N<sub>4</sub> composite coatings. The corrosion resistance of ED Ni-B-Si<sub>3</sub>N<sub>4</sub> composite coating is relatively higher than ED Ni-B coatings, both in as-plated and heat-treated conditions, due to the decrease in the effective metallic area prone to corrosion.
- ❖ The level of incorporation of Si<sub>3</sub>N<sub>4</sub> particles in the EL Ni-B matrix increases with increase in its concentration in the bath up to 10 g/L, beyond which it gets saturated. The maximum level of incorporation is 2 wt.% at a bath loading of 10 g/l of Si<sub>3</sub>N<sub>4</sub> particles. The above composite coating contains 91.7 wt.% Ni; 6.0 wt.% B; 0.3 wt.% Ti; and 2 wt.% Si<sub>3</sub>N<sub>4</sub> particles.
- ❖ The incorporation of Si<sub>3</sub>N<sub>4</sub> particles in the EL Ni-B matrix increases the surface roughness of the coatings. The average surface roughness ( $R_a$ ) is of the order of 0.92  $\mu\text{m}$ . The surface morphology shows the uniform distribution of Si<sub>3</sub>N<sub>4</sub> particles in the EL Ni-B matrix.

- ❖ Incorporation of  $\text{Si}_3\text{N}_4$  particles in the EL Ni-B matrix has a very little influence on the structure of EL Ni-B matrix. The grain size of EL Ni-B- $\text{Si}_3\text{N}_4$  composite coatings is of the same order as that of EL Ni-B coatings; 2-3 nm in as-plated condition and 8-10 nm after heat-treatment at 450°C for 1 hour.
- ❖ The microhardness of as-plated EL Ni-B- $\text{Si}_3\text{N}_4$  composite coatings is 670  $\text{HV}_{0.1}$  and it increases to 946  $\text{HV}_{0.1}$  and 1012  $\text{HV}_{0.1}$ , when the coating is heat-treated at 350 and 450°C for 1 hour, respectively. The microhardness of EL Ni-B- $\text{Si}_3\text{N}_4$  composite coatings is relatively higher than that of EL Ni-B coatings, due to the combination strengthening of solid solution hardening of the matrix and dispersion hardening induced by particle incorporation.
- ❖ The wear resistance is higher for heat-treated EL Ni-B- $\text{Si}_3\text{N}_4$  composite coatings compared to those obtained in as-plated condition. The wear resistance of EL Ni-B- $\text{Si}_3\text{N}_4$  composite coatings is relatively higher than that of EL Ni-B coatings, both in as-plated and heat-treated conditions, due to the double strengthening effect of the hard  $\text{Si}_3\text{N}_4$  particles and precipitation strengthening of the Ni-B alloy matrix. The wear mechanism of EL Ni-B and EL Ni-B- $\text{Si}_3\text{N}_4$  composite coatings is similar - Adhesive wear appears to be the most likely mechanism during the wear process of EL Ni-B- $\text{Si}_3\text{N}_4$  composite coatings.
- ❖ Surface heterogeneity and columnar structure are primarily responsible for the observed corrosion behaviour of the EL Ni-B- $\text{Si}_3\text{N}_4$  composite coating in their as-plated condition. The corrosion resistance decreases further up

on heat-treatment due to the crystallization of the coating, increase in the grain boundary region and formation of nickel boride phases. EIS studies indicate that the electrolyte has penetrated through the pores in the EL Ni-B-Si<sub>3</sub>N<sub>4</sub> composite coatings. The corrosion resistance of EL Ni-B-Si<sub>3</sub>N<sub>4</sub> composite coating is relatively higher than EL Ni-B coatings, both in as-plated and heat-treated conditions, due to the decrease in the effective metallic area prone to corrosion

- ❖ EL Ni-P/Ni-B and EL Ni-B/Ni-P duplex coatings are amorphous in as-plated condition. Heat-treatment at 450°C for 1 hour leads to the formation of both Ni<sub>3</sub>P and Ni<sub>3</sub>B phases.
- ❖ The microhardness of EL Ni-P/Ni-B and EL Ni-B/Ni-P duplex coatings is higher than that of single layer EL Ni-P and EL Ni-B coatings of similar thickness, both in as-plated and heat-treated (450°C for 1 hour) conditions.
- ❖ Between the two types of duplex coatings, those having EL Ni-B coating as the outer layer exhibits a higher hardness and better wear resistance whereas those having EL Ni-P coating as the outer layer offers better corrosion resistance.
- ❖ The possibility of preparing ED Ni-B multilayer and graded coatings is explored. The attempt made in the present investigation provides new avenues to manipulate the ED Ni-B coatings with desirable characteristics.
- ❖ Comparison of Ni-B and Ni-B-Si<sub>3</sub>N<sub>4</sub> composite coatings obtained by electro- and electroless deposition process reveals that the rate of deposition

is higher for coatings obtained by electroless deposition process. The level of incorporation of  $\text{Si}_3\text{N}_4$  particles in the Ni-B matrix is relatively higher when the coatings are prepared by electrodeposition. The hardness of Ni-B, or Ni-B- $\text{Si}_3\text{N}_4$  composite coatings, obtained by both electro- and electroless deposition processes, is comparable. Ni-B and Ni-B- $\text{Si}_3\text{N}_4$  composite coatings obtained by electroless deposition process offer a better resistance to wear and corrosion than the coatings obtained by electrodeposition.

## **FUTUROLOGY**

- ❖ Preparation of Ni-B coatings by pulsed current electrodeposition
- ❖ Identification of an alternative stabilizer in place of thallium salts for borohydride-reduced electroless plating baths
- ❖ Structural characterization and evaluation of tribological properties and corrosion resistance of ED Ni-B multilayer and graded coatings.

## REFERENCES

1. **Abdel Hamid, Z. and Ghayad, I.M.** (2002) Characteristics of electrodeposition Ni-polyethylene composite coatings. *Materials Letters*, 53, 238-243.
2. **Abdel Hamid, Z. and Abou Elkhair, M.T.** (2002) Development of electroless nickel-phosphorus composite deposits for wear resistance of 6061 aluminium alloy. *Materials Letters*, 57, 720-726.
3. **Abdel Hamid, Z. Ghayad, I.M. and Ibrahim, K.M.** (2005) Electrodeposition and characterization of chromium–tungsten carbide composite coatings from a trivalent chromium bath. *Surface and Interface Analysis*, 37, 573–579.
4. **Agarwala, R.C. and Agarwala, V.** (2003) Electroless alloy/composite coatings: A review. *Sadhana*, 28.3-4, 474-493.
5. **Ahmed, I. Greco, V.P. and Barranco, J.M.** (1967) Reinforcement of nickel with some high-strength filaments. *Journal of Composite Materials*, 1, 18-29.
6. **Allen, R.M. and Vander Sande, J.B.** (1982) The structure of electroless Ni-P films as a function of composition. *Scripta Metallurgica*, 16, 1161-1164.
7. **Alirezai, S., Monirvaghefi, S., Salehi, M. and Saatchi, A.** (2004) Effect of alumina content on surface morphology and hardness of Ni-P-Al<sub>2</sub>O<sub>3</sub>( $\alpha$ ) electroless composite coatings. *Surface and Coatings Technology*, 184, 170-175.
8. **Amblard, J., Froment, M. and Spyrellis, N.** (1977) Origine des textures dans les depots electrolytiques de nickel. *Surface Technology*, 5.3, 205-234.
9. **Amblard, J., Epelboin, I., Froment, M. and Maurin, G.** (1979) Inhibition and nickel electrocrystallization. *Journal of Applied Electrochemistry*, 9.2, 233-242.
10. **Apachitei, I., Duszczyk, J., Katgerman, L. and Overkamp, P.J.B.** (1998a) Electroless Ni-P composite coatings: The effect of heat treatment on the microhardness of substrate and coating. *Scripta Materialia*, 38.9, 1347-1353.

11. **Apachitei, I., Duszczek, J., Katgerman, L. and Overkamp, P.J.B.** (1998b) Particles co-deposition by electroless nickel. *Scripta Materialia*, 38.9, 1383-1389.
12. **Apachitei, I., Tichelaar, F.D., Duszczek, J. and Katgerman, L.** (2001) Solid-state reactions in low-phosphorus autocatalytic NiP–SiC coatings. *Surface and Coatings Technology*, 148(2-3), 284-295.
13. **Apachitei, I., Tichelaar, F.D., Duszczek, J. and Katgerman, L.** (2002) The effect of heat-treatment on the structure and abrasive wear resistance of autocatalytic Ni-P and Ni-P-SiC coatings. *Surface and Coatings Technology*, 149.23, 263-278.
14. **Argyriou, A. and Spyrellis, N.** (1993) Nickel electrodeposition from all-sulphate and chloride baths-texture and microhardness. *Transactions of the Institute of Metal Finishing*, 71, 82.
15. **Aruna, S.T., Bindu, C.N., Ezhil Selvi, V., William Grips, V.K. and Rajam, K.S.** (2006) Synthesis and properties of electrodeposited Ni/ceria nanocomposite coatings. *Surface and Coatings Technology*, 200, 6871-6880.
16. **ASM Handbook**, “Alloy Phase Diagrams”, Volume 3, American Society for Materials, Material Park, Ohio, 1991.
17. **ASTM G 40-88**, Standard terminology relating to wear and erosion. *Annual Book of ASTM Standards*, American Society for Testing and Materials, Philadelphia, 1993.
18. **Assoul, M., Pena-Munoz, E. and Roizard, X.** (1998) A tribological study of electrolytic nickel-PTFE composite coatings. *Journal of Synthetic Lubrication*, 15.2, 107-116.
19. **Atkinson, A. and Smart, D.W.** (1988) Transport of nickel and oxygen during the oxidation of nickel and dilute nickel/chromium alloy. *Journal of the Electrochemical Society*, 135.11, 2886-2893.
20. **Ayyappa Raju, J., Ramesh Bapu, G.N.K., Devaraj, G. and Guruviah, S.** (1989) Electrodeposition of Zinc-Titania Composites. *Bulletin of Electrochemistry*, 5.5, 340-342.
21. **Balaraju, J.N. and Seshadri, S.K.** (1998) Synthesis and corrosion behavior of electroless Ni-P-Si<sub>3</sub>N<sub>4</sub> composite coatings, *Journal of Material Science Letters*, 17, 1297-1299.



22. **Balaraju, J.N. and Seshadri, S.K.** (1999) Preparation and characterization of electroless Ni-P and Ni-P-Si<sub>3</sub>N<sub>4</sub> composite coatings. *Transactions of Institute of Metal Finishing*, 77.2, 84.
23. **Balaraju, J.N.** (2000), Electroless nickel composite coatings: Preparation and surface characterization, Ph.D. Thesis, Indian Institute of Technology- Madras, Chennai.
24. **Balaraju, J.N., Sankara Narayanan, T.S.N. and Seshadri, S.K.** (2001) Evaluation of the corrosion resistance of electroless Ni-P and Ni-P composite coatings by electrochemical impedance spectroscopy, *Journal of Solid State Electrochemistry*, 5.5, 334-338.
25. **Balaraju, J.N., Sankara Narayanan, T.S.N. and Seshadri, S.K.** (2003) Electroless Ni-P composite coatings. *Journal of Applied Electrochemistry*, 33, 807-816.
26. **Balaraju, J.N., Kalavati and Rajam, K.S.** (2006a) Influence of particle size on the microstructure, hardness and corrosion resistance of electroless Ni-P-Al<sub>2</sub>O<sub>3</sub> composite coatings, *Surface and Coatings Technology*, 200, 3993-3941.
27. **Balaraju, J.N., Sankara Narayanan, T.S.N. and Seshadri, S.K.** (2006b) Structure and phase transformation behaviour of electroless Ni-P composite coatings, *Materials Research Bulletin*, 60, 1990-1995.
28. **Balathandan, S. and Seshadri, S.K.** (1992a) Electroforming of Nickel-cerium dioxide composites. *Metal Finishing*, 90, 51-53.
29. **Balathandan, S. and Seshadri, S.K.** (1992b) Nickel-Ceria-Zirconia Electro-composite Coatings. *Bulletin of Electrochemistry*, 8.3, 119-121.
30. **Banovic, S.W., Petronis, C.M., Barmak, K. and Marder, A.R.** in: *Elevated Temperature Coatings*, Dahotre, N.B. and Hampikian, J.M. (Eds.), TMS, Warrendale, 1996, p. 89.
31. **Banovic, S.W., Barmak, K. and Marder, A.R.** (1999) Characterization of single and discretely stepped electro-composite coatings of nickel-alumina. *Journal of Materials Science*, 34, 3203-3211.
32. **Baskaran, I., Sankara Narayanan, T.S.N. and Stephen, A.** (2006a) Pulsed electrodeposition of nanocrystalline Cu-Ni alloy films and evaluation of their characteristic properties. *Materials Letters*, 60.16, 1990-1995.

33. **Baskaran, I., Sakthikumar, R., Sankara Narayanan, T.S.N. and Stephen, A.** (2006b) Formation of electroless Ni-B coatings from low temperature bath and evaluation of their characteristic properties. *Surface and Coatings Technology*, 200.24, 6888-6894.
34. **Baudrand, D.W.**, "Electroless Plating", in: ASM Handbook, Surface Engineering, Volume 5, American Society of Metals, Philadelphia, 1994, p. 290.
35. **Bazzard, R. and Boden, P.J.** (1971) Ni-Cr alloys by codeposition. Part I - Codeposition of chromium particles in a nickel matrix. *Transactions of Institute of Metal Finishing*, 50, 63.
36. **Bedingfield, P.B., Lewis, D.B., Datta, P.K., Gray, J.S. and Wells, P.B.** (1991) Studies of electroless nickel-boron alloy coatings, *Transactions of Institute of Metal Finishing*, 70.1, 19-23.
37. **Bell, T. (1991)** Surface Engineering: Past, present and future. *Surface Engineering*, 6.1, 31-40.
38. **Benea, L., Mitoseriu, O., Galland, J., Wenger, F. and Ponthiaux, P.** (2000) Corrosion study of copper composite coating by impedance spectroscopy method. *Materials and Corrosion*, 51, 491-495.
39. **Benea, L., Bonora, P.L., Borello, A. and Martelli, S.** (2002a) Effect of SiC size dimensions on the corrosion wear resistance of the electro-deposited composite coating. *Materials and Corrosion*, 53, 23-29.
40. **Berkh, O., Bodnevas, A. and Zahavi, J.** (1995) Electrodeposited Ni-P-SiC Composite Coatings. *Plating and Surface Finishing*, 82.11, 62-66.
41. **Berkh, O., Eskin, S. and Zahavi, J.** (1996) Properties of Electro-deposited Ni-P-SiC Composite Coatings. *Metal Finishing*, 94, 35-40.
42. **Bestgen, H.**, *Rapidly Quenched Metals*, Elsevier, Amsterdam, 1985.
43. **Bielinski, J., Krol, J. and Bielinska, A.** (1990) Inorganic Additives in the Solutions for Electroless Nickel-Boron Alloy Deposition. *Bulletin of Electrochemistry*, 6.10, 828-831.
44. **Bonino, J.P., Loubiere, S. and Rousset, A.** (1998) Reactivity and Codeposition of  $\text{Co}_3\text{O}_4$  powders with nickel in a watts bath. *Journal of Applied Electrochemistry*, 28, 1227-1233.

45. **Bowden, F.P. and Tabor, D.,** *The Friction and Lubrication of solids.* Part-II. Clarendon Press, Oxford, 1964.
46. **Bozzini, B., Martini, C., Cavallotti, P.L. and Lanzoni, E.** (1999) Relationships among crystallographic structure, mechanical properties and tribological behavior of electroless Ni-P(9%)/B<sub>4</sub>C films. *Wear*, 225-229, 806-813.
47. **Bozzini, B.** (2000) Mass-transport effects on texture formation of nickel electrodeposits. *Materials Chemistry and Physics*, 66 (2-3), 278-285.
48. **Bozzini, B., Boniardi, M., Fanigliulo, A. and Bogani, F.** (2001a) Tribological properties of electroless Ni-P/diamond composite films. *Materials Research Bulletin*, 36, 1889-1902.
49. **Bozzini, B., Cavallotti, P.L. and Parisi, G.** (2001b) Corrosion and erosion-corrosion of electrodeposited Ni-P/B<sub>4</sub> C composites. *British Corrosion Journal*, 36.1, 49-55.
50. **Brandes, E.A. and Goldthorpe, D.** (1967) Electrodeposition of cermets. *Metallurgia*, 76, 195-198.
51. **Brenner, A.,** *Electrodeposition of Alloys: Principles and Practices, Volumes 1 and 2*, Academic Press, New York, 1963.
52. **Broszeit, E.** (1982) Mechanical, thermal and tribological properties of electro- and chemodeposited composite coatings. *Thin Solid Films*, 95, 133-142.
53. **Brown, L.** (1985) Electroless nickel composites – The state of the art. *Transactions of the Institute of Metal Finishing*, 63, 139-141.
54. **Cârâc, G., Benea, L., Iticescu, C., Lampke, T., Steinhäuser, S. and Wielage, B.** (2004) Codeposition of cerium oxide with nickel and cobalt: Correlation between microstructure and microhardness. *Surface Engineering*, 20.5, 353-359.
55. **Carbajal, J.L. and White, R.E.** (1988) Electrochemical production and corrosion testing of amorphous Ni-P. *Journal of the Electrochemical Society*, 135.12, 2952-2957.
56. **Celis, J.P. and Roos, J.R.** (1977) Kinetics of the deposition of alumina particles from copper sulphate plating bath. *Journal of Electrochemical Society*, 124, 1508-1511.

57. **Celis, J.P., Roos, J.R. and Buelens, C.** (1987) A mathematical model for the electrolytic codeposition of particles with a metallic matrix. *Journal of Electrochemical Society*, 134.6, 1402-1408.
58. **Chang, L.M., An, M.Z. and Shi, S.Y.** (2006) Microstructure and characterization of Ni-Co/Al<sub>2</sub>O<sub>3</sub> composite coatings by pulse reversal electrodeposits. *Materials Chemistry and Physics*, (doi:10.1016/j.matchemphys.2006.01.035).
59. **Changgeng, X., Zonggeng, D. and Lijun, Z.** (1988) The properties of electrodeposited Ni-P-SiC composite coatings. *Plating and Surface Finishing*, 75.10, 54-57.
60. **Chao, T.Y., Shen, G.R. and Cheng, Y.T.** (2006) Comparative study of Ni-P-diamond and Ni-P-CNT nanocomposite films. *Journal of the Electrochemical Society*, 153.1, G98-G104.
61. **Chen, C.K., Feng, H.M., Lin, H.C. and Hon, M.H.** (2002a) The effect of heat treatment on the microstructure of electroless Ni-P coatings containing SiC particles. *Thin Solid Films*, 416, 31-37.
62. **Chen, W.X., Tu, J.P., Xu, Z.D., Tenne, R., Rosenstveig, R., Chen, W.L. and Gan, H.Y.** (2002b) Wear and Friction of Ni-P Electroless Composite Coating Including Inorganic Fullerene-WS<sub>2</sub> Nanoparticles. *Advanced Engineering Materials*, 4.9, 686-690.
63. **Chen, W.X., Tu, J.P., Gan, H.Y., Xu, Z.D., Wang, Q.G., Lee, J.Y., Liu, Z.L. and Zhang, X.B.** (2002c) Electroless preparation and tribological properties of Ni-P-Carbon nanotube composite coatings under lubricated condition. *Surface and Coatings Technology*, 160, 68-73.
64. **Chen, W.X., Tu, J.P., Wang, L.Y., Gan, H.Y., Xu, Z.D. and Zhang, X.B.** (2003a) Tribological application of nanotubes in a metal-based composite coating and composites. *Carbon*, 41, 215-222.
65. **Chen, W.X., Tu, J.P., Xu, Z.D., Chen, W.L., Zhang, X.B. and Cheng, D.H.** (2003b) Tribological properties of Ni-P-multi-walled carbon nanotubes electroless composite coating. *Materials Letters*, 57, 1256-1260.
66. **Chen, X.H., Chen, C.S., Xiao, H.N., Cheng, F.Q., Zhang, G. and Yi, G.J.** (2005) Corrosion behaviour of carbon nanotubes-Ni composite coating, *Surface and Coatings Technology*, 191, 351-356.

67. **Chen, X.H., Chen, C.S., Xiao, H.N., Liu, H.B., Zhou, L.P., Li, S.L. and Zhang, G.** (2006a) Dry friction and wear characteristics of nickel/carbon nanotube electroless composite deposits. *Tribology International*, 39.1, 22-28.
68. **Chen, Z., Ng, A., Yi, J. and Chen, X.** (2006b) Multi-layered electroless Ni-P coatings on powder-sintered Nd-Fe-B permanent magnet. *Journal of Magnetism and Magnetic Materials*, 302, 216-222.
69. **Contreras, A., Leon, C., Jimenez, O., Sosa, E. and Perez, R.** (2006) Electrochemical behaviour and microstructural characterization of 1026 Ni-B coated steel. *Applied Surface Science*, (Article in press)
70. **Cui, C.Q. and Lee, J.Y.** (1995) Nickel deposition from unbuffered neutral chloride solutions in the presence of oxygen. *Electrochimica Acta*, 40.11, 1653-1662.
71. **Czerwinski, F. and Szpunar, J.A.** (1999) Controlling the thermal stability of texture in single-phase electrodeposits. *Nanostructured Materials*, 11.5, 669-676.
72. **Dadvand, N., Kipouros, G.J. and Caley, W.F.** (2003) Electroless nickel boron plating on AA6061. *Canadian Metallurgical Quarterly*, 42.3, 349-364.
73. **Daly, B.P. and Barry, F.J.** (2003) Electrochemical nickel-phosphorus alloy formation. *International Materials Reviews*, 48.5, 326-338.
74. **Das, C.M., Grover, A.K. and Suri, A.K.** (2002) Codeposition of luminescent particles with electroless nickel. *Transactions of the Institute of Metal Finishing*, 80.4, 128-131.
75. **Das, C.M., Limaye, P.K., Grover, A.K. and Suri, A.K.** (2006) Preparation and characterization of silicon nitride codeposited electroless nickel composite coatings. *Journal of Alloys and Compounds*, (Article in Press) (doi:10.1016/j.jallcom.2006.07.036).
76. **Delaunois, F., Petitjean, J.P., Lienard, P. and Jacob-Dulier, M.** (2000) Autocatalytic electroless nickel-boron plating on light alloys. *Surface and Coatings Technology*, 124, 201-209.
77. **Delaunois, F. and Lienard, P.** (2002) Heat treatments for electroless nickel-boron plating on aluminium. *Surface and Coatings Technology*, 160, 239-248.

78. **Dennis, J.K., Sheikh, S.T. and Silverstone, E.C.** (1981) Electroless composite coatings for wear resistant applications. *Transactions of the Institute of Metal Finishing*, 59.3, 118-122.
79. **Dennis, J.K. and Sagoo, K.S.** (1991) Wear behavior of engineering coatings and surface treatments. *Metal Finishing*, 89.6, 111-122.
80. **Desyatkova, G.I., Yagodkina, L.M., Savochkina, I.E. and Khaldeev, G.V.** (2002) Composite Nickel-Based Electroplates. *Protection of Metals*, 38.5, 466–470.
81. **Duncan, R.N. and Arney, T.L.** (1984) Operation and use of sodium borohydride reduced electroless nickel, *Plating and Surface Finishing*, 71.12, 49-54.
82. **Duncan, R.N.** (1986) Corrosion resistance of high –phosphorus electroless nickel coatings. *Plating and Surface Finishing*, 73.7, 52-57.
83. **Duncan, R.N. and Arney, T.L.** (1989) Galvanic corrosion behavior of electroless nickel in sea water. *Plating and Surface Finishing*, 76.10, 60-62.
84. **Ebdon, P.R.** (1987) Composite electroless nickel/PTFE coatings: Industrial Case Studies. *Surface Engineering* 3.2, 114-116.
85. **Ebdon, P.R.** (1988) The Performance of Electroless Nickel/PTFE Composites. *Plating and Surface Finishing* 75.9, 65-68.
86. **Erler, F., Jakob, C., Romanus, H., Spiess, L., Wielage, B., Lampke, T. and Steinhauser, S.** (2003) Interface behaviour in nickel composite coatings with nano-particles of oxidic ceramic. *Electrochimica Acta*, 48, 3063-3070.
87. **Ettmayer, P. and Lengauer, W.,** in: Ullmann's Encyclopedia of Industrial Chemistry, Elvers, B., Hankins, S. and Schmdz, G. (Eds.), 5<sup>th</sup> Completely Revised Edition, Volume A-17, 1991, pp. 341-361.
88. **Evans, W.T. and Schlesinger, M.** (1994) The effect of solution pH and heat-treatment on the properties of electroless nickel boron films. *Journal of the Electrochemical Society*, 141.1, 78-82.
89. **Feldstein, N., Lancsek, T., Lindsay, D. and Salerno, L.** (1983) Electroless composite plating. *Metal Finishing*, 81.8, 35-41.

90. **Filiatre, C., Towarnicki, L., Mange, F. and Foissy, A.** (1999) A parallel plate flow cell for the investigation of the role of surfactants in the codeposition of polymer particles in nickel electroplating. *Journal of Applied Electrochemistry*, 29, 1393-1400.
91. **Fellner, P. and Cong, P.K.** (1996) Ni-B and Ni-Si composite electrolytic coatings. *Surface and Coatings Technology*, 82, 317-319.
92. **Fransaer, J., Celis, J.P. and Roos, J.R.** (1992) Analysis of the electrolytic codeposition of non-Brownian particles with metals. *Journal of the Electrochemical Society*, 139, 413-425.
93. **Fratari, R.Q. and Robin, A.** (2006) Production and characterization of electrolytic nickel–niobium composite coatings. *Surface and Coatings Technology*, 200 (12-13), 4082-4090.
94. **Fritz, T., Cho, H.S., Henker, K.J., Mokwa, W. and Schnakenberg, U** (2002) Characterization of electroplated nickel. *Microsystem Technologies*, 9, 87.
95. **Furukawa, N. and Hayashi, T.** (1984) Sur./Fin.'84, Proceedings 71<sup>st</sup> Annual Technical Conference, July 16-20, New York, Dispersion Coating II, 2<sup>nd</sup> paper.
96. **Futterer, B.**, Dutch Patent, 6,708,227 (1967).
97. **Gaevskaya, T.V., Novotortseva, I.G. and Tsybulskaya, L.S.** (1996) The effect of Boron on the Microstructure and Properties of Electrodeposited Nickel Films. *Metal Finishing*, 94.6, 100-103.
98. **Garcia, I., Fransaer, J. and Celis, J.P.** (2001) Electrodeposition and sliding wear resistance of nickel composite coatings containing micron and submicron SiC particles. *Surface and Coatings Technology*, 148, 171-178.
99. **Garcia, I., Conde, A., Langelaan, G., Fransaer, J. and Celis, J.P.** (2003) Improved corrosion resistance through microstructural modifications induced by codepositing SiC-particles with electrolytic nickel. *Corrosion Science*, 45, 1173-1189.
100. **Gawne, D.T. and Ma, U.** (1987a) Wear mechanisms in electroless nickel coatings. *Wear*, 120, 125-149.
101. **Gawne, D.T. and Ma, U.** (1987b) Structure and wear of electroless nickel coatings. *Materials Science and Technology*, 33, 228-238.

102. **Gawrilov, G.G.**, *Chemical (Electroless) nickel plating*, Portcullis Press Ltd., Surrey, 1979.
103. **Ge, J-P., Che, R.X. and Wang, X.Z.** (1998) Structure and properties of electroless Ni-P-B<sub>4</sub>C composite coatings. *Metal Finishing*, 96.10, 69-73.
104. **Ger, M.D. and Hwang, B.J.** (2002) Effect of surfactants on codeposition of PTFE particles with electroless Ni-P coating. *Materials Chemistry and Physics*, 76, 38-45.
105. **Ger, M.D., Hou, K.H., Wang, L.M. and Hwang, B.J.** (2003) The friction and wear of Ni-P-PTFE composite deposits under water lubrication. *Materials Chemistry and Physics*, 77, 755-764.
106. **Ghouse, Md., Viswanathan, M. and Ramachandran, E.G.** (1980) Occlusion Plating of copper-silicon carbide composites. *Metal Finishing*, 78, 31-35.
107. **Gierlotka, D., Rowinski, E., Budniok, A. and Lagiewka, E.** (1997) Production and Properties of Electrolytic Ni-P-TiO<sub>2</sub> Composite Layers. *Journal of Applied Electrochemistry*, 27, 1349-1354.
108. **Gladman, T., Holmes, B. and McIvor, I.D.** (1971) Effects of second phase particles on strength, toughness and ductility. In *Effect of second phase particles on the mechanical properties of steel*. Iron and Steel Institute, London, pp. 68-78.
109. **Gorbunova, K.M., Ivanov, M.V. and Moiseev, V.P.** (1973) Electroless deposition of nickel-boron alloys, *Journal of the Electrochemical Society*, 120.5, 613-618.
110. **Gould, A.J.** (1988) Electroless nickel - A wear resistant coating. *Transactions of the Institute of Metal Finishing*, 66, 58-62.
111. **Graham, A.H. and Gibbs, T.W.**, in: *Properties of electrodeposit: Their measurements and significance*, Sard, R., Leidheiser, H. Jr. and Ogburun, F. (Eds.), Electrochemical Society, New Jersey, 1975.
112. **Greco, V.P. and Baldauf, T.W.** (1968) Electrodeposition of Ni-Al<sub>2</sub>O<sub>3</sub>, Ni-TiO<sub>2</sub> and Cr-TiO<sub>2</sub> dispersion hardened alloys. *Plating*, 55, 250-257.
113. **Grosjean, A., Rezrazi, M. and Tachez, M.** (1997) Study of the surface charge of silicon carbide (SiC) particles for electroless composite deposits: nickel-SiC. *Surface and Coatings Technology*, 96, 300-304.



114. **Grosjean, A., Rezrazi, M., Bercot, P. and Tachez, M.** (1998) Adaptation of a Mathematical Model to the Incorporation of Silicon Carbide Particles in an Electroless Nickel Deposit. *Metal Finishing*, 76.4, 14-17.
115. **Grosjean, A., Rezrazi, M., and Bercot, P.** (2000) Some morphological characteristics of the incorporation of silicon carbide particles into electroless nickel deposits. *Surface and Coatings Technology*, 130, 252-256.
116. **Grosjean, A., Rezrazi, M., Takadoun, J. and Bercot, P.** (2001) Hardness, friction and wear characteristics of nickel-SiC electroless composite coatings. *Surface and Coatings Technology*, 137, 92-96.
117. **Growcock, F.B. and Jasinski, R.J.** (1989) Time-resolved impedance spectroscopy of mild steel in concentrated hydrochloric acid. *Journal of the Electrochemical Society*, 136.8, 2310-2314.
118. **Guglielmi, N.** (1972) Kinetics of the deposition of inert particles from electrolytic baths. *Journal of Electrochemical Society*, 119, 1009-1012.
119. **Gu, C., Lian, J.S., Li, G., Niu, L. and Jiang, Z.** (2005a) High corrosion-resistant Ni-P/Ni/Ni-P multilayer coatings on steel. *Surface & Coatings Technology*, 197, 61-67.
120. **Gu, C., Lian, J.S. and Jiang, Z.** (2005b) Multilayer Ni-P coating for improving the corrosion resistance of AZ91D magnesium alloy. *Advanced Engineering Materials*, 7.11, 1032.
121. **Guo, Z.C., Zhu, X.Y. and Yang, X.W.** (2001) Corrosion resistance of electrodeposited RE-Ni-W-P-SiC composite coating. *Transactions of Nonferrous Metals Society of China*, (English Edition), 11.3, 413-416.
122. **Guo, Z. and Zhu, X.** (2003) Studies on properties and structure of electrodeposited RE-Ni-W-B-SiC composite coating *Materials Science and Engineering*, A363, 325-329.
123. **Guo, Z., Keong, K.G. and Sha, W.** (2003) Crystallization and phase transformation behaviour of electroless nickel phosphorus platings during continuous heating. *Journal of Alloys and Compounds*, 358 (1-2), 112-119.
124. **Gupta, B.K., Tiwari, A.N. and Agarwal, B.K.** (1982) Electro-codeposition and mechanical properties of Ni-tungsten carbide cermets. *Transactions of the Japan Institute of Metals*, 23, 320-327.

125. **Hadley, J.S. and Harland, L.E.** (1987) Electroless Nickel/PTFE Composite Coatings. *Metal Finishing*, 67.12, 51-53.
126. **Halling, J.**, *Principles of Tribology*, McMillan Publishers, London, 1975.
127. **Halling, J.** (1983) The tribology of surface films. *Thin Solid Films*, 108, 103-115.
128. **Hansen, P.L. and Moller, P.** (1990) The microstructure of electroless nickel containing TiC particles. *Journal of Materials Science Letters*, 9, 152-154.
129. **Henry, J.** (1990) A new fluorinated electroless nickel codeposit. *Metal Finishing*, 88.10, 15-18.
130. **Hiratsuka, K., Takago, S., Sasaki, T. and Hirose, Y.** (2001) Residual stress in composite film (Ni-Co-P/Si<sub>3</sub>N<sub>4</sub>) film. *Thin Solid Films*, 398-399, 476-479.
131. **Homma, T., Tamaki, A., Nakai, H. and Osaka, T.** (2003) Molecular orbital study on the reaction process of dimethylamine borane as a reductant for electroless deposition. *Journal of Electroanalytical Chemistry*, 559, 131-136.
132. **Hou, K.H. and Ger, M.D., Wang, L.M. and Ke, S.T.** (2002) The wear behavior of electro-codeposited Ni-SiC composites. *Wear*, 253, 994-1003.
133. **Hu, C.C., Lin, C.Y. and Wen, T.C.** (1996) Textural and electrochemical properties of Watts nickel-deposited titanium electrodes. *Materials Chemistry and Physics*, 44.3, 233-238.
134. **Hu, X., Dai, C., Li, J. and Wang, D.** (1997) Zeta potential and codeposition of PTFE particles suspended in electroless nickel solution. *Plating and Surface Finishing*, 84.3, 51-53.
135. **Huang, Y.S., Zeng, X.T., Annergren, I. and Liu, F.M.** (2003) Development of electroless Ni-P-PTFE-SiC composite coating. *Surface and Coatings Technology*, 167, 207-211.
136. **Huang, Y.S., Zeng, X.T., Hu, X.F. and Liu, F.M.** (2004) Corrosion resistance properties of electroless nickel composite coatings, *Electrochimica Acta*, 49, 4313-4319.

137. **Huang, Y.S., Zeng, X.T., Hu, X.F. and Liu, F.M.** (2005) Heat treatment effects on EN-PTFE-SiC composite coatings, *Surface and Coatings Technology*, 198, 173– 177.
138. **Hubbell, F.N.** (1978a) Chemically deposited composites – A new generation of electroless coatings. *Transactions of the Institute of Metal Finishing*, 56, 65-69.
139. **Hubbell, F.N.** (1978b) Chemically deposited composites – A new generation of electroless coatings. *Plating and Surface Finishing*, 65.12, 58-62.
140. **Hur, K.H., Jeong, J.H., and Lee, D.N.** (1990) Microstructures and crystallization of electroless Ni-P deposits. *Journal of Materials Science*, 25, 2573-2584.
141. **Hussain, M.S. and Such, T.E.** (1981) Deposition of composite autocatalytic nickel coatings containing particles. *Surface Technology*, 13, 119-125.
142. **Hwang, B.J. and Hwang, C.S.** (1993) Mechanism of codeposition of silicon carbide with electrolytic cobalt. *Journal of Electrochemical Society* 140.4, 979-984.
143. **Indira Rajagopal**, in: *Surface Modification Technologies: An Engineering Guide*, Sudarshan, T S (Ed.), Marcel Dekker, New York, 1989.
144. **Izzard, M. and Dennis, J.K.** (1987) Deposition and properties of electroless nickel/graphite coatings. *Transactions of the Institute of Metal Finishing*, 65, 85-89.
145. **Jacobson, B.E. and Sliwa, J.W.** (1972) Structure and mechanical properties of electrodeposited nickel. *Plating and Surface Finishing* 9, 42.
146. **Jiaqiang, G., Lei, L., Yating, W., Bin, S. and Wenbin, H.** (2006) Electroless Ni–P–SiC composite coatings with superfine particles. *Surface and Coatings Technology*, 200, 5836-5842.
147. **John, S.S., Srinivasan, K.N., Kavimani, P.M., Krishnan, K.H., Praveen, J. and Ganesan, M.** (2005) Electroless Ni-P-TiO<sub>2</sub> - Based composite coatings for surface engineering applications *Plating and Surface Finishing*, 92.5, 62-66.

148. **Joshi, M.N. and Totlani, M.K.** (1981) Electrodeposition of Nickel-Silicon nitride composites. *Proceedings of the 2<sup>nd</sup> National Conference on Electroplating and Metal Finishing*, Totlani, M K and Joshi, M N (Eds.), 1981.
149. **Jun, L., Changsong, D., Dianlong, W. and Xinguo, H.** (1997) Electroforming of nickel and partially stabilized zirconia (Ni+PSZ) gradient coating. *Surface and Coatings Technology*, 91, 131-135.
150. **Kalantary, M.R., Holbrook, K.A. and Wells, P.B.** (1993) Optimization of a bath for electroless plating and its use for the production of nickel-phosphorus-silicon carbide coatings. *Transactions of the Institute of Metal Finishing*, 71.2, 55-61.
151. **Kanani, N.** (1991) Tribological behavior of electroless nickel. *Transactions of the Institute of Metal Finishing*, 70.1, 14-18.
152. **Kariappar, A.M.J. and Foster, J.** (1974) Further studies on the mechanism of formation of electrodeposited composite coatings. *Transactions of Institute of Metal Finishing*, 52, 87-91.
153. **Kedward, E.C. and Kiernan, B.** (1967) Electrodeposited composite coatings for wear resistance. *Metal Finishing*, 13, 116-118.
154. **Kedward, E.C.** (1972) Electrodeposited composite coatings. *Electroplating and Metal Finishing*, 25, 20-24.
155. **Keong, K.G., Sha, W. and Malinov, S.** (2002a) Crystallization kinetics and phase transformation behaviour of electroless nickel-phosphorus deposits with high phosphorus content. *Journal of Alloys and Compounds*, 334 (1-2), 192-199.
156. **Keong, K.G., Sha, W. and Malinov, S.** (2002b) Crystallization and phase transformation behaviour of electroless nickel-phosphorus deposits with low and medium phosphorus contents under continuous heating. *Journal of Materials Science*, 37, 20.
157. **Kerr, C., Barker, D., Walsh, F. and Archer, J.** (2000) The electro-deposition of composite coatings based on metal matrix included particle deposits. *Transactions of Institute of Metal Finishing*, 78.5, 171-178.
158. **Kim, S.K. and Yoo, H.J.** (1998) Formation of bilayer Ni-SiC composite coatings by electrodeposition. *Surface and Coatings Technology*, 108-109, 564-569.

159. **Kozlov, V.M. and Peraldo-Bicelli, L.** (2003) Texture formation of electrodeposited fcc metals. *Materials Chemistry and Physics*, 77, 289-293.
160. **Kosov, A.M., Yu, V., Makarov, V.F. and Flerov, V.N.** (1989) Stepped Reaction of Dimethylamineborane in Chemical Nickel Plating Solutions. *Elektrokhimiya*, 25.11, 1546-1566.
161. **Kurozaki, K.** (1979) *Journal of Japanese Institute of Metals*, 10, 48-52.
162. **Laitinen, G.A.** (1991) Electroless nickel and composite coatings for engineering applications. *Metal Casting and Surface Finishing*, 37(11-12) 17-20.
163. **Laitinen, G.A.** (1992) Electroless nickel and their applications in the aircraft industry. *Metal Finishing*, 90.4, 13-15.
164. **Lancaster, J.K.** (1983) Composites for increased wear resistance: Current achievements and future prospects, in: New direction in lubrication materials, wear and surface interactions- Tribology in 80's, Loomis, W R (Ed.), Noyes, p. 320.
165. **Lantelme, F., Seghioer, A. and Derja, A.** (1998) Model of nickel electrodeposition from acidic medium. *Journal of Applied Electrochemistry*, 28.9, 907-913.
166. **Lausmann, G.A.** (1984) Electrolytic dispersion coating of Nickel/Silicon carbide in a fully automatic operating system for multiple cylinder blocks in line. *Sur/Fin'84 - Proceedings of the 71<sup>st</sup> AES Annual Technical Conference*, Session - Dispersion coatings, 4<sup>th</sup> paper, New York.
167. **Lee, D.N.** (2001) A stability criterion for deformation and deposition textures of metals during annealing. *Journal of Materials Processing Technology*, 117.3, 307-310.
168. **Lee, D.N.** (2002) Texture Development in Thin Films. *Materials Science Forum*, 408-412, 75-94.
169. **Lee, W.H., Tang, S.C. and Chung, K.C.** (1999) Effect of direct current and pulse-plating on the co-deposition of nickel and nanometer diamond powder. *Surface and Coatings Technology*, 120-121, 607-611.

170. **Lee, K.H., Chang, D. and Kwon, S.C.** (2005) Properties of electrodeposited nanocrystalline Ni–B alloy films. *Electrochimica Acta*, 50.23, 4538-4543.
171. **Lekka, M., Kouloumbi, N., Gajo, M. and Bonora, P.L.** (2005) Corrosion and wear resistant electrodeposited composite coatings. *Electrochimica Acta*, 50, 4551–4556.
172. **Leon, O.A., Staia, M.H. and Hintermann, H.E.** (1998) Deposition of Ni–P–BN(h) composite autocatalytic coatings. *Surface and Coatings Technology*, 108–109, 461–465.
173. **León, O.A., Staia, M.H. and Hintermann, H.E.** (1999) Influence of the heat treatment on the tribological behavior of a Ni–P–BN(h) autocatalytic composite coating. *Surface and Coatings Technology*, 120-121, 641-645.
174. **Leon, O.A., Staia, M.H. and Hintermann, H.E.** (2003) High temperature wear of an electroless Ni–P–BN (h) composite coating. *Surface and Coatings Technology*, 163 –164, 578–584.
175. **Lewis, D.B. and Marshall, G.W.** (1996) Investigation into the structure of electrodeposited nickel-phosphorus alloy deposits. *Surface and Coatings Technology*, 78 (1-3), 150-156.
176. **Li, Y.** (1997) Investigation of Electroless Ni-P-SiC Composite Coatings *Plating and Surface Finishing* 84, 77-81.
177. **Li, X. and Li, Z.** (2003) Nano-sized Si<sub>3</sub>N<sub>4</sub> reinforced Ni-Fe nanocomposites by electroplating. *Materials Science and Engineering*, A358, 107-113.
178. **Li, J., Sun, Y., Sun, X. and Qiao, J.** (2005) Mechanical and corrosion-resistance performance of electrodeposited titania-nickel nanocomposite coatings. *Surface and Coatings Technology*, 192, 331-335.
179. **Li, Z.H., Wang, X.Q., Wang, M., Wang, F.F. and Ge, H.L.** (2006) Preparation and tribological properties of the carbon nanotubes–Ni–P composite coating *Tribology International*, 39.9, 953-957.
180. **Lin, C.S., Lee, C.Y., Chen, F.J. and Li, W.C.** (2005) Structural evolution and internal stress of nickel-phosphorus electrodeposits. *Journal of The Electrochemical Society*, 152.6, C370-C375.

181. **Liqun, Z., Qunpeng, Z. and Jianhua, L.** (2001) Amorphous Nickel-Tungsten-Boron Composite Electrodeposits with Zirconium Oxide Particles *Metal Finishing*, 99.7, 28-30.
182. **Lo, Y.L. and Hwang, B.J.** (1994) Decomposition of  $\text{NaBH}_4$  in an Electroless Nickel Bath. *Industrial Engineering Chemistry Research*, 33, 56-61.
183. **Lo, P.H., Tsai, W.T., Lee, J.T. and Hung, M.P.** (1995) The electrochemical behaviour of electroless plated Ni-P alloys in concentrated NaOH solution. *Journal of the Electrochemical Society*, 142.1, 91-96.
184. **Low, C.T.J., Wills, R.G.A. and Walsh, F.C.** (2006) Electrodeposition of composite coatings containing nanoparticles in a metal deposit. *Surface and Coatings Technology*, Volume 201.1-2, 371-383.
185. **Lowenheim, F.A.**, *Modern Electroplating*, 3<sup>rd</sup> Edition, Wiley, 1974.
186. **Lukschandel, J.** (1978) Diamond – containing electroless nickel coatings. *Transactions of the Institute of Metal Finishing*, 56.3, 118-120.
187. **Mahoney, M.W. and Dynes, P.J.** (1985) The effects of thermal history and phosphorus level on the crystallization of electroless nickel. *Scripta Metallurgica*, 19, 539-542.
188. **Mallory, G.O.** (1971) The Electroless Nickel-Boron Plating Bath; Effects of Variables on Deposit Properties. *Plating*, 55.4, 319-327.
189. **Mallory, G.O. and Hajdu, J.B. (Eds.)**, *Electroless Plating: Fundamentals and Applications*, AESF, Orlando, 1991.
190. **Malfatti, C.F., Ferreira, J.Z., Santos, C.B., Souza, B.V., Fallavena, E.P., Vaillant, S. and Bonino, J.P.** (2005) NiP/SiC composite coatings: The effects of particles on the electrochemical behaviour. *Corrosion Science*, 47, 567–580.
191. **Mansfeld, F., Kending, M. and Tsai, S.** (1982) Evaluation of corrosion behaviour of coated metals with AC impedance measurements. *Corrosion*, 38, 478.
192. **Masui, K., Masuda, M., Maruno, S. and Kawaguchi, T.** (1985) Preparation of electroless Ni-B alloys and heat-induced structural changes. *Journal of Metal Finishers Society of Japan*, 36.2, 50-57.

193. **Masui, K.** (1986) Heat induced Structural Changes on Electroless Ni-B Alloys. *Metal Finishing*, 84.8, 34-36.
194. **Matsuda, H., Nishira, M., Kiyono, Y. and Takano, O.** (1995) Effect of Surfactants addition on the suspension of PTFE particles in electroless plating solutions. *Transactions of the Institute of Metal Finishing*, 73(1), 16-18.
195. **McCormack, A.G., Pomeroy, M.J. and Cunnane, V.J.** (2003) Microstructural Development and Surface Characterization of Electrodeposited Nickel/Yttria Composite Coatings. *Journal of The Electrochemical Society*, 150.5, C356-C361.
196. **Medeliene, V., Gladkovas, M. and Matulionis, E.** (2001) Corrosion of Nickel Electroplates in Neutral and Acidic Salt-Spray-Fog *Protection of Metals*, 37.4, 331–336.
197. **Medeliene, V.** (2002) The influence of B<sub>4</sub>C and SiC additions on the morphological, physical, chemical and corrosion properties of Ni coatings. *Surface and Coatings Technology*, 154,104–111.
198. **Metzger and Florian, Th.** (1976) The deposition of dispersion hardened coatings by means of electroless nickel. *Transactions of the Institute of Metal Finishing*, 54, 174-177.
199. **Mitoseriu, L. and Mitoseriu, O.** (2002) Ni-P/SiC composite coatings obtained by chemical methods *Science and Engineering of Composite Materials*, 10.1, 51-54.
200. **Mohanty, U.S., Tripathy, B.C., Singh, P. and Das, S.C.** (2002) Effect of Cd<sup>2+</sup> on the electrodeposition of nickel from sulfate solutions. Part I: Current efficiency, surface morphology and crystal orientations. *Journal of Electroanalytical Chemistry*, Volume 526 (1-2), 63-68.
201. **Moller, A. and Hahn, H.** (1999) Synthesis and characterization of nanocrystalline Ni/ZrO<sub>2</sub> composite coatings. *Nanostructured Materials*, 12, 259-262.
202. **Moonir-Vaghefi, S.M. and Saatchi, A.** (1997a) The Effect of Agitation on Electroless Nickel-Phosphorus-Molybdenum Disulphide Composite Plating. *Metal Finishing*, 95.6, 102-106.
203. **Moonir-Vaghefi, S.M. and Saatchi, A.** (1997b) Deposition and Properties of Electroless Nickel-Phosphorus-Molybdenum Disulphide Composites. *Metal Finishing*, 95.11, 46-52.



204. **Moonir-Vaghefi, S.M., Saatchi, A. and Hejazi, J.** (1997c) Tribological behaviour of electroless Ni-P-MoS<sub>2</sub> composite coatings. *Zeitsfur Metallkunde*, 88.6, 498-501.
205. **Moonir-Vaghefi, S.M., Saatchi, A. and Hoseinabadi, M.E.** (2003) Deposition and properties of electroless Ni-P-B<sub>4</sub>C composite coatings. *Surface and Coatings Technology*, 168, 259-262.
206. **Morikawa, T., Nakade, T., Yokoi, M., Fukumotot, Y. and Iwakura, C.** (1997) Electrodeposition of Ni-P alloys from Ni-citrate bath, *Electrochimica Acta*, 42.1, 115-118.
207. **Muller, C., Sarret, M. and Benballa, M.** (2002) ZnNi/SiC composites obtained from an alkaline bath. *Surface and Coatings Technology*, 162, 49-53.
208. **Musiani, M.** (2000) Electrodeposition of composites: An expanding subject in electrochemical materials science. *Electrochimica Acta*, 45.20, 3397-3402.
209. **Narayan, R. and Narayana, B.H.** (1981) Electrodeposited Chromium-graphite composite coatings. *Journal of Electrochemical Society*, 128, 1704-1708.
210. **Narayanan, R. and Seshadri, S.K.** (2001) Chromium-Ceria electrodeposition using nitrate additives. *Metal Finishing*, 99.2, 84-89.
211. **Ng, P.K., Synder, D.D. and Lasala, J.** (1988) Structure and Crystallization of Nickel-Phosphorus Alloys Prepared by High-Rate Electrodeposition. *Journal of the Electrochemical Society*, 135, 1376-1381.
212. **Nishira, M. and Takano, O.** (1994) Friction and wear characteristics of electroless Ni-P-PTFE composite coatings. *Plating and Surface Finishing*, 81.1, 48-50.
213. **Nishira, M., Yamagishi, K., Matsuda, H., Suzuki, M. and Takano, O.** (1996) Uniform Dispersibility of PTFE Particles in Electroless Composite Plating. *Transactions of the Institute of Metal Finishing*, 74(2), 62-64.
214. **Novakovic, J., Vassiliou, P., Samara, Kl. and Argyropoulos, Th.** (2006) Electroless NiP–TiO<sub>2</sub> composite coatings: Their production and properties. *Surface and Coatings Technology*, 201, 895–901.

215. **Nowak, P., Socha, R.P., Kaisheva, M., Fransaer, J., Celis, J.P. and Stoinov, Z.** (2000) Electrochemical investigation of the codeposition of SiC and SiO<sub>2</sub> particles with nickel. *Journal of Applied Electrochemistry*, 30, 429-437.
216. **Oh, I.H., Lee, J.Y., Han, J.K., Lee, H.J., and Lee, B.T.** (2005) Microstructural characterization of Al<sub>2</sub>O<sub>3</sub>-Ni composites prepared by electroless deposition *Surface and Coatings Technology*, 192.1, 39-42.
217. **Okinaka, Y., Osaka, T., Gerischer and Tobias, C.W.** (Eds.), *Advances in Electrochemical Science and Engineering*, Volume 3, VCH, Weinheim, Germany, 1994, p. 55.
218. **Onoda, M., Shimizu, K., Tateishi, Y. and Watanabe, T.** (1998) Preparation of Ni-B amorphous alloy films by electrodeposition using a rotating electrode and their structural changes. *Transactions of the Institute of Metal Finishing*, 76.1, 41-44.
219. **Onoda, M., Shimizu, K., Tateishi, Y. and Watanabe, T.** (1999) Mechanism of boron codeposition in electrodeposited Ni-B alloy films and calculation of the amount of codeposited boron. *Transactions of the Institute of Metal Finishing*, 77.1, 44-48.
220. **Panagopoulos, C.N., Agathocleous, P.E., Papachristos, V.D. and Michaelides, A.** (2000a) Sliding wear behaviour of zinc-iron alloy electrodeposits. *Surface and Coatings Technology*, 123.1, 62-71.
221. **Panagopoulos, C.N., Papachristos, V.D., Wahlstrom, U., Leisner, P. and Christoffersen, L.W.** (2000b) Ni-P-W multilayered alloy coatings produced by pulse plating, *Scripta Materialia*, 43, 677-683.
222. **Panagopoulos, C.N., Georgarakis, K.G. and Agathocleous, P.E.** (2003) Sliding wear behaviour of Zinc-Nickel alloy electrodeposits. *Tribology International*, 36.8, 619-623.
223. **Parker, K.** (1972) Recent Advances in Electroless Nickel Deposits. *Proceedings of the 8<sup>th</sup> International Conference*, Forster-Verlag, Zurich, Switzerland, pp. 202-207.
224. **Parker, K.** (1974) Hardness and wear resistance tests of electroless nickel deposits. *Plating*, 61.9, 834-841.
225. **Paunovic, M.** (1968) Electrochemical aspects of electroless deposition of metals. *Plating*, 55.11, 1161-1167.

226. **Pena-Munoz, E., Bercot, P., Grosjean, A., Rezrazi, M. and Pagetti, J.** (1998) Electrolytic and Electroless coatings of Ni-PTFE composites: Study of some characteristics. *Surface and Coatings Technology*, 107, 85-93.
227. **Plumier, F., Chassiang, E., Terwagne, G., Delhalle, J. and Mekhalif, Z.** (2003) Electrolytic co-deposition of a nickel-fluorographite composite layer on polycrystalline copper. *Applied Surface Science*, 212-213, 271-278.
228. **Pushpavanam, M. and Shenoi, B.A.** (1977) Nickel-aluminum oxide composite coatings. *Metal Finishing*, 75.4, 38-43.
229. **Pushpavanam, M., Balakrishnan, K. and Natarajan, S.R.** (1989) Properties of  $\text{TiO}_2$  Dispersed Nickel Deposits. *Bulletin of Electrochemistry*, 5.3, 161-165.
230. **Pushpavanam, M., Varadarajan, G. Krishnamoorthy, S., Thangappa, R., Shenoi, B.A. and Udupa, H.V.K.** (1974) Occlusion plating with nickel-codeposition of titanium oxide particles. *Metal Finishing*, 72, 46-52.
231. **Pushpavanam, M.** (1992) Electroless Ni-P- $\text{Al}_2\text{O}_3$  composites. *Bulletin of Electrochemistry*, 8.8, 399-401.
232. **Pushpavanam, M. and Natarajan, S.R.** (1992) Ni-ZrB<sub>2</sub> Electrocomposites. *Bulletin of Electrochemistry*, 8.8, 396-398.
233. **Pushpavanam, M. and Natarajan, S.R.** (1995) Nickel-boron nitride electrocomposites. *Metal Finishing*, 93, 97-99.
234. **Qu, N.S., Zhu, D. and Chan, K.C.** (2006) Fabrication of Ni-CeO<sub>2</sub> nanocomposite by electrodeposition. *Scripta Materialia*, 54, 1421-1425.
235. **Rajam, K.S., Indira Rajagopal, Rajagopalan, S.R. and Viswanathan, B.** (1993) DSC, X-ray and magnetic studies on electroless Ni-P films grown in alkaline ethanolamine baths. *Materials Chemistry and Physics*, 33, 289-297.
236. **Rajiv, E.P. and Seshadri, S.K.** (1993) Characteristics of Electro-Codeposition of Cobalt-Titania Composites. *Plating and Surface Finishing*, 80.10, 66-72.
237. **Ramakrishna,** (1990) Characteristics of nickel-colloidal silica. *B.Tech. Dissertation*, Indian Institute of Technology- Madras, Chennai.

238. **Ramesh, C.S., Seshadri, S.K. and Iyer, K.J.L.** (1990) *Proceedings of the Second International Ceramic Science and Technology Congress*, Orlando, Florida, U S A., 12-15 Nov.1990.
239. **Ramesh, C.S., Seshadri, S.K. and Iyer, K.J.L.** (1991) Characteristics of nickel-flyash electrocomposite coatings. *Plating and Surface Finishing*, 78, 52-54.
240. **Ramesh, C.S. and Seshadri, S.K.** (2003) Tribological Characteristics of Nickel Based Composite Coatings. *Wear*, 255, 893-902.
241. **Ramesh Babu, G.N.K., Ayyapparaju, J., Mahalingam, R., Devaraj, G. and Guruviah, S.** (1990) Composite plating of aluminium-A direct method. *Bulletin of Electrochemistry*, 6.2, 245-246.
242. **Ramesh Babu, G.N.K., Muralidharan, V.S. and Vasu, K.I.** (1991) Mechanism of the codeposition of titania particles with nickel from fluoborate baths. *Plating and Surface Finishing*, 78.5, 126-132.
243. **Ramesh Babu, G.N.K.** (1994) Electrocodeposition and characterization of nickel-titanium carbide composites. *Surface and Coatings Technology*, 67, 105-110.
244. **Ramesh Babu, G.N.K.** (1995) Characteristics of Ni-BN electrocomposites. *Plating and Surface Finishing*, 82, 70-73.
245. **Rao, Q., Haowei, W., Kun, Z., Xiaolan, F. and Yoahe, Z.** (2001) Effects of heat-treatment processes on the electroless Ni-B coating and its natural aging mechanism, *Transactions of the Institute of Metal Finishing*, 79.2, 56-59.
246. **Ratzker, M., Lashmore, D.S. and Pratt, K.W.** (1986) Electrodeposition and corrosion performance of nickel-phosphorus amorphous alloys. *Plating and Surface Finishing*, 73.9, 74-82.
247. **Reddy, V.V.N., Ramamoorthy, B. and Kesavan Nair, P.** (2000) Study on the wear resistance of electroless Ni-P/diamond composite coatings. *Wear*, 239, 111-116.
248. **Revenko, V.G., Kozlova, T.V., Astakhov, G.A., Chernova, G.P. and Bogdashkina, N.L.** (2003) Corrosion and Electrochemical Behavior of Composite Electrolytic, Iron-Based Coatings. *Protection of Metals*, 39.1, 77-80.
249. **Riedel, W.,** *Electroless Plating*, ASM International, Ohio, 1991.

250. **Rossi, S., Chini, F., Straffelini, G., Bonora, P.L., Moschini, R. and Stampali, A.** (2003) Corrosion protection properties of electroless Nickel/PTFE, Phosphate/MoS<sub>2</sub> and Bronze/PTFE coatings applied to improve the wear resistance of carbon steel. *Surface and Coatings Technology*, 173, 235-242.
251. **Ruimi Michel and Martinou, R.** (1989) Nickel-cobalt alloy electrolytic coatings incorporating ceramic particles. *Metal Finishing*, 87, 7-10.
252. **Saifullin, R.S. and Kahlilova, R.G.** (1970) *Journal of Applied Chemistry (USSR)*, 43, 1266.
253. **Saito, T., Sato, E., Matsuoka, M. and Iwakura, C.** (1998) Electroless deposition of Ni-B, Co-B and Ni-Co-B alloys using dimethylamineborane as a reducing agent. *Journal of Applied Electrochemistry*, 28.5, 559-563.
254. **Sale, J.M.,** Coatings for Corrosion Prevention. American Society of Metals, Metal Park, Ohio, 1979, pp. 90-102.
255. **Sampath Kumar, P. and Kesavan Nair, P.** (1995) Crystallization of Electroless Ni-B Deposits, *Metals Materials and Processes*, 7.2, 131-138.
256. **Sankara Narayanan, T.S.N., Krishnaveni, K. and Seshadri, S.K.** (2003) Electroless Ni-P/Ni-B duplex coatings: preparation and evaluation of microhardness, wear and corrosion resistance. *Materials Chemistry and Physics*, 82.3, 771-779.
257. **Sankara Narayanan, T.S.N. and Seshadri, S.K.** (2004) Formation and characterization of borohydride reduced electroless nickel deposits. *Journal of Alloys and Compounds*, 365(1-2), 197-205.
258. **Sankara Narayanan, T.S.N., Baskaran, I., Krishnaveni, K. and Parthiban, S.** (2006) Deposition of electroless Ni-P graded coatings and evaluation of their corrosion resistance. *Surface and Coatings Technology*, 200.11, 3438-3445.
259. **Sasame, T.,** Japanese patent, 74,48,051 (1974).
260. **Sautter, F.K.** (1963) Electrodeposition of dispersion hardened nickel Al<sub>2</sub>O<sub>3</sub> alloys. *Journal of Electrochemical Society*, 110, 557-560.
261. **Schlesinger, M. and Paunovic, M.** (Eds.), Modern Electroplating, Fourth Edition, John Wiley & Sons., New York, 2000.

262. **Serek, A. and Budniok, A.** (2003) Electrodeposition and thermal treatment of nickel layers containing titanium. *Journal of Alloys and Compounds*, 352, 290-295.
263. **Shao, I., Vereecken, P.M., Chien, C.L., Searson, P.C. and Cammarata, R.C.** (2002) Synthesis and characterization of particle-reinforced Ni/Al<sub>2</sub>O<sub>3</sub> nanocomposites. *Journal of Materials Research*, 17.6, 1412-1418.
264. **Sharp, W.F.** (1975) Properties and applications of composite diamond coatings, *Wear*, 32, 315-325.
265. **Sheela, G. and Pushpavanam, M.** (2002) Diamond-Dispersed Electroless Nickel Coatings. *Metal Finishing*, 100.1, 45-47.
266. **Shi, Y.L., Yang, Z., Xu, H., Li, M.K. and Li, H.L.** (2004) Preparation of electroplated Ni-P-ultrafine diamond, Ni-P-carbon nanotubes composite coatings and their corrosion properties, *Journal of Material Science*, 39, 5809-5815.
267. **Shi, L., Sun, C.F., Zhou, F. and Liu, W.M.** (2005) Electrodeposited nickel-cobalt composite coating containing nano-sized Si<sub>3</sub>N<sub>4</sub>. *Materials Science and Engineering*, A 397, 190-194.
268. **Shi, L., Sun, C., Gao, P., Zhou, F. and Liu, W.** (2006) Mechanical properties and wear and corrosion resistance of electrodeposited Ni-Co/SiC nanocomposite coating. *Applied Surface Science*, 252.10, 3591-3599.
269. **Shibli, S.M.A., Jabeera, B. and Anupama, R.I.** (2006) Incorporation of nano zinc oxide for improvement of electroless nickel plating. *Applied Surface Science*, In Press (doi:10.1016/j.apsusc.2006.02.063)
270. **Shibli, S.M.A., Jabeera, B. and Anupama, R.I.** (2006) Development of ZnO incorporated composite Ni-ZnO-P alloy coating *Surface and Coatings Technology*, 200 (12-13), 3903-3906.
271. **Shoeib, M.A., Mokhtar, S.M. and Abd El-Ghaffar, M.A.** (1998) Mechanical and corrosion protection properties of electroless nickel-polymer composite coatings. *Metal Finishing*, 96.11, 58-59.
272. **Shrestha, N.K., Sakurada, K., Masuko, M. and Saji, T.** (2001) Composite coatings of nickel and ceramic particles prepared in two steps. *Surface and Coatings Technology*, 140, 175-181.

273. **Shrestha, N.K., Masuko, M. and Saji, T.** (2003) Composite plating of Ni/SiC using azo-cationic surfactants and wear resistance of coatings *Wear*, 254, 555-564.
274. **Sinha, P.K., Dhananjayan, N. and Chakrabarti, H.K.** (1973) Electrodeposited nickel-alumina composites. *Plating*, 60, 55-59.
275. **Socha, R.P., Laajalehto, K. and Nowak, P.** (2002) Influence of the surface properties of silicon carbide on the process of SiC particles codeposition with nickel. *Colloids and Surfaces A: Physicochemical and Engineering Aspects*, 208, 267-275.
276. **Srinivasan, K.N. and John, S.** (2005) Studies on electroless nickel-PTFE composite coatings. *Surface Engineering*, 21.2, 156-160.
277. **Srivastava, A., Mohan, S., Agarwala, V. and Agarwala, R.C.** (1992a) Factors Influencing the Deposition Rate of Ni-B Electroless Films. *Zeitsfur Metallkunde*, 83.4, 251-253.
278. **Srivastava, A., Mohan, S., Agarwala, V. and Agarwala, R.C.** (1992b) On the crystallization Behavior of an Amorphous Ni-17.8 at% B Electroless Deposit. *Zeitsfur Metallkunde*, 83.4, 254-257.
279. **Staia, M.H., Castillo, E.J., Puchi, E.S., Lewis, D.B. and Hintermann, H.E.** (1996) Wear performance and mechanism of electroless Ni-P coating. *Surface and Coatings Technology*, 86/87, 598-602.
280. **Staia, M.H., Conzono, A., Cruz, M.R., Roman, A., Lesage, J., Chicot, D. and Mesmacque, G.** (2002) Wear Behaviour of Silicon Carbide/Electroless Nickel Composite Coatings at high temperature *Surface Engineering*, 18.4, 265-269.
281. **Starosta, R. and Zielinski, A.** (2004) Effect of chemical composition on corrosion and wear behaviour of the composite Ni-Fe-Al<sub>2</sub>O<sub>3</sub> coatings. *Journal of Material Processing Technology*, 157-158, 434-441.
282. **Straffelini, G., Colombo, D. and Molinari, A.** (1999) Surface durability of electroless Ni-P composite deposits. *Wear*, 236, 179-188.
283. **Subramanian, C. and Pallotta, E.** (1996) Two-body abrasive wear of electroless nickel composite coatings. *Tribology Letters*, 2.2, 133-150.

284. **Surender, M., Balasubramaniam, R. and Basu, B.** (2004a) Electrochemical behaviour of electrodeposited Ni-WC composite coatings. *Surface and Coatings Technology*, 187, 93-97.
285. **Surender, M., Basu, B. and Balasubramaniam, R.** (2004b) Wear characterization of electrodeposited Ni-WC composite coatings. *Tribology International*, 37, 743-749.
286. **Surviliene, S., Bellozor, S., Kurtinaitiene, M. and Safonov, V.A.** (2004) Protective properties of the chromium–titanium carbonitride composite coatings. *Surface and Coatings Technology*, 176, 193–201.
287. **Susan, D.F., Barmak, K. and Marder, A.R.** (1997) Electrodeposited Ni-Al particle composite coatings. *Thin Solid Films*, 307, 133-140.
288. **Szasz, A., Fabian, D.J., Paal, Z. and Kojnok, J.** (1988) Chemical mechanisms in electroless deposition. A study on the role of hydrogen in layer formation. *Journal of Non-Crystalline Solids*, 103, 21-27.
289. **Szczygiel, B. and Kolodziej, M.** (2005a) Composite Ni/Al<sub>2</sub>O<sub>3</sub> coatings and their corrosion resistance. *Electrochimica Acta*, 50, 4188–4195.
290. **Szczygiel, B. and Kolodziej, M.** (2005b) Corrosion resistance of Ni/Al<sub>2</sub>O<sub>3</sub> coatings in NaCl solution. *Transactions of the Institute of Metal Finishing*, 83.4, 181-187.
291. **Szeptycka, B.** (2002) Electroplated hybrid composite coatings. *Galvanotechnik*, 93.3, 663-671.
292. **Szeptycka, B. and Gajewska, A.** (2005) Investigation of the electrochemical corrosion resistance of hybrid Ni-SiC-fluoropolymer composite coatings. *Materials and Manufacturing Processes*, 20.1, 23-34.
293. **Teranishi, A. and Gijutsu, H.** (2000) The application of electroless-deposited composite plating. *Journal of the Surface Finishing Society of Japan*, 5.11, 1078-1080.
294. **Tomaszewski, T.W., Tomaszewski, L.C. and Brown, H.** (1969) Codeposition of finely dispersed particles with metals. *Plating*, 56, 1234-1238.
295. **Tulsi, S.S.** (1983a) Composite PTFE – nickel coatings for low friction applications. *Metal Finishing*, 7.11, 14-18.



296. **Tulsi, S.S.** (1983b) Electroless nickel-PTFE composite coatings. *Transactions of the Institute of Metal Finishing*, 61, 147-149.
297. **Tulsi, S.S.** (1985) A new composite PTFE-nickel coating for low friction wear applications, in: Thermal Spraying, Testing of Coatings, Wear-resistant Coatings, Bucklow, I A (Ed.), Proceedings of the 1<sup>st</sup> International Conference on Surface Engineering, Volume 1, pp. 193-201.
298. **Valdes, J.L.**, Deposition of colloidal particles in electrochemical systems. Ph.D. Thesis. Columbia University, New York, 1987.
299. **Valles, E., Pollina, R. and Gomez, E.** (1993) Relation between the presence of inhibitors and deposit morphology in nickel deposition. *Journal of Applied Electrochemistry*, 23, 508-515.
300. **Valsiunene J.** (1988) Electroless Plating Using Boron Tetrahydride. *Corrosion Week Conference Scientific Society of Mechanical Engineers Hungary* 11-15 Apr. 1988 461-467.
301. **Van Der Kouwe, E.T.** (1993) EIS as a means of evaluating electroless nickel deposits. *Electrochimica Acta*, 38.14, 2093-2097.
302. **Veleva, L., Ballote, L.D. and Wipf, D.O.** (2003) An *In-Situ* Electrochemical Study of Electrodeposited Nickel and Nickel-Yttrium Oxide Composite Using Scanning Electrochemical Microscopy. *Journal of The Electrochemical Society*, 150.1, C1-C6.
303. **Vidrine, A.B. and Podlaha, E.J.** (2001) Composite electrodeposition of ultrafine gamma alumina particles in nickel matrices. Part I Nickel and Citrate Electrolytes. *Journal of Applied Electrochemistry*, 31, 461-468.
304. **Viswanathan, M.** (1973) Occlusion plating to form nickel cermets. *Metal Finishing*, 71, 38-43.
305. **Viswanathan, M. and Ghouse, Md.** (1979) Occlusion plating of nickel graphite composites. *Metal Finishing*, 77, 67-69.
306. **Wang, W., Guo, H.T., Gao, J.P., Dong, X.H. and Qin, Q.X.** (2000) XPS, UPS and ESR studies on the interfacial interaction in Ni-ZrO<sub>2</sub> composite plating. *Journal of Materials Science*, 35, 1495-1499.

307. **Wang, Y., Brogan, K. and Tung, S.C.** (2001) Wear and scuffing characteristics of composite polymer and nickel/ceramic composite coated piston skirts against aluminium and cast iron cylinder bores. *Wear*, 250, 706-717.
308. **Wang, C.B., Wang, D.L., Chen, W.X. and Wang, Y.Y.** (2002a) Tribological properties of nanostructured WC/CoNi and WC/CoNiP coatings produced by electro-deposition. *Wear*, 253, 563-571.
309. **Wang, H., Yao, S. and Matsumura, S.** (2002b) Preparation, characterization and the study of the thermal strain in Ni-W gradient deposits with nanostructure, *Surface and Coatings Technology*, 157, 166-170.
310. **Wang, S.C. and Wei, W.C.J.** (2003a) Kinetics of electroplating process of nano-sized ceramic particle/Ni composite. *Materials Chemistry and Physics* 78, 574-580.
311. **Wang, S.C. and Wei, W.C.J.** (2003b) Characterization of electroplated Ni/SiC and Ni/Al<sub>2</sub>O<sub>3</sub> composite coatings bearing nanoparticles. *Journal of Materials Research* 18.7, 1566-1574.
312. **Wang, L., Gao, Y., Xu, Y. and Xue, Q.** (2006a) Corrosion resistance and lubricated sliding wear behaviour of novel Ni-P graded alloys as an alternative to hard Cr deposits. *Applied Surface Science*, 252.20, 7361-7372.
313. **Wang, L., Gao, Y., Xu, Y. and Xue, Q.** (2006b) A comparative study on the tribological behavior of nanocrystalline nickel and cobalt coatings correlated with grain size and phase structure. *Materials Chemistry and Physics*, 99.1, 96-103.
314. **Warren, B.E.,** *X-ray diffraction*, Addison-Weseley Publishing Company, 1969.
315. **Wasserman, A.** (1989) Occlusion of particles in electrodeposits. *Metal Finishing*, 87.8, 47-49.
316. **Watanabe, T. and Tanabe, Y.** (1976) Formation and morphology of Ni-B amorphous alloy deposited by electroless plating, *Materials Science and Engineering*, 23(2-3), 97-100.
317. **Watanabe, T. and Tanabe, Y.** (1983) The Lattice Images of Amorphous-like Ni-B Alloy Films Prepared by Electroless Plating Method. *Transactions of the Japan Institute of Metals*, 24.6, 396-404.

318. **Webb, P.R. and Robertson, N.L.** (1994) Electrolytic codeposition of nickel  $\gamma$ -alumina thin films. *Journal of the Electrochemical Society*, 141, 669-673.
319. **Wehner, S., Bund, A., Lichtenstein, U., Plieth, W., Dahms, W. and Richtering, W.** (2003) Electrochemical investigations on the influence of electrolyte composition of Watts baths with special regard to throwing power. *Journal of Applied Electrochemistry*, 33, 457-463.
320. **White, C. and Foster, J.** (1981) Factors affecting the entrapment of alumina particles during the electrodeposition of copper. *Transactions of the Institute of Metal Finishing*, 59, 8-12.
321. **Wu, Y.C., Li, G.H., Zhang, L. and Bo, Y.** (2000a) Study on Constitution and Wear Resistance of Nickel Phosphorus Alloy-Silicon Carbide Composite Coatings. *Zeitsfur Metallkunde*. 91.9, 788-793.
322. **Wu, Y.C., Li, G.H. and Zhang, L.** (2000b) Wear Resistance of Electroless Deposited Ni-P and Ni-P/SiC Composite on low alloy cast iron. *Surface Engineering*, 16.6, 506-510.
323. **Wu, F.B., Chen, Y.I., Peng, P.J., Tsai, Y.Y. and Duh, J.G.** (2002) Fabrication, thermal stability and microhardness of sputtered Ni-P-W coating. *Surface and Coatings Technology*, 150, 232-238.
324. **Wu, G., Li, N., Zhou, D. and Mitsuo, K.** (2003) Electrodeposited Co-Ni- $\text{Al}_2\text{O}_3$  composite coatings. *Surface and Coatings Technology*, 176, 157-164.
325. **Wu, Y., Gao, J., Shen, B., Liu, L., Hu, W. and Ding, W.** (2005) Process and properties of electroless Ni-P-PTFE composite coatings. *Plating and Surface Finishing*, 92.8, 38-42.
326. **Wu, Y.T., Liu, L., Gao, J.Q., Shen, B., Hu, W.B. and Ding, W.J.** (2005b) Process and properties of self-lubricant Ni-P-PTFE composite coating. *Shanghai Jiaotong Daxue Xuebao/Journal of Shanghai Jiaotong University*, 39.2, 206-210.
327. **Wu, Y., Liu, H., Shen, B., Liu, L. and Hu, W.** (2006) The friction and wear of electroless Ni-P matrix with PTFE and/or SiC particles composite. *Tribology International*, 39.6, 553-559.
328. **Xiang, Y., Zhang, J. and Jin, C.** (2001) Study of Electroless Ni-P-Nanometer Diamond Composite Coatings. *Plating and Surface Finishing*, 88.2, 64-67.

329. **Xinguo, H. and Naichao, L.** (1990) A study of the kinetics of electroless composite plating, in: *Proceedings of Asia Pacific Inter Finish '90*. The Australian Institute of Metal Finishing, Melbourne, pp. 26.1 - 26.9.
330. **Xinmin, H. and Zonggang, D.** (1992) The wear characteristics of Ni-P-SiC composite coatings. *Transactions of the Institute of Metal Finishing*, 70.2, 84-86.
331. **Xinmin, H. and Zonggang, D.** (1993) A wear- resistant composite coating. *Plating and Surface Finishing*, 80.2, 62-65.
332. **Xu, H., Yang, Z., Li, M.K., Shi, Y.L., Huang, Y. and Li, H.L.** (2005) Synthesis and properties of electroless Ni-P-Nanometer Diamond composite coatings, *Surface and Coatings Technology*, 191, 161– 165.
333. **Xue, Y.J., Jia, X.Z., Zhou, Y.W., Ma, W. and Lee, J.S.** (2006) Tribological performance of Ni-CeO<sub>2</sub> composite coatings by electrodeposition. *Surface and Coatings Technology*, 200, 5677-5681.
334. **Yagodkina, L.M., Loginova, I.D. and Savochkina, I.E.** (1997) *Russian Journal of Applied Chemistry*, 70.10, 1556-1560.
335. **Yang, Z Xu, H Li, M-K Shi, Y-L Huang, Y and Li, H-L** (2004a) Preparation and properties of Ni/P/single-walled carbon nanotubes composite coatings by means of electroless plating, *Thin Solid Films*, 466, 86– 91.
336. **Yang, F.Z., Ma, Z.H., Huang, L., Xu, S.K., and Zhou, S.M.** (2004b) Electrodeposition, Structure and Properties of an Amorphous Ni-W-B/ZrO<sub>2</sub> Composite Coating. *Acta Physico - Chimica Sinica*, 20.12, 1411-1416.
337. **Yang, Z., Xu, H., Shi, Y.L., Li, M.K., Huang, Y. and Li, H.L.** (2005) The fabrication and corrosion behavior of electroless Ni-P-carbon nanotube composite coatings. *Materials Research Bulletin*, 40, 1001– 1009.
338. **Yeh, S.H. and Wan, C.C.** (1994) Codeposition of SiC powders with nickel in a watts bath. *Journal of Applied Electrochemistry*, 24, 993-1000.

339. **Yeh, S.H. and Wan, C.C.** (1995) Influence of Plating conditions on tribology behavior of Ni-SiC composite deposit. *Materials Science and Technology*, 11, 589-593.
340. **Yeh, S.H. and Wan, C.C.** (1997) A study of SiC/Ni Composite Plating in the Watts Bath. *Plating and Surface Finishing*, 84.3, 54-58.
341. **Yu, L.G. and Zhang, X.S.** (1994) The friction and wear properties of electroless Ni-polytetrafluoroethylene composite coating *Thin Solid Films*, 245 (1-2), 98-103.
342. **Zahavi, J. and Kerbel, H.** (1982) Properties of electrodeposited composite coatings. *Plating and Surface Finishing*, 69, 76-82.
343. **Zahavi, J. and Hazan, J.** (1983) Electrodeposited Nickel Composites Containing Diamond Particles. *Plating and Surface Finishing*, 70.2, 57-61.
344. **Zeller III, R.L.** (1991) Electrochemical corrosion testing of high phosphorus electroless nickel in 5% NaCl. *Corrosion*, 47.9, 692-702.
345. **Zhao, Q., Liu, Y., Muller-Steinhagen, H. and Liu, G.** (2002) Graded Ni-P-PTFE coatings and their potential applications. *Surface and Coatings Technology*, 155, 279-284.
346. **Zhao, Q. and Liu, Y.** (2004) Investigation of graded Ni-Cu-P-PTFE composite coatings with antiscaling properties, *Applied Surface Science*, 229, 56-62.
347. **Zhao, Q. and Liu, Y.** (2005) Comparisons of corrosion rates of Ni-P based composite coatings in HCl and NaCl solutions. *Corrosion Science*, 47.11, 2807-2815.
348. **Zhao Q. and Liu, Y.** (2005) Electroless Ni-Cu-P-PTFE composite coatings and their anticorrosion properties. *Surface and Coatings Technology*, 200.7, 2510-2514.
349. **Zhang, H., Zhang, X.J. and Zhang, Y.K.** (1993) Structure and properties of electroless nickel-boron alloy, *Plating and Surface Finishing*, 80.4, 80-84.
350. **Zhang, Y.Z., Wu, Y.Y. Sun, K.N. and Yao, M.** (1998) Characterization of electroless Ni-P-PTFE composite deposits. *Journal of Materials Science Letters*, 17, 119-122.

351. **Zimmerman, A.F., Clark, D.G., Aust, K.T. and Erb, U.** (2002a) Pulse electrodeposition of Ni-SiC nanocomposite. *Materials Letters*, 52, 85-90.
352. **Zimmerman, A.F., Palumbo, G., Aust, K.T. and Erb, U.** (2002b) Mechanical properties of nickel silicon carbide nanocomposites. *Materials Science and Engineering*, A328, 137-146.
353. **Zonggang, D. and Xinmin, H.** (1987) Study of wear resistance of electroless codeposited Ni-P-SiC. Proceedings of the conference - Heat-treatment'87, pp. 55-59.

## LIST OF PUBLICATIONS

1. **K. Krishnaveni, T.S.N. Sankara Narayanan and S.K. Seshadri**  
Electrodeposited Ni-B alloy films: Preparation and Structural aspects  
*Transactions of Indian Institute of Metals*, **56**(4) (2003) 1-6.
2. **T.S.N. Sankara Narayanan, K. Krishnaveni and S.K. Seshadri**  
Electroless Ni-P/Ni-B duplex coatings: preparation and evaluation of microhardness, wear and corrosion resistance  
*Materials Chemistry and Physics*, **82** (2003) 771-779.
3. **K. Krishnaveni, T.S.N. Sankara Narayanan and S.K. Seshadri**  
Electroless Ni-B coatings: Preparation and evaluation of hardness and wear resistance  
*Surface and Coatings Technology*, **190** (2005) 115-121.
4. **T.S.N. Sankara Narayanan, I. Baskaran, K. Krishnaveni and S. Parthiban**  
Deposition of electroless Ni-P graded coatings and evaluation of their corrosion resistance  
*Surface and Coatings Technology* **200** (2006) 3438-3445.
5. **K. Krishnaveni, T.S.N. Sankara Narayanan and S.K. Seshadri**  
Electrodeposited Ni-B coatings: Formation and evaluation of hardness and wear resistance  
*Materials Chemistry and Physics*, **99** (2006) 300-308.